JOURNAL OF CAVE AND KARST STUDIES

DEDICATED TO THE ADVANCEMENT OF SCIENCE, EDUCATION, AND EXPLORATION

Front cover: Phreatic lakes of Frasassi Caves, Italy

FSC
www.fsc.org
MIX
Paper from
responsible sources
FSC® C006300

EVALUATION OF STRATEGIES FOR THE DECONTAMINATION OF EQUIPMENT FOR *GEOMYCES DESTRUCTANS*, THE CAUSATIVE AGENT OF WHITE-NOSE SYNDROME (WNS)

Virginia Shelley[1], Samantha Kaiser[1], Elizabeth Shelley[1], Tim Williams[1], Marcelo Kramer[1], Katie Haman[2], Kevin Keel[2], and Hazel A. Barton[1,3*]

Abstract: White-nose syndrome is an emerging infectious disease that has led to a dramatic decline in cave-hibernating bat species. White-nose syndrome is caused by the newly described fungal pathogen *Geomyces destructans*, which infects the ear, muzzle, and wing membranes of bats. Although the exact mechanism by which the fungus causes death is not yet understood, *G. destructans* leads to a high mortality rate in infected animals. While the primary mechanism of infection appears to be bat-to-bat transfer, it is still unclear what role human activity may play in the spread of this pathogen. Here we evaluate the effectiveness of decontamination protocols that can be utilized by speleologists to reduce the likelihood of spreading this dangerous pathogen to naïve bats or uninfected hibernacula. Our results show that pre-cleaning to remove muds and/or sediments followed by the use of commercially available disinfectants can effectively remove *G. destructans* from caving fabrics. Alternatively, immersion in water above 50 °C for at least 20 minutes effectively destroys the fungal spores. These results have allowed the development of a decontamination protocol (http://www.fws.gov/WhiteNoseSyndrome/cavers.html) that, when appropriately followed, can greatly reduce the likelihood of the human mediated transfer of *G. destructans* from an infected to uninfected site.

INTRODUCTION

In 2006 the bat population in Howe Caverns, a commercial cave in New York, USA, contained a large number of dead or dying bats (Blehert et al., 2009). A common link between all of the dying bats was that they had a white, powder-like substance around their muzzles, ears, and wing-membranes; this white substance caused the disease to be named White-nose Syndrome (WNS). WNS is believed to cause a greater than 70% mortality rate (range 30 to 99%) in bat populations of infected hibernacula and has been associated with a mass bat die-off in the northeastern US, with an estimated 5.5 million deaths (USFWS, 2012). To date, eighteen states have either confirmed WNS [demonstrating bats with histological evidence of a WNS infection: (Meteyer et al., 2009)] and/or bats that test positive for the presence of the etiological agent, the fungus *Geomyces destructans*. These states are Connecticut, Delaware, Kentucky, Maine, Maryland, Massachusetts, Missouri, New Hampshire, New Jersey, New York, North Carolina, Ohio, Oklahoma, Pennsylvania, Tennessee, Vermont, Virginia, and West Virginia. The fungus is also now affecting bat populations in Canada, including the provinces of New Brunswick, Nova Scotia, Ontario, and Quebec. As of December 2011, more than two hundred bat hibernacula have been affected by WNS, which has resulted in a significant decrease in cave-hibernating bat

populations in the Northeast (Kunz and Tuttle, 2009). At the current rate of both mortality and spread, WNS is likely to cause the regional extinction of the little brown bat *Myotis lucifugus* within the next twenty years (Frick et al., 2010).

Koch's postulates were recently satisfied for *G. destructans* (Lorch et al., 2011), demonstrating that *G. destructans* was the sole agent of WNS. While this paper demonstrated that *G. destructans* could be spread directly through bat-to-bat contact, airborne movement of the pathogen was inconclusive, and the role of fomites was not investigated. Whatever the mechanisms of transport, Chaturvedi et al. (2010) demonstrated that a single strain of *G. destructans* was responsible for WNS in over one hundred bats from geographically diverse regions. These investigators used random amplification of polymorphic DNA (RAPD) to demonstrate that all tested isolates had identical RAPD patterns using differential primer sets. Further evidence suggests that *G. destructans* may be an introduced pathogen is provided by the discovery of morphologically and genetically similar *Geomyces* strains from France

* Corresponding author: bartonh@uakron.edu
[1] Department of Biological Sciences, Northern Kentucky University, Highland Heights, KY 41099
[2] UC Davis, School of Veterinary Medicine, Dept. Pathology, Microbiology and Immunology, One Shields Ave. Davis, CA 95616
[3] Department of Biology, University of Akron, Akron, OH 44325

(Puechmaille et al., 2010). This European fungus has since been confirmed in three additional countries: Germany, Switzerland, and Hungary (Wibbelt et al., 2010). However, DNA sequencing across a range of genes will be needed to confirm that this strain is the source of the WNS epidemic. The high mortality rates caused by WNS in the US have not been observed among European bats infected with *G. destructans*. Although the susceptibility of European bat species to WNS has not been fully evaluated, they do demonstrate different hibernation patterns, which may reflect the influence of past epidemics on the populations (Puechmaille, personal communication, 2010).

Past epizootics demonstrate the role human activity can play in the spread of animal pathogens, including foot-and-mouth disease virus (Savill et al., 2006) and the chytrid fungus *Batrachochytrium dendrobatidis* (Daszak et al., 2000). In these epidemics, human activity has contributed to the spread of the pathogen, while altered behavior and disinfection have been shown to limit or prevent its dissemination (Savill et al., 2006, Webb et al., 2007). At this time, we have no understanding of *G. destructans* viability in the environment or how many fungal cells or spores are sufficient to infect a bat or colonize a cave environment. Until this information is available, it is critical that decontamination protocols are used to eliminate the possibility of WNS spread by human activity. In this paper we assess potential physical and chemical methods to decontaminate the fabrics and materials used by speleologists. Our results demonstrate that safe and effective methods of disinfection are possible to limit the anthropomorphic spread of *G. destructans*.

MATERIALS AND METHODS

FUNGAL STRAINS AND GROWTH CONDITIONS

The following strains were obtained from the American Type Culture Collection (ATCC; Manassas, Virginia): *Geomyces pannorum* var *pannorum* (ATCC 16222), *Aspergillus brasiliensis* (née *niger*, ATCC 9642) and *Penicillium pinophilum* (ATCC 9644). These species were grown in *Geomyces* media (40 g dextrose, 10 g peptone L^{-1}) to which 2% agarose was added as a gelling agent for solid media. *Geomyces destructans* was obtained from a little-brown bat collected in Hell Hole Cave, West Virginia, sent to the SCWDS and confirmed by cell morphology, PCR, and an invasive histology diagnostic of WNS. Growth was carried out at room temperature (RT) for all strains except *G. destructans*, which was grown at 7 °C. Mueller-Hinton agar for disk-diffusion assays was obtained from BD Difco/BBL (Franklin Lakes, New Jersey).

SPORE SUSPENSIONS

Conidiospores (spores) from all fungi were harvested from fungal plates in liquid *Geomyces* media using the American Society for Testing and Materials protocol G21-09 (ASTM, 2002), with 0.1% sodium dioctyl sulfosuccinate (DSS) as a wetting agent. DSS was tested for toxicity against each of the fungal strains and demonstrated no inhibitory effect on growth or spore germination. Spore suspensions were counted using a hemocytometer and resuspended in liquid *Geomyces* media to a stock concentration of 1×10^6 spores mL^{-1}. Once made, all spore suspensions were stored at 4 °C and used within four days.

SURVIVAL ASSAYS

Three assays were carried out on spore suspensions to determine spore killing (sporicidal) or fungal growth inhibition (fungistatic) activity of treatments. All assays were carried out in triplicate and the average of each treatment was recorded.

Sporocidal assay – Suspensions of spores at 1×10^3, 1×10^4 and 1×10^5 spores mL^{-1} were filtered onto a 25-mm-diameter 5.0 μm PFTE membrane (Cat # LSWG02500, Millipore, Billerica, Massachusetts; *Geomyces* spores are ~17 mm Ø) using a sterile glass membrane filtration unit (Millipore Cat # XX1002502). While still in the filtration unit, the membranes were exposed to chemical treatment for ten minutes, washed three times with 10 mL sterile distilled water, then aseptically removed and placed on culture media for growth. Following all treatments, the membrane plates were incubated until colonies were observed: up to six days for *G. pannorum* and nine days for the slower growing *G. destructans*. Germination/ outgrowth rates were calculated as the number of colonies divided by the total number of viable spores applied; viability was determined from untreated controls.

Disk diffusion assays – Approximately 1×10^4 spores of *G. pannorum* or *G. destructans* were streaked across the entire surface of either a Mueller-Hinton or *Geomyces*-media plate. The agar plate was allowed to dry until surface moisture was no longer evident, and a 6 mm sterile Whatman paper disk (Whatman, Piscataway, New Jersey) soaked in a single test chemical was placed directly on the plate, using aseptic techniques. Plates were allowed to incubate until confluent fungal growth was observed, and the diameter of the zone of inhibition was measured. To examine the effectiveness of disinfection on *G. pannorum* in the presence of other materials, a top agar containing *Geomyces* media, 1% agar, and 2% of the test material (organic material, muds and sediment) was added. This top agar had been autoclaved and was poured over the surface of *Geomyces*-media plates to a depth of 2 mm. Testing was then carried out using the standard disk-diffusion assay. The organic material, mud and sediment (weathered sandstone) was obtained of a Kentucky cave within the Ste. Genevieve Formation.

CHEMICALS TESTED FOR POTENTIAL EFFECTIVENESS AGAINST GEOMYCES SPP.

Lab grade chemicals were obtained from Sigma-Aldrich (St. Louis, Missouri). The off-the-shelf chemicals were obtained from local retail stores. Household bleach

(Clorox, 6% HOCl) was diluted 1:10 (0.6%) prior to use in all the assays described. The chemical formulations for products evaluated were obtained from publically available material safety data sheets (MSDS). Initial screening was carried out using the disk diffusion assay (Bauer 1966) on both Mueller-Hinton and *Geomyces* media plates.

Heat Treatments of Spores

Dry-Air Treatments

Suspensions of 10^3–10^4 *G. pannorum* or *G. destructans* spores were placed on membrane filters as previously described, placed in sterile petri dishes and exposed to air temperatures of 50 °C, 60 °C, 70 °C, 80 °C, 90 °C, or 100 °C for fifteen minutes. The membrane filters were then placed on *Geomyces* media and incubated at 7 °C for three weeks.

Submersion Treatments

One mL of a 3×10^5 per mL spore suspension of *G. pannorum* or *G. destructans* was placed in conical centrifuge tubes and immersed in water at 30 °C, 40 °C, 50 °C, 60 °C, or 70 °C for twenty minutes. A 100 µL aliquot of the suspension was spread on an SDA plate and incubated at 7 °C for forty days, with colony numbers, in a randomly placed 4 × 4 cm grid, recorded at days seven and forty. All heat treatments were done in replicates of three.

Autoclaving

Preparations of *G. pannorum* and *G. destructans* spores and hyphae were heated to 121 °C at 15 psi (103 kPa) for fifteen minutes using an AMSCO 3013 autoclave sterilizer (STERIS Corporation, Mentor, Ohio). All heat treatments were done in replicates of three. A variety of caving equipment, such as oversuits, helmets, and ropes were treated in the autoclave under the same conditions.

Surface Treatment Assays

New nylon caving fabrics appeared to carry a charge from the nylon or contained water-repellent coatings, preventing the attachment or penetration of spore suspensions. As a result, these materials were not used. Instead a 1000-denier Cordura caving oversuit manufactured by Warmbac (Glastonbury, England) that had been heavily used for four years was used in the surface-treatment assays. One-inch tubular webbing, Sterling 11 mm HTP polyester rope, and Sterling 11 mm Superstatic nylon rope were obtained from Sterling Rope (Biddeford, Maine).

Surface Sterilization Assays

Treatment assays were carried out according to the standard protocol for testing the resistance of synthetic polymeric materials to fungi (ASTM G21-09; ASTM, 2002). Briefly, sections of test fabric were cut into roughly 3 × 3 cm squares, while rope and webbing sections were cut into approximately 3 cm pieces using a heated 1 mm wire. All samples were autoclaved prior to treatment, with sterile control samples demonstrating no fungal growth. Surfaces were sprayed with 250 µL of a 1×10^6 spores per mL suspension, allowed to air-dry for one hour to overnight, depending on the material, and were then exposed to the treatment. After exposure, the material was washed twice by immersion in 500 mL of sterile distilled water, allowed to air-dry, and then either pressed or rolled (in the case of rope) onto the surface of solid *Geomyces* media to deposit spores. The total number of colonies per plate was counted to determine the number of colonies divided by the number of viable applied spores. In the case of adherent fungi, which were not transferred from the fabric to the media, the remaining material was placed in 40 mL *Geomyces* media. Any growth indicated spore survival following disinfection.

Rope-Strength Testing

To test the strength of safety equipment following treatment, 4 m lengths of rope or 1 m sewn webbing loops were treated under the conditions deemed most effective at decontaminating ropes: washing in a front-loading washing machine with the manufacturer's recommended concentration of Woolite detergent, rinsing with water, soaking in a 1:64 dilution of Lysol IC for ten minutes, and rinsing twice in water. That concentration of Lysol IC was used to chemically stress the material, although we showed that a 1:128 dilution is sufficient for disinfection. To test whether this altered the strength of the rope or webbing, three replicate samples were subjected to one or five rounds of treatment (Woolite wash, rinse, treat with Lysol IC, rinse twice). The strength of these materials was then tested at Sterling Rope on a custom-built pull apparatus using a 60 kN hydraulic ram according to the Cordage Institute standard 1801 and calibrated by American Calibration, Inc. (ISO/IEC 17025 accredited, Crystal Lake, Illinois). Pull data was captured by means of a load cell attached to a PAXS strain gage meter (Red Lion Controls, York, Pennsylvania) with a sample rate of 20 Hz. Statistical analysis was performed on grouped samples using a paired *t*-test with a *p*-value of 0.05.

Results

In order to determine the effectiveness of all treatments, we began by autoclaving *G. pannorum* and *G. destructans* cultures. These tests demonstrated that autoclaving at 15 psi (103 kPA) for fifteen minutes killed 100% of *Geomyces* spores and hyphae, even at fairly high concentrations (e.g., 1×10^7 spores per mL). Most caving equipment did not withstand autoclave conditions: ropes became permanently fixed in shape, oversuits became friable, and the lining and cradle fabrics of helmets melted, although the plastics retained their shape. Given the gross physical changes, no attempt was made to determine how autoclaving affected the strength of these fabrics.

Spores of *G. pannorum*, *A. brasiliensis*, and *P. pinophilum* were all resistant to killing by baking (dry heat) above 50 °C (Table 1). At 50 °C, germination and growth of *G.*

Table 1. Number of viable spores following 15 minutes of dry-air heating at 50 °C.

Species	Spores/mL	Treatment			
		Control[a]	5 min	10 min	15 min
Geomyces pannorum	1×10^4	TNTC	TNTC	TNTC	21
	1×10^3	TNTC	TNTC	NG	NG
Aspergillus brasiliensis	1×10^4	TNTC	TNTC	TNTC	TNTC
	1×10^3	TNTC	TNTC	TNTC	TNTC
Penicillium pinophilum	1×10^4	TNTC	TNTC	TNTC	TNTC
	1×10^3	TNTC	TNTC	TNTC	2

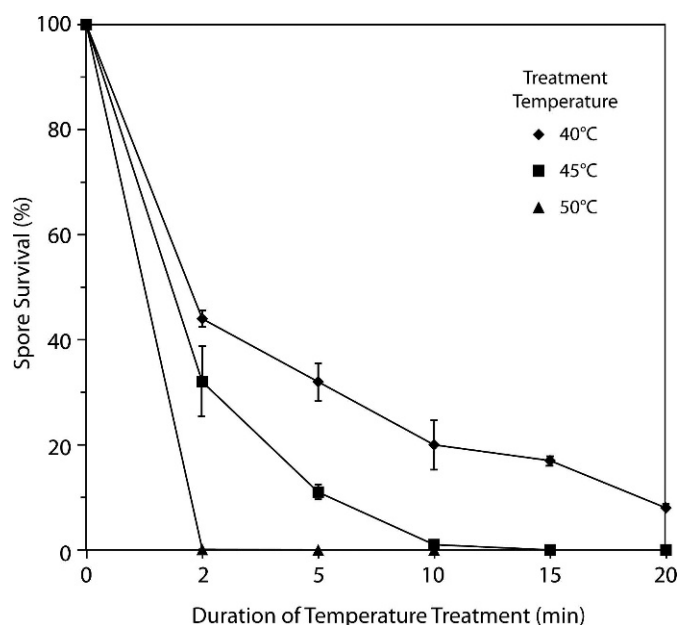[a] Untreated spore suspension.
TNTC = Too numerous to count.
NG = No growth.

pannorum spores was 82.7% of the untreated controls. At the same temperature, 35.3% of *G. destructans* spores were able to germinate by day seven. When the treatments were increased to 70 °C, no *G. destructans* spores germinated. Nonetheless, the spores of *G. destructans* were not as resistant to immersion in hot water. When *G. destructans* spore suspensions were treated at 50 °C for even two minutes, germination of spores after seven days was eliminated (Fig. 1), while unheated controls had abundant growth (data not shown). Exposure to 40 °C and 45 °C also reduced the viability of *G. destructans* spores (Fig. 1), but by day forty, viable colonies were observed. Repeated

Figure 1. Effects of immersive heating on spore suspensions of *G. destructans*. Spore suspensions were heated in a water bath, then plated on culture media and incubated at 6°C for seven days. The average spore growth (percentage) compared to the original inoculum of three separate assays is shown. Error bars indicate the standard deviation from this average. Inhibited growth of *G. destructans* was confirmed for up to forty days post-treatment.

assays demonstrated that only immersion at $\geq$ 50 °C for a minimum of twenty minutes resulted in sterilization of *G. destructans* spores.

Commercially available cleaning agents, disinfectants, and chemicals (Table 2) were screened for their ability to either kill *Geomyces* spores (sporicidal) or limit the germination and growth of the fungus (sporostatic). In all, forty-four commercially available disinfection products were screened against *G. pannorum, A. brasiliensis*, and *P. pinophilum* (Table 2). As expected, some traditional disinfecting agents, such as hydrogen peroxide (H_2O_2), crystal violet, and iodine demonstrated good inhibition of fungal growth. Other effective chemicals contained quaternary ammonium compounds as a disinfectant, including Lysol IC (*n*-alkyl (C8–18) dimethylbenzylammonium chloride), Formula 409 [*n*-alkyl (C12-16) dimethylbenzyl ammonium chloride], and Oust Surface and Air cleaner (*n*-Alkyl dimethyl benzyl ammonium saccharinate). Lysol IC comes in concentrated form (20 to 25%), and our work demonstrates that a 1:128 dilution (0.15 to 0.20% final concentration) of Lysol IC is the minimum effective concentration. Agents containing a detergent also appeared to be effective, including Dawn, Ivory, and Palmolive products, all of which contain ionic and non-ionic detergents. Agents that contain both a disinfectant and a detergent, such as Clorox Toilet Bowl Cleaner (disinfectant: NaClO 1 to 5%), Tide with Bleach (disinfectant: benzenesulfonic acid 10%), Woolite (disinfectant: benzenesulfonic acid), and Dawn Antibacterial Dish Soap (disinfectant: Triclosan, undisclosed percent), are also effective against the growth of *Geomyces* species.

Other chemicals demonstrated less effectiveness. Alcohols did not demonstrate strong activity against *G. pannorum,* either directly (chemical-grade 70% alcohol) or in the following products: Purell Hand Sanitizer, Quick Care, Listerine, Exo Balance, and Cal Stat. Acids and bases also failed to demonstrate any significant effect against *Geomyces* growth, including those found in Grease Lightning, Cascade Gel, Jump Ultra Fabric Softner, and food-grade vinegar. Finally, Tilex Fresh Shower, which contains the cation-chelating agent ethylenediaminetetraacetic acid (EDTA), Seventh Generation Fabric Softner,

V. Shelley, S. Kaiser, E. Shelley, T. Williams, M. Kramer, K. Haman, K. Keel, and H.A. Barton

Table 2. Resistance of fungal spores to various disinfectants based on Kirby-Bauer disk-diffusion assays.

Disinfectant/ Chemical Agent	Zone of Inhibition, mm		
	G. pannorum	*Aspergillus*	*Penicillium*
crystal violet stain	39	20	28
Dawn Simple Pleasures	35	27	32
Chlorox Toilet Bowl Cleaner	35	28	24
Palmolive pure and clean	34	24	18
Tide with Bleach	34	35	25
Oust Surface and Air	34	10	14
Meyer's Clean Day	34	24	27
Hydrogen Peroxide (3%)	34	NZ	NZ
Dawn Dish Liquid	33	27	33
anti-bacterial hand soap	31	21	13
Woolite	31	NZ	20
Penguin Sport-Wash	30	25	26
Formula 409	29	25	13
Ivory Hand soap	28	NZ	12
iodine	25	12	NZ
Cascade Gel	25	NZ	NZ
Pine-Sol	25	9	29
Hibiclens	24	18	14
Scope	22	NZ	NZ
Vick's Early Defense	18	17	16
70% ethanol	18	4	10
Scotchguard Oxy Pet Spot Stain Cleaner	17	NZ	NZ
household bleach (1:10)	16	NZ	18
decolorizer	14	26	NZ
Lysol IC Disinfectant Cleaner (1:128)	15	NZ	NZ
Tabasco	13	–	–
Vesphene Disinfectant	13	–	–
Hydrogen Peroxide (0.3%)	12	–	–
SporiCLEAN	11	–	–
Grease Lightning	9	–	–
vinegar	9	–	–
Cascade Actionpack	NZ	–	–
Purell Hand Sanitizer	NZ	–	–
silver nitrate	NZ	–	–
Quick Care	NZ	–	–
Listerine	NZ	–	–
Cal Stat	NZ	–	–
Tilex Fresh Shower	NZ	–	–
Jump Ultra Fabric Softner	NZ	–	–
Seventh Generation Fabric Softner	NZ	–	–
PureGreen 24	NZ	–	–
Virkon (1%)	NZ	–	–
Exo Balance	NZ	–	–

NZ = No zone of inhibition (growth up to disk).
Dashes indicate test not done.

which contains the palm-oil extract dihydrogenated palmoylethyl hydroxyethylmonium methosulfate, and Virkon, which contains potassium peroxymonosulfate, all failed to demonstrate any effect on fungal growth. Based on some discussion within the WNS scientific community, we also examined products that contained silver as a disinfectant [PureGreen24 (colloidal silver) and silver nitrate (1% AgNO$_3$)], as well as enzymatic cleaners such as SporiCLEAN; however, none of these products demonstrated significant antifungal activity.

Table 3. Comparative resistance of *G. pannorum* and *G. destructans* spores to disinfectants based on the disk-diffusion assays.

| | Zone of Inhibition, mm | | |
| | *Geomyces pannorum* | | *Geomyces destructans* |
Treatment	Day 7	Day 30	Day 30
control	NZ	NZ	NZ
Lysol	23	23	31
bleach (1:10)	67	45	NG
ethanol (70%)	11	NZ	7
Woolite	27	24	44
Formula 409	27	24	31

NZ = No zone of inhibition (growth up to disk).
NG = Fungus was completely cleared from the plate.

Following this preliminary screen, the agents chosen for further study either demonstrated effectiveness against *G. pannorum* (Woolite, Formula 409) or had known activity against fungi (Lysol IC, household bleach, and alcohol). A number of agents that demonstrated strong antifungal activity in the *G. pannorum* assays were not examined due to practical disinfection issues, such as staining of materials (crystal violet and iodine), the concentrations necessary to generate antifungal activity (Dawn Dish Soap), or potential damage to fabrics (Clorox Toilet Bowl Cleaner). Before additional, more extensive testing was carried out, Lysol IC, Woolite, Formula 409, household bleach, and 70% alcohol were also tested for their effectiveness against the pathogen *G. destructans* in a disk-diffusion assay. The results for *G. destructans* and *G. pannorum* were similar, although *G. destructans* appeared to be more susceptible to the same chemical treatments as *G. pannorum* (Table 3), confirming the choice of these compounds.

Disk-diffusion assays only demonstrate the susceptibility of an organism to grow in the presence of a particular disinfectant; they do not demonstrate the effectiveness of that agent as an exposure-based disinfectant. We therefore used the filtration assay to test the effectiveness of exposure to Formula 409, Woolite, Lysol IC, bleach, and 70%

ethanol in preventing *G. pannorum* and *G. destructans* germination. Due to the sub-leathal damage that can occur from such treatments, *G. destructans* spores were allowed to recover for up to forty days following exposure (Russell, 1990). The results (Table 4) demonstrated that direct exposure to household bleach (1:10), Formula 409, and Lysol IC (1:128) completely inactivated *Geomyces* spores following exposure. Woolite demonstrated a reduced level of sporicidal activity (Table 3), suggesting that the activity of this agent in disk-diffusion assays is fungistatic. Alcohol did not demonstrate any effective killing of fungal spores in these assays (Table 4).

While these approaches demonstrate the effectiveness of chemical disinfection in the laboratory, they do not necessarily translate to efficient disinfection in the field. We therefore examined factors that may affect the effectiveness of these disinfectants under real-world conditions.

Cave explorers use a number of different fabrics due to their durability and abrasion resistance, as well as critical life-support equipment, including rope, webbing, and harnesses. The structure of these fabrics, with multiple niches for spore attachment, protection, and chemical absorption, may affect the penetration and effectiveness of chemical disinfectants. Therefore, we took fabrics used by cavers and examined disinfection efficiency following the direct application of fungal spores to the surface. Approximately 2.5×10^4 spores per cm^2 were applied to ballistic nylon (used under cave conditions), and treatment was carried out with Formula 409, household bleach (1:10), and Lysol IC (1:128) for 5, 10, and 15 minutes. The results (Table 5) demonstrated that fungal spores are effectively and reproducibly disinfected on these surfaces with no remaining viable spores when treatment is applied for a minimum of 10 minutes. Woolite greatly reduced the number of viable spores, but did not act as a disinfectant in this assay, while alcohol had comparatively little activity.

During exploration, caving fabrics become covered in mud, clay, or other sediments and organic debris, which could limit the effectiveness of disinfecting agents against fungal spores (Russell, 1990). To this end, organic material,

Table 4. Sporicidal activity of disinfectants against *G. destructans* compared to *G. pannorum* following a 10-minute exposure.

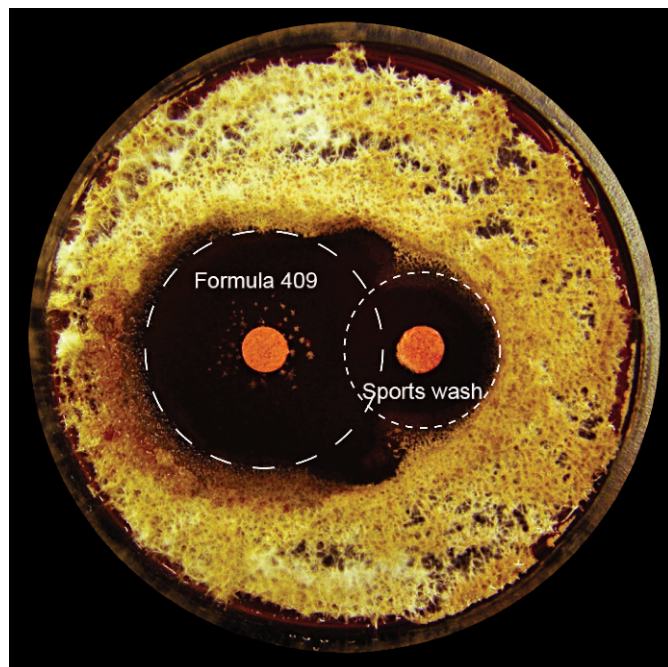| | | | Treatments | | | | | |
Species	Days after Treatment	spores/mL	control	Formula 409	Woolite	Lysol (1:100)	bleach (1:10)	ethanol (70%)
G. pannorum	4	1×10^4	56	49	26	13	0	6
	5	1×10^4	TNTC	53	32	TNTC	0	35
	6	1×10^4	TNTC	TNTC	TNTC	TNTC	0	TNTC
G. destructans	7	1×10^4	TNTC	0	0	0	0	177
	8	1×10^4	TNTC	0	0	0	0	TNTC
	9	1×10^4	TNTC	0	1	0	0	TNTC

TNTC = Too numerous to count.

Table 5. Effectiveness of Disinfectants against *G. pannorum* in the Presence of Various Cave Sediments.

| | Disk Diffusion | | | | Fabric Treatment (Rope) | | | |
| | Zone of Inhibition, mm | | | | Colonies | | | |
Disinfectant	Control	Clay	Sand	Silt	Control	Clay	Sand	Silt
Bleach (1:10)	67	12	NZ	NZ	TNTC	0	11	9
Lysol IC (1:128)	23	NZ	12	12	TNTC	0	0	0
Formula 409	27	32	NZ	NZ	TNTC	0	0	0

TNTC = Too numerous to count.
NZ = No zone of inhibition (growth up to disk).

mud, and sediment were added to the disk-diffusion assays to determine how great an effect the presence of these materials could have on disinfection. The results (Table 5) demonstrate that cave detritus can have a dramatic impact on the effectiveness of these disinfectants. We therefore repeated our cave fabric disinfection protocol with mud applied along with the fungal spores. The results (Table 5) demonstrated that these substances also dramatically reduced the effectiveness of disinfection on these surfaces, arguing for a pre-cleaning treatment prior to disinfection.

Figure 2. Synergistic effects of multiple treatments on the growth of *G. pannorum*. Disk diffusion assays were set up using various combinations of disinfecting agents. The combination of Formula 409 (left disk) and Penguin Sport-Wash (right disk) is shown. While a zone where each chemical prevents the growth of the fungus around each disk is observed, the combination of the two chemicals generates a greater zone of inhibition than each alone (larger zone between the two disks).

To test this, we carried out a disk diffusion assay to determine if specific detergents and disinfectants were compatible; such combinations can often be problematic as cationic disinfectants and anionic detergents can bind to each other, precipitate, and negate the effect of both products. In these assays we compared the inhibition of fungal growth by combinations of both Woolite and Meyer's Clean Day washing detergents with Formula 409, household bleach (1:10), and Lysol IC (1:128). The results (for example, Fig. 2) suggested that these products lead to a greater inhibition of fungal growth together than each does individually. It therefore appears that a pre-wash with a detergent such as Woolite can remove inhibitory substances while contributing to overall disinfection.

In addition to fabrics, speleologists use a number of pieces of critical life support equipment, including harnesses, webbing, and ropes. The nylon in this equipment gives the ropes or webbing strength; however, it is also susceptible to ionic attack, by substances such as bleach, which can damage the structural integrity and strength of the material. Consequently, we wanted to examine the ability of disinfection protocols to remove or kill spores on this material without harming its strength. Given the negative potential effects of bleach on nylon, we examined the ability of Woolite (which is traditionally used by speleologists to wash ropes) and Lysol IC (which can be made up in large volumes) to disinfect sewn webbing and nylon ropes. Treatment was carried out by washing in Woolite, rinsing with sterile water, soaking in a 1:64 dilution of Lysol IC for ten minutes, and rinsing twice in sterile water. The results demonstrated 100% killing of 2.5×10^5 spores applied to rope and webbing samples (Table 5). A higher concentration of Lysol IC (1:64) was used to chemically stress the material, although a 1:128 dilution has been shown to be 100% effective in this assay. To test whether this altered the strength of the webbing or rope, we treated samples of one-inch tubular webbing, Sterling 11 mm HTP rope, and Sterling 11 mm Superstatic rope, for one or five rounds of treatment. The strength of these materials was then tested, and the average breaking strength (in kN) was recorded (Fig. 3). Similar rope tests have not been carried out on samples returned to other rope manufacturers despite repeated requests.
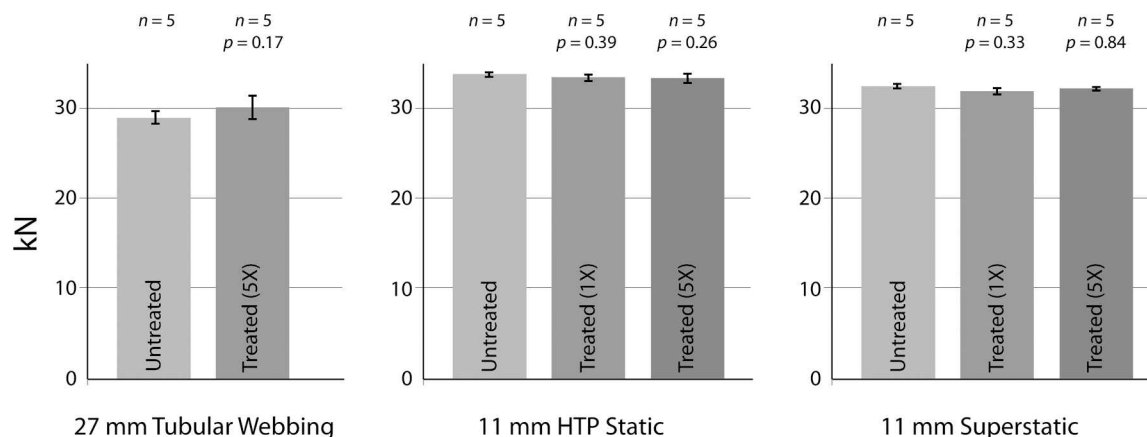
Figure 3. Rope and webbing post-treatment strength tests. Samples of rope and webbing were treated in triplicate with either one or five rounds of chemical treatment. The samples were then subjected to strength tests to determine the average breaking strength (in kN). The standard deviation of the combined results is shown as error bars. Based on a paired t-test ($p = 0.05$) there was no significant difference between the strength of the treated and untreated samples.

DISCUSSION

We carried out our preliminary assays in the non-pathogenic *G. pannorum* due to the ease of cultivation and comparatively short generation time for this species in the laboratory (five days to confluent growth versus approximately one month for *G. destructans*); however, to confirm the effectiveness of our decontamination protocols, we repeated key assays with *G. destructans.* Our results demonstrated a strong correlation between the effectiveness of these agents in *G. pannorum* and *G. destructans,* arguing for the appropriateness of *G. pannorum* as a model organism for preliminary assay development. We also chose to concentrate our assays on spores, the more resistant form of the *G. destructans* fungus (Deacon, 2005). Conidiospores are made by fungi for dispersal of the parent organism and, as such, are intrinsically resistant to environmental stressors such as UV and desiccation (Deacon, 2005, Gottlieb, 1950, Russell, 1990). Indeed, this can be seen by the relative resistance of these spores to both heat treatments and alcohols, and that heat stress actually promotes the germination and outgrowth of fungal spores (Table 1), even in the case of this psychrophilic fungi (Deacon, 2005, Russell, 1990).

Our results demonstrate that certain compounds, such as Formula 409 or bleach, are viable means of *G. destructans* disinfection to prevent the spread of WNS. Given the ineffectiveness of alcohols, protocols that suggest cavers should wipe exposed skin with alcohol swabs or alcohol-based hand sanitizer should be met with skepticism. The fact that most speleologists wear gloves that can be decontaminated suggests that standard personal hygiene practices (hand washing, bathing) likely represent a much more practical approach to limiting the spread of WNS on human skin.

In addition to chemical treatments, immersive heating of materials able to withstand submersion could be useful for reducing contamination by *G. destructans* spores. It is important to note that such conditions are not normally achieved in a standard washing machine, although sterilizing washing machines that can heat and maintain the temperature above 50 °C for twenty minutes would be a practical alternative. Given the difficulty in establishing and maintaining dry-air temperatures above 70 °C without laboratory-type controlled ovens or autoclaves, this mechanism of disinfection is not advised for anyone without access to, and training in the use of, such equipment. Regardless of these practical considerations, if heat treatment is the primary mechanism of disinfection, it is also important to consider the risks of contaminating external surfaces of containers, instruments, or surrounding surfaces. Limiting contact of contaminated gear or subsequent disinfection of such surfaces with effective chemical agents would help mitigate this risk.

Our chemical-disinfection experiments demonstrate the effectiveness of a number of agents that are known to be sporostatic but not sporicidal, including quarternary ammonium compounds and detergents (Russell, 1990). These results actually align well with those for bacterial spores and sporicidal agents (Russell, 1990 and references therein) and the work of Chaturvedi et al. (2011) against *G. destructans.* The effectiveness of these agents may well be due to a phenomenon by which these agents become attached to the spore coat and are hard to remove (other than by neutralization; Russell, 1990), suggesting that these agents do not act specifically on the spores, but rather act on germ tube formation during germination (Deacon, 2005). In all our assays, the presence of a long-chain alkyl group in the most effective antifungal agents suggests that such chemical structures play an important role in

preventing the growth of *Geomyces* spp. (Table 2). The specificity of such activity may help to identify whether *Geomyces*-restrictive antifungal agents could be identified for the in situ treatment of hibernating bats.

There were some differences between the results found in the disk-diffusion assay and the spore assay, specifically as they relate to bleach. These differences can probably be accounted for by adsorption of the reactive chlorite ions (ClO_2^-) to reagents in the media. This effect was amplified by the addition of clays, sand, and silt to the media. Mud consists of insoluble clay particles that remain after speleogenesis. The composition of these muds depends on the rock formation from which they were derived. In the Ste. Genevieve Formation (used in these assays), these muds are primarily silica (SiO_2), but also contain kalsilite ($KAlSiO_4$), iron (Fe_2O_3) and aluminum (Al_2O_3) oxides (Preston and Denver, 1967). Such clays contain numerous reactive surfaces, such as hydroxyl (OH^-) or siloxane [$(SiO^-)_n$] groups, which can be bound by reactive ions (Sposito et al., 1999). Indeed, such clays are often used as adsorption agents in a variety of settings, including hydrocarbon extraction and absorptive chemical liners (Sposito et al., 1999). It is therefore likely that such compounds adsorb the reactive ions of disinfectants, negating some of the antifungal properties of these agents. Although disk-diffusion assays yielded similar results for both *G. pannorum* and *G. destructans*, the sporicidal activity of agents differed for the two fungi, possibly due to differences in the spore coats. This assay involved treating spores with the agent of interest, thoroughly washing the spores, then culturing the washed spores. Differences in spore coats could result in differential adherence of certain compounds to the spores of the two species examined.

The chemicals chosen in the development of these protocols (Table 2) were based on their commercial availability and ability to be included in a disinfection protocol that could be carried out by untrained personnel in the field. Chemicals were also selected that could disinfect without damaging the potentially life-supporting materials of recreational cavers. Our data demonstrate the effectiveness of protocols that can be used on caving equipment to decontaminate *Geomyces* fungal spores from surfaces in a short time (~15 minutes) and that the chemicals did not significantly alter the strength of Sterling rope (Fig. 3). Our protocols and results led to the development of the USFWS standard decontamination protocols (http://www.fws.gov/WhiteNoseSyndrome/cavers.html) and demonstrate the ability to kill all of 2.5×10^4 spores, an effective kill rate of greater than 99.995%, although it is possible that this kill rate may actually be higher.

In the food and pharmaceutical industries, hygiene protocols aim not to sterilize pharmaceuticals and cosmetics, but to remove sufficient microorganisms to prevent human infections (Baird et al., 2000). As such, much lower concentrations of disinfectants, used for longer periods,

may reduce the fungal spore burden down to a level that is considered safe (Gupta et al., 2001). At this time, no information is available about spore loading during human visits to a cave or the minimum infective dose of *G. destructans* to initiate WNS in bats or contaminate the cave environment. The spread of WNS along bat migration routes (Frick et al., 2010) and the lack of numerous geographic epicenters may also suggest that human-vectored transport of *G. destructans* may be rare. Nonetheless, until the exact mechanism of *G. destructans* transport and environmental survival is known, it is critical to remove the potential impact of human transport. However draconian the proposed decontamination measures seem, a high level of adoption within the caving community can ensure continued access to both popular recreational sites and demonstrate to landowners and management agencies the commitment of cavers to both protect the fragile underground wilderness and care for the only other mammalian species that penetrates as deeply into this subterranean world.

References

ASTM, 2002, Standard Practice for Determining Resistance of Synthetic Polymeric Materials to Fungi, West Conshohocken, Pennsylvania, American Society of Testing and Materials standard G21-09, 5 p.

Baird, R.M., Hodges, N.A., and Denyer, S.P., eds., 2000, Handbook of Microbiological Quality Control: Pharmaceuticals and Medical Devices, Boca Raton, Florida, CRC Press, 280 p.

Bauer, A.W., Kirby, W.M.M., Sherris, J.C., and Turck, M., 1966, Antibiotic susceptibility testing by a standardized single disk method: *American Journal of Clinical Pathology*, v. 36, p. 493–496.

Blehert, D.S., Hicks, A.C., Behr, M., Meteyer, C.U., Berlowski-Zier, B.M., Buckles, E.L., Coleman, J.T.H., Darling, S.R., Gargas, A., Niver, R., Okoniewski, J.C., Rudd, R.J., and Stone, W.B., 2009, Bat white-nose syndrome: an emerging fungal pathogen?: *Science*, v. 323, 227 p. doi:10.1126/science.1163874.

Chaturvedi, S., Rajkumar, S.S., Li, Xiaojiang, Hurteau, G.J., Shtutman, M., and Chaturvedi, V., 2011, Antifungal testing and high-throughput screening of a compound library against *Geomyces destructans*, the etiologic agent of geomycosis (WNS) in bats: *PLoS One*, v. 6, paper e17032, 6 p. doi:10.1371/journal.pone.0017032.

Chaturvedi, V., Springer, D.J., Behr, M.J., Ramani, R., Li, Xiaojiang, Peck, M.K., Ren, P., Bopp, D.J., Wood, B., Samsonoff, W.A., Butchkoski, C.M., Hicks, A.C., Stone, W.B., Rudd, R.J., and Chaturvedi, S., 2010, Morphological and molecular characterizations of psychrophilic fungus *Geomyces destructans* from New York bats with white-nose syndrome (WNS): *PLoS One*, v. 5, paper e10783, 12 p. doi:10.1371/journal.pone.0010783.

Daszak, P., Cunningham, A.A., and Hyatt, A.D., 2000, Emerging infectious diseases of wildlife—threats to biodiversity and human health: *Science*, v. 287, p. 443–449. doi:10.1126/science.287.5452.443.

Deacon, J.W., 2005, Fungal Biology, Indianapolis, Wiley-Blackwell, 384 p.

Frick, W.F., Pollock, J.F., Hicks, A.C., Langwig, K.E., Reynolds, D.S., Turner, G.G., Butchkoski, C.M., and Kunz, T.H., 2010, An emerging disease causes regional population collapse of a common North American bat species: *Science*, v. 329, p. 679–682. doi:10.1126/science.1188594.

Gottlieb, D., 1950, The physiology of spore germination in fungi: *The Botanical Review*, v. 16, p. 229–257. doi:10.1007/BF02873609.

Gupta, A.K., Ahmad, I., and Summerbell, R.C., 2001, Comparative efficacies of commonly used disinfectants and antifungal pharmaceutical spray preparations against dermatophytic fungi: *Medical Mycology*, v. 39, p. 321–328.

Kunz, T., and Tuttle, M., 2009, Science Strategies for White Nose Syndrome. WNS Science Strategy II Meeting May 27–28, 2009, Austin, Texas.

Lorch, J.M., Meteyer, C.U., Behr, M.J., Boyles, J.G., Cryan, P.M., Hicks, A.C., Ballmann, A.E., Coleman, J.T.H., Redell, D.N., Reeder, D.M., and Blehert, D.S., 2011, Experimental infection of bats with *Geomyces destructans* causes white-nose syndrome: *Nature*, v. 480, p. 376–378. doi:10.1038/nature10590.

McGrain, P., and Denver, G.R., Jr., 1967, Limestone resources in the Appalachian region of Kentucky: Lexingon, Kentucky Geological Survey bulletin ser. 10, no. 4, 12 p.

Meteyer, C., U. Buckles, E.L., Blehert, D.S., Hicks, A.C., Green, D.E., Shearn-Bochsler, V., Thomas, N.J., Gargas, A., and Behr, M.J., 2009, Histopathologic criteria to confirm white-nose syndrome in bats: *Journal of Veterinary Diagnostic Investigation*, v. 21, p. 411–414. doi:10.1177/104063870902100401.

Puechmaille, S.J., Verdeyroux, P., Fuller, H., Ar Gouilh, M., Bekaert, M., and Teeling, E.C., 2010, White-nose syndrome fungus (*Geomyces destructans*) in a bat, France: *Emerging Infectious Diseases*, v. 16, p. 290–293. doi:10.3201/eid1602.091391.

Russell, A.D., 1990, Bacterial spores and chemical sporicidal agents: *Clinical Microbiological Reviews*, v. 3, p. 99–119. doi:10.1128/CMR.3.2.99.

Savill, N.J., Shaw, D.J., Deardon, R., Tildesley, M.J., Keeling, M.J., Woolhouse, M.E.J., Brooks, S.P., and Grenfell, B.T., 2006, Topographic determinants of foot and mouth disease transmission in the UK 2001 epidemic: *BMC Veterinary Research*, v. 2, article 3, 9 p. doi:10.1186/1746-6148-2-3.

Sposito, G., Skipper, N.T., Sutton, R., Park, S.-H., Soper, A.K., and Greathouse, J.A., 1999, Surface geochemistry of the clay minerals: *Proceedings of the National Academy of Sciences of the United States of America*, v. 96, p. 3358–3364. doi:10.1073/pnas.96.7.3358.

USFWS, 2012, North American bat death toll exceeds 5.5 million from white-nose syndrome: [Arlington, Virginia, Office of Communications] http://www.fws.gov/whitenosesyndrome/pdf/WNS_Mortality_2012_NR_FINAL.pdf [Accessed February 22, 2012]

Webb, R., Mendez, D., Berger, L., and Speare, R., 2007, Additional disinfectants effective against the amphibian chytrid fungus, *Batrachochytrium dendrobatidis*: *Diseases of Aquatic Organisms*, v. 74, p. 13–16. doi:10.3354/dao074013.

Wibbelt, G., Kurth, A., Hellmann, D., Weishaar, M., Barlow, A., Veith, M., Prüger, J., Görföl, T., Grosche, L., Bontadina, F., Zöphel, U., Seidl, H.-P., Cryan, P.M., and Blehert, D.S., 2010, White-nose syndrome fungus (*Geomyces destructans*) in bats, Europe: *Emerging Infectious Diseases*, v. 16, p. 1237–1242. doi:10.3201/eid1608.100002.

OSTRACOD ASSEMBLAGES IN THE FRASASSI CAVES AND ADJACENT SULFIDIC SPRING AND SENTINO RIVER IN THE NORTHEASTERN APENNINES OF ITALY

Dawn E. Peterson[1], Kenneth L. Finger[1*], Sanda Iepure[2], Sandro Mariani[3], Alessandro Montanari[4], and Tadeusz Namiotko[5]

Abstract: Rich, diverse assemblages comprising a total (live + dead) of twenty-one ostracod species belonging to fifteen genera were recovered from phreatic waters of the hypogenic Frasassi Cave system and the adjacent Frasassi sulfidic spring and Sentino River in the Marche region of the northeastern Apennines of Italy. Specimens were recovered from ten sites, eight of which were in the phreatic waters of the cave system and sampled at different times of the year over a period of five years. Approximately 6900 specimens were recovered, the vast majority of which were disarticulated valves; live ostracods were also collected. The most abundant species in the sulfidic spring and Sentino River were *Prionocypris zenkeri*, *Herpetocypris chevreuxi*, and *Cypridopsis vidua*, while the phreatic waters of the cave system were dominated by two putatively new stygobitic species of *Mixtacandona* and *Pseudolimnocythere* and a species that was also abundant in the sulfidic spring, *Fabaeformiscandona* ex gr. *F. fabaeformis*. *Pseudocandona* ex gr. *P. eremita*, likely another new stygobitic species, is recorded for the first time in Italy. The relatively high diversity of the ostracod assemblages at Frasassi could be attributed to the heterogeneity of groundwater and associated habitats or to niche partitioning promoted by the creation of a chemoautotrophic ecosystem based on sulfur-oxidizing bacteria. Other possible factors are the geologic age and hydrologic conditions of the cave and karst aquifer system that possibly originated in the early–middle Pleistocene when topographic uplift and incision enabled deep sulfidic waters to reach the local carbonate aquifer. Flooding or active migration would have introduced the invertebrates that now inhabit the Frasassi Cave system.

INTRODUCTION

Due to their toxic level of H$_2$S and critically low concentration of dissolved oxygen, the environment of a sulfur-based chemoautotrophic groundwater ecosystem is considered harsher than other subsurface settings (Engel, 2007). Despite the stressful sulfidic environment, it is remarkable that their crustacea-dominated fauna appear to be as diverse as those in non-sulfidic karst ecosystems, especially when considering endemics (Culver and Sket, 2000; Iliffe, 2004). Since the discoveries of thermal vent communities in the 1970s (Jannasch, 1985; Deming and Barross, 1993) and the Movile Cave in 1986 (Sarbu, 1990; Sarbu et al., 1996), several subsurface ecosystems associated with sulfidic waters, particularly in caves, were documented worldwide as hotspots for subterranean biodiversity (Iliffe, 2004). However, the ostracod fauna are almost unknown for most of the discovered sulfidic cave and karst aquifers.

The best-known hotspot of ostracod biodiversity is the anchialine Walshingham Cave System in Bermuda, with nineteen ostracod species out of a total thirty animal species registered (Iliffe, 2004). Other hotspots of subterranean crustacean biodiversity are known in continental sulfidic karst systems, but their associated ostracod faunas

are less diverse. The Movile Cave in Romania hosts one endemic ostracod species of *Pseudocandona* (awaiting formal description) out of a total of eighteen aquatic species (Sarbu et al., 1996; Sarbu et al., 2000). The large Edwards Aquifer in Texas, from which springs provide the base flow of the Guadalupe River system, also hosts only one known ostracod species, *Sphaeromicola moria* Hart, among its fifty-five known aquatic taxa (Longley, 1981, 1986). Ostracods have yet to be studied in other sulfidic ecosystems that support diverse communities of stygobitic crustaceans, such as the thermohaline sulfidic spring complex of El Hamma in Tunisia (Por, 1963), the Dead Sea rift valley and the Ayalon Cave in Israel (Por, 1963, 2007, 2011), the springs of Grotta di Fiume Coperto in Italy (Latella et al., 1999), Lower Kane Cave in Wyoming, USA (Porter et al., 2002; Engel, 2007), and Cueva de Villa Luz in Mexico (Engel, 2007).

* Corresponding author: kfinger@berkeley.edu
[1] University of California Museum of Paleontology, 1101 Valley Life Sciences Building, Berkeley, CA 94720-4780, USA
[2] Speleological Institute "Emil Racovitza", Department of Biospeleology, Clinicilor 5, 400006, Cluj Napoca, Romania
[3] Gruppo Speleologico CAI Fabriano, Via Alfieri 9, 60044 Fabriano, Italy
[4] Osservatorio Geologico di Coldigioco, Cda. Coldigioco 4, 62021 Apiro, Italy
[5] University of Gdańsk, Department of Genetics, Laboratory of Limnozoology, Kładki 24, 80-822 Gdańsk, Poland
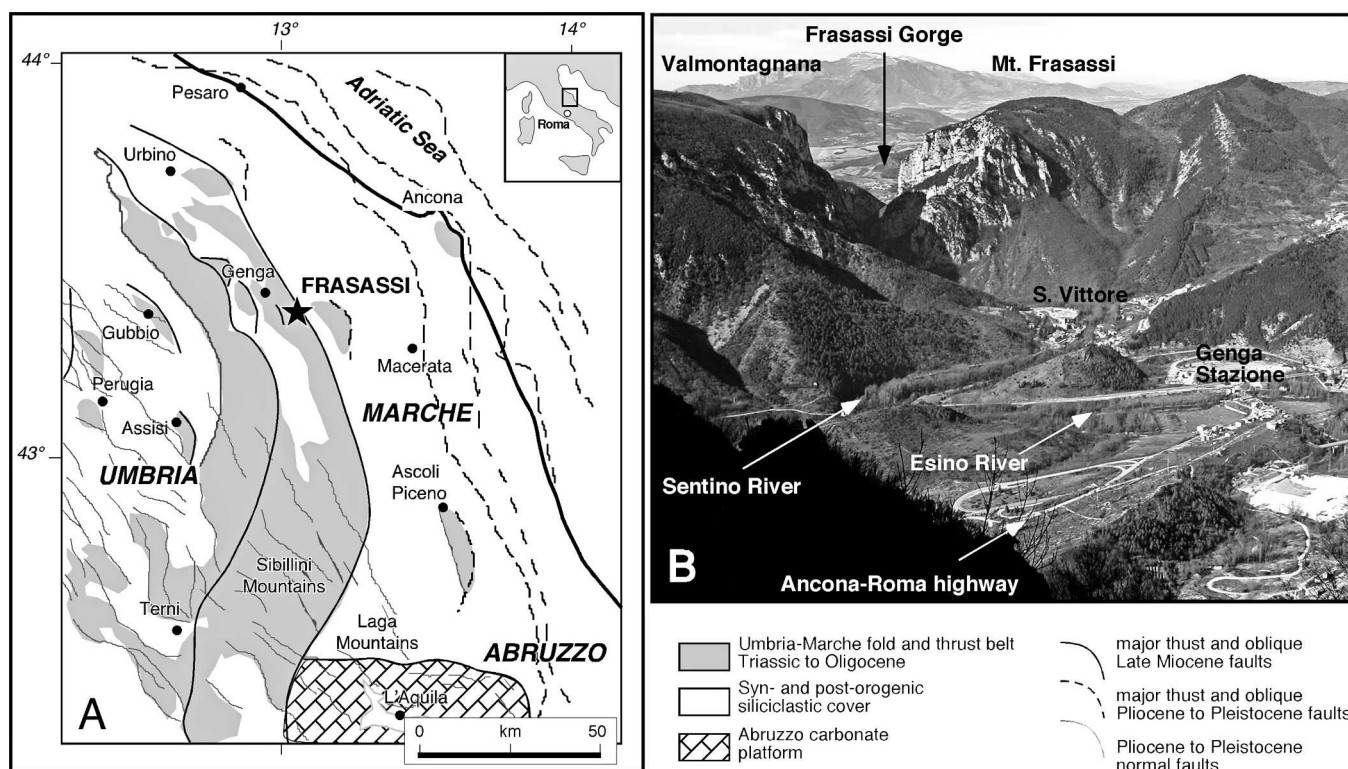
Figure 1. (A) Simplified geostructural map of the Umbria-Marche region and location of the Frasassi area. (B) Panoramic view of the Frasassi area looking west.

During a joint expedition in 2001, speleologists of the Gruppo Speleologico of the Club Alpino Italiano from Fabriano and the Gruppo Speleologico Marchigiano in Ancona discovered and explored a new large extension in the deepest reaches of the Grotta del Fiume in the Marche region of central Italy, which, along with another dozen or so other caves, is part of the sulfidic chemioautotrophic ecosystem of the hypogenic karst of Frasassi (Fig. 1; entrance coordinates: 43°24′03″N; 12°57′48″E). In this newly discovered part of the cave, named New Mexico, the speleologists found the bones and skin of hundreds of subfossil eels (*Anguilla anguilla* L.) lying on the subvertical banks of large phreatic lakes up to about 5 m above the water table (Fig. 2).

Taphonomy and carbon-isotope analysis of the eel remains indicate that the animals periodically entered the cave from the Sentino River that flows outside the cave through the deep Frasassi Gorge. The eels survived in this hypogean environment feeding on sulfur bacteria (Mariani et al., 2007), which still flourish in the sulfidic bottom-water layer of these phreatic lakes (Macalady et al., 2008a, b). These chemosynthetic, autotrophic sulfur bacteria are the food source for a number of stygobionts endemic to the cave, including protozoans (Buonanno et al., 2009), annelids (Erséus, 2009), rotifers (Claudia Ricci, personal communication, January 2010), gastropods (Bodon et al., 2009), copepods (Diana Galassi, personal communication,

October 2009), and amphipods (Bauermeister, 2009; Dattagupta, 2009; Karaman et al., 2010; also see review by Montanari, 2010). After dying, the decomposing eels floated on the surface of these phreatic pools, and after heavy rains the slow northward backflow of vadose bicarbonate water washed them up onto the rocky banks (Mariani et al., 2007). Through accurate radiocarbon dating of the eel remains, Mariani et al. (2007) obtained corrected ^{14}C ages that increased with height above present mean water table from 2200 BP at 63 cm, to 2600 BP at 215 cm, to 7200 BP at 395 cm. Using a radiocarbon age of 8400 BP from a calcite rind contouring the lakes at 465 cm, Mariani et al. (2007) estimated that the water table dropped at a mean rate of about 0.55 mm y^{-1} during the Holocene because of the incision of the Sentino River and the tectonic uplifting of the Frasassi area.

While preparing samples for radiocarbon dating, Mariani et al. (2007) recovered numerous well-preserved shells of microgastropods and ostracods that had been intimately mixed with the eel debris (Fig. 2C). Stygobitic hydrobiid microgastropods (~1 mm) belonging to the genus *Islamia* were first reported in the sulfidic sections of the Frasassi caves by Sarbu et al. (2000) as a component of its hypogean fauna that included fourteen other species of mostly terrestrial invertebrates, five of which were new taxa and seven of which were endemic to these caves. They reported only two inhabitants of the aqueous environment
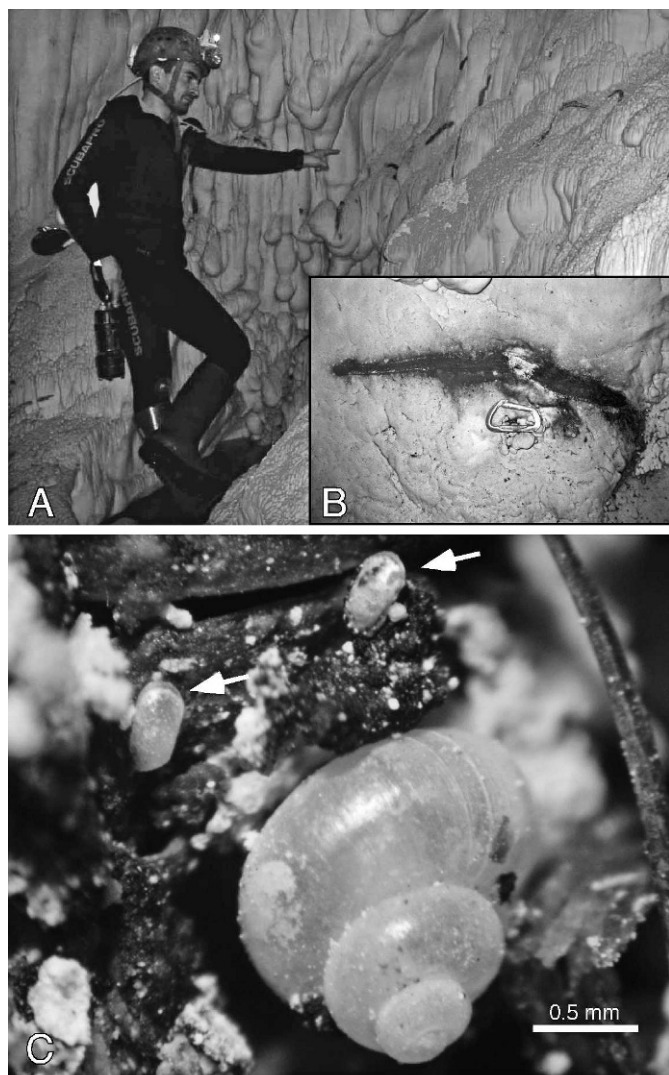
Figure 2. (A) Subfossil eels attached to a vertical concretioned bank of Lago delle Anguille. (B) Detail of a sampled eel found at about 2 m above the water table. (C) Photomicrograph of subfossil eel debris (skin and bones; sample LDA/09/09-200 cm) with a shell of the gastropod *Islamia* sp. 2 and two carapaces of the ostracod *Pseudolimnocythere* sp. (arrows).

in the cave, the amphipod *Niphargus ictus* Karaman and the microgastropod *Islamia pusilla* (Piersanti). In a subsequent study on these microgastropods, Bodon et al. (2009) identified them as *Islamia* sp. 2, an undescribed species known only from this cave system and provisionally identified from a few sulfidic springs in Umbria and Latium.

The discovery of abundant ostracod shells among the remains of subfossil (Holocene but not recent) eels prompted our study of them in several phreatic lakes and pools throughout the cave system, as well as in and around a sulfidic spring outside the cave and on the banks of the Sentino River. In this paper, we present a reconnaissance

of these ostracod assemblages that focuses on their ecological characteristics and distribution. We highlight two new stygobitic species, here reported in open nomenclature as *Mixtacandona* sp., which is apparently endemic to the Frasassi cave system, and an elusive yet intriguing *Pseudolimnocythere* sp., which is represented by more than one thousand subfossil carapaces and valves recovered from various sites in the cave. We report also on a third presumably new stygobitic or stygophilic species, *Pseudocandona* ex gr. *P. eremite* that was recovered rarely and only from the Frasassi sulfidic spring, and eighteen other ostracod species collected from localities along the riverbanks and the sulfidic spring. Detailed taxonomic descriptions of the three new species will be addressed in the future.

GEOLOGIC SETTING

The Frasassi Cave system is a 25 km karstic maze located in the Mt. Frasassi–Mt. Valmontagna blind-thrust anticline, which is part of the Umbria-Marche Apennines thrust-and-fold belt of central Italy (Fig. 1). The core of the anticline is made of a 800 m thick succession of massive carbonate platform limestone layers of the Calcare Massiccio Formation (earliest Jurassic), overlain by a succession of Jurassic to Eocene pelagic limestone formations (Fig. 3). The Calcare Massiccio rests on top of the uppermost Triassic Burano Formation, which consists of a 2000 m thick succession of evaporitic anhydrites, black shales, and bituminous limestones (Martinis and Pieri, 1964). The Burano evaporites are not exposed in the Frasassi area, but are present in deep boreholes, and they are quarried in some localities near Perugia, in Umbria.

The anticline is dissected by the deep Frasassi Gorge, which was incised by the eastward-flowing Sentino River, a tributary of the Esino River. The Sentino flows at piezometric level in the Frasassi Gorge, which corresponds to the height of the water table in the cave system, at about 205 m above mean sea level toward the eastern end of the gorge. The incision of the gorge was the result of a combined process of antecedence and superposition beginning during the Pleistocene (Mazzanti and Trevisan, 1978; Alvarez, 1999). The core of the anticline was karstified during this time, with the formation of the giant Frasassi Cave system, which comprises seven main subhorizontal levels connected by narrow, steep to nearly vertical shafts (Fig. 4). This is the result of alternating erosion and deposition controlled by successive Quaternary glacial-interglacial cycles during a steady, regional tectonic uplift (Cattuto, 1976; Bocchini and Coltorti, 1990; Galdenzi and Menichetti, 1995; Mayer et al., 2003; Cyr and Granger, 2008; Wegman and Pazzaglia, 2008). Some large rooms, such as the 250 m high Abisso Ancona (estimated at 10^6 m^3), were created by the collapse of the thin rock layers separating the hypogean levels. The lowest level is flooded by the water table and represents the piezometric level of the cave system.
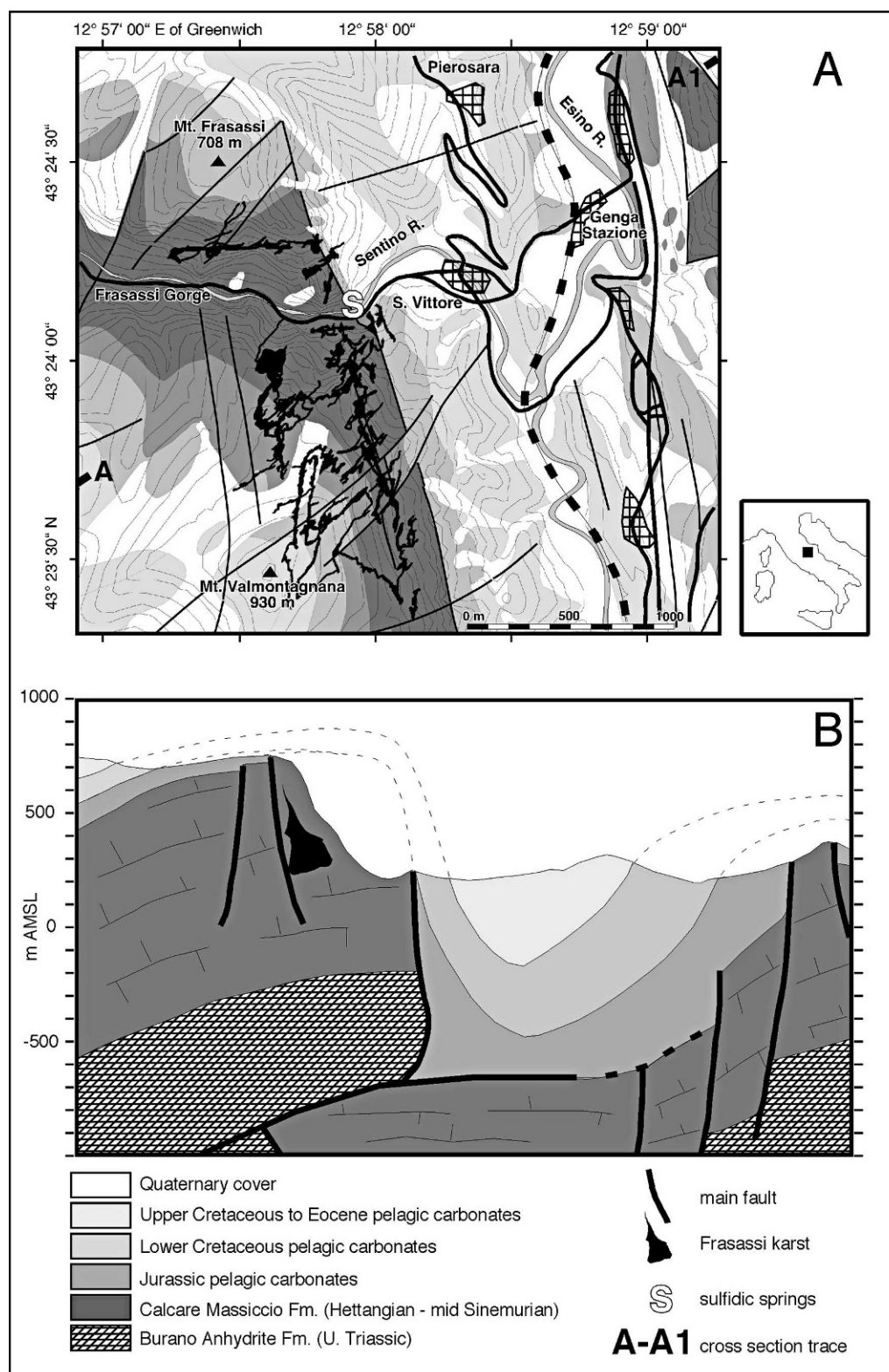
Figure 3. (A) Simplified geologic map. (B) Cross-section of the Frasassi area. (Redrawn from Mariani et al., 2007.)
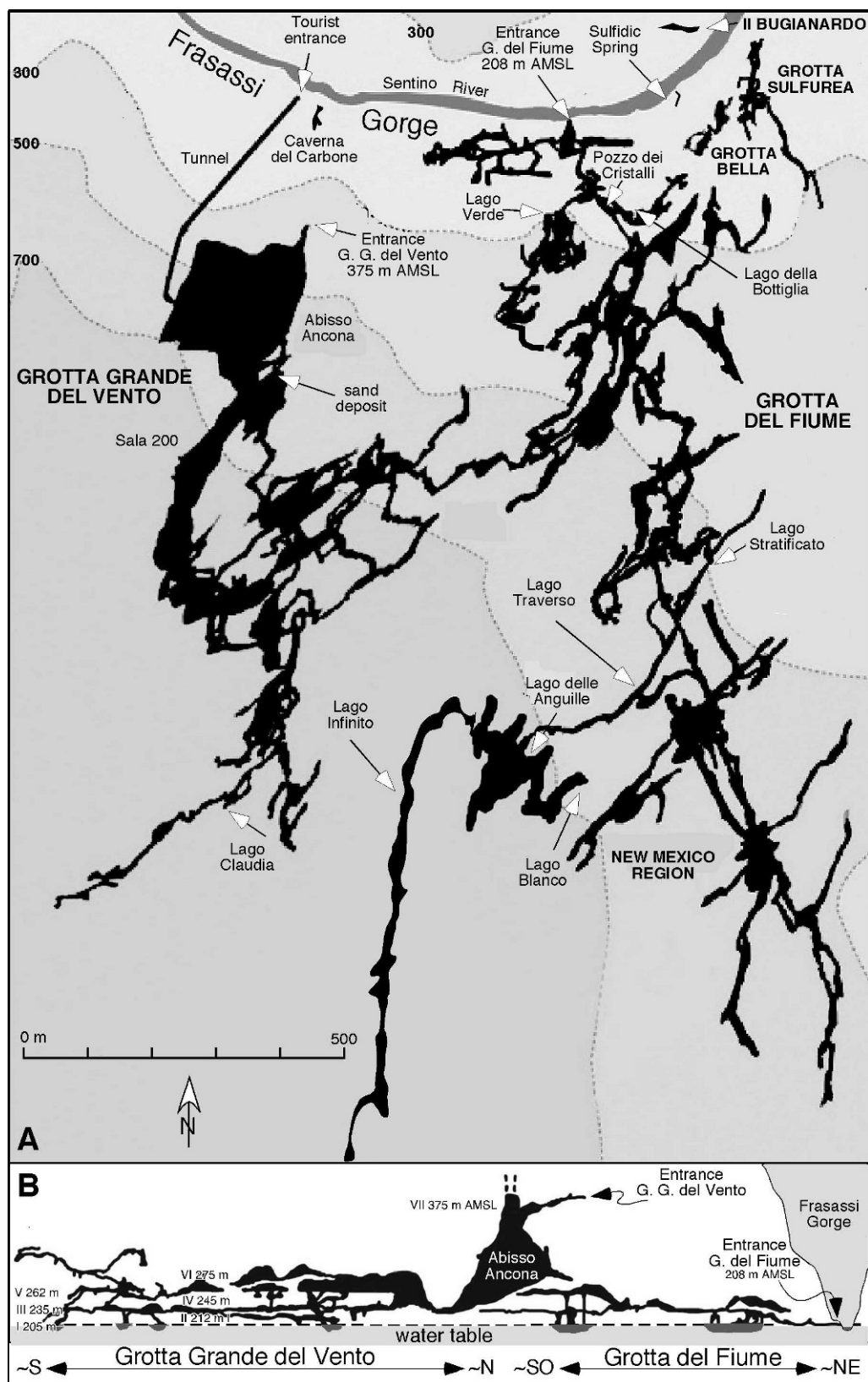
Figure 4. (A) Simplified map of the Grotta Grande del Vento–Grotta del Fiume cave system (base map from Mariani et al., 2007) with location of sites cited in the text. (Note: this plane view of the complex cave system does not show the vertical extent of the first four levels of the cave from its base level of 205 m AMSL to ~245 m elevation). **(B)** Idealized cross-section of the caves showing the arrangement of horizontal hypogean levels.

Deep groundwater contacting the Burano Formation reduces the anhydrite, allowing sulfidic H$_2$S-rich water to well up along the fault that bounds the east side of the Frasassi anticlinal massif, eventually emerging along the intersection of this fault with the Sentino River bed (see Fig. 3).

The presence in the Burano Formation of anhydrite (CaSO$_4$) as a sulfate source and black shale as an organic carbon source provides the conditions for bacterial sulfate reduction in deep groundwater to form H$_2$S. Bacterial action is necessary in this reducing process because H$_2$S would not be produced inorganically at any significant rate at temperatures below 200°C (Druschel et al., 2009). The H$_2$S-rich water wells up along the fracture network until it interacts with oxygen brought in either as dissolved O$_2$ in meteoric water percolating from above through the Calcare Massiccio limestone or as atmospheric O$_2$ in the open spaces of the cave system. At this point, the H$_2$S interacts with the oxygen, creating conditions for sulfur-oxidizing bacteria to accelerate the rate of the overall reaction and liberate H$^+$ to form sulfuric acid $(H_2S+2O_2{\rightarrow}2H^+)$ that corrodes and dissolves the limestone (CaCO$_3$) of the Calcare Massiccio, thus forming the hypogenic cave system within the water table. Such a reaction, which would be extremely slow without the action of the sulfur bacteria, precipitates gypsum (CaSO$_4$·2H$_2$O), which, being soluble in water, is carried away out of the cave system with the slow but continuous flow of vadose water. In some parts of the cave, sulfidic water reaches the surface, exhaling H$_2$S directly into the cave atmosphere. This causes corrosion of the limestone vaults, formation of microcrystalline gypsum slush masses (Galdenzi and Maruoka, 2003), and the growth of extremely acidic pendulous biofilms (snottites) attached to the walls of the cave (Macalady et al., 2007, Jones et al., 2012). In summary, the giant Frasassi Cave system is the result of sulfidic hypogenic karstification in which sulfur-oxidizing bacteria play a major role in the massive corrosion of the Calcare Massiccio limestone (Galdenzi et al., 1999, 2008; Macalady et al., 2006, 2008a). Continuous and abundant production of organic matter by the H$_2$S-oxidizing bacterial activity is the basis of a complex stygobitic ecosystem.

Materials and Methods

During 2005–2010, eighty samples were collected for ostracods from ten Frasassi localities). These included fifteen small samples of subfossil eel remains (bones and skin), ranging from 0.1 to 5.0 g each, collected in 2005–2007 at eight different heights above water table (50, 70, 150, 200, 215, 300, 370, and 395 cm) on the banks of Lago delle Anguille in the New Mexico region of the Grotta del Fiume (see Fig. 4A for location). Ostracod carapaces and valves were separated from organic eel remains with a moist fine brush and mounted on micropaleontological slides for examination.

A total of twenty-two sediment samples were systematically collected at different times of the year from spring 2005 to winter 2010 from eight phreatic lakes in the Grotta del Fiume–Grotta Grande del Vento complex. In order of progressively greater distance from the natural entrance of the Grotta del Fiume, these are Lago Verde, L. della Bottiglia, L. Stratificato, L. Traverso, L. Blanco, L. delle Anguille, L. Infinito, and L. Claudia (Fig. 4A). Arm length limited substrate sampling to water depths ranging up to 60 cm. Except for Lago della Bottiglia, where sampling was done in 2009 and 2010 using a plankton net, all sediment samples were collected in 3 L sealable plastic bags containing abundant cave water using an ordinary 7 cm diameter metal tea strainer as a scooper. A few hours after their collection, samples were wet-screened at the Geological Observatory of Coldigioco to remove sediment smaller than 63 μm and greater than 2 mm; the residues were preserved in 50 mL Falcon tubes with 70% ethanol for transport to the University of California Museum of Paleontology, where the residues were again washed through a 63 μm sieve. Each dried residue was split into 63, 125 and 250 μm fractions for stereomicroscopic examination; all ostracod specimens were picked and sorted on micropaleontological slides. Images of selected specimens were obtained using the Hitachi TM-1000 Tabletop Scanning Electron Microscope at the Robert M. Ogg Electron Microscope Laboratory, University of California, Berkeley.

It is important to point out that, despite our intention to perform sampling in the most systematic and consistent way possible, difficult environmental conditions that vary between lakes and sampling sites hindered our attempts to obtain a sample collection that would be appropriate for an accurate quantitative assessment of the ostracod assemblages in the cave. Only experienced and technically proficient cavers can reach many of the sites, particularly the inner lakes of the Grotta del Fiume (Fig. 5). Hence, sampling was limited to sites where a lake's bank is relatively easy to reach and has a gentle or flat slope that enabled us to easily collect fine sediment from shallow depths.

At Lago della Bottiglia (Fig. 5A) in the Grotta del Fiume and in all the larger, up to 8 m deep lakes in the New Mexico region of the cave, the sulfidic water layer is usually at a depth of approximately 4 m (Mariani et al., 2007). Therefore samples were collected well above the chemocline, in oxygenated bicarbonate water. On the other hand, at Lago Verde and Lago Claudia (Figs. 6C, D), sulfidic water often reaches the water table, and the sediment along the banks is usually black in color, reduced, and rich in hydrogen sulfide (Figs. 6B, D). In most cases, cave-lake sediments were usually made of micro- or cryptocrystalline calcite or clay, sometimes containing iron-sulfide grains, and, at the Lago Infinito sampling site, microcrystals of gypsum. Where the bank of the lake is a talus slope, as at Lago Verde and Lago Claudia, the sediment consists of fine grains to large angular fragments of limestone. In contrast, the sparse sediment attached to the steep, rocky bank of Lago della Bottiglia at the bottom of Pozzo dei Cristalli (Fig. 4A) consists of calcite microcrystals and fecal pellets of the hygrobiid gastropod *Islamia* sp. 2.

One sample was collected at Lago Claudia in summer 2008 experimenting with a suction pump with a 63 μm polyester monofilament cloth as catching filter and kept in water to be observed in a 12 cm diameter Petri dish at the Coldigioco lab. From this sample, live ostracod specimens were separated and preserved in 70% ethanol for later identification. After discovering live specimens at Lago Claudia, in 2009 we adopted the use of a 20 cm diameter polyester plankton net with a 44 μm mesh and a 50 mL Falcon tube as terminal catcher for further sampling in this relatively accessible site, and we also used it at Lago della Bottiglia (see Fig. 4A for locations).

Twenty-four sediment samples from the Frasassi sulfidic spring were collected at different times of the year from winter 2006 through summer 2009. The sampling site is a small, ephemeral pond on the left side of the sulfidic stream, which flows for a few meters out of the calcareous massif through a small cave before merging into the right bank of the Sentino River (Fig. 7A). The pond is protected from the direct flow of the river by boulders. The reduced, sulfidic sediment of the pond includes lime, calcareous sand, and pebbles derived from the various formations of the Umbria-Marche sedimentary succession, mostly pelagic limestones and chert from the Jurassic to Oligocene part of the succession, and siliceous sand, silt, and clay from the Miocene flysch succession (Marnoso-Arenacea Formation). All samples from this site contained abundant leaf and woody litter. Collecting was performed during low river flow. During prolonged periods of heavy rains, usually in the early winter and early spring, the Sentino River floods, rising to 3 m above normal level. During these events, the ephemeral sulfidic spring and pond are completely submerged by the rushing, muddy river water (Fig. 7B). It usually takes a week or more of dry weather for the Sentino to return to its low, normal flow regime and for the sulfidic environment of our sampling site to regenerate.

Seven riverbed sediment samples were taken in 2006 and 2009 along the right bank of the Sentino 15 and 30 m upstream and 5 and 10 m downstream from the sulfidic Spring. One sample was also collected on the left bank about 15 m directly across the river from the sulfidic spring site. These fluvial deposits were used for comparison with samples from the cavern and sulfidic spring.

Due to the difficulty of sampling the bottom waters of the hypogean lakes, there are no measurements of their oxygen concentrations. Among profiles of redox potential measurements versus depth obtained in 2009 for a few lakes, those for Lago Infinito and Lago Profondo showed they were well stratified, with a sharp chemocline above water with oxygen below detection limits of ~6 μg L^{-1} or 0.2 μmol L^{-1}. The well-mixed sulfidic stream was not anoxic, but had very low oxygen levels. (J. Macalady, pers. comm.)

Results

In total, sixty-six of the eighty Frasassi samples yielded 6850 ostracod specimens representing twenty-one species-group taxa (Table 1; Figure 8) belonging to fifteen genera and five families (Candonidae, Ilyocyprididae, Cyprididae, Limnocytheridae, and Loxoconchidae). The seventy-seven assemblage slides prepared in this study reside in the University of California Museum of Paleontology microfossil collection as UCMP 46331–46407. Table 1 records the numbers of valves and live specimens of each taxon at the ten Frasassi localities. However, it must be pointed out that the number of valves per species in Table 1 is not a standardized measure of the absolute abundance relative to a unit of sediment surface, mass, or volume, nor is it of the abundance of specimens in one site relative to another. Each site was sampled multiple times, some more times than others, and the amount of sediment recovered varied. The total amount of sediment analyzed also varies from site to site. Nevertheless, the specimen counts reveal the relative abundance of each species at each location.

Out of the twenty-one species identified, three stygobites are of particular interest. Numerous valves and live individuals identified as *Mixtacandona* sp. (Fig. 8G) most likely represent a new species that closely resembles *Mixtacandona talianae* Gliozzi and Mazzini and *M. italica* Karanovic and Pesce. *Mixtacandona talianae* was described from valves recovered from Holocene cave deposits in Grotta del Lago in Umbria, central Italy (Gliozzi and Mazzini, 1998a), while *M. italica* was collected live from groundwater accessed through wells in Puglia, southeastern Italy (Karanovic and Pesce, 2000). Our specimens are similar to these two species in having a trapezoidal left valve, a height:length ratio greater than 55%, and remarkable dorsal protuberances. But *Mixtacandona* sp. can be distinguished by its straight or only slightly concave valve margin in the anterodorsal and posterodorsal sections, unlike that of *M. talianae* and *M. italica*, where it is distinctly concave, and by its larger size (valve length 0.70 to 0.75 mm vs. 0.54 to 0.57 mm for *M. talianae* and 0.57 to 0.62 mm of *M. italica*). The Frasassi specimens differ also in soft-part features that await detailed study and description.

Triangular valves of other putative new stygobitic candonid species found in sediments of the Frasassi sulfidic spring were assigned to *Pseudocandona* ex gr. *P. eremita* (Fig. 8F) based on the diagnosis of Namiotko and Danielopol (2004). This open nomenclature is used because several species belonging to this group presently cannot be unambiguously separated without thorough analysis of valve shape and male genital morphology (see Iepure et al., 2007). Although the taxonomic status of our specimens remains to be determined by further study, the occurrence of *Pseudocandona* ex gr. *P. eremita* in the sulfidic spring allows us to extend the known geographical distribution of the *P. eremita* group, as this is the first record of a representative of this stygobitic ostracod group in Italy. It also allows us to revise the ecological valences of this group previously known only from non-sulfidic waters.

As for *Pseudolimnocythere* sp., the third stygobitic ostracod found at Frasassi (Fig. 8U), it shows closest
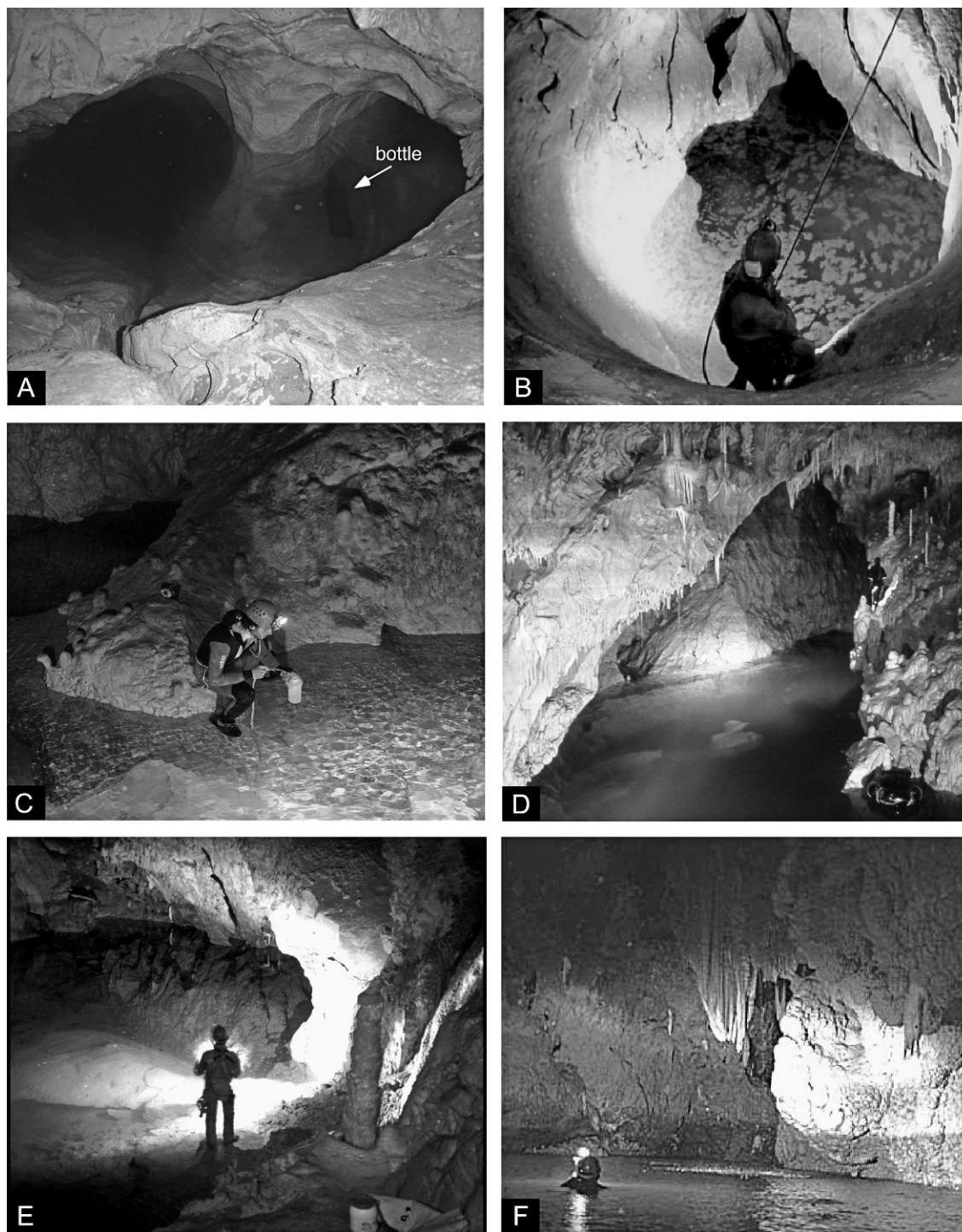
Figure 5. Phreatic lakes of the Frasassi caves sampled for this study (see Fig. 4). (A) Lago della Bottiglia; arrow points to a whiskey bottle at the bottom of a 30 cm deep pond on the right side of the pool; the sample site is on the steep rocky bank at the lower left. (B) Lago Stratificato; note the rafts of microcrystalline calcite that form at the water surface during the dry season. (C) Lago Traverso. (D) Lago delle Anguille; inner tube of tire and caver climbing on the right side provide scale. (E) Lago Blanco, so named because of the white lime on the shallow lake bottom. (F) Lago Infinito, which is in the farthest reaches of the Grotta del Fiume and is the largest lake in the cave, at approximately 200 m long and 8 m deep. Sampling site LIN is in the northern part of the lake.
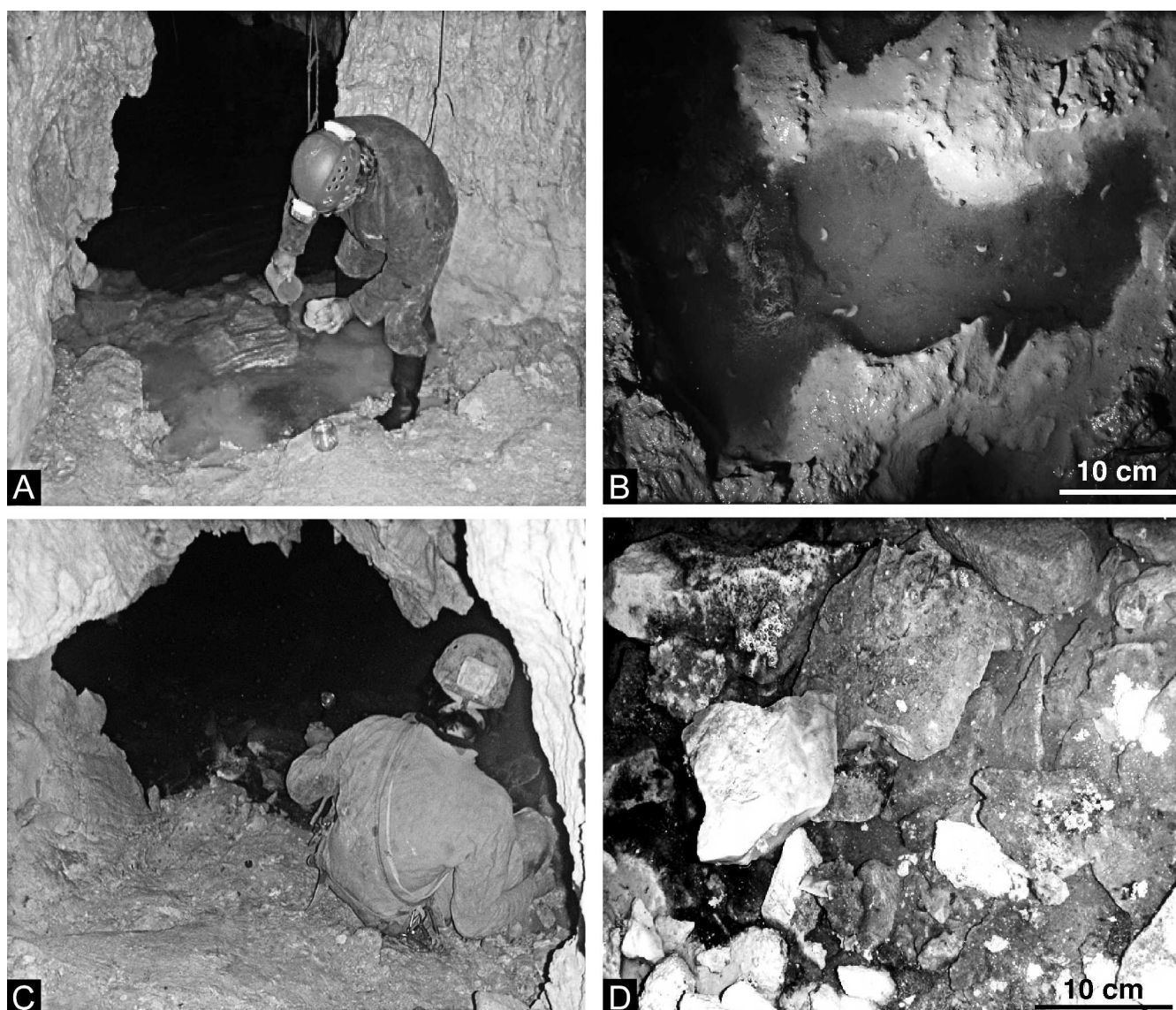
Figure 6. (A) Lago Verde, the phreatic pool closest to the natural entrance of the Grotta del Fiume cave sampled in this study. Samples were taken from the shallow, muddy edge of the pool, beyond which the lake drops several meters. The concentration of H_2S in the superficial water layer may change considerably through time due to the seasonally variable water table and the relatively shallow sulfidic water layer. (B) Closeup of the sampling site on the shore of Lago Verde. Note the numerous amphipods *Niphargus ictus* pasturing in a 5 cm deep pond on the shore of the lake. The lake bottom consists of black, reduced, sulfidic mud mixed with rocks from the bank's scree. (C) Lago Claudia, the sampled phreatic pool farthest from the natural entrance of the cave. (D) Shallow bottom along margin of Lago Claudia showing the angular limestone clasts derived from the talus slope that distinguish it from Lago Verde.

affinity to *P. hypogea* Klie, originally described from material collected from groundwater in southern Italy (Klie, 1938) and subsequently recorded in caves and wells in Puglia by Pesce and Pagliani (1999) and Karanovic and Pesce (2001). More recently, individuals of this genus were reported in northern Apennine springs (Bottazzi et al., 2008; Stoch et al., 2009), but they were not described. It is unfortunate that none of the Frasassi *Pseudolimnocythere* sp. specimens retain their soft parts, as the limb and genital morphology in the genus are better characteristics for

distinguishing species than valve morphology alone. Future detailed study on the valve morphology and additional material with soft parts will enable us to confirm the taxonomic status of our specimens.

Some other taxa in the studied material are also left in open nomenclature (Table 1, genus and species indeterminate) to indicate that the identification to the species level was provisional, uncertain, or impossible due to the lack of soft parts or an insufficient number of well-preserved adult valves. The senior author tentatively identified some
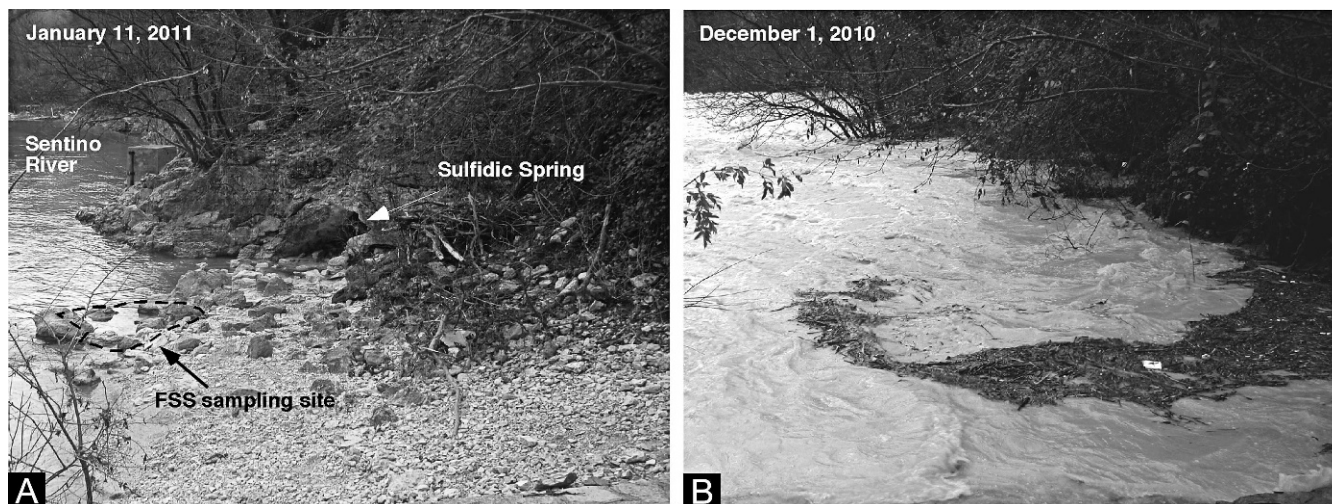
Figure 7. (A) View of the sulfidic spring site taken on January 11, 2011; the sampling site is delimited by a dashed line. (B) The same site during heavy flooding of the Sentino River on December 1, 2010, when both the small pond of the sampling site and the cave where the sulfidic water flows out from the mountain and into the Sentino are completely submerged by muddy river water.

broken valves from the sulfidic spring as belonging to two other species of *Mixtacandona* and one species of *Cryptocandona*, suggesting a greater species diversity of groundwater-associated ostracod assemblages in the Frasassi cave system. However, as verification of this material was impossible, these taxa were excluded from further study pending the availability of sufficient material.

Apart from the three presumably new species (*Mixtacandona* sp., *Pseudocandona* ex gr. *P. eremita*, and *Pseudolimnocythere* sp.), two candonid species identified only to the species group (*Candona* ex gr. *C. neglecta* and *Fabaeformiscandona* ex gr. *F. fabaeformis*), and an unidentified species of *Paralimnocythere*, all taxa listed in Table 1 have been previously reported from various habitats elsewhere in Europe (Meisch, 2000). They have been also recorded from various present-day water bodies and late Pliocene to Holocene deposits in the Italian Peninsula, Sardinia, and Sicily (e.g., Ambrosetti et al., 1995; Barberi et al., 1995; Calderini et al., 1998; Gliozzi and Mazzini, 1998b; Gliozzi, 2000; Meisch, 2000; Karanovic and Pesce, 2001; Rossi et al., 2003, 2004; Rossetti et al., 2004, 2005, 2006; Pieri et al., 2006, 2007, 2009; Rossi et al., 2010).

In the epigean site of the sulfidic spring pool (FSS in Table 1), live specimens collected were limited to *Candona* ex gr. *C. neglecta*, *Fabaeformiscandona* ex gr. *F. fabaeformis*, *Ilyocypris monstrifica*, *Prionocypris zenkeri*, *Cypridopsis vidua*, *Potamocypris zschokkei*, and *Limnocythere inopinata*. *Prioncypris zenkeri* was the most abundant taxon, represented by 1541 valves and six live individuals from the sulfidic spring. Valves of most of these species were also recovered from non-sulfidic sediment samples collected along the banks of the Sentino River, but the live fauna recovered consisted only of eight specimens of *Fabaeformiscandona* ex gr. *F. fabaeformis* (FSR in Table 1).

Inside the cave at Lago Verde, the sampled phreatic pool closest to the natural entrance of the Grotta del Fiume (~150 m straight-line distance), we found 281 valves of many of the taxa recovered outside plus one live specimen of *Pseudocandona albicans*. The most abundant ostracod species at Lago Verde, represented by 82 valves, is *Candona* ex gr. *C. neglecta* (LVE in Table 1). Two live juveniles of this taxon were recovered elsewhere, one from the sulfidic spring and another, interestingly enough, at Lago Claudia, the most remote lake in the inner part of the Grotta Grande del Vento, about 1.2 km straight-line distance from the natural entrance of that cave (Fig. 4A).

Hundreds of specimens of *Mixtacandona* sp., *Pseudolimnocythere* sp., and *Fabaeformiscandona* ex gr. *fabaeformis* were recovered from the most remote sites of the cave system, as well as a very few valves of *Candona neglecta*, *Candona* ex gr. *C. neglecta*, *Pseudocandona albicans*, *Herpetocypris chevreuxi*, and *Cypridopsis vidua*, rarely found in sites closer to an entrance.

Of the three most abundant species in the hypogean environment of Frasassi, only *Mixtacandona* sp. was found live and abundant at Lago della Bottiglia and Lago Claudia. Empty valves of this species were present in all the other sampled cave sites, as well as the sulfidic spring outside the cave, but none were recognized in any of the samples from the freshwater sites along the Sentino River banks. Lago Blanco yielded a disproportionate 383 valves of *Mixtacandona* sp., 325 of which were in sample LBL/07-21/04. Valves of this species were also found among subfossil eel remains at Lago delle Anguille, at 395, 300, 150, and 70 cm above the present water table. The limy sediment of Lago Blanco also produced a disproportionate number of *Fabaeformiscandona* ex gr. *F. fabaeformis*, which occurred as 435 valves, 325 of which were in the same

Table 1. Composite numbers of ostracodes recovered from Frasassi localities, 2006–2009.

Figure 8 Images	Species	Localities Outside of Cave			Hypogean Lakes							Total
		FSS	FSR	LVE	LDB	LST	LTR	LDA[a]	LBL	LIN	LCL	...
A	*Candona candida*	96	31	1								128
B	*Candona neglecta*	63	11	26								102
C	*Candona* ex gr. *C. neglecta*	73-**1**	6	82					1		3-**1**	165
D	*Fabaeformiscandona* ex gr. *F. fabaeformis*	299-**3**	48-**8**	61		5		5	435		1	854
E	*Pseudocandona albicans*	176	47	14-**1**		2						239
F	*Pseudocandona* ex gr. *P. eremita*[b]	11-**3**	1									12
G	*Mixtacandona* sp.[b]	3		36	50-**11**	7	6	15	383	13	121-**6**	634
H	*Cypria* cf. *C. ophtalmica*	4	4	5								13
I	*Ilyocypris bradyi*	6										6
J	*Ilyocypris* cf. *I. inermis*	60	7									67
K	*Ilyocypris monstrifica*	9-**3**	6									15
L	*Prionocypris zenkeri*	1541-**6**	131	7								1679
M	*Herpetocypris chevreuxi*	687	21	36					4			748
N	*Psychrodromus olivaceus*	193	15	2								210
O	*Heterocypris* cf. *H. reptans*	99	9	1								109
P	*Cypridopsis vidua*	347-**4**	11	8					1			368
Q	*Potamocypris fulva*	28	9									37
R	*Potamocypris zschokkei*	56-**2**	26									82
S	*Limnocythere inopinata*	191-**10**	15	2								208
T	*Paralimnocythere* sp.	2										2
U	*Pseudolimnocythere* sp.[b]	9	3			2	14	448	176	505	3	1160
	genus and species indeterminate	10						2				12
	Total number of valves at each locality	3963	401	281	50	18	20	470	1001	518	128	6850

[a] All specimens collected on the remains of subfossil eels.
[b] Stygobitic species.
Note: Numerical data in plain typeface refers to single valves counts; boldface indicates live specimens.
FSS = sulfidic spring, FSR = Sentino River, LVE = Lago Verde, LDB = Lago della Bottiglia, LST = Lago Stratificato, LTR = Lago Traverso, LDA = Lago delle Anguille, LBL = Lago Blanco, LIN = Lago Infinito, LCL = Lago Claudia.
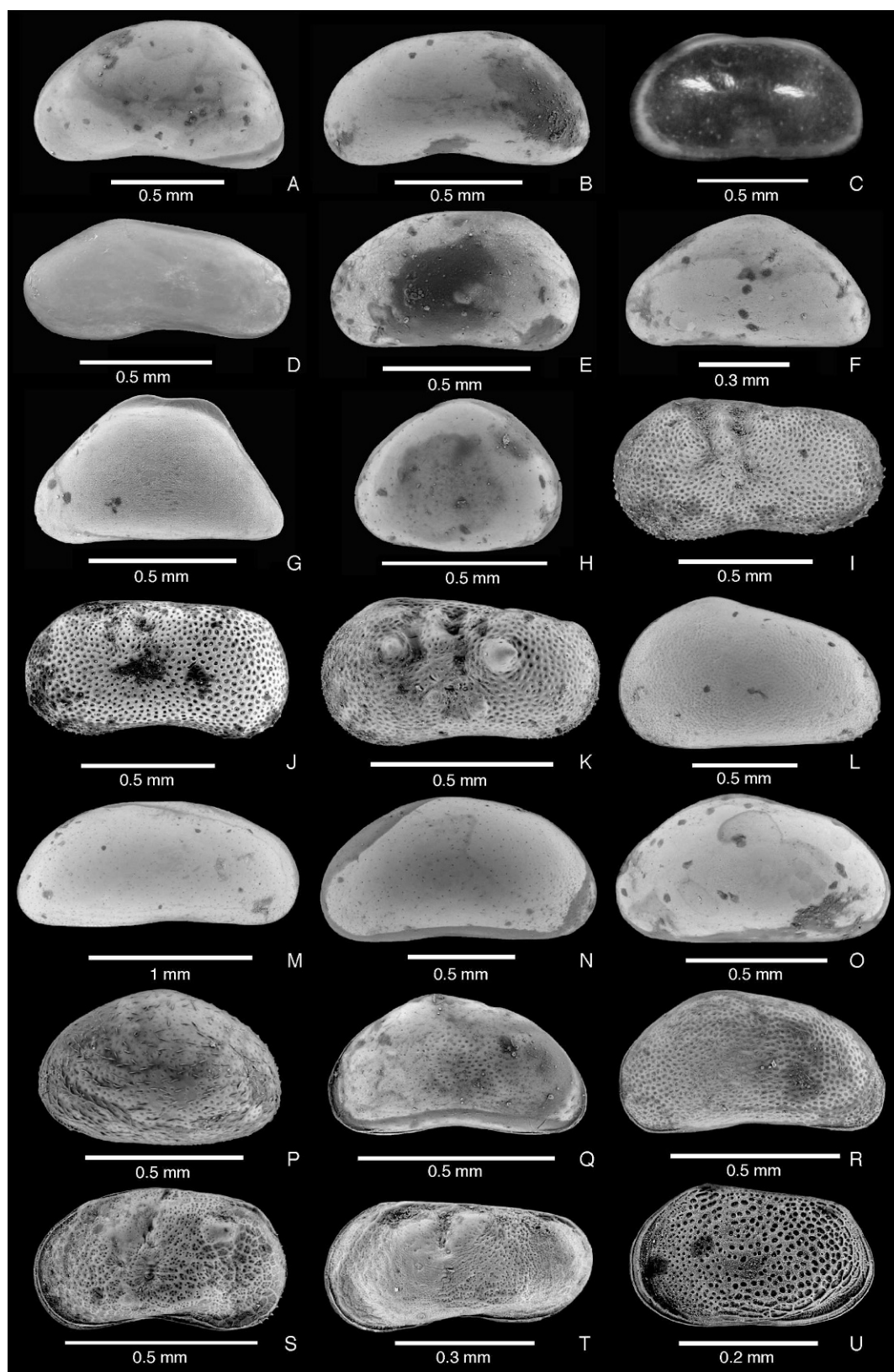
Figure 8. External lateral views of ostracod valves from the Sentino River, sulfidic spring, and cave complex at Frasassi. All are SEM images except C, which is a photomicrograph. LV = left valve; RV = right valve. (A) *Candona candida* **(Müller, 1776), LV. (B)** *Candona neglecta* **Sars, 1887, LV. (C)** *Candona* **ex gr.** *C. neglecta***, LV. (D)** *Fabaeformiscandona* **ex gr.** *F.*

sediment sample that yielded the same number of *Mixtacandona* sp.

The distribution of *Pseudolimnocythere* sp. is intriguing, because this species is represented in our collection by 1160 carapaces and valves but no live specimens. Only nine disarticulated valves were found at the sulfidic spring site, where 3954 valves belonging to other species were recovered. Just three valves were found in nonsulfidic riverbank sediments, where 398 valves of other species were counted. Few separate valves were recovered from samples collected at the hypogean sites of Lago Stratificato, Lago Traverso, and Lago Claudia. Yet 176 valves (articulated carapaces counted as two valves) of *Pseudolimnocythere* sp. were counted in samples from Lago Blanco, 505 valves at Lago Infinito, and an abnormally large total number of 448 valves were recovered from eight small samples of subfossil eel remains collected at 50, 70, 150, 200, 215, 300, 375, and 395 cm above the present water table at Lago delle Anguille. Considering that a total of only five valves of *Fabaeformiscandona* ex gr. *F. fabaeformis* and fifteen valves of *Mixtacandona* sp. were recovered from the subfossil eel samples, it appears that *Pseudolimnocythere* sp., though probably extinct by now, had been the dominant ostracod species of the Frasassi cave system in the recent past.

In the studied material, *Pseudolimnocythere* sp. was represented predominantly by separate adult valves, which may indicate some evidence of taphonomic postmortem disturbance or biological activity (Boomer et al., 2003). However, in samples large enough to provide a significant number of specimens (ca. >150), separate valves were accompanied by closed carapaces with the mean valve:carapace ratio $\pm$SD = 21.8 $\pm$ 9.7 (based on four abundant samples from Lago Blanco, Lago Infinito, and Lago delle Anguille). At Lago delle Anguille, *Pseudolimnocythere* sp. was found in seventeen samples with varied abundances, six of which had only separate valves. The other eleven samples had valve:carapace ratios that ranged from 1:1 to 75:1 with the mean value $\pm$SD = 12.2 $\pm$ 21.7. This predominance of valves, however, may be biased, because carapaces of this very small species (adult length < 0.35 mm), especially juveniles, are more prone than those of larger species to disarticulation resulting from chemical and biological decomposition of soft parts, as well as physical separation during sample collection and processing. Nevertheless, we believe that our record represents an autochthonous assemblage preserved in situ (i.e., thanatocoenosis *sensu* Boomer et al., 2003), and as such, it is a good indicator of an accumulation representing an in situ life environment.

Discussion

Habitats

From this reconnaissance study, our first impression is that the main selective factor for the Frasassi ostracod assemblages is the hydrogen sulfide contained in the waters of the sulfidic spring and the hypogean lakes that requires special adaption to both the toxicity of H_2S and the hypoxia in these environments. Sulfur bacteria, which thrive in these sulfidic waters, provide a limitless and constant food source for those ostracods that can adapt to the conditions and diet. In contrast, in non-sulfidic, epigean waters, the food source normally consists of algae and other vegetal or animal matter. In terms of environmental or ecologic characteristics, the main difference between the sulfidic spring and the cave sites is that the latter are aphotic. In addition, the environmental conditions in the phreatic pools of the cave are much more stable than those of the sulfidic spring pond, which gets obliterated several times a year by floodwaters of the Sentino River.

It is remarkable that *Mixtacandona* sp. and *Candona* ex gr. *C. neglecta* seem to be the only ostracods living permanently, at least since the early Holocene, in the phreatic waters of the cave system. Our *Mixtacandona* sp. displays morphological traits typical for a stygobite dweller with a long evolutionary history of isolation underground, being diaphanous, depigmented, transparent, small-sized, and anophtalmic.

Hypogean Colonization

Some questions remain about how and when ostracods colonized the groundwater habitats of the Frasassi Cave system. They either entered gradually by actively passing through interstices and fractures of the limestone bedrock below the water table or they were introduced passively *en mass* via episodic flooding of the cave when the Sentino River flowed at the same elevation as large natural entrances. However, the ostracod richness and endemicity in the Frasassi area is probably due to both species-habitat specialization and

←

fabaeformis (Fischer, 1851), RV. (E) *Pseudocandona albicans* (Brady, 1864), LV. (F) *Pseudocandona* ex gr. *P. eremita* (Vejdowský, 1882), LV. (G) *Mixtacandona* sp., LV. (H) *Cypria ophtalmica* (Jurine, 1820), LV. (I) *Ilyocypris bradyi* Sars, 1890, LV. (J) *Ilyocypris* cf. *I. inermis* Kaufmann, 1900, LV. (K) *Ilyocypris monstrifica* (Norman, 1862), LV. (L) *Prionocypris zenkeri* (Chyzer & Toth, 1858), LV. (M) *Herpetocypris chevreuxi* (Sars, 1896), RV. (N) *Psychrodromus olivaceus* (Brady & Norman, 1889), LV. (O) *Heterocypris reptans* (Kaufmann, 1900), LV. (P) *Cypridopsis vidua* (Müller, 1776), LV. (Q) *Potamocypris fulva* (Brady, 1868), LV. (R) *Potamocypris zschokkei* (Kaufmann, 1900), LV. (S) *Limnocythere inopinata* (Baird, 1843), LV. (T) *Paralimnocythere* sp., LV. (U) *Pseudolimnocythere* sp., RV.

the general factors that act in any subterranean ecosystem, like the age of the system, karst isolation, and the underground colonization history at the regional level.

At present, a number of cave systems' entrances are located on the Mt. Valmontagnana (southern) side of the Frasassi Gorge at elevations between 350 and 500 m above msl (e.g., Buco Cattivo, Grotta del Paradiso, Grotta dell'Infinito, Buco del Diavolo, Grotta dell'Inferno; see Cattuto, 1976). Although karstic morphology and rare residual gypsum deposits in these caves indicate that sulfidic activity was present in the phreatic environment when the Sentino River was flowing at these elevations, the lack of geochronological data prevent an accurate assessment of the age of formation of these upper and older karstic levels. Moreover, no evidence of fossil stygobitic animals has yet been found in the sediments of these caves. Cyr and Granger (2008) obtained an Al/Be cosmogenic age of 760 ± 250 ka from a fluvial deposit preserved in the Grotta della Beata Vergine, on the Mt. Frasassi (northern) side of the gorge at an elevation of 325 m. This suggests that a sulfidic hypogean environment capable of supporting a complex chemoautotrophic ecosystem was present in this area in the late-early Pleistocene and that the Sentino River could have transported epigean organisms in the cave system via episodic floods.

The only natural cave entrance known on the slopes of the Frasassi Gorge at an elevation lower than 325 m, besides the Grotta del Fiume, is that of the Caverna del Carbone, a small cave located near the tourist entrance of the Grotta Grande del Vento, at 236 m (i.e., ~31 m above present river level). The floor of the Caverna del Carbone is alluvium, mostly clay, some sand, and pebbles. An impenetrable clay deposit presently obstructs the inner tunnel of the cave that leads southward toward the Grotta Grande del Vento. Coincidently, a well-sorted, fine-sand fluvial deposit preliminarily dated with the optical-stimulated-luminescence method on quartz at 111 ± 17 ka (Markus Fiebic, pers. comm. on work in progress) is located in the northernmost end of Sala 200 (see Fig. 4A for location) in the Grotta Grande del Vento, at an elevation of 234 m, corresponding to the third level of the cave system. In both these fluvial deposits, we found well-preserved ostracod valves representing essentially the same species that we collected from the Sentino River site. Besides *Candona candida*, *C. neglecta*, *C.* ex gr. *C. neglecta*, *Ilyocypris bradyi*, *I. gibba*, *Potamocypris* sp., and juvenile cyprid valves that most probably represent species found today in the Sentino River, such as *Heterocypris* cf. *H. reptans* or *Psychrodromus olivaceus*), as well as rare valves of *Mixtacandona* sp., these paleoassemblages include two other species, *Cyclocypris* cf. *C. ovum* (Jurine) and *Potamocypris fallax* Fox, that were not recorded in the Sentino River, sulfidic spring, or Frasassi Cave system. These observations allow no doubt that the Sentino River was flooding the cave during the Riss-Würm interglacial period, importing organisms from outside the cave into the cave's phreatic environment.

At present, the Sentino River flows approximately 3 m below the natural entrance of the Grotta del Fiume. The study by Mariani et al. (2007) on the subfossil eels demonstrates that there have been, as far back as 7200 years ago, open passages below the water table through which these fish were able to enter the hypogean environment and swim to the deepest and farthest reaches of the cave system. It is reasonable to think that other outsiders were able to enter the cave along with the eels, and some of them were able to adapt to its environment. We found valves of three ostracod species mixed with the subfossil remains of these eels: *Mixtacandona* sp., *Fabaeformiscandona* ex gr. *F. fabaeformis*, and unusually abundant *Pseudolimnocythere* sp. Of these, only *Mixtacandona* sp. presently lives exclusively in the same cave environments. In recent years, eels have been observed swimming in a small pool in the Grotta Solfurea about 80 m from the Sentino River (Fig. 4A; pers. comm. by Piero Mirabella and Sandro Galdenzi and sighting by Alessandro Montanari in 1973). If anything, this indicates that there must be at least one direct connection between the Sentino River and the cave system. Alternatively, it may be that exceptionally heavy flooding of the Sentino River, like the one in the winter of 2010, would have swollen the river level high enough to reach the Grotta del Fiume entrance, allowing the river water to rush into the cave transporting sediment and live aquatic animals, including fish and ostracods. Further research on the cave sediments will hopefully provide greater insight on the history of ostracod colonization of this extraordinary cave system.

Ecology and Trophic Adaptation

The recovery of only one live specimen, a juvenile, of *Candona* ex gr. *C. neglecta* at Lago Claudia and only one live *Pseudocandona albicans* at Lago Verde prevents us from making any assessment on the ecology and trophic adaptations of these ostracods living today in the phreatic environment of the Frasassi cave system. On the other hand, something can be said in regard to *Mixtacandona* sp., which thrives in the phreatic waters of Lago della Bottiglia and Lago Claudia. The accessibility and morphology of the Lago della Bottiglia (Fig. 5A) makes possible a rough estimate of how many specimens live in a square meter of the lake's bank at any time. This small yet deep lake has a stratified water column, with a layer of well-oxygenated bicarbonate water at the surface and a layer of sulfidic water down to a depth of 3 to 4 m. During an expedition to this site in September 2009, live specimens of *Mixtacandona* sp. were captured by gently brushing the 20 cm diameter rigid rim of a conical plankton net against the steep, rocky banks of the lake with slow, repeated movements from about 50 cm depth upward to the surface. During thirty such strokes, about 2 m³ of water passed through the net over about 0.5 m² of the lake's rocky bank, with a total catch of about 25 cm³ of fine sediment containing twenty-five shells of the hygrobiid gastropod

Islamia sp. 2, several *Niphargus ictus,* a few nematodes, a few dozen copepods, about fifty disarticulated ostracod valves, and eleven live individuals of *Mixtacandona* sp. No other ostracod species were recognized in the catch. Sampling was repeated at different times in the following year at this site using the same procedure (thirty strokes over the same bank surface), and a catch of ten to fifteen live specimens was consistently obtained, leading to the conclusion that, at this site, twenty to thirty specimens were living on a square meter of rocky bank. As mentioned above, the sparse sediment attached to the rocky bank is mostly made of *Islamia* sp. 2 fecal pellets. Direct observation of this gastropod in mesocosms over a period of three years (see review by Montanari, 2010), revealed that it feeds on bacteria by pasturing on the glass wall of the tank along the boundary between the deep sulfidic water layer and the overlying bicarbonate water layer, where the highest concentration of benthic microorganism such as bacteria, protozoans, nematodes, platyhelminthes, and rotifers were found. But for most of the time, the gastropods crawl on the glass walls of the mesocosms well above the chemocline, in oxygenated, bicarbonate waters, and never descend into the euxinic bottom-water layer. These observations led us to hypothesize that ostracods and other stygobitic meiofauna such as copepods find gastropod fecal pellets to be an important trophic resource in Lago della Bottiglia.

The trophic situation at Lago Claudia is different than that deduced at Lago della Bottiglia. At Lago Claudia, the sulfidic bottom-water layer often reaches the lake's surface, with H$_2$S escaping into the cave's atmosphere. The northern bank of this deep pool is the base of a gentle limestone talus slope (Figs. 6C, D) that is often reached by the chemocline, particularly during the dry season in summer and early autumn. In these times, the bottom of the shallow bank is sulfidic and reduced, and it is capped by a layer of bicarbonate water just a few centimeters thick. Live specimens of *Mixtacandona* sp. were recovered from this site in July 2008 (sample LCL/08.07/04) and observed in a Petri dish, where they were distinctly seen grazing on threads and feathers of sulfur-oxidizing bacteria on rocks and clay in the substrate sample.

An additional distinct trophic adaptation is suggested by the presence of *Mixtacandona* sp., *Fabaeformiscandona* ex gr. *F. fabaeformis*, and abundant *Pseudolimnocythere* sp. on the remains of subfossil eels at Lago delle Anguille (Table 1), along with numerous shells of the gastropod *Islamia* sp. 2. Our samples of these remains were small scrapings from which it was impossible to determine if the microgastropods and ostracods had been ingested by the eels or if they had been feeding on the remains. However, a complete specimen collected later clearly shows them scattered on the outer surface of the skin, suggesting that they were necrophagous. We believe the presence of these organisms on the eel carcasses is somewhat analogous to the extreme, ephemeral deep-sea ecosystem that develops on a fallen whale (Dominici

et al., 2009, and references therein). These carcasses, such as the Pliocene whale studied by Dominici et al. (2009) in Tuscany, serve as a long-lasting food source for a well-diversified invertebrate fauna dominated by gastropods, bivalves, decapods, and worms in an otherwise extreme, oligotrophic, and mainly chemosymbiotic environment.

All considered, we conclude that *Mixtacandona* sp., as well as other endemic ostracod species found in the phreatic waters of the Frasassi cave system, are benthonic stygobitic grazers dwelling in oxygenated waters not far from a sulfidic chemocline, which constantly provides them with a limitless food supply of sulfur bacteria. The ostracods are opportunistic feeders that adapt to local trophic provisions, such as abundant fecal pellets of gastropods and occasional fallen eels.

Conclusions

The 6850 specimens of twenty-one species of ostracods recovered over five years of sampling at the Frasassi cave system and the adjacent sulfidic spring and Sentino River constitute the largest and most diversified collection to date of these microcrustaceans from a continental sulfidic cave and karst aquifer. The dominant species differ between the assemblages inside and outside the cave. The cave fauna includes three apparently new stygobitic species. Import by river floods and gradual migration, trophic opportunism, and environmental heterogeneity have contributed to and maintained the species diversity at a relatively higher level than is typical for freshwater environments. Future studies of this sort should enable us to better understand the ecology and evolution of hypogeal ostracods, and, in turn, the ostracods may find utility in deciphering the evolution and environmental health of individual cave systems.

Acknowledgements

References

Alvarez, W., 1999, Drainage on evolving fold-thrust belts: a study of transverse canyons in the Apennines: Basin Research, v. 11, p. 267–284. doi: 10.1046/j.1365-2117.1999.00100.x.

Ambrosetti, P., Basilici, G., Capasso Barbato, L., Carboni, M.G., Di Stefano, G., Esu, D., Gliozzi, E., Petronio, C., Sardella, R., and Squazzini, E., 1995, Il Pleistocene inferiore nel ramo Sud-Occidentale del Bacino Tiberino (Umbria): aspetti litostratigrafici e biostratigrafici: Il Quaternario, v. 8, p. 19–36.

Barberi, R., Cavinato, G.P., Gliozzi, E., and Mazzini, I., 1995, Late Pliocene–Early Pleistocene paleoenvironmental evolution of the Rieti basin (central Apennines): Il Quaternario, v. 8, p. 515–534.

Bauermeister, J., 2009, Ecology and diversity of an amphipod–bacterial ectosymbiosis from the Frasassi cave complex in central Italy: Abstracts with Program, The Frasassi Stygobionts and Their Sulfidic Environment, Genga, September 10–13, 2009, 7 p.

Bocchini, A., and Coltorti, M., 1990, Il complesso carsico Grotta del Fiume-Grotta Grande del Vento e l'evoluzione geomorfologica della Gola di Frasassi: Memorie dell'Istituto Italiano di Speleologia, ser. 2, v. 4, p. 155–180.

Bodon, M., Cianfanelli, S., and Montanari, A., 2009, Mollusks of the Frasassi karstic complex and adjacent sulfidic spring: Abstracts with Program, The Frasassi Stygobionts and Their Sulfidic Environment, Genga, September 10–13, 2009, p. 9–11.

Boomer, I., Horne, D.J., and Slipper, I.J., 2003, The use of ostracods in palaeoenvironmental studies, or what can you do with an ostracod shell?, in Park, L.E., and Smith, A.J., eds., Bridging the Gap: Trends in the Ostracode Biological and Geological Sciences, Ithaca, New York, Paleontological Society Papers no. 9, p. 153–179.

Bottazzi, E., Bruno, M.C., Mazzini, M., Pieri, V., and Rossetti, G., 2008, First report on Copepoda and Ostracoda (Crustacea) from northern Apenninic springs (n. Italy): a faunal and biogeographical account: Journal of Limnology, v. 67, p. 56–63. doi:10.4081/jlimnol.2008.56.

Buonanno, F., Chandramohan, B., Di Pretoro, B., La Terza, A., Ortenzi, C., and Kumar, S., 2009, The protozoan ciliates of the Frasassi caves: a potential source of bioactive molecules for biotechnological applications: Abstracts with Program, The Frasassi Stygobionts and Their Sulfidic Environment, Genga, September 10–13, 2009, 19 p.

Calderini, G., Calderoni, G., Cavinato, G.P., Gliozzi, E., and Paccara, P., 1998, The upper Quaternary sedimentary sequence at the Rieti basin (central Italy): a record of sedimentary response to environmental changes: Palaeogeography, Palaeoclimatology, Palaeoecology, v. 140, p. 97–111. doi:10.1016/S0031-0182(98)00024-8.

Cattuto, C., 1976, Correlazione tra piani carsici ipogei e terrazzi fluviali nella valle del Fiume Esino (Marche): Bollettino della Società Geologica Italiana, v. 95, p. 313–326.

Culver, D.C., and Sket, B., 2000, Hotspots of subterranean biodiversity in caves and wells: Journal of Cave and Karst Studies, v. 62, p. 11–17.

Cyr, A.J., and Granger, D.E., 2008, Dynamic equilibrium among erosion, river incision, and coastal uplift in the northern and central Apennines, Italy: Geology, v. 36, p. 103–106. doi:10.1130/G24003A.1.

Dattagupta, S., 2009, The Niphargus symbiosis from the Frasassi Cave ecosystem: a case of multiple partners?: Abstracts with Program, The Frasassi Stygobionts and Their Sulfidic Environment, Genga, September 10–13, 2009, 21 p.

Deming, J.W., and Baross, J.A., 1993, Deep-sea smokers: windows to a subsurface biosphere?: Geochimica et Cosmochimica Acta, v. 57, p. 3219–3230. doi:10.1016/0016-7037(93)90535-5.

Dominici, S., Cioppi, E., Danise, S., Betocchi, U., Gallai, G., Tangocci, F., Valleri, G., and Monechi, S., 2009, Mediterranean fossil whale falls and the adaptation of mollusks to extreme habitats: Geology, v. 37, p. 815–818. doi:10.1130/G30073A.1.

Druschel, G.K., Eastman, D., and Macalady, J., 2009, Biological controls on detailed sulfur cycling and the formation of the Frasassi caves: Abstracts with Program, The Frasassi Stygobionts and Their Sulfidic Environment, Genga, September 10–13, 2009, p. 23–24.

Engel, A., 2007, Observations on the biodiversity of sulfidic karst habitats: Journal of Cave and Karst Studies, v. 69, p. 187–206.

Erséus, C., 2009, A possibly opportunistic clitellate annelid belonging to the genus Potamothrix (family Naididae) in the microbial ecosystems of the Frasassi caves (Italy): Abstracts with Program, The Frasassi Stygobionts and Their Sulfidic Environment, Genga, September 10–13, 2009, p. 27–28.

Galdenzi, S., and Maruoka, T., 2003, Gypsum deposits in the Frasassi caves, central Italy: Journal of Cave and Karst Studies, v. 65, p. 111–125.

Galdenzi, S., and Menichetti, M., 1995, Occurrence of hypogenic caves in a karst region: examples from central Italy: Environmental Geology, v. 26, p. 39–47. doi:10.1007/BF00776030.

Galdenzi, S., Menichetti, M., Sarbu, S.M., and Rossi, A., 1999, Frasassi caves: a biogenic hypogean karst system?, in Audora, P., ed., Proceedings of the European Conference Karst 99, Université de Provence, Études de Géographie Physique, no. 28, p. 101–106.

Galdenzi, S., Cocchioni, M., Morichetti, L., Amici, V., and Scuri, S., 2008, Sulfidic ground-water chemistry in the Frasassi caves, Italy: Journal of Cave and Karst Studies, v. 70, p. 94–107.

Gliozzi, E., 2000, Tardiglacial–Holocene freshwater ostracod assemblages from Ripasottile wells (Rieti basin, Latium, central Italy): Giornale di Geologia, v. 3, p. 159–172.

Gliozzi, E., and Mazzini, I., 1998a, Mixtacandona talianae n. sp. (Crustacea, Ostracoda) from the Holocene of Grotta del Lago (Ubria, central Italy): Micropaleontology, v. 44, p. 441–446.

Gliozzi, E., and Mazzini, I., 1998b, Palaeoenvironmental analysis of the 250.000-year Quaternary sediment core of Valle di Castiglione (Latium, Italy) using ostracods, in Crasquin Soleau, S., Braccini, E., and Lethiers, F., eds., What about Ostracoda!, Actes du 3e Congrès Européen des Ostracodologistes, 1966, Pau, France, Bulletin du Centres des Recherches ELF Exploration et Production Memoir, v. 20, p. 69–82.

Iepure, S., Namiotko, T., and Danielpol, D.L., 2007, Evolutionary and taxonomic aspects within the species group Pseudocandona eremita (Vejdovský) (Ostracoda, Candonidae): Hydrobiologia, v. 585, p. 159–180. doi:10.1007/s10750-007-0636-3.

Iliffe, T.M., 2004, Walsingham Caves, Bermuda: biospeleology, in Gunn, J., ed., Encyclopedia of Caves and Karst Science, New York, Fitzroy Dearborn, p. 767–769.

Jannasch, H.W., 1985, The chemosynthetic support of life and the microbial diversity at deep-sea hydrothermal vents: Proceedings of the Royal Society of London, Ser. B, Biological Sciences, v. 225, p. 277–297. doi:10.1098/rspb.1985.0062.

Jones, D.S., Albrecht, H.L., Dawson, K.S., Shaperdoth, I., Freeman, K.H., Pi, Yundan, Pearson, A., and Macalady, J.L., 2012, Community genomic analysis of an extremely acidophilic sulfur-oxidizing biofilm: The ISME Journal, v. 6, p. 158–170. doi:10.1038/ismej.2011.75.

Karaman, G.S., Borowsky, B., and Dattagupta, S., 2010, Two new species of the genus *Niphargus* Schiödte, 1849 (Amphipoda, fam. Niphargidae) from the Frasassi cave system in central Italy: Zootaxa, no. 2439, p. 35–52.

Karanovic, I., and Pesce, G.L., 2000, *Trapezicandona italica* n. sp. from the underground waters of southern Italy (Crustacea, Ostracoda): Fragmenta Entomologica, Roma, v. 32, p. 213–224.

Karanovic, I., and Pesce, G.L., 2001, Ostracodes (Crustacea, Ostracoda) from underground waters of Puglia (southern Italy), with a redescription of *Pseudolimnocythere hypogea* Klie, 1938: Thalassia Salentina, v. 25, p. 11–39. doi:10.1285/i15910725v25p11.

Klie, W., 1938, Ostracoden aus unterirdischen Gewässern in Süditalien: Zoologischer Anzeiger, v. 123, p. 148–155.

Latella, L., Di Russo, C., De Pasquale, L., Dell'Anna, L., and Rampini, M., 1999, Ecological study in a new sulfurous cave from central Italy, *in* Holcer, D., and Šašic, M., eds., Abstracts of the 14th International Symposium of Biospeleology, Makarska, Croatia 19th–26th September 1999, Croatian Biospeleological Society, 54 p.

Longley, G., 1981, The Edwards Aquifer: Earth's most diverse groundwater ecosystem? International Journal of Speleology, v. 11, p. 123–128.

Longley, G., 1986, The biota of the Edwards Aquifer and the implications for paleozoogeography: *in* Abbot, P.L., and WoodruffC.M. Jr., eds., The Balcones Escarpment: Geology, Hydrology, Ecology and Social Development in Central Texas, San Antonio, Texas, Geological Society of America, p. 51–54.

Macalady, J.L., Lyon, E.H., Koffman, B., Albertson, L.K., Meyer, K., Galdenzi, S., and Mariani, S., 2006, Dominant microbial populations in limestone-corroding stream biofilms, Frasassi Cave system, Italy: Applied and Environmental Microbiology, v. 72, p. 5596–5609. doi:10.1128/AEM.00715-06.

Macalady, J.L., Jones, D.S., and Lyon, E.H., 2007, Extremely acidic, pendulous cave wall biofilms from the Frasassi Cave system, Italy. Environmental Microbiology, v. 9, p. 1402–1414. doi:10.1111/j.1462-2920.2007.01256.x.

Macalady, J.L., Dattagupta, S., Schaperdoth, I., Jones, D.S., Druschel, G.K., and Eastman, D., 2008a, Niche differentiation among sulfur-oxidizing bacterial populations in cave waters: The ISME Journal, v. 2, p. 590–601. doi:10.1038/ismej.2008.25.

Macalady, J.L., Jones, D.S., Schaperdoth, I., Bloom, D., and McCauley, R., 2008b, Meter-long microbial ropes from euxinic cave lakes: American Geophysical Union Fall Meeting 2008, abstract B53C-0514.

Mariani, S., Mainiero, M., Barchi, M., van der Borg, K., van der, Vonhof, H., and Montanari, A., 2007, Use of speleologic data to evaluate Holocene uplifting and tilting: an example from the Frasassi anticline (northeastern Apennines, Italy): Earth and Planetary Science Letters, v. 257, p. 313–328. doi:10.1016/j.epsl.2007.02.045.

Martinis, B., and Pieri, M., 1964, Alcune notizie sulla formazione evaporitica del Triassico superiore nell'Italia centrale e meridionale: Memorie della Società Geologica Italiana, v. 4, p. 649–678.

Mayer, L., Menichetti, M., Nesci, O., and Savelli, D., 2003, Morphotectonic approach to the drainage analysis in the north Marche region, central Italy: Quaternary International, v. 101–102, p. 157–167. doi:10.1016/S1040-6182(02)00098-8.

Mazzanti, R., and Trevisan, L., 1978, Evoluzione della rete idrografica nell'Appennino centro-settentrionale: Geografia Fisica e Dinamica Quaternaria, v. 1, p. 55–62.

Meisch, C., 2000, Freshwater Ostracoda of western and central Europe, Heidelberg, Spektrum Akademischer Verlag, Süßwasserfauna von Mitteleuropa, v. 8/3, 522 p.

Montanari, A., 2010, ed., Stigobionti: vita acquatica nelle grotte di Frasassi, Jesi, Italy, Federazione Speleologica Marchigiana, 120 p.

Namiotko, T., and Danielopol, D.L., 2004, Review of the *eremita* species-group of the genus *Pseudocandona* Kaufmann (Ostracoda, Crustacea), with the description of a new species: Revista Española de Micropaleontologia, v. 36, p. 117–134.

Pesce, G.L., and Pagliani, T., 1999, Gli ambientali anchialini della Puglia e la loro fauna, *in* Belmonti, G., Ciccarese, G., and Ruggiero, L., eds., Il Carsismo nell-Area Mediterranea, Thalassia Salentina, Supplement to no. 23, p. 89–102.

Pieri, V., Martens, K., Naselli-Flores, L., Marrone, F., and Rossetti, G., 2006, Distribution of Recent ostracods in inland waters of Sicily (southern Italy). Journal of Limnology, v. 65, p. 1–8. doi:10.4081/jlimnol.2006.1.

Pieri, V., Caserini, C., Gomarasca, S., Martens, K., and Rossetti, G., 2007, Water quality and diversity of the Recent ostracod fauna in lowland springs from Lombardy (northern Italy): Hydrobiologia, v. 585, p. 79–87. doi:10.1007/s10750-007-0630-9.

Pieri, V., Martens, K., Stoch, F., and Rossetti, G., 2009, Distribution and ecology of non-marine ostracods (Crustacea, Ostracoda) from Friuli Venezia Giulia (NE Italy): Journal of Limnology, v. 68, p. 1–15. doi:10.4081/jlimnol.2009.1.

Por, F.D., 1963, The relict aquatic fauna of the Jordan Rift Valley: new contributions and review: Israel Journal of Zoology, v. 12, p. 47–58.

Por, F.D., 2007, Ophel: a groundwater biome based on chemoautotrophic resources: The global significance of the Ayalon Cave finds, Israel: Hydrobiologia, v. 592, p. 1–10. doi:10.1007/s10750-007-0795-2.

Por, F.D., 2011, Groundwater life: some new biospeological views resultly from the Ophel paradigm. Travaux Institut de Speologie Emile Racovitza, v. 50, p. 61–76.

Porter, M.L., Russell, S., Engel, A.S., and Stern, L., 2002, Population studies of the endemic snail *Physa spelunca* (Gastropoda: Physidae) from Lower Kane Cave, Wyoming (abstract): Journal of Cave and Karst Studies, v. 64, 181 p.

Rossi, V., Benassi, G., Veneri, M., Bellavere, C., Menozzi, P., Moroni, A., and McKenzie, K.G., 2003, Ostracoda of the Italian ricefields thirty years on: new synthesis and hypothesis: Journal of Limnology, v. 62, p. 1–8. doi:10.4081/jlimnol.2003.1.

Rossi, V., Gandolfi, A., Gentile, G., Geiger, W., and Menozzi, P., 2004, Low genetic variability in the ancient asexual ostracod *Darwinula stevensoni*: Italian Journal of Zoology, v. 71, p. 135–142. doi:10.1080/11250000409356564.

Rossi, V., Pioti, A., Geiger, W., Benassi, G., and Menozzi, P., 2010, Genetic structure of Austrian and Italian populations of *Limnocythere inopinata* (Crustacea, Ostracoda): a potential case of post-glacial parthenogenetic invader?: Annales Zoologici Fennici, v. 47, p. 133–143.

Rossetti, G., Bartoli, M., and Martens, K., 2004, Limnological charateristics and recent ostracods (Crustacea, Ostracoda) of freshwater wetlands in the Parco Oglio Sud (northern Italy): Annales de Limnologie, v. 40, p. 329–341. doi:10.1051/limn/2004030.

Rossetti, G., Pieri, V., and Martens, K., 2005, Recent ostracods (Crustacea, Ostracoda) found in lowland springs of the Provinces of Piacenza and Parma (northern Italy): Hydrobiologia, v. 542, p. 287–296. doi:10.1007/s10750-004-2566-7.

Rossetti, G., Martens, K., Meisch, C., Tavernelli, S., and Pieri, V., 2006, Small is beautiful: diversity of freshwater ostracods (Crustacea, Ostracoda) in marginal habitats of the Province of Parma (northern Italy). Journal of Limnology, v. 65, p. 121–131. doi:10.4081/jlimnol.2006.121.

Sarbu, S.M., 1990, The unusual fauna of a cave with thermomineral waters containing H_2S from southern Dobrogea, Romania: Mémoires de Biospéologie, v. 17, p. 191–195.

Sarbu, S.M., Galdenzi, S., Menichetti, M., and Gentile, G., 2000, Geology and biology of the Frasassi caves in central Italy: An ecological multi-disciplinary study of a hypogenic underground karst system, *in* Wilkens, H., Culver, D.C., and Hamphreys, W.F., eds., Subterranean Ecosystems, New York, Elsevier, Ecosystems of the World no. 30, p. 359–378.

Sarbu, S.M., Kane, T.C., and Kinkle, B.K., 1996, A chemoautotrophically based groundwater ecosystem: Science, v. 272, p. 1953–1955. doi:10.1126/science.272.5270.1953.

Stoch, F., Pieri, V., Sambugar, B., and Zullini, A., 2009, La fauna delle acque sotterranee dell'alta Val Secchia (Appennino Reggiano): Memorie dell'Istituto Italiano di Speleologia, s. 2, v. 22, p. 145–163.

Wegman, K.W., and Pazzaglia, F.J., 2008, Late Quaternary fluvial terraces of the Romagna and Marche Apennines, Italy: climatic, lithologic, and tectonic controls on terrace genesis in an active orogen: Quaternary Science Reviews, v. 28, p. 137–165. doi:110.1016/j.quascirev.2008.1010.1006.

ELECTRICAL TOMOGRAPHY APPLIED TO THE DETECTION OF SUBSURFACE CAVITIES

J. Martínez-López[1], J. Rey[2*], J. Dueñas[3], C. Hidalgo[2], and J. Benavente[4]

Abstract: We have analyzed the geoelectric response produced by three cavities cut into different geological substrata of granite, phyllite, and sandstone that had previously been characterized by direct methods. We also examined a mining void excavated in granite. In each case, we applied three different geoelectric arrays (Wenner-Schlumberger, Wenner and dipole-dipole) and several inter-electrode spacings. The survey results suggest that electrical resistivity tomography is a viable geophysical tool for the detection and monitoring of mining voids and other subsurface cavities. The results vary depending on a wide range of factors, such as the depth and diameter of the cavity, the multi-electrode array used, the inter-electrode spacing, the geological model, and the density of the data. The resolution capacity of the Wenner- Schlumberger array for the detection of these cavities was greater than that of the Wenner array and slightly better than the dipole-dipole. There is a direct relationship between inter-electrode spacing and diameter of the cavity. In general, we observed a loss of resolution as the distance between the electrodes increased. The most efficient detection was achieved when the inter-electrodes distance was less than or equal to the diameter of the cavity itself. In addition, cavity detection became increasingly less precise with its depth beneath the surface. Cavities with a radius of about 1.5 m were located by both the Wenner-Schlumberger method and the dipole-dipole at depths of more than 4.6 m, which means that prospecting can be carried out at depths 3 times the radius of the cavity.

INTRODUCTION

The detection of underground cavities, whether of natural origin such as karstic cavities or of anthropogenic origin such as mining galleries, is of vital importance in land-use planning. In construction projects, and in particular in civil engineering, it is necessary to identify any deep-lying cavities beneath the construction site, as these could cause undesired effects at the surface such as subsidence or complete collapse (De Bruyn and Bell, 2001; Waltham et al., 2005). The use of a suitable geophysical prospecting procedure for the identification and characterization of these underground anomalies renders it unnecessary to use destructive methods, such as drilling boreholes, that are much more expensive and environmentally damaging.

In general, geophysical prospecting involves a number of different techniques that help identify anomalies in the physical and chemical properties of the subsoil, including the propagation of electromagnetic, gravity, acoustic, electrical, or magnetic signals. One of these techniques, electrical resistivity tomography, involves determination of the subsurface distribution of electrical resistivity. This is done by taking a very large number of readings either from the surface or from perforations (Telford et al., 1990; Store et al., 2000). The varying geoelectric response in the area under investigation enables users to obtain 2D profiles and 3D images of the distribution of the resistivities under the ground, which makes it a very effective, non-destructive tool for analyzing and characterizing possible discontinu-

ities in the subsoil (Sasaki, 1992; Store et al., 2000). The depth range may vary from just a few meters to hundreds of meters in depth. This technique has numerous possible applications when one is faced with various problems in different geological settings (Caputo et al., 2003; Colella et al., 2004). It is increasingly used in environmental studies, hydrogeology (Maillet et al. 2005; Šumanovac, 2006; Martínez et al., 2009), and geotechnics (Naudet et al., 2008), among other fields. This technique has also been used for detection of natural crevice-type caves (van Schoor, 2002; Gutiérrez et al., 2009; Pánek et al., 2010; Gambetta et al., 2011) and in some cases, to locate man-made mining cavities (Maillol et al., 1999; Martínez-López et al., 2007).

The aim of this work was to analyze the resolution of images under different geological conditions and assess the potential for using this technique for locating cavities. Our general objective was to develop a suitable method for the optimum interpretation of resistivity images obtained by electrical tomography so as to be able to characterize cavities in the subsoil. We therefore (i) analyzed the criteria for selecting the best inter-electrode spacings and the most

* Corresponding author: jrey@ujaen.es
[1] Dpto. Ingeniería Mecánica y Minera, Escuela Politécnica Superior de Linares, Universidad de Jaén, 23700 Linares (Jaén), Spain
[2] Dpto. de Geología, Escuela Politécnica Superior de Linares, Universidad de Jaén, 23700 Linares (Jaén), Spain
[3] Dpto. Ingeniería Gráfica, Diseño y Proyectos, Escuela Politécnica Superior de Linares, Universidad de Jaén, 23700 Linares (Jaén), Spain
[4] Instituto del Agua, Universidad de Granada, C/Ramón y Cajal 4, 18071 Granada, Spain

suitable multi-electrode array for the characterization of each specific type of cavity, (ii) the capacity of the different techniques to detect the size and shape of the cavity, and (iii) the influence of depth and the nature of the rock substrata on the resolution capacity of each type of array.

We conducted our research at a number of geologically well-documented sites to be able to assess the electrical response afforded by different subsoil structures. The study was mainly carried out in the former mining district of Linares (Jaén Province, southern Spain), where we studied the response to two drainage adits and a cavity formed by a mine chamber over a vein (sites A, B, and D in Fig. 1). Our last site was outside this district in an old mining roadway near Canena, also in the province of Jaén (C in Fig. 1). In cases A, B and C, we conducted a topographic survey (including underground topographic survey, Fig. 2) to chart the underground route of the cavities, their depths, and their dimensions and shapes (Fig. 2). In case D it was not possible to visit the mine, but we have historical information on its geometry.

Methods

We used electrical resistivity tomography. This is a geoelectric method that analyzes the materials in the subsoil on the basis of their electrical behavior and can provide two and even three-dimensional high-resolution electrical images of the subsurface (Reynolds, 1997; Colella et al., 2004). The method requires numerous electrodes and a system of cables to be installed above the section to be profiled. The distance between the electrodes depends upon the resolution and depth of the particular objectives being sought. In general, the shorter the distance between the electrodes the greater the resolution, and the greater the resolution the greater the depths that it is possible to investigate. Technically, an electrical-resistivity tomography survey can be carried out using different electrode arrays (dipole-dipole, Wenner, Schlumberger) that are spread across the surface above the objective (Loke and Barker, 1996; Reynolds, 1997; Dahlin and Zhou, 2004). Electric current is injected into the ground and the voltage signals are measured. From the configuration of the array it is then possible to calculate the apparent electrical resistivity.

The electrical tomography equipment used in this study is the RESECS model, manufactured by Deutsche Montan Technologie. This is a multi-electrode array with an integrated computer that can handle up to 960 electrodes. The power source is 250 W and 2.5 A, which generates impulses of 880 V peak-to-peak. It has a built-in transmitter, receiver, and power supply. Other interesting features include the automatic processing of apparent resistivity and chargeability, real-time resistivity control in 2D and 3D, control of the current and voltage injection curve, regulation of injection time, built-in PC and integrated switching processor.

The electrical tomography profiles were interpreted using the RES2DINV resistivity and induced-polarization interpretation software. This calculation program is based on the least-square method with an enforced smoothness constraint, modified with the quasi-Newton optimization technique. The inversion method constructs a model of the subsoil using rectangular prisms and determines the resistivity value for each of them, minimizing the differences between the observed and calculated apparent resistivity values (Loke and Barker, 1996; Loke and Dahlin, 2002).

We collected a total of fourteen electrical tomography profiles at the four sites selected (A, B, C, and D in Fig. 1). At the first three sites, we made a detailed topographic survey of the underground cavities and the positions of the profiles (Fig. 2). Various experiments were conducted at these sites, trying always to ensure that the profile was perpendicular to and centered over the course of the drainage adit. Once we knew the size of the cavity investigated, we used a spacing that was either slightly less than or almost the same as the diameter of the cavity (1.5 m), or considerably greater (3 m). We used the Wenner-Schlumberger, dipole-dipole, and Wenner arrays to determine which technique best detected the cavity.

The question of which is the most effective array is a matter of some debate in the literature (see for example the discussions in studies by Zhou et al., 2000; Zhou and Dahlin, 2003; Dahlin and Zhou, 2004; Drahor 2006; Pánek et al., 2010). Some authors consider that the Wenner array is most sensitive to changes in the vertical resistivity of the subsoil (Griffiths and Turnbull, 1985; Griffiths and Barker, 1993), the average reliable depth for investigation being around half that of the spacing (Edwards, 1977). Because it has a small geometric factor, leads to a strong signal even in areas with electromagnetic background noise.

The dipole-dipole array is very sensitive to changes in horizontal resistivity and relatively insensitive to vertical changes. Thus it is useful in the detection of vertical structures such as buried walls, cavities, and contamination plumes. Of the three arrays, the dipole-dipole achieves the greatest average depth of investigation, although its performance is adversely affected in areas with electromagnetic noise.

The Wenner-Schlumberger array is a hybrid between the Wenner and the Schlumberger arrays. According to Pazdirek and Bláha (1996), this array is moderately sensitive to both horizontal and vertical structures. The average investigation depth is greater than with the Wenner array and the intensity of the signal is lower than that of the Wenner, but greater than that of the dipole-dipole.

At sites A, B, and C we used eighty electrodes over a length of 120 m with a spacing of 1.5 m. At site B we repeated the test with an inter-electrode spacing of 3 meters. We used spacings that were equal to or greater than the diameter of the cavity to enable us to prospect for cavities at depths of between 2 and 4 meters with sufficient
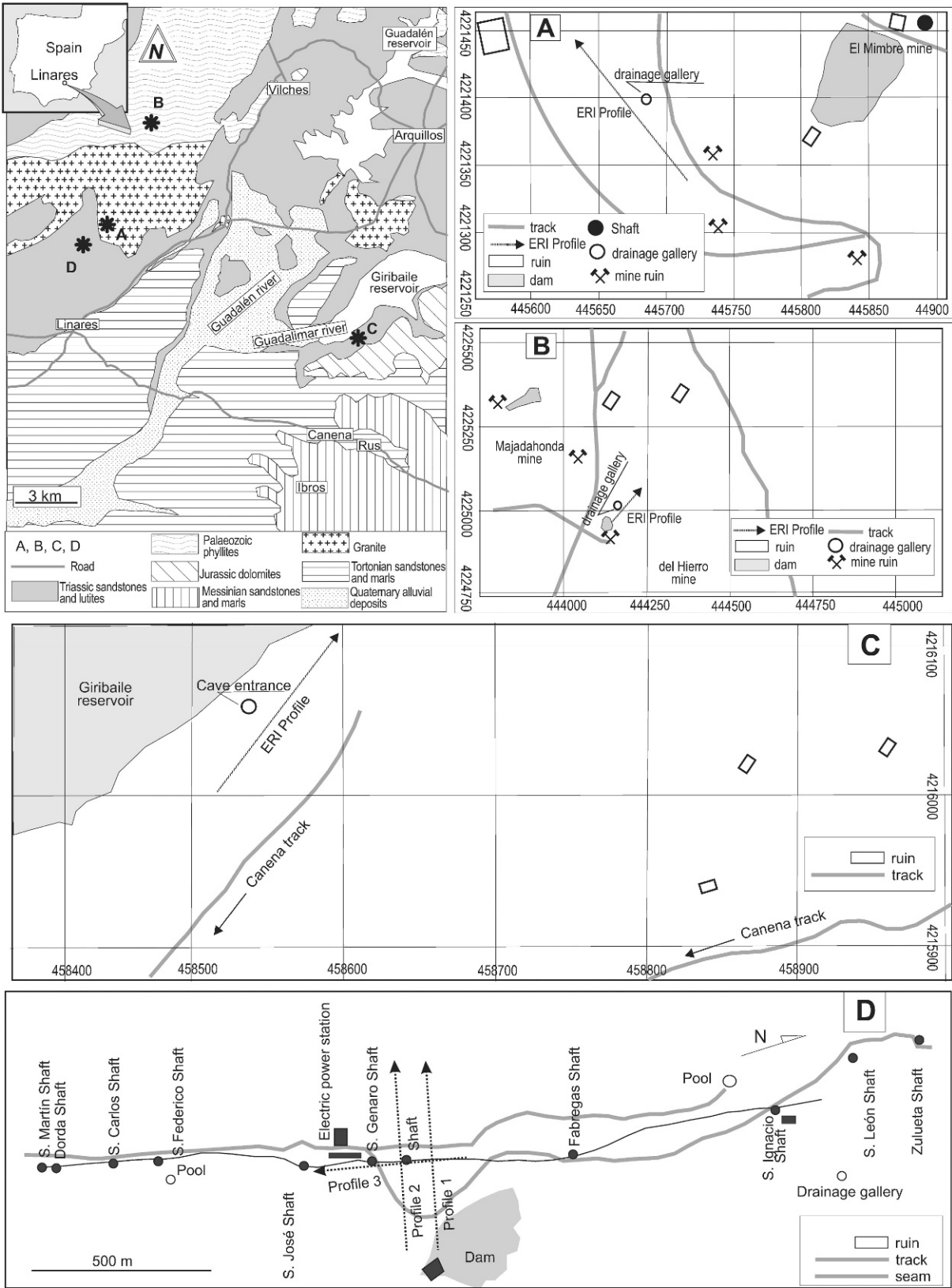
Figure 1. Geographical locations and geological context of the four sites studied, A, B, C, and D.

Figure 2. 2.1: Surveying inside the drainage adit at site A, the Mimbre Cavity. 2.2: Topographic surveying at the surface above the tomography profile at site A. 2.3: Route of the electrode array at site B, the Grupo Cobo Cavity, and the entrance to the drainage gallery. 2.4: The entrance to the drainage adit at site B. 2.5: Interior of the mine tunnel that is site C, the Canena Cavity. 2.6: Collapse associated with the caved seam at site D, the Arrayanes caved seam.

resolution. At site D, three profiles (Fig. 1D) were made using a Wenner-Schlumberger array with a spacing of 5 m, a value similar to the size of the chambers above the seam. To do this, we used eighty electrodes over a distance of 400 m.

Site A, the Mimbre Cavity, is a drainage adit, currently dry and empty, that was excavated in granite in a northeast-southwest direction. Its average cross-section is 1.60 m^2, and it is located at a depth of from 4.6 to 6.4 m. The location of the profiles is in Figure 1A. Figure 3 shows examples of pseudo-sections of real resistivities obtained for each of the arrays we used. With a electrode-spacing of 1.5 m, we took 1,325 measurements of apparent resistivity for the Wenner-Schlumberger array, and a maximum investigation depth of 14.4 m was reached, with an RMS of 11.4 (Fig. 3A). A total of 1,025 measurements of apparent resistivity were taken for the Wenner array, and a maximum investigation depth of 19.2 m was reached, with an RMS of 4.2 (Fig. 3B). A total of 2,492 measurements of apparent resistivity were taken for the dipole-dipole array, reaching a maximum investigation depth of 11.9 m, with an RMS of 23.3 (Fig. 3C).

The drainage adit at Site B, the Grupo Cobo Cavity, currently dry and empty, is cut into Palaeozoic phyllites, in a northwest-southeast direction. The average cross-section is 1.8 m^2, and it is located at a depth of from 4 to 5.8 m. The location of the profiles is in Figure 1B. The lithology and the depth (slightly shallower) are therefore different from the previous experiment. The electrode arrays and spacings were arranged according to the same criteria as at Site A. Figure 4 shows examples of the pseudo-sections of the real resistivities obtained for each of the arrays applied. We took 1,232 readings for the Wenner-Schlumberger array with a spacing of 1.5 m between each electrode. A depth of 12.7 m was reached and an RMS of 16.7 was obtained (Fig. 4A). We took 970 readings with the Wenner array; a depth of 15.4 meters was reached and a RMS of 6.7 was obtained (Fig. 4B). We took 2,942 readings with the dipole-dipole array; a depth of 11.9 m was reached and an RMS of 36.3 was obtained (Fig. 4C). At this site, the Wenner-Schlumberger array was repeated with a spacing of 3 m. We took 225 readings that gave an RMS of 8.2.

Site C, the Canena Cavity, an old mining roadway currently dry and empty was cut into Triassic sandstones in a northwest-southeast direction. The average section is 2.5 m^2, and it is located at a depth from 1.8 to 4 m. The lithology is again different, and the depth is the least of our sites. The location of the profiles are in Figure 1C. The electrode arrays and spacings were arranged the same as at Sites A and B. Parts A–C of Figure 5 show the pseudo-sections of the real resistivities obtained for each of the arrays applied. We took 1,232 readings for the Wenner-Schlumberger array; a depth of 12.7 m was reached and an RMS of 42.4 was obtained. We took 970 readings with the Wenner array; a depth of 15.4 m was reached and an RMS of 47.4 was obtained. We took 2,942 readings with the

dipole-dipole array; a depth of 11.9 m was reached and an RMS of 34.4 was obtained.

At Site D, three profiles were taken near the San Genaro shaft in the Arrayanes caved seam (locations in Fig. 1D). Profile 2, running 113° to 293° and perpendicular to the path of the seam, has been selected. Lutites and Triassic sandstones, lying over Palaeozoic granite, crop out at the surface. Although in this case, we were unable to carry out a topographic survey, the exact position and morphology of the cavity produced after mining the seam is known. This cavity is up to 5 m thick and, due to the collapse of the structure, is partially filled at the top with lutites. The profiles had a inter-electrode spacing of 5 m in a Wenner-Schlumberger array. The total length was 400 m and it contained eighty electrodes, reaching an investigation depth of 75 m. We took 1,419 readings and obtained an RMS of 8.3 (Fig. 5D).

RESULTS

From a geophysical point of view, the geologic structure at Site A behaves like a two-layer model with all three arrays. It has a 2 to 4 m thick surface layer that shows low resistivity values (< 300 ohm-m) that consists of altered granite with varying degrees of water saturation. Below this, there is a more resistive mass that is composed of unaltered granite.

Using a spacing of 1.5 m, similar to the diameter of the cavity, with the Wenner-Schlumberger configuration we detected a resistivity feature that coincided with the position of the cavity (Fig. 3A). The position of the structure could not be defined with the Wenner method because low resistivity values were obtained compared to the readings in the previous experiment (Fig. 3B). With the dipole-dipole array the cavity was located but the RMS numbers were higher (Fig. 3C).

At Site B the geologic structure behaves like a three-layer model. There is a 1 to 2 m thick surface layer with high resistivity values (> 300 ohm-m) that probably consists of breccia and the remains of an old spoil-heap. Beneath this, there is a layer of altered phyllites. The irregular distribution of areas with varying degrees of alteration, fractures, and water saturation may explain the large oscillations in the resistivity values between 20 and 200. Below this, is another layer that has the highest resistivity values. These values (up to 1200 ohm-m) coincide with the least altered phyllites.

Using the Wenner-Schlumberger array with a spacing of 1.5 m, similar to the diameter of the cavity, we detected an increase in resistivity in an area that coincided with the position of the cavity. Two additional peaks in resistivity were observed at a depth of about 6 m (Fig. 4A). These may correspond to two service galleries near the seam. The dipole-dipole array appeared to detect the same structure with high resistivity values, although its morphology was less precise (Fig. 4C). The Wenner array detected the structures but the resolution was lower (Fig. 4B).
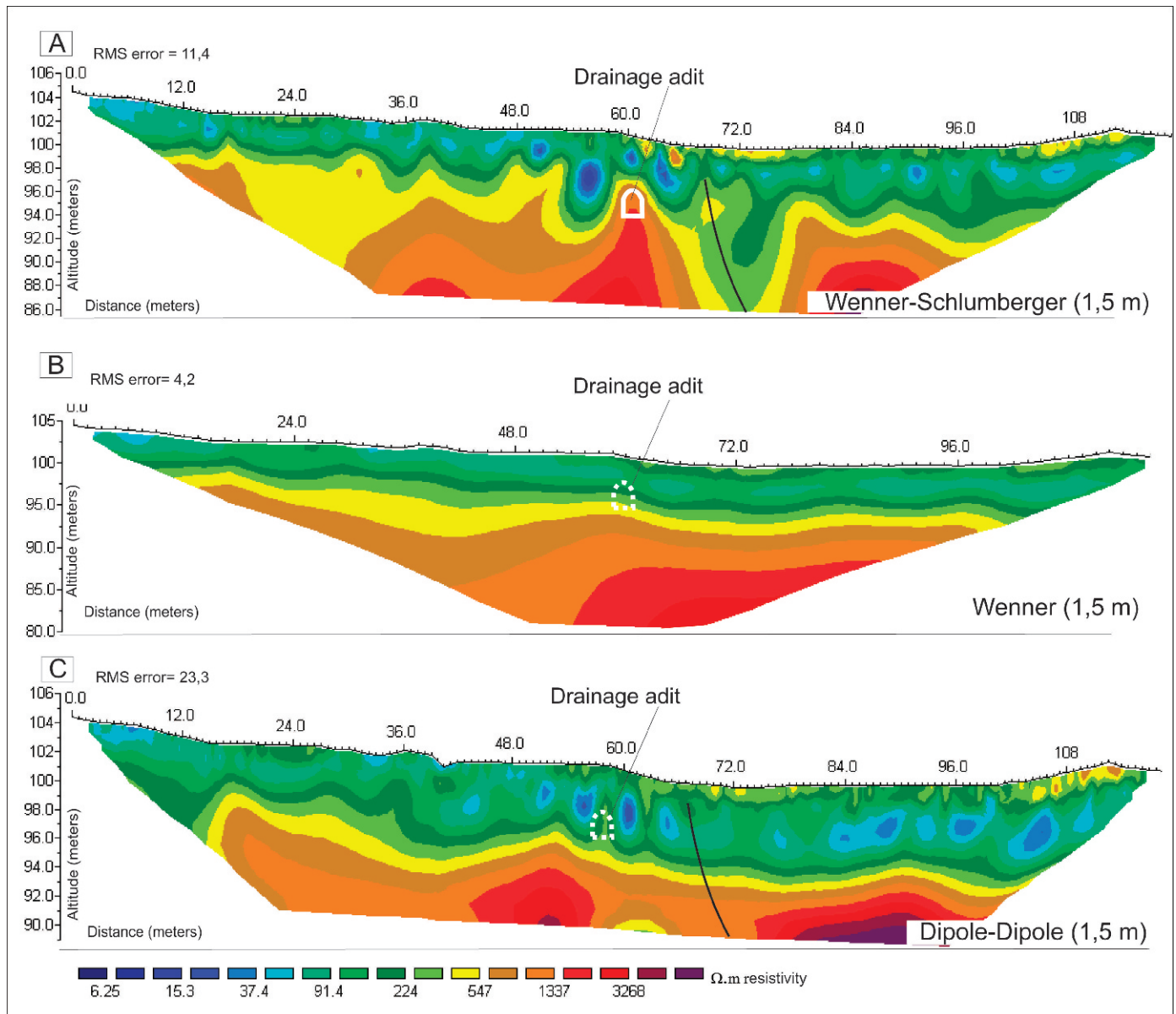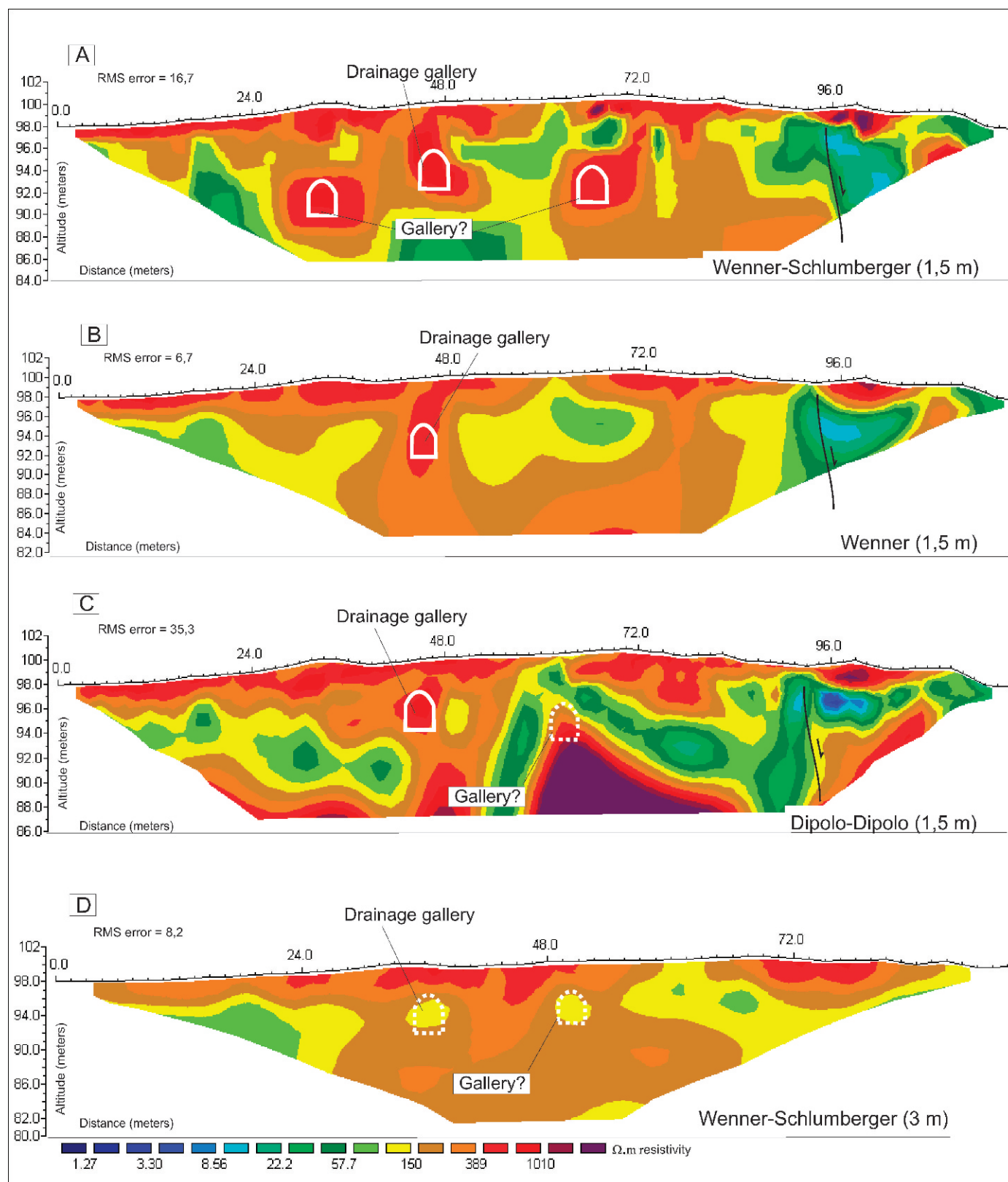
Figure 3. Electrical resistivity tomography profiles obtained at the site A in granite, using the arrays and electrode spacing indicated. Note that the vertical scales are all different.

A loss of resolution was noted as the spacing between the electrodes increased. As a result, with a spacing of 3m (double the diameter of the cavity) the gallery could not be defined (Fig. 4D).

In the Site C profiles with all three arrays, the geologic structure of this sector behaves like a two-layer model. In addition to a discontinuous surface level of breccia that shows high resistivities of up to 2,000 ohm-m, two distinct units can be seen. There is a 1 to 10 m thick surface layer that shows low resistivity values ($<$ 350) and is probably composed of calcarenites. Underneath this layer, a more resistive facies appears, with values ranging from 1,000 to 2,500 ohm-m, that would appear to be a siliceous conglomerate. The contact between the two units is affected by fractures.

With the Wenner-Schlumberger array, the anomaly was clearly indicated by high resistivity values (Fig. 5A). With the dipole-dipole array, the gallery was located as an area with medium resistivity levels (Fig. 5C). The gallery could not be detected with the Wenner array (Fig. 5B).

A two-layer geophysical model can also be applied to Site D, the caved seam. There is a surface level with low resistivity ($<$ 250) that would appear to be formed by either Triassic lutite or highly altered granite. Beneath this layer, there is an increase in resistivity that would appear to coincide with somewhat less altered granite. Using the Wenner-Schlumberger array with a spacing of 5 m, similar to the diameter of the cavity, we detected a very well defined maximum resistivity that corresponds to a mined

Figure 4. Electrical resistivity tomography profiles obtained at site B in phyllite, using the arrays and electrode spacing indicated. Note that the vertical scales are all different and the horizontal scale in part D is different.
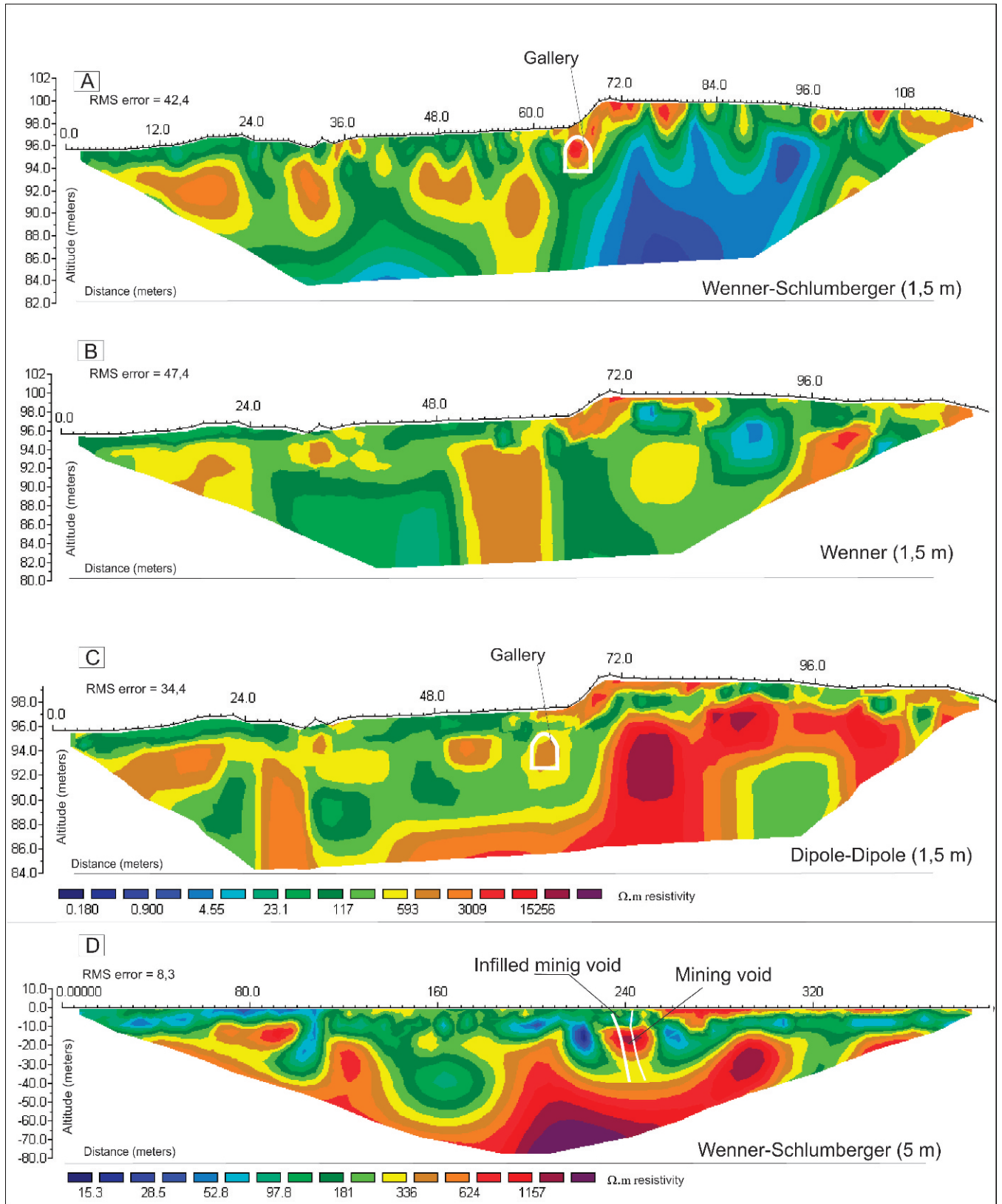
Figure 5. A–C, electrical resistivity tomography profiles obtained at site C in sandstone, using the array and electrode spacing indicated. Note that the vertical scales are all different. Part D, profile 2 at site D, the collapsed mine chamber.

chamber orientated along the previous path of the seam (Fig. 5D). The cavity shows two different types of behavior. In the upper part, the collapse of the protective surface layer has resulted in a partial infill of lutites, so that in the sector closest to the surface the caved seam behaves like a conductor ,with values ranging from 60 to 160 ohm-m. At greater depths, the empty chamber shows higher resistivity, with values ranging from 600 to 1500 ohm-m.

DISCUSSION AND CONCLUSIONS

Electrical resistivity tomography is a geophysical prospecting technique that can detect cavities in the subsoil. We describe here several cases in which this prospecting method has been used to detect cavities associated with past mining work in the Linares mining district and another cavity near Canena (Jaén Province, southern Spain). In all these examples, the position, shape, and characteristics of the structures were well known and documented, and the aim of our electrical tomography experiments was to test the efficacy of the technique itself.

Our results varied depending upon a multitude of physical factors, such as the depth and diameter of the cavity and the local geology, and the method factors, such as the array configuration, the inter-electrode spacing, and the density of data. In addition, when the cavity was empty, there was an anomaly with a steep gradient and very high resistivity values as the air filling the cavity is dielectric. When the cavities were filled with fine, loose material, usually saturated in water, the electrical resistance was lower, as both water and clay are good conductors of electric current (see Pánek et al, 2010). In this situation, electrical tomography shows an anomaly with a low resistivity value, as near the surface in Figure 5D.

Of the three arrays types we used, the Wenner-Schlumberger array offered the highest resolution in the three cases studied of cavities excavated in a variety of different lithologies. This array also identified the presence of the mine chamber. The results obtained with the dipole-dipole array were positive in the case of the phyllites (a resistive rock) and negative in the case of sandstones (resistive) and altered granites (low resistivity). The Wenner array produced poorer results with all three cavities. The quality of the results was correlated with the RMS numbers, which were always lower and more stable with Wenner-Schlumberger and higher and more unstable with dipole-dipole and Wenner.

There was a maximum inter-electrode spacing above which the arrays we used could not detect the cavities. The quality of cavity detection was at its best when the distance between the electrodes was less than or equal to the diameter of the cavity (compare the Fig. 4A and Fig. 4D). When the spacing was greater than the diameter of the cavity, at best, only vague traces of the cavities could be identified, but these profiles did not include identifying images.

As far as the depth of the cavity was concerned, those that were closest to the surface could be located more efficiently. In general, cavity detection was less precise with an increase in depth. Using the Wenner-Schlumberger method, and to a lesser extent the dipole-dipole, we located cavities with a radius of about 1.5 m at depths of over 4.6 m, which means that prospecting can be carried out at depths of 3 times the radius of the cavity.

ACKNOWLEDGEMENTS

REFERENCES

Caputo, R., Piscitelli, S., Oliveto, A., Rizzo, E., and Lapenna, V., 2003, The use of electrical resistivity tomographies in active tectonics: Examples from the Tyrnavos Basin, Greece: Journal of Geodynamics, v. 36, p. 19–35. doi:10.1016/S0264-3707(03)00036-X.

Colella, A., Lapenna, V., and Rizzo, E., 2004, High-resolution imaging of the High Agri Valley Basin (Southern Italy) with electrical resistivity tomography: Tectonophysics, v. 386, p. 29–40. doi:10.1016/j.tecto.2004.03.017.

Dahlin, T., and Zhou, Bing, 2004, A numerical comparison of 2D resistivity imaging with 10 electrode arrays: Geophysical Prospecting, v. 52, p. 379–398. doi:10.1111/j.1365-2478.2004.00423.x.

De Bruyn, I.A., and Bell, F.G., 2001, The occurrence of sinkholes and subsidence depressions in the far West Rand and Gauteng Province, South Africa, and their engineering implications: Environmental and Engineering Geoscience, v. 7, p. 281–295. doi:10.2113/gseegeosci.7.3.281.

Drahor, M.G., 2006, Integrated geophysical studies in the upper part of Sardis archaeological site, Turkey: Journal of Applied Geophysics, v. 59, p. 205–223. 10.1016/j.jappgeo.2005.10.008.

Edwards, L.S., 1977, A modified pseudosection for resistivity and induced-polarization: Geophysics, v. 42, p. 1020–1036. doi:10.1190/1.1440762.

Gambetta, M., Armadillo, E., Carmisciano, C., Stefanelli, P., Cocchi, L., and Tontini, F.C., 2011, Determining geophysical properties of a near-surface cave through integrated microgravity vertical gradient and electrical resistivity tomography measurements: Journal of Cave and Karst Studies, v. 73, p. 11–15. doi:10.4311/jcks2009ex0091.

Griffiths, D.H., and Barker, R.D., 1993, Two-dimensional resistivity imaging and modelling in areas of complex geology: Journal of Applied Geophysics, v. 29, p. 211–226. doi:10.1016/0926-9851(93)90005-J.

Griffiths, D.H., and Turnbull, J., 1985, A multi-electrode array for resistivity surveying: First Break, v. 3, no. 7, p. 16–20.

Gutiérrez, F., Galve, J.P., Lucha, P., Bonachea, J., Jordá, L., and Jordá, R., 2009, Investigation of a large collapse sinkhole affecting a multi-storey building by means of geophysics and the trenching technique (Zaragoza city, NE Spain) Environmental Geology, v. 58, p. 1107–1122. doi:10.1007/s00254-008-1590-8.

Loke, M.H., and Barker, R.D., 1996, Rapid least-squares inversion of apparent resistivity pseudosections by a quasi-Newton method: Geophysical Prospecting: v. 44, p. 131–152. doi:10.1111/j.1365-2478.1996.tb00142.x.

Loke, M.H., and Dahlin, T., 2002, A comparison of the Gauss-Newton and quasi-Newton methods in resistivity imaging inversion: Journal of Applied Geophysics, v. 49, p. 149–162. doi:10.1016/S0926-9851(01)00106-9.

Maillet, G.M., Rizzo, E., Revil, A., and Vella, C., 2005, High resolution electrical resistivity tomography (ERT) in a transition zone environment:

Application for detailed internal architecture and infilling processes study of a Rhône River paleo-channel: Marine Geophysical Research, v. 26, p. 317–328. doi:10.1007/s11001-005-3726-5.

Maillol, J.M., Seguin, M.-K., Gupta, O.P., Akhauri, H.M., and Sen, N., 1999, Electrical resistivity tomography survey for delineating uncharted mine galleries in West Bengal, India: Geophysical Prospecting: v. 47, p. 103–116. doi:10.1046/j.1365-2478.1999.00126.x.

Martínez, J., Benavente, J., García-Aróstegui, J.L., Hidalgo, M.C., and Rey, J., 2009, Contribution of electrical resistivity tomography to the study of detrital aquifers affected by seawater intrusion-extrusion effects: The River Vélez delta (Vélez-Málaga, southern Spain): Engineering Geology, v. 108, p. 161–168. doi:10.1016/j.enggeo.2009.07.004.

Martínez-López, J., Rey, J., Sandoval, S., and Rodríguez, M., 2007, La tomografía eléctrica: una herramienta para la detección de huecos mineros (concesión de Arrayanes, Linares-Jaén): Geogaceta, v. 42, p. 43–46.

Naudet, V., Lazzari, M., Perrone, A., Loperte, A., Piscitelli, S., and Lapenna, V., 2008, Integrated geophysical and geomorphological approach to investigate the snowmelt-triggered landslide of Bosco Piccolo village (Basilicata, southern Italy): Engineering Geology, v. 98, p. 156–167. doi:10.1016/j.enggeo.2008.02.008.

Pánek, T., Margielewski, W., Tábořík, P., Urban, J., Hradecký, J., and Szura, C., 2010, Gravitationally induced caves and other discontinuities detected by 2D electrical resistivity tomography: Case studies from the Polish Flysch Carpathians: Geomorphology, v. 123, p. 165–180. doi:10.1016/j.geomorph.2010.07.008.

Pazdîrek, O., and Bláha, V., 1996, Examples of resistivity imaging using ME-100 resistivity field acquisition system. EAGE 58th Conference and Technical Exhibition Extended Abstracts, Amsterdam, P050.

Reynolds, J.M., 1997, An Introduction to Applied and Environmental Geophysics: Chichester, England, John Wiley & Sons, 796 p.

Sasaki, Y., 1992, Resolution of resistivity tomography inferred from numerical simulation: Geophysical Prospecting, v. 40, p. 453–463. doi:10.1111/j.1365-2478.1992.tb00536.x.

Šumanovac, F., 2006, Mapping of thin sandy aquifers by using high resolution reflection seismics and 2-D electrical tomography: Journal of Applied Geophysics, v. 58, p. 345–346. doi:10.1016/j.jappgeo.2005.06.005.

Store, H., Storz, W., and Jacobs, F., 2000, Electrical resistivity tomography to investigate geological structures of earth's upper crust: Geophysical Prospecting, v. 48, p. 455–471. doi:10.1046/j.1365-2478.2000.00196.x.

Telford, W.M., Geldart, L.P., and Sheriff, R.E., 1990, Applied Geophysics, second edition: Cambridge, Cambridge University Press, 770 p.

van Schoor, M., 2002, Detection of sinkholes using 2D electrical resistivity imaging: Journal of Applied Geophysics, v. 50, p. 393–399. doi:10.1016/S0926-9851(02)00166-0.

Waltham, T., Bell, F., and Culshaw, M., 2005, Sinkholes and Subsidence: Karst and Cavernous Rocks in Engineering and Construction: Chichester, England, Springer, 382 p.

Zhou, Wanfang, Beck, B.F., and Stephenson, J.B., 2000, Reliability of dipole-dipole electrical resistivity tomography for defining depth to bedrock in covered karst terranes: Environmental Geology, v. 39, p. 760–766. doi:10.1007/s002540050491.

Zhou, Bing, and Dahlin, T., 2003, Properties and effects of measurements errors on 2D resistivity imaging: Near Surface Geophysics, v. 1, p. 105–117. doi:10.3997/1873-0604.2003001.

TEMPORAL VARIABILITY OF CAVE-AIR CO$_2$ IN CENTRAL TEXAS

BRIAN D. COWAN[1]*, MICHAEL C. OSBORNE[2], AND JAY L. BANNER[3]

Abstract: The growth rate and composition of cave calcite deposits (speleothems) are often used as proxies for past environmental change. There is, however, the potential for bias in the speleothem record due to seasonal fluctuations in calcite growth and drip-water chemistry. It has been proposed that the growth rate of speleothem calcite in Texas caves varies seasonally in response to density-driven fluctuations in cave-air CO$_2$, with lower growth rates in the warmer months when cave-air CO$_2$ is highest. We monitored CO$_2$ in three undeveloped caves and three tourist caves spread over 130 km in central Texas to determine whether seasonal CO$_2$ fluctuations are confined to tourist caves, which have been modified from their natural states, and the extent to which cave-air CO$_2$ is controlled by variations in cave geometry, host rocks, cave volume, and soils. Nearly 150 lateral transects into six caves over three years show that CO$_2$ concentrations vary seasonally in five of the caves monitored, with peak concentrations in the warmer months and lower concentrations in the cooler months. The caves occur in six stratigraphic units of lower Cretaceous marine platform carbonate rocks and vary in volume (from 100 to >100,000 m^3) and geometry. Seasonal CO$_2$ fluctuations are regional in extent and unlikely due to human activity. Seasonal fluctuations are independent of cave geometry, volume, depth, soil thickness, and the hosting stratigraphic unit. Our findings indicate that seasonal variations in calcite deposition may introduce bias in the speleothem record, and should be considered when reconstructing paleoclimate using speleothem proxies.

INTRODUCTION

It is important to understand the mechanisms that control speleothem growth and calcite composition. It has long been known that the concentration of CO$_2$ in cave air can affect the growth rate of speleothems (Holland et al., 1964), but until recently, the extent to which cave-air CO$_2$ fluctuations might introduce bias into the speleothem record was not fully appreciated (Fairchild et al., 2007). Recent studies in the United States (Banner et al., 2007; Wong et al., 2011), Austria (Spötl et al., 2005), and Ireland (Baldini et al., 2008) have demonstrated that there is potential for bias in the paleoclimate record due to changes in speleothem deposition rate and drip-water chemistry caused by cave-air CO$_2$ fluctuations.

A recent study of calcite growth rates in four central Texas tourist caves reveals that in three of the caves, calcite growth varies seasonally and is inversely correlated with cave-air CO$_2$ concentrations (Banner et al., 2007). In the caves that experienced growth-rate variations, calcite deposition peaked in the cooler months, when cave-air CO$_2$ concentrations were low, while in the warmer months, elevated cave-air CO$_2$ concentrations inhibited drip water degassing, resulting in a significant decrease or cessation of calcite deposition. Drip rate variations were not the primary control on seasonal fluctuations in calcite growth rate, but did account for site-to-site variability in the magnitude of calcite growth rate within individual caves. The tourist caves with variable growth rates were located

over a distance of 130 km, suggesting that the potential for a regionally extensive seasonal bias in the speleothem record exists. Such regional biases in speleothem proxies (e.g., seasonal growth-rate variations, isotopic shifts) might be incorrectly interpreted as a direct result of climate conditions, not as a result of speleothem deposition being affected by cave meteorology. Therefore, it is important to determine if seasonal cave-air CO$_2$ fluctuations in central Texas caves are confined to tourist caves, which are modified from their natural state and receive a large number of visitors, or if they are naturally occurring.

Seasonal CO$_2$ fluctuations in tourist caves may result from modifications to their natural connectivity with the surface atmosphere during their development for tourism, significant human visitation, or non-anthropogenic influences. Variations in non-anthropogenic factors, such as cave volume, stratigraphic unit, cave geometry, and soil thickness, may also influence the extent and timing of CO$_2$ fluctuations. The hypothesis that seasonal CO$_2$ fluctuations in central Texas caves are regional in extent and are not unique to tourist caves was tested.

* Corresponding author
[1] Zara Environmental, LLC, 1707 FM1626, Manchaca, TX, USA 78652, bc1774@gmail.com
[2] Department of Geological and Environmental Sciences, Stanford University, 450 Serra Mall, Stanford, CA 94305, osbornem@stanford.edu
[3] Department of Geological Sciences C-1100, Jackson School of Geosciences, The University of Texas at Austin, Austin, TX, USA 78712, banner@jsg.utexas.edu
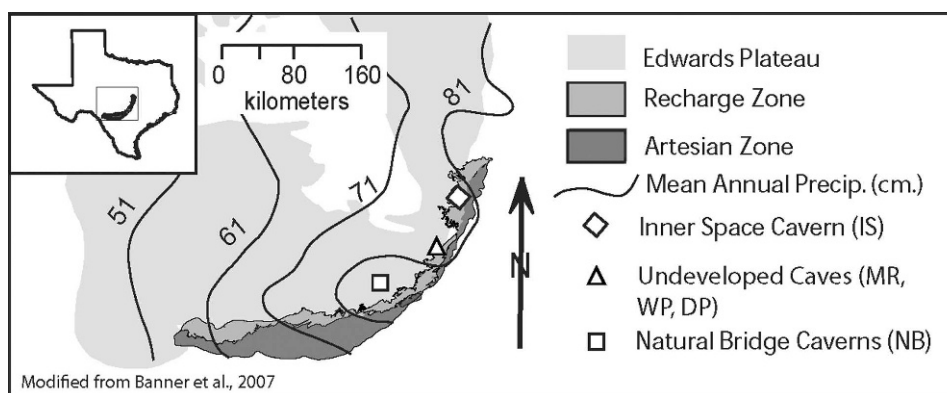
Figure 1. Map of Edwards Aquifer and cave locations on the Edwards Plateau in central Texas, USA. Note the undeveloped caves are located within 5 km of each other and are depicted as a single triangle. The two parts of Natural Bridge Caverns are adjacent and shown by a single symbol. Average annual precipitation in centimeters is shown as contours.

The timing and magnitude of CO_2 fluctuations in three undeveloped caves, District Park, Whirlpool, and Maple Run, were compared with those measured in the tourist caves with variable speleothem grown rates that were studied by Banner et al. (2007), Natural Bridge North Cavern, Natural Bridge South Cavern, and Inner Space Cavern. The undeveloped caves chosen for comparison with the tourist caves are centrally located between the tourist caves, are formed in similar stratigraphic units as the tourist caves, are overlain by similar soil and vegetation, receive similar rainfall amounts, experience similar surface temperature fluctuations, and receive little visitation outside of the monitoring trips (Fig. 1; Table 1).

Study Area

The study area is located near Austin, Texas, on the Edwards Plateau, which is composed of karstified Lower Cretaceous marine carbonates overlain by a thin calcareous clay soil that supports oak and juniper savannah. Soils across the study area are thin mollisols (typically < 30 cm) and commonly contain limestone fragments sourced from the underlying bedrock (Cooke, 2005). The undeveloped caves are overlain by stony clay loams, Inner Space is overlain by silty clays and stony clays, and the two parts of Natural Bridge are overlain by extremely stony clays and gravely clay loams (U.S. Department of Agriculture, Web Soil Survey).

All study caves, with the exception of Natural Bridge North and Natural Bridge South, are located within the Edwards Limestone, an Early Cretaceous marine limestone unit with interbedded dolomitic layers. Within the study area, the Edwards Group can be subdivided into several hydrostratigraphic units with different structural and hydrologic characteristics (Fig. 2) (Maclay and Small, 1976; Small et al., 1996). The Natural Bridge caves are located within the interbedded limestone and dolomitic units of the upper Glen Rose and lower Walnut

formations, which are also Early Cretaceous in age. Those two caves are adjacent to each other, not well connected, and have separate entrances. More detailed descriptions of the hydrology and morphology of Inner Space Caverns and the Natural Bridge caves is given by Musgrove et al. (2001), Musgrove and Banner (2004), and Banner et al. (2007).

The entrances of Natural Bridge North and Natural Bridge South are sealed by double glass doors that are only opened when tour groups enter and exit. During the development of Inner Space Cavern, an entrance tunnel approximately 4 m in diameter was excavated, and it remains unsealed. To increase visitor comfort, man-made ventilation shafts equipped with fans were installed in all three tourist caves. Ventilation fans are manually controlled and are typically used during the daytime hours in the summer months.

Controls on Cave-Air CO_2

Cave Ventilation

Cave ventilation is an important control on cave-air CO_2 concentrations, both seasonally and on shorter timescales, and is dependent on multiple factors, including fluctuations of the outside air temperature and barometric pressure, cave geometry and prevailing winds (e.g., Villar et al., 1985; Fernández et al., 1986; Hoyos et al., 1998; Buecher, 1999; Bourges et al., 2001; Spötl et al., 2005; Baldini et al., 2006; Denis et al., 2005; Bourges et al., 2006; Baldini et al., 2008; Kowalczk and Froelich, 2010). At mid latitudes, density differences between cave and outside air caused by seasonal temperature variability exert a first order control on the seasonal ventilation of caves (James and Banner, 2007). In many caves, air temperature is near the mean annual surface temperature and varies by only a few degrees over the seasons (Moore and Sullivan, 1997), and thus, cave ventilation is primarily controlled by surface air temperature and changes in barometric pressure

Table 1. Characteristics of monitored caves and overlying soils.

Cave name	Hydrostratigraphic Unit	Cave volume (m³) <accuracy>	Soil thickness (cm) <stdev>	USDA soil type	USDA soil series	Tourist cave	Stormwashed debris	Min/Max CO_2 (ppm)	R^2 average CO_2 vs. distance from entrance	Transect length (m)
Inner Space Cavern (IS)	Cyclic and Marine Members of Edwards Group	75,000 <1,000>	26.2 <10.2>	Silty clays stony clays	Eckrant	Yes	None	400/7,600	0.87	450
Natural Bridge Cavern North (NBN)	Upper Glen Rose and Walnut Formation	250,000 <10,000>	23.1 <20.9>	Stony clay, gravely clay loam, exposed bedrock	Comfort & Eckrant Rock Complex	Yes	None	370/9,500	0.79	200
Natural Bridge Caverns South (NBS)	Upper Glen Rose and Walnut Formation	150,000 <2,000>	32 <17.6>	Stony clay, gravely clay loam, exposed bedrock	Comfort & Eckrant Rock Complex	Yes	None	470/38,000	0.25	400
Maple Run Cave (MR)	Leached and Collapsed Member, Grainstone Member, and Regional Dense Member of Edwards Group	450 <10>	41.9 <14.4>	Stony Clay Loam	Speck	No	Little	570/23,000	0.05/0.29[a]	42
Whirlpool Cave (WP)	Grainstone Member and Kirschberg Member of Edwards Group	22,000 <100>	31 <21.7>	Stony Clay Loam	Speck	No	None	420/22,000	0.84	125
District Park Cave[b] (DP)	Kirschberg Member of Edwards Group	100 <2>	37.8 <18.9>	Stony Clay Loam	Speck	No	Significant	500/31,000	•••	5

[a] denotes that R^2 value is calculated for average CO_2 and depth from cave entrance.
[b] R^2 value not calculated for DP, because there are only two stations in the cave.
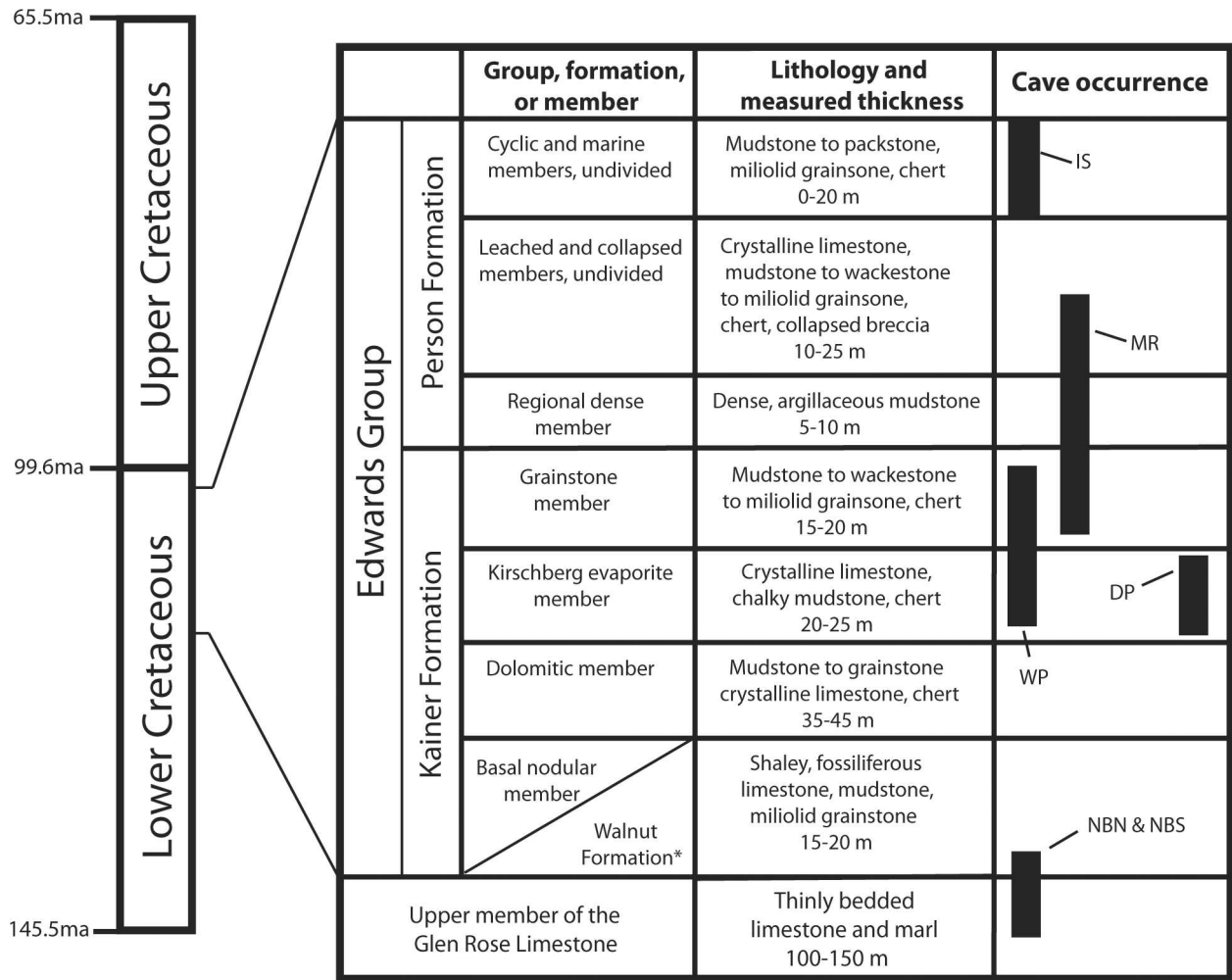
Figure 2. Stratigraphic section of the study area showing the intervals of occurrence of the caves of this study. The undeveloped caves (MR=Maple Run, DP=District Park, and WP=Whirlpool) are formed within several members of the Kainer and Person Formations. Note that MR and WP are formed in more than one member. The two parts of Natural Bridge Cavern (NBS and NBN) are adjacent and formed in the same member. Adapted from Maclay and Small (1976), Kastning (1983), and Small et al. (1996).

(Fairchild et al., 2006). Here we focus on seasonal fluctuations of cave-air CO_2 fluctuations that are primarily controlled by seasonal surface temperature fluctuations.

During warmer months, cave-air temperatures remain below outside temperature, causing the cooler, denser cave air to stagnate. During this time, the cave can be thought of as a semi-closed system, as ventilation is less efficient. As long as CO_2 sources such as degassing of drip water or advection through fractures are present ,the concentration of CO_2 in the cave air will continue to rise until CO_2 inputs reach equilibrium with CO_2 removal. When cave-air temperatures are warmer than outside temperatures, ventilation becomes more efficient, because the denser outside air flows into the cave, mixing with and displacing the CO_2-rich cave air, and causing CO_2 levels within the cave to decrease. This process only applies to caves in which most of their volume is lower in elevation than the entrance(s).

The intensity of cave ventilation is governed by cave geometry (e.g., vertical vs. horizontal, large passages vs. numerous constrictions), density differences between the cave air and outside air, distance from the cave entrance, other connections with the surface via pores and fracture networks that primarily depend on the stratigraphic position of the cave, and cave volume (Batiot-Guilhe et al., 2007). In general, stronger ventilation occurs at sites near the entrance and at sites that are not separated from the entrance by constrictions (Bourges et al., 2006). Where ventilation is limited by constrictions or distance from the entrance, CO_2 levels may remain relatively constant, governed by the balance between sources and losses other than ventilation.

CAVE CO_2 SOURCES

Known sources of cave-air CO_2 include decomposition of soil organic matter by microbes (soil respiration), root

respiration, in-cave decomposition of organic matter, diffusion from deep sources, animal respiration, and degassing from CO_2-rich groundwater (Troester and White, 1984; Ek and Gewelt, 1985; Hanson et al., 2000; Baldini et al., 2006; Bourges et al., 2001; Batiot-Guilhe et al., 2007; Crossey et al., 2006). The rate of CO_2 input into a cave is dependent on several factors that may vary on multiple timescales.

Degassing of CO_2-rich vadose water is a significant input of CO_2 in most caves. The concentration of CO_2 in vadose water is primarily controlled by the concentration of CO_2 in the soil air. Soil and root respiration is likely the dominant source of soil CO_2 in the study area. The rate of respiration is affected by changes in soil temperature and soil moisture, and the highest CO_2 production occurs when soils are moist and in warm months (Amundson and Smith, 1988; Daly et al., 2008; Lloyd and Taylor, 1994; Raich and Schlesinger, 1992). As the water flows through the soil zone, it becomes enriched in CO_2 until the partial pressure of CO_2 of the water is equal to the pCO_2 of the soil or the water drops below the soil zone. When CO_2-charged water comes into contact with a lower pCO_2 environment such as a cave, CO_2 degassing occurs, and the air within that environment becomes slightly more CO_2-rich. Advection or diffusion of vadose-zone air through fractures, cracks, and dissolution cavities is also a significant means of transporting CO_2 to the cave atmosphere (Baldini et al., 2006; Batiot-Guilhe et al., 2007; Perrier and Richon, 2010).

Carbon dioxide generated from decaying organic material within caves is a significant CO_2 source for caves that collect detritus or bat guano. The significance of this contribution of CO_2 is likely to vary, depending on the ability of a given cave to capture storm-washed debris or the presence of a significant bat population. Overland flows of water into caves, sinkholes, or soil piping features are required for a significant amount of organic debris to enter the caves that we monitored. Only District Park Cave receives significant amounts of organic debris via overland stormflow.

Animal respiration is another significant source of CO_2 in a cave environment, particularly in tourist caves. The concentration of CO_2 in a human breath is approximately 40,000 ppm (Miotke, 1974). A recent study of the impacts of respired CO_2 in a cave in the Czech Republic demonstrated that human respiration is a significant source of CO_2 that is proportional to the number of people in a cave and the duration of visits (Faimon et al., 2006). Likewise Liñán et al. (2008) noted that cave CO_2 concentrations in Nerja Cave, Spain, were correlated with visitation during certain times of the year. However, some data suggests that these elevated levels of CO_2 dissipate rapidly (Faimon et al., 2006; Hoyos et al., 1998).

Three of the monitored caves are tourist caves and receive <100 to >1,000 visitors per day, while the undeveloped caves receive few visitors outside of our monitoring trips. Visitation varies greatly, but generally the greatest numbers of visits to the tourist caves occur in mid-March and the summer months of May through August. Animals inhabiting caves will affect CO_2 concentrations in similar ways, depending on population size. A few bats are commonly found in the Natural Bridge caves, Inner Space, and Maple Run, but not in numbers significant enough to be counted (Jim Kennedy, Bat Conservation International, personal communication, April 8, 2009) or to significantly raise the concentration of CO_2 in the caves. Large mammals are unlikely to enter any of the undeveloped caves, as they are gated to exclude large mammals but allow for unimpeded airflow.

Degassing of CO_2 from phreatic water is another potential source within caves, especially where cave passages intersect the water table. Degassing occurs when high-pCO_2 phreatic water comes in contact with lower-pCO_2 cave air and will continue until the water reaches equilibrium with the air or it leaves the air-filled cave at a spring or a sump. The contribution of CO_2 from degassing of phreatic water will likely vary seasonally and in response to recharge events. Degassing of phreatic water might be a significant source of CO_2 in Inner Space and the Natural Bridge caves, as they are known to flood when aquifer levels rise after particularly heavy rainfalls. Flooding of these caves does not occur on a regular basis (seasonally), but only after prolonged periods of unusually wet conditions. A small stream flows through Natural Bride North occasionally. Degassing of phreatic water is not likely a significant source of CO_2 in Whirlpool, Maple Run, or District Park, as they are located approximately 50 m above the phreatic zone and are not known to flood.

METHODS

CO_2 concentrations were measured along transects inward from the cave entrances at sample points shown in Figure 3 using a portable Telaire 7001 CO_2 meter. From August 2006 to August 2007 the Telaire CO_2 meter was calibrated to an average atmospheric value of 380 ppm. Local atmospheric CO_2 concentrations likely differ from 380 ppm due to anthropogenic and natural variations, however these variations are likely within the instrument's range of uncertainty of 50 ppm or 5% of the total CO_2 concentration. Beginning in June 2007, a zero-point calibration was performed using argon gas. Atmospheric CO_2 concentrations were measured before and after each field transect to check for post-calibration drift. When a drift of greater than 100 ppm was detected, all data from that transect were considered unreliable and are not reported here.

Although the caves were monitored with varying frequency, ranging from weekly to monthly, each cave was visited multiple times during each season in order to assess seasonal variability. Cave-air CO_2 concentrations in tourist caves Inner Space, Natural Bridge North, and Natural Bridge South were monitored every four to six
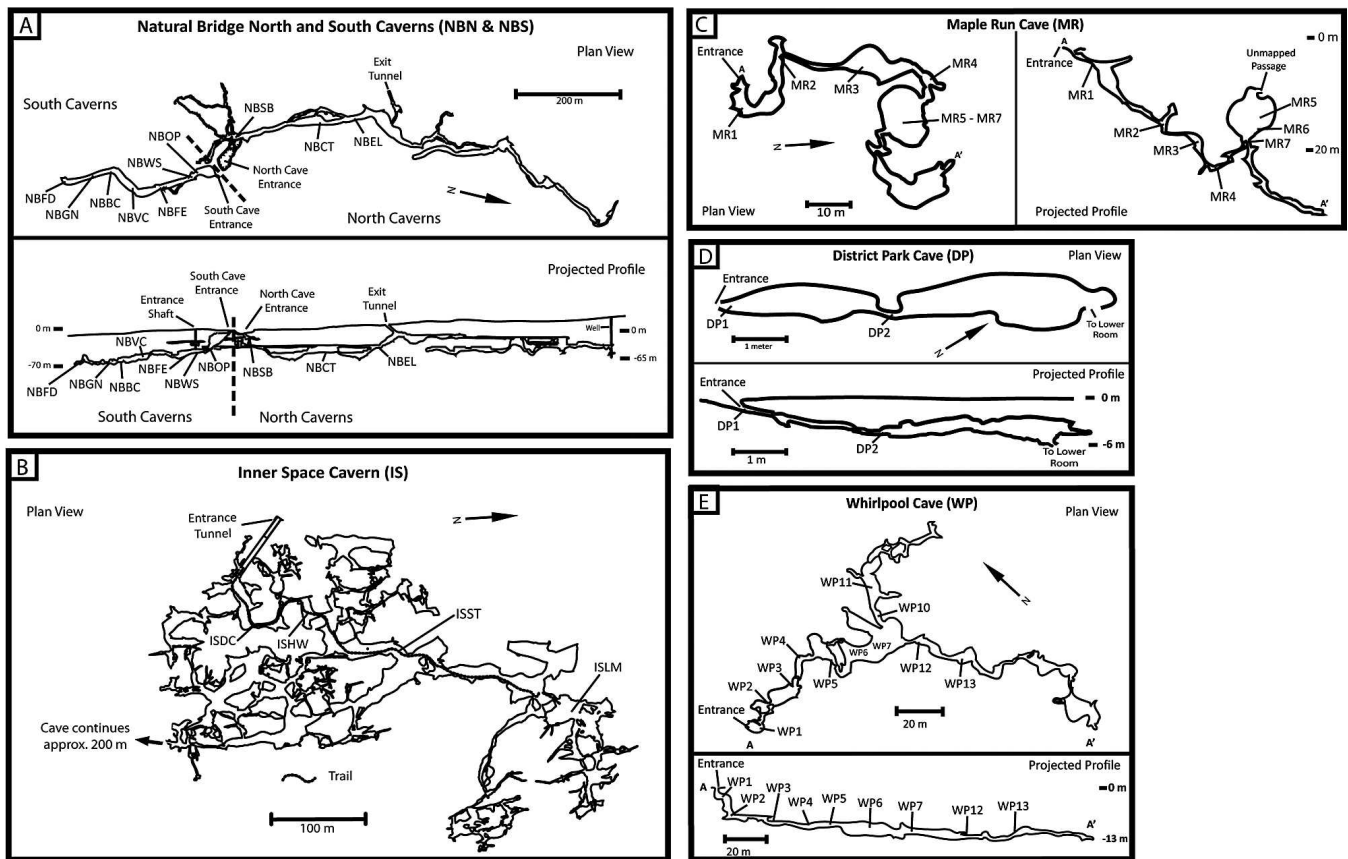
Figure 3. Maps of central Texas caves and locations of monitoring stations. Note that the entrance to cave NBN is taken as the datum for indicated depths for both NBN and NBS. Cave entrances are taken as the datum for all other depths reported. IS map adapted from Atkinson (2003), NBN and NBS maps adapted from Atkinson (2004), MR map adapted from Scott (2000), WP map adapted from Russell (1979), and DP map adapted from Russell (1988).

weeks from 2001 to May 2010. Maple Run, Whirlpool, and District Park caves were each visited two to four times monthly between July 2006 and October 2007. No transects were taken in those three caves from November 2007 to July 2008. In August 2008, monitoring resumed in those caves and continued through July 2009.

Significant increases in CO_2 concentration due to operator respiration have been reported (Baldini et al., 2006). Due to the ruggedness of the undeveloped caves, it was impractical to wear CO_2 scrubbing respirators or other devices that remove exhaled CO_2 from where measurements were being taken. Several experiments to estimate operator-caused bias were performed. Upon arriving at a measurement site, the initial CO_2 concentration was recorded. The operators then waited for a period of five minutes to determine if there was a rise in CO_2 concentration as a result of respiration. This experiment was repeated at several sites within each undeveloped cave. No increase in CO_2 concentration greater than the instrument error (50 ppm) was measured, and occasionally small decreases (20 to 30 ppm) within instrument error were measured. The meter was turned on and allowed to warm up and stabilize before reaching each measurement

site as to minimize the time required for the meter to equilibrate with the atmosphere at each measurement site. Measurements reported here were typically recorded within two to three minutes of arrival at each site, and no measurements were recorded after spending five minutes at a site. Based on this protocol, operator bias is considered to be insignificant, especially when compared to the magnitude of seasonal cave-air CO_2 fluctuations observed. The volumes of the tourist caves are so large that operator respiration is unlikely to have been a problem.

Total cave volume is reported for each cave in Table 1. All volumes were estimated from survey maps and physical measurements, and are presented here to compare relative cave volumes. To facilitate comparison between caves and between visits to each cave, a weighted mean CO_2 concentration was calculated for each transect as weighted mean = $[(C_{s1} \, V_{s1}) + (C_{s2} \, V_{s2}) + ...] / V_t$, where C_{sx} is the CO_2 concentration measured at site x, V_{sx} is the volume of passage at site x, and V_t is the total volume of transect passages. Because cave-air CO_2 concentrations are both temporally and spatially variable, the weighted means are displayed in Figure 4 as an estimation of the magnitude and timing of seasonal variability.

Tourist Caves
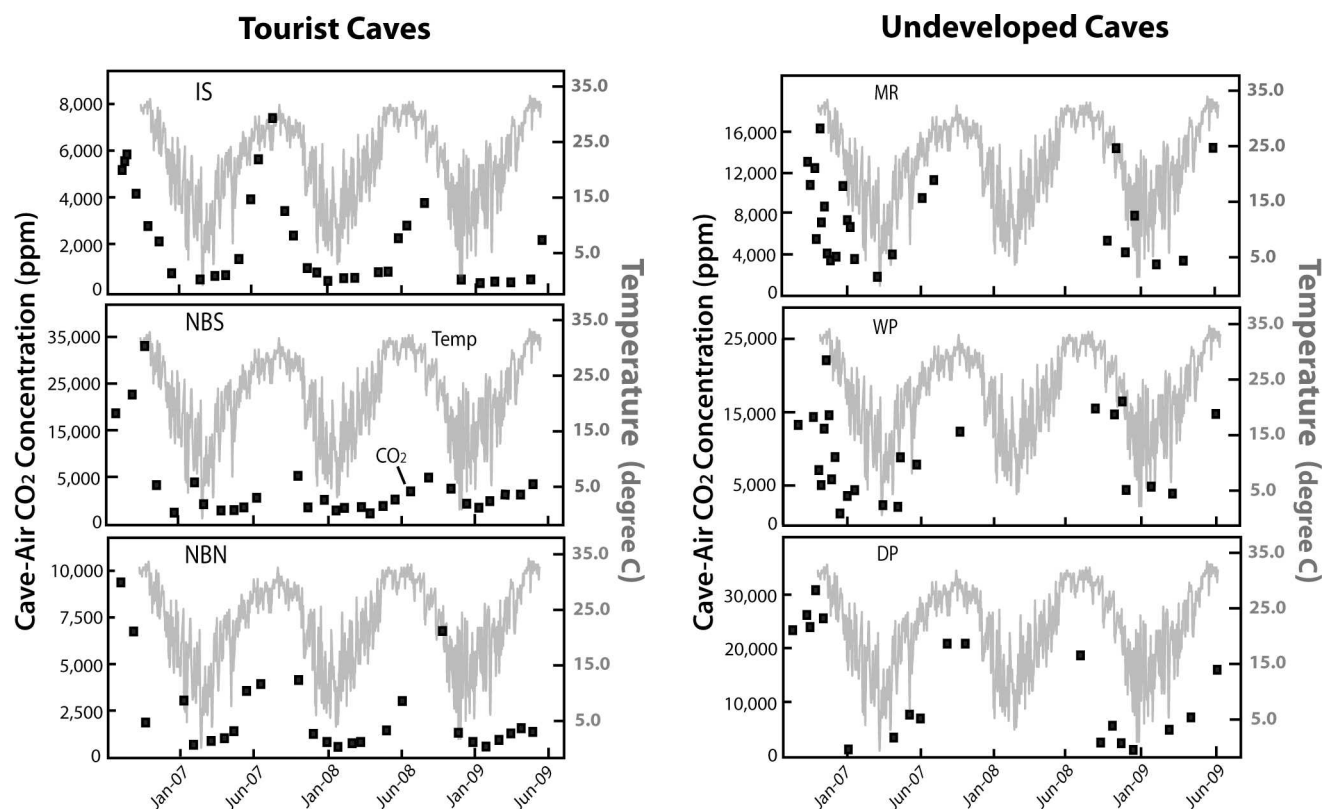
Undeveloped Caves

Figure 4. Time series of volume-weighted mean cave-air CO_2 concentrations measured during each transect of tourist and undeveloped caves (black squares) and outside air temperature (gray solid lines). Instrument error (5% of measurement or 50 ppm) is smaller than symbols used to represent CO_2 concentrations. Air temperature was measured at a National Climate Data Center weather station located in Austin, Texas; COOP ID: 410428). For weighted mean calculation, see text. IS is Inner Space Cavern, NBS and NBN are the parts of Natural Bridge Cavern, MR is Maple Run Cave, WP is Whirlpool Cave, and DP is District Park Cave.

Soil thicknesses were measured above each cave by hammering a 1.7-meter stake with a radius of 1 cm into the soil as far as possible (Table 1). Measurements were taken every 10 m along a 60 m transect, and a minimum of three transects were measured above each cave. Average soil thicknesses ranged from 23 cm above Natural Bridge Caverns North to 42 cm above Maple Run Cave (Table 1). Impervious cover was visually estimated by superimposing cave maps on satellite images of the land surface above the caves. Part of Inner Space is overlain by engineered fill for Interstate Highway 35 that is several meters thick, and approximately 35% of the cave is overlain by impervious cover. Natural Bridge North is overlain by approximately 20% impervious cover, and Natural Bridge South is overlain by approximately 10% impervious cover. There is no impervious cover over District Park, Whirlpool, or Maple Run caves.

Results

The volume-weighted means over time of the cave-air CO_2 concentrations are presented in Figure 4. Daily

average surface temperature measured at a National Climate Data Center weather station (COOP ID: 410428) located in Austin, Texas, are also in Figure 4.

The concentration of CO_2 in the tourist and undeveloped caves show strong seasonal variability. The timing of seasonal CO_2 fluctuations was consistent between all caves, but the magnitude of CO_2 fluctuations varied considerably, especially between the undeveloped and tourist caves. CO_2 concentrations were lowest during the cooler season (November through April) and elevated throughout the warm season (May through October), and concentrations generally increased with increasing distance from the cave entrances (Fig. 5). With the exception of Maple Run and District Park, the average CO_2 concentration at each station was well correlated ($R^2 > 0.25$) with distance from the entrance (Table 1, Fig. 6). At Maple Run there is not a strong correlation between average CO_2 concentration at each station and distance from the entrance ($R^2 = 0.0$, but there is a stronger correlation between average CO_2 concentration at each station and depth ($R^2 = 0.29$; data not shown). The small size and limited number of points for District Park Cave prevented this calculation there.
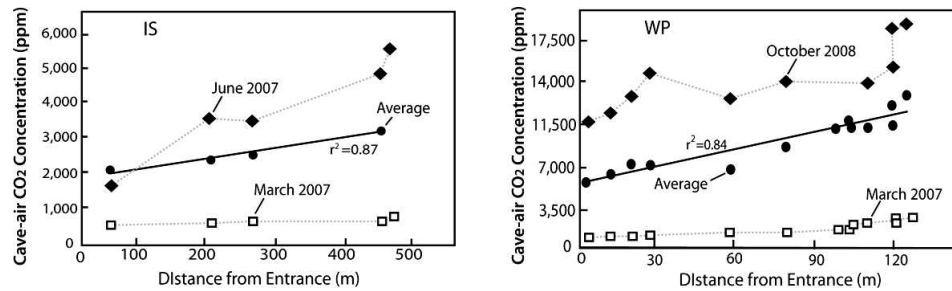
Figure 5. Representative individual warm- and cool-season CO$_2$ transects at Inner Space Caverns (IS) and Whirlpool Cave (WP). Mean CO$_2$ concentration measured during all transects at each station during study.

DISCUSSION

REGIONAL CONTROLS OF CAVE-AIR CO$_2$

Cave-air CO$_2$ concentrations varied significantly in all caves monitored. Higher CO$_2$ concentrations were measured during the warmer months and lower concentrations were measured during the cooler months (Fig. 4). Seasonal ventilation differences are likely driven by density differences between outside and cave air caused by seasonal differences in outside temperatures. If anthropogenic effects were responsible for the seasonal fluctuations of cave-air CO$_2$, then significant CO$_2$ fluctuations would only occur in tourist caves; but large seasonal fluctuations of cave-air CO$_2$ were observed in all caves.

Although seasonal fluctuations of cave-air CO$_2$ were observed in the undeveloped caves and tourist caves,
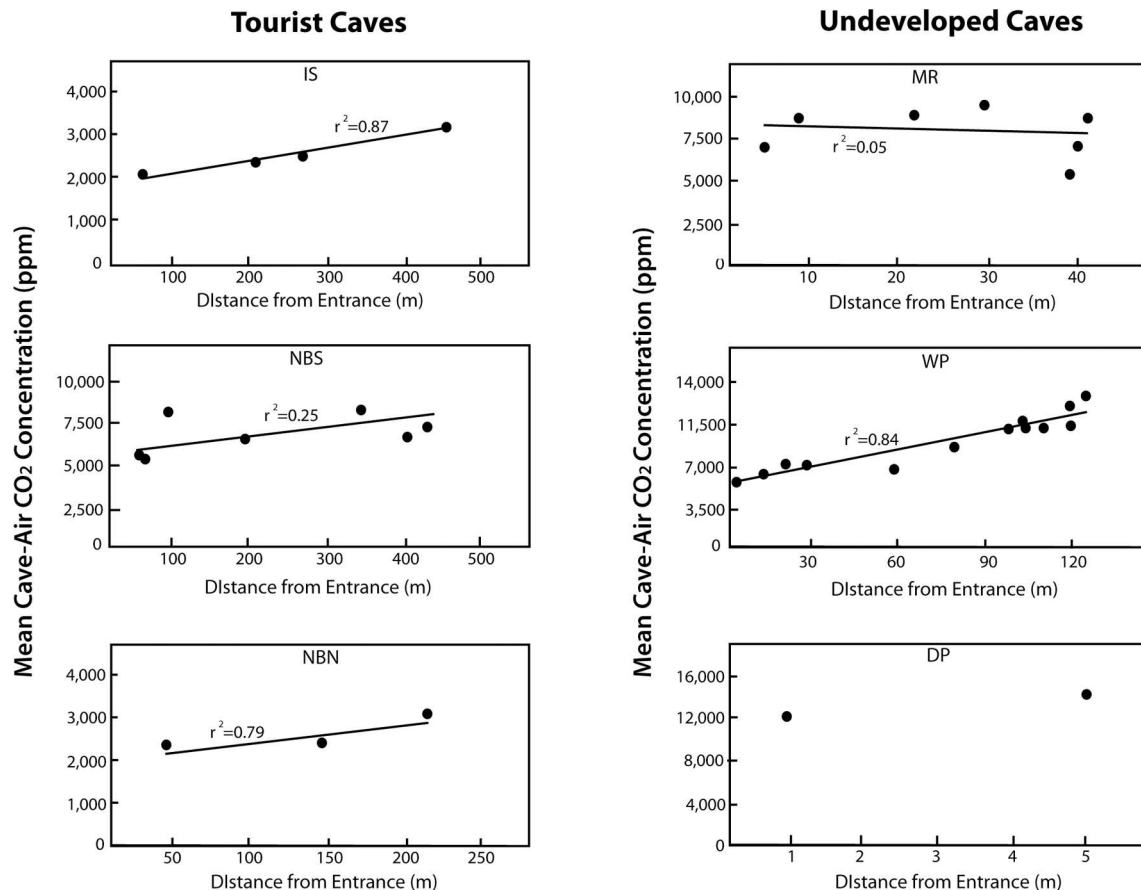

Figure 6. Mean CO$_2$ concentration measured at each station versus distance from the cave entrance. IS refers to Inner Space Cavern, NBS and NBN are the parts of Natural Bridge Cavern, MR is Maple Run Cave, WP is Whirlpool Cave, and DP is District Park Cave. No statistically valid r^2 value can be presented for District Park, as there are only two stations within the cave.

visitation cannot be dismissed as a significant source of CO_2 in the tourist caves without closer examination. Visitation to all three tourist caves reaches a maximum during the summer, when cave-air CO_2 levels are most elevated. There are, however, two key observations that suggest visitor respiration is not the primary control on seasonal CO_2 fluctuations. Visitation rates peak in March and July each year, but CO_2 concentrations remain elevated throughout the summer and not in March; and the highest CO_2 concentrations occur in Natural Bridge South, the least visited tourist cave (Banner et al., 2007). These lines of evidence suggest that the seasonal CO_2 fluctuations observed in the tourist caves are indeed a natural phenomenon and not due to visitation.

It is also important to note that the tourist caves use ventilation fans to remove some of the CO_2-rich air from the caves during the summer months. No detailed record of fan usage exists, but preliminary data from logging CO_2 meters installed in both caves exhibit high summertime cave-air CO_2 concentrations with no intermittent excursions to near atmospheric values. Although diurnal CO_2 fluctuations >500 ppm were routinely detected, the maximum CO_2 concentrations were measured during the afternoon hours, when fans were typically turned on. The lowest CO_2 concentrations were typically measured during the overnight hours, when the ventilation fans were typically not in use. This suggests that CO_2 inputs are sufficient to maintain elevated concentrations throughout the warmer months, even though ventilation fans undoubtedly remove CO_2-rich air from the caves. Similar diurnal patterns were observed in all undeveloped caves for which logging meters were deployed.

There was significant variety in the magnitude of seasonal cave-air CO_2 fluctuations (Fig. 4), but seasonal weather patterns cannot explain the inter-cave variability. All of the caves are located within 130 km of each other and experience similar seasonal weather patterns. Additionally, the three undeveloped caves are located within 5 km of each other and experience nearly identical seasonal and storm-scale weather patterns, yet the magnitude and exact timing of CO_2 fluctuations within these caves are not identical, suggesting that some site-specific parameters play a role in cave ventilation.

SITE-SPECIFIC CONTROLS OF CAVE-AIR CO_2

Soil thickness does not appear to be an important control on cave-air CO_2 variability in the study area. If soil thickness were an important control on cave-air CO_2 concentrations, we would expect to see variations in the average CO_2 concentrations at monitoring stations that are overlain by thicker soils relative to other stations in the same cave. At Inner Space, sites ISHW and ISST (Fig. 3) are overlain by engineered fill that is several meters thick and sites ISDC and ISLM are overlain by much thinner soils (approximately 26 cm; Table 1). If soil thickness were an important control on cave-air CO_2 variability at Inner

Space, there would likely be a weaker correlation between CO_2 concentration and distance from the cave entrance due to the highly variable soil thickness above the cave. Instead, there is a strong correlation ($R^2 = 0.87$) between average CO_2 concentration and distance from the entrance (Fig. 6).

The large differences in peak CO_2 concentrations at the caves shown in Table 1 also suggest that soil thickness is not a major control on cave-air CO_2 concentrations in the study area. Soil type and thickness (Table 1) and extent of vegetative cover are relatively uniform across the study sites, with the exception of Inner Space, but peak CO_2 concentrations vary by more than 30,000 ppm between caves. This is best illustrated by comparing the north and south parts of Natural Bridge Cavern. Vegetative cover and soil type and thickness are nearly identical above both caves (33 cm at Natural Bridge South and 34 cm at Natural Bridge North), and the caves are located adjacent to one another. Nevertheless, peak CO_2 values in the north cave did not exceed 10,000 ppm at any site, while peak CO_2 values in the south cave consistently exceeded 20,000 ppm during the summer months of 2006 and were consistently higher than the CO_2 concentrations in the north cave the following two summers (Fig. 4). It is important to note that these two caves are overlain by different amounts of impervious cover (approximately 10% of Natural Bridge South and 20% of Natural Bridge North), which could account for some of the difference in peak CO_2, but probably not the magnitude observed.

The data suggest that cave volume is an important control on the magnitude of seasonal cave-air CO_2 fluctuations. With the notable exception of Natural Bridge South during the summer of 2006, peak CO_2 concentrations in the tourist caves were significantly lower than those in the undeveloped caves (Table 1). The large passages in the tourist caves imply a greater volume of cave under a given area of the surface, so larger caves will require a greater flux of CO_2 per unit of surface area to achieve the same magnitude increase in CO_2 concentration as a smaller cave. The soils in the study area are all similar in composition and thickness, so it is likely that the amount of CO_2 production per unit area above each cave is similar. The tourist caves might have a greater flux of CO_2 into them compared to the undeveloped caves, but the volumes of the tourist caves relative to their surface footprints are much greater; and therefore, the flux of CO_2 into the tourist caves per unit volume may actually be less than the flux of CO_2 per unit volume in the undeveloped caves. Cave-air CO_2 concentrations in the smaller, undeveloped caves rarely dropped below 4,000 ppm, the threshold above which Banner et al. (2007) noticed a significant decrease in calcite growth. This suggests that smaller caves may have higher cave-air CO_2 concentrations on average, leading to less speleothem growth than larger caves located in the same region.

In the study area, cave geometry is influenced by stratigraphy (Russell, 2007; Hauwert, 2009). For example,

much of Maple Run Cave is within units that are more conducive to cave formation via leaching and collapse (Rose, 1972), and mean CO_2 concentration is better correlated with depth of the monitoring stations than distance from the entrance (Table 1). The better correlation with depth might be attributed to the ease with which air can circulate through the rock units in which the cave is formed. Much of the cave consists of connected voids in a collapsed rubble pile (Fig. 2). Airflow through the subsurface at Maple Run is likely not only through the known cave passages, but also through the void spaces within the rubble pile that surrounds much of the cave.

Initial results from high frequency monitoring at Inner Space, Maple Run, and Whirlpool verify that strong seasonal CO_2 fluctuations do occur in the caves monitored with the exception of Maple Run, which did not experience seasonal cave-air CO_2 fluctuations, but did experience large diurnal CO_2 fluctuations (Cowan et al., 2009). The lack of seasonal fluctuations in Maple Run can be attributed to diurnal ventilation of the cave caused by barometric-pressure fluctuations and its porous geologic situation. Airspeed measurements taken at the cave reveal that a volume of air nearly 15 times greater than the volume of known passage flows from it during a 9-hour period. These daily ventilation patterns in Maple Run appear to be due to the global atmospheric tide (Melcior, 1983; Wallace and Hobbs, 2006) that has been shown to affect cave meteorology (e.g., Sondag et al., 2003; Bourges et al., 2006). The apparent seasonality of cave-air CO_2 data taken in Maple Run for this study that appear in Figure 4 can be attributed to the timing of cave ventilation caused by seasonal shifts in the atmospheric tide and the timing of the visits, which typically occurred between 12:00 and 15:00 CST. Initial results from logging CO_2 meters confirm that CO_2 concentrations in Inner Space and Whirlpool do fluctuate both seasonally and diurnally. Logging CO_2 meters were only deployed in Natural Bridge North for two months and recorded diurnal CO_2 fluctuations there as well.

In contrast to Maple Run, Whirlpool, Inner Space, and Natural Bridge North are formed in stratigraphic units known for lateral cave development (Hauwert, 2009), and CO_2 concentrations in these caves is well correlated with distance from the entrance (Fig. 6). It is important to note that the undeveloped caves are in different stratigraphic units than the tourist caves (Fig. 2), and it is likely that the stratigraphic characteristics of the hosting and overlying units affect the ventilation and CO_2 inputs of the caves. Therefore, it is possible that the smaller seasonal cave-air CO_2 fluctuations in the tourist caves could be attributed to the stratigraphic units that the caves are located in, not their larger volumes. While the data suggest that stratigraphic control promoting horizontal or vertical development does influence the spatial variability of CO_2 within the caves, more monitoring of a larger number of caves in a wide range of stratigraphic units is needed to fully understand the relative importance of this control on cave-air CO_2.

With the exception of Maple Run Cave (and maybe District Park, for which very limited data are available), cave-air CO_2 concentrations were correlated with distance from the cave entrance (Fig. 6). This is likely related to ventilation efficiency. As cooler outside air flows into a cave, it will come into contact with the cave walls, which remain at a relatively stable temperature year-round. As the denser outside air is continually warmed by the cave walls, its density will decrease and ventilation will become less efficient with distance from the entrance.

IMPLICATIONS FOR SPELEOTHEM PALEOCLIMATE STUDIES

Recent studies have proposed that there is potential for bias in the speleothem paleoclimate record due to changes in deposition rates and drip-water chemistry caused by cave-air CO_2 fluctuations (Spötl et al., 2005; Banner et al., 2007). This bias may affect speleothem proxies such as growth rate and isotope and trace element geochemistry (Baldini et al., 2008; Wong et al., 2011). These studies highlight the need to better understand the causes of cave-air CO_2 fluctuations, on what time scales the fluctuations occur, and whether cave-air CO_2 fluctuations occur on a regional scale or are specific to individual caves. The findings presented herein suggest that seasonal cave-air CO_2 changes are a regional phenomenon caused by seasonal differences in cave ventilation. Elevated CO_2 concentrations were detected in all caves during the warmer months, and lower concentrations during cooler months. This observation implies that even in regions where paleoclimate proxies are reproducible among spatially separated sites in a region, seasonal fluctuations of cave-air CO_2 may cause a seasonal bias in the speleothem paleoclimate record.

Speleothem growth-rate is often used as a proxy for rainfall. It is typically assumed that growth-layer thickness and hiatuses in growth are controlled by drip rate, which is controlled by changes in rainfall (Baker et al., 1993; Genty and Quinif, 1996; Qin et al., 1999; Musgrove et al., 2001; Polyak and Asmerom, 2001). It is likely that this assumption is valid in many instances, but there is evidence that high cave-air CO_2 concentrations can inhibit speleothem growth rates (Banner et al., 2007; Baldini et al., 2008), so the possibility should be considered that a growth rate proxy may be affected by cave-air CO_2 variations.

Cave-air CO_2 fluctuations may also affect the trace-element composition of speleothems, which has also been used as a proxy for rainfall. In caves where trace-element composition in drip water varies seasonally, periods of non-deposition due to high cave-air CO_2 concentrations might cause speleothem calcite composition to be biased toward times when cave-air CO_2 is lower and speleothem growth is faster. Precipitation of calcite from the water upgradient from the point where a speleothem is being

deposited has been shown to affect the concentration of trace elements in speleothem-forming drip water (Fairchild et al., 2006; Mattey et al., 2010; Wong, 2008) and might be reflected in the speleothem record. As modeled by Wong et al. (2011), a speleothem with a pattern of seasonally varying trace-element concentrations due to seasonal cave-air CO_2 fluctuations might be incorrectly interpreted as reflecting changes in rainfall or vadose flow paths.

Carbon and oxygen stable isotope variations are commonly used as proxies for vegetation and rainfall amounts and temperature. Similar to the bias in trace element proxies, stable isotope variations may also preserve a bias that would affect the accuracy of climate interpretations (Baldini et al., 2008). Studies have shown that $\delta^{13}C$ and $\delta^{18}O$ values respond not only to environmental changes, but also to in-cave processes as well. Drip-water may undergo significant kinetic isotope effects due to rapid CO_2 degassing or Rayleigh distillation that causes departures from equilibrium isotope fractionation between HCO_3^- and $CaCO_3$ (Mickler et al., 2004, 2006). Because the rate of drip-water degassing is largely controlled by the difference between the pCO_2 of the drip water and cave air, the magnitude of departure from equilibrium isotope fractionation, may change as cave-air CO_2 concentrations fluctuate. In fact, a study of a modern stalagmite by Mattey et al. (2010) showed that annual growth lamina preserved seasonal $\delta^{13}C$ and $\delta^{18}O$ cycles that were attributed to cave ventilation. If this effect is not accounted for, then changes in the $\delta^{13}C$ and $\delta^{18}O$ composition of speleothems might be incorrectly interpreted as reflecting climatic changes and not in-cave processes.

Although seasonal cave-air CO_2 fluctuations could introduce bias into the speleothem climate record, these fluctuations may also leave seasonal markers in speleothem calcite growth layers, which could greatly increase the resolution of paleoclimate reconstructions. With advances in analytical techniques, such as laser-ablation inductively coupled plasma mass spectrometry, it may be possible to achieve annual or sub-annual resolution from speleothems deposited in caves that experience seasonal CO_2 fluctuations. This is an exciting prospect considering that some speleothem records cover the past 200,000 years (e.g., Wang et al., 2008).

Summary and Conclusions

The results of nearly 150 lateral transects into six caves over three years show that CO_2 concentrations vary seasonally in all of the caves monitored, with peaks in CO_2 concentration in the warmer months and lower concentrations in the cooler months. These seasonal CO_2 fluctuations are attributed to seasonally variable cave ventilation that is controlled by outside temperature fluctuations. Cave-air CO_2 concentrations are lowest in the cooler months due to stronger ventilation. In the cooler months, when the outside air is cooler and denser than the

cave-air, outside air sinks into the cave and mixes with the CO_2-rich cave air, causing a decrease in the cave-air CO_2 concentration. In the warmer months, when the outside air is less dense, cave ventilation becomes much weaker and CO_2 concentrations increase.

Seasonal CO_2 fluctuations in the study area do not appear to be caused by anthropogenic influences such as cave visitation. If anthropogenic influences were controlling seasonal CO_2 fluctuations in the study area, it would be unlikely that seasonal CO_2 fluctuations would occur in the undeveloped caves, as they have not been modified greatly and receive a relatively small number of visitors. Instead, the largest CO_2 fluctuations were observed in the undeveloped caves. The timing of peak CO_2 concentrations in the tourist caves does not coincide with visitation, which peaks in March and July each year. Instead, CO_2 concentrations remain elevated throughout the summer and September. Additionally, the highest CO_2 concentrations occur in Natural Bridge South, the least visited tourist cave.

Seasonal fluctuations occurred regardless of cave volume, geometry, depth, soil thickness, and hosting stratigraphic unit. Significant seasonal CO_2 fluctuations were measured in all caves, but the magnitude of CO_2 fluctuations does appear to be influenced by cave volume and geometry. In general, the peak CO_2 concentrations in the smaller caves were much greater than peak concentrations in the larger caves. Additionally, the caves are located in seven distinct stratigraphic units. Portions of Inner Space are overlain by engineered fill that is several meters thick, but significant CO_2 fluctuations were nevertheless measured there.

It is important to note that the presence of seasonal CO_2 fluctuations does not necessarily indicate that seasonal variations in calcite deposition rates are occurring. The rate of calcite deposition is dependent on the interplay of multiple factors, including temperature, CO_2 concentration, relative humidity, the concentration of calcium in the drip water, and the drip rate. The CO_2 concentration in some caves was seldom below 4,000 ppm, the concentration at which Banner et al. (2007) observed a decrease in calcite precipitation.

To understand modern and ancient changes in speleothem deposition, it is essential that the mechanisms controlling cave ventilation be understood in greater detail. Future research should focus on seasonal and short-term (e.g., diurnal or storm scale) variations in cave ventilation and the influence of ventilation on disequilibrium calcite precipitation or periods of cessation of calcite deposition. It is clear that continuous monitoring with logging CO_2 meters will help address the complexities of cave ventilation.

Acknowledgements

References Cited

Amundson, R.G., and Smith, V.S., 1988, Annual cycles of physical and biological properties in an uncultivated and an irrigated soil in the San Joaquin Valley of California: Agriculture, Ecosystems and Environment, v. 20, p. 195–208. doi:10.1016/0167-8809(88)90111-9.

Atkinson, G.L., 2003, Inner Space Cavern (Laubach Cave) Williamson County, Texas, Texas Speleological Survey.

Atkinson, G.L., 2004, Natural Bridge Caverns Comal County, Texas, Texas Speleological Survey.

Baker, A., Smart, P.L., and Ford, D.C., 1993, Northwest European palaeoclimate as indicated by growth frequency variations of secondary calcite deposits: Palaeogeography, Palaeoclimatology, Palaeoecology, v. 100, p. 291–301. doi:10.1016/0031-0182(93)90059-R.

Baldini, J.U.L., Baldini, L.M., McDermott, F., and Clipson, N., 2006, Carbon dioxide sources, sinks, and spatial variability in shallow temperate zone caves: Evidence from Ballynamintra Cave, Ireland: Journal of Cave and Karst Studies, v. 68, p. 4–11.

Baldini, J.U.L., McDermott, F., Hoffmann, D.L., Richards, D.A., and Clipson, N., 2008, Very high-frequency and seasonal cave atmosphere PCO_2 variability: Implications for stalagmite growth and oxygen isotope-based paleoclimate records: Earth and Planetary Science Letters, v. 272, p. 118–129. doi:10.1016/j.epsl.2008.04.031.

Banner, J.L., Gilfoyle, A., James, E.W., Stern, L.A., and Musgrove, M., 2007, Seasonal variations in modern speleothem calcite growth in Central Texas, U.S.A.: Journal of Sedimentary Research, v. 77, p. 615–622. doi:10.2110/jsr.2007.065.

Batiot-Guilhe, C., Seidel, J.-L., Jourde, H., Hébrard, O., and Bailly-Comte, V., 2007, Seasonal variations of CO_2 and ^{222}Rn in a Mediterranean sinkhole-spring (Causse d'Aumelas, SE France): International Journal of Speleology, v. 36, p. 51–56.

Bourges, F., Genthon, P., Mangin, A., and D'Hulst, D., 2006, Microclimates of l'Aven d'Orgnac and other French limestone caves (Chauvet, Esparros, Marsoulas): International Journal of Climatology, v. 26, p. 1651–1670. doi:10.1002/joc.1327.

Bourges, F., Mangin, A., and D'Hulst, D., 2001, Carbon dioxide in karst cavity atmosphere dynamics: the example of the Aven d'Orgnac (Ardeche): Comptes Rendus de l'Academie des Sciences, Series IIA Earth and Planetary Science, v. 333, p. 685–692.

Buecher, R.H., 1999, Microclimate study of Kartchner Caverns, Arizona: Journal of Cave and Karst Studies, v. 61, p. 108–120.

Cooke, M.J., 2005, Soil formation and erosion in central Texas: Insights from relict soils and cave deposits [PhD thesis]: University of Texas at Austin, 219 p.

Cowan, B.D., Osborne, M.C., and Banner, J.L., 2009, Temporal variability of cave-air CO_2 in central Texas, in Proceedings of the 15th International Congress of Speleology, v. 2, p. 1018–1023.

Crossey, L., Springer, A., Kalstrom, K., Newell, D., Atudorei, V., Fischer, T., and Hilton, D., 2006, CO_2 degassing in high volume springs in the Southern Colorado Plateau region—Understanding deep inputs and geochemical mixing in regional groundwater: Geological Society of America, Rocky Mountain Section Abstracts with Programs, v. 38, no. 6, 5 p.

Daly, E., Oishi, A.C., Porporato, A., and Katul, G.G., 2008, A stochastic model for daily subsurface CO_2 concentration and related soil respiration: Advances in Water Resources, v. 31, p. 987–994. doi:10.1016/j.advwatres.2008.04.001.

Denis, A., Lastennet, R., Huneau, F., and Malaurent, P., 2005, Identification of functional relationships between atmospheric pressure and CO_2 in the cave of Lascaux using the concept of entropy of curves: Geophysical Research Letters, v. 32, L05810, doi:10.1029/2004GL022226.

Ek, C., and Gewelt, M., 1985, Carbon dioxide in cave atmospheres: New results in Belgium and comparison with some other countries: Earth Surface Processes and Landforms, v. 10, p. 173–187. doi:10.1002/esp.3290100209.

Faimon, J., Štelcl, J., and Sas, D., 2006, Anthropogenic CO_2 flux into cave atmosphere and its environmental impact: A case study in the Císařská Cave (Moravian Karst, Czech Republic): Science of the Total Environment, v. 369, p. 231–245. doi:10.1016/j.scitotenv.2006.04.006.

Fairchild, I.J., Frisia, S., Borsato, A., and Tooth, A.F., 2007, Speleothems, in Nash, D.L., and McLaren, S.J., eds., Geochemical Sediments and landscapes, Malden, Mass., Blackwell Publishing, p. 200–245.

Fairchild, I.J., Smith, C.L., Baker, A., Fuller, L., Spötl, C., Mattey, D., and McDermott, F., 2006, Modification and preservation of environmental signals in speleothems: Earth Science Reviews, v. 75, p. 105–152. doi:10.1016/j.earscirev.2005.08.003.

Fernández, P.L., Gutierrez, I., Quindós, L.S., Soto, J., and Villar, E., 1986, Natural ventilation of the Paintings Room in Altamira Cave: Nature, v. 321, p. 586–588. doi:10.1038/321586a0.

Genty, D., and Quinif, Y., 1996, Annually laminated sequences in the internal structure of some Belgian stalagmites; importance for paleoclimatology: Journal of Sedimentary Research, v. 66, p. 275–288. doi:10.1306/D426831A-2B26-11D7-8648000102C1865D.

Hanson, P.J., Edwards, N.T., Garten, C.T., and Andrews, J.A., 2000, Separating root and soil microbial contributions to soil respiration: A review of methods and observations: Biogeochemistry, v. 48, p. 115–146. doi:10.1023/A:1006244819642.

Hauwert, N.M., 2009, Groundwater flow and recharge within the Barton Springs Segment of the Edwards Aquifer, Southern Travis and Northern Hays Counties, Texas [PhD thesis]: University of Texas at Austin. 328 p.

Holland, H.D., Kirsipu, T.V., Huebner, J.S., and Oxburgh, U.M., 1964, On some aspects of the evolution of cave waters: Journal of Geology, v. 72, p. 36–67.

Hoyos, M., Soler, V., Cañaveras, J.C., Sánchez-Moral, S., and Sanz-Rubio, E., 1998, Microclimate characterization of a karstic cave: human impact on micro environmental parameters of a prehistoric rock art cave (Candamo Cave, northern Spain): Environmental Geology, v. 33, p. 231–242. doi:10.1007/s002540050242.

James, E.W., and Banner, J.L., 2007, Preservation bias in speleothem proxy records due to seasonal ventilation of caves: Geological Society of America, Abstracts with Programs, v. 39, no. 6, 583 p.

Kastning, E.H., 1983, Geomorphology and hydrogeology of the Edwards Plateau karst, central Texas [PhD thesis]: University of Texas at Austin. 656 p.

Kowalczk, A.J., and Froelich, P.N., 2010, Cave air ventilation and CO_2 outgassing by radon-222 modeling: How fast do caves breathe?: Earth and Planetary Science Letters, v. 289, p. 209–219. doi:10.1016/j.epsl.2009.11.010.

Liñán, C., Vadillo, I., and Carrasco, F., 2008, Carbon dioxide concentration in air within the Nerja Cave (Malaga, Andalusia, Spain): International Journal of Speleology, v. 37, p. 99–106.

Lloyd, J., and Taylor, J.A., 1994, On the temperature dependence of soil respiration: Functional Ecology, v. 8, p. 315–323.

Mattey, D.P., Fairchild, I.J., Atkinson, T.C., Latin, J.-P., Ainsworth, M., and Durell, R., 2010, Seasonal microclimate control of calcite fabrics, stable isotopes and trace elements in modern speleothem from St. Michaels Cave, Gibraltar, in Pedley, H.M., and Rogerson, M., eds., Tufas and Speleothems: Unravelling the Microbial and Physical Controls, Geological Society of London Special Publications, v. 336, p. 323–344. doi:10.1144/SP336.17.

Maclay, R.W., and Small, T.A., 1976, Progress report on geology of the Edwards Aquifer, San Antonio area, Texas, and preliminary interpretation of borehole geophysical and laboratory data on carbonate rocks: U.S. Geological Survey Open-File Report 76–627, 65 p. plus 5 folded map plates.

Melchior, P.J., 1993, The Tides of Planet Earth (2nd ed.): New York, Pergamon Press, 609 p.

Mickler, P.J., Banner, J.L., Stern, L., Asmerom, Y., Edwards, R.L., and Ito, E., 2004, Stable isotope variations in modern tropical speleothems: Evaluating equilibrium vs. kinetic isotope effects: Geochimica et Cosmochemica Acta, v. 68, p. 4381–4393. doi:10.1016/j.gca.2004.02.012

Mickler, P.J., Stern, L.A., and Banner, J.L., 2006, Large kinetic isotope effects in modern speleothems: Geological Society of America Bulletin, v. 118, p. 65–81. doi:10.1130/B25698.1.

Miotke, F.D., 1974, Carbon dioxide and the soil atmosphere: Abhandlungen zur Karst-Und Höhlenkunde, Reihe A, Speläologie, v. 9, p. 1–49.

Moore, G.W., and Sullivan, N., 1997, Speleology: Caves and the cave environment (3rd ed.), St. Louis, Cave Books, 176 p.

Musgrove, M.L., and Banner, J.L., 2004, Controls on the spatial and temporal variability of vadose dripwater geochemistry: Edwards Aquifer, central Texas: Geochimica et Cosmochimica Acta, v. 68, p. 1007–1020. doi:10.1016/j.gca.2003.08.014.

Musgrove, M., Banner, J.L., Mack, L.E., Combs, D.M., James, E.W., Cheng Hai, and Edwards, R.L., 2001, Geochronology of Late Pleistocene to Holocene speleothems from central Texas: Implications for regional paleoclimate: Geological Society of America Bulletin, v. 113, p. 1532–1543. doi:10.1130/0016-7606(2001)113<1532:GOLPTH>2.0.CO;2.

Perrier, F., and Richon, P., 2010, Spatiotemporal variation of radon and carbon dioxide concentrations in an underground quarry: coupled processes of natural ventilation, barometric pumping and internal mixing: Journal of Environmental Radioactivity, v. 101, p. 279–296. doi:10.1016/j.jenvrad.2009.12.003.

Polyak, V.J., and Asmerom, Y., 2001, Late Holocene climate and cultural changes in the southwestern United States: Science, v. 294, p. 148–151. doi:10.1126/science.1062771.

Qin, Xianguang, Tan, Ming, Liu, Tungsheng, Wang, Xianfeng, Li, Tieying, and Lu, Jinpo, 1999, Spectral analysis of a 1000-year stalagmite lamina-thickness record from Shihua Cavern, Beijing, China, and its climatic significance: The Holocene, v. 9, p. 689–694. doi:10.1191/095968399671019413.

Raich, J.W., and Schlesinger, W.H., 1992, The global carbon dioxide flux in soil respiration and its relationship to vegetation and climate: Tellus, v. 44B, p. 81–99. doi:10.1034/j.1600-0889.1992.t01-1-00001.x.

Rose, P.R., 1972, Edwards Group, Surface and Subsurface, Central Texas, Austin, University of Texas Bureau of Economic Geology Report of Investigations no. 74, 198 p.

Russell, W.H., 1979Whirlpool Cave Travis County, Texas, Barton Underground Research Project.

Russell, W.H., 1988District Park Cave, Dick Nichols District Park, Travis County, Texas, Texas Speleological Survey.

Russell, W.H., 2007, Stratigraphic distribution of cave volume in the Edwards Limestone, Southern Travis County, Texas: Austin Geological Society Bulletin, v. 3, p. 37–42.

Scott, 2000, Maple Run Cave Travis, County Texas, Aggie Speleological Society.

Small, T.A., Hanson, J.A., and Hauwert, N.M., 1996, Geologic Framework and Hydrogeologic Characteristics of the Edwards Aquifer Outcrop (Barton Springs Segment), Northeastern Hayes and Southwestern Travis Counties, Texas, U.S. Geological Survey Water-Resources Investigation Report 96-4306, 21 p.

Sondag, F., van Ruymbeke, M., Soubiès, F., Santos, R., Somerhausen, A., Seidel, A., and P. Boggiani, P., 2003, Monitoring present day climatic conditions in tropical caves using an Environmental Data Acquisition System (EDAS): Journal of Hydrology, v. 273, p. 103–118. doi:10.1016/S0022-1694(02)00362-1.

Spötl, C., Fairchild, I.J., and Tooth, A.F., 2005, Cave air control on drip water geochemistry, Obir Caves (Austria): Implications for speleothem deposition in dynamically ventilated caves: Geochimica et Cosmochemica Acta, v. 69, p. 2451–2468. doi:10.1016/j.gca.2004.12.009.

Troester, J.W., and White, W.B., 1984, Seasonal fluctuations in the carbon dioxide partial pressure in a cave atmosphere: Water Resources Research, v. 20, p. 153–156. doi:10.1029/WR020i001p00153.

Villar, E., Fernandez, P.L., Quindos, L.S., and Soto, J., 1985, Natural temporal evolution of the CO_2 content in the air of the "Paintings Chamber" at Altamira Cave: NSS Bulletin, v. 47, p. 12–16.

Wallace, J.M., P.V. HOBBS, P.V., 2006, Atmospheric Science, an Introductory Survey (2nd ed.) Burlington, Massachusetts, Elsevier Academic Press, 483 p.

Wang, Yongjin, Cheng, Hai, Edwards, R.L., Kong, Xinggong, Shao, Xiaohua, Chen, Shitao, Wu, Jiangyin, Jiang, Xiouyang, Wang, Xianfeng, and An, Zhisheng, 2008, Millennial- and orbital-scale changes in the East Asian monsoon over the past 224,000 years: Nature, v. 451, p. 1090–1093. doi:10.1038/nature06692.

Wong, C., Banner, J.L., and Musgrove, M., 2011, Seasonal dripwater Mg/Ca and Sr/Ca variations driven by cave ventilation: Implications for and modeling of speleothem paleoclimate records, Geochimica et Cosmochimica Acta, v. 75, p. 3514–3529.

HIGH RESOLUTION SEISMIC REFLECTION METHODS TO DETECT NEAR SURFACE TUFF-CAVITIES: A CASE STUDY IN THE NEAPOLITAN AREA, ITALY

Vincenzo Di Fiore[1], Antimo Angelino[1], Salvatore Passaro[1*], and Angelo Bonanno[2]

Abstract: The Neapolitan region of Italy is plagued by the presence of shallow man-made cavities in lithoid tuffs that cause problems for communities because they produce building damages and loss of human lives. A high resolution P-wave seismic-reflection technique was successfully used to define a cavity 6 m by 10 m in horizontal dimensions and with a height of about 6 m located in a tuff layer 10 to 19 m below ground level. Such a cavity was located at Afragola (near Naples) where the local geology is typical of the Neapolitan area. The seismic dataset was acquired by using end-on spread geometry, with 0.25 m spacing for shots and 0.5 m for receivers. The application of band–pass filtering (30–150 Hz) allowed us to remove incoherent noise from the data, while an additional equivalent slope (Vs^{-1}) of 0.005 s m^{-1} cut in the FK transform results in ground-roll noise removal. Both the acquisition and processing methods have been necessary to investigate and define the shape and dimensions of the targeted cavity.

INTRODUCTION

An important problem in civil engineering is the detection of natural and man-made cavities, because they often produce subsurface subsidence and collapses. This problem is particularly frequent when dealing with karst terranes, where natural cavities are formed from rock dissolution. Of course, the detection of cavities is mainly carried out by using geophysical prospecting methods, but the interaction of several factors, such as porosity, groundwater, locally complex geological contexts, and logistics may result in severe uncertainty as to the best choice for geophysical techniques. Electrical-resistivity tomography may be appropriate in dolomitic rocks (e.g., van Schoore, 2002) as well as in masses of flysh (e.g., Pánek et al., 2010), while ground-penetrating radar gives optimal results for shallow cavities in the absence of groundwater (Grandjean and Leparoux, 2004) or in glacial environments (Taurisano et al., 2006). High-resolution seismic-reflection methods can be used to detect shallow cavities. The extreme contrast of elastic properties between a water- or air-filled void and the surrounding rocks provides an excellent reflecting interface. Several authors (Hunter et al., 1984; Branham and Steeples, 1988; Steeples and Miller, 1987, 1990; Miller and Steeples, 1991; Bruno and Rapolla, 1997; Inazaki et al., 2004) applied high resolution reflections of seismic P-waves to detect cavities, including evaluating the risk of an active sinkhole located at 7 m depth in 0.6 m thick coal seam (Miller and Steeples, 1991). Inazaki et al. (2004) successfully applied the seismic-reflection technique to detect cavities smaller than 2 m in diameter located 5 to 10 m in depth.

However, many authors suggest the use of more than one geophysical prospecting technique to reduce the ambiguities inherent in each method (Pueyo-Anchuela et al., 2010; Frumkin et al., 2011).

In the Campanian Region and in the Neapolitan area, in particular, there are several sites characterized by the presence of shallow cavities between 10 and 50 meters in depth in lithoid tuff that was extensively quarried in historical times for building materials. We designed a high-resolution seismic-reflection survey to maximize the potential for detection of the shape and dimensions of a lithoid tuff cavity located at Afragola, Naples. Shallow voids in tuff in urbanized areas are a known problem in the Campanian Plain, and they often produce heavy damages and loss of human lives as a consequence of collapses, such as that at Casalnuovo di Napoli in August 2011, the last fatal event. Cavities are often located in the urban areas and buildings are located above them. Therefore, they represent a clear threat to the stability of the buildings, as can be seen by the large number of edifices damaged by collapse into the cavity underneath. Often the locations of the cavities are unknown, because they are not recorded, location maps are not available, or access holes are concealed. Some cavities are located at small sites in urbanized areas where it is difficult to use geophysical methods such seismic refraction or electrical resistivity. A search for these cavities is important to reduce the risk; and therefore, it is important to develop a non-invasive survey method.

A seismic profile was acquired for this cavity by using specifically adapted parameters to allow for the best result for the investigated area. The result obtained was compared with the theoretical model using the finite

---

* Corresponding Author: salvatore.passaro@cnr.it
[1] Istituto per l'Ambiente Marino Costiero, CNR - Calata Porta di Massa Porto di Napoli, 80 - 80133 Naples – Italy
[2] Istituto per l'Ambiente Marino Costiero, CNR - Sezione di Capo Granitola, Via del Faro, 3 - 91021 Campobello di Mazara (TP) – Italy
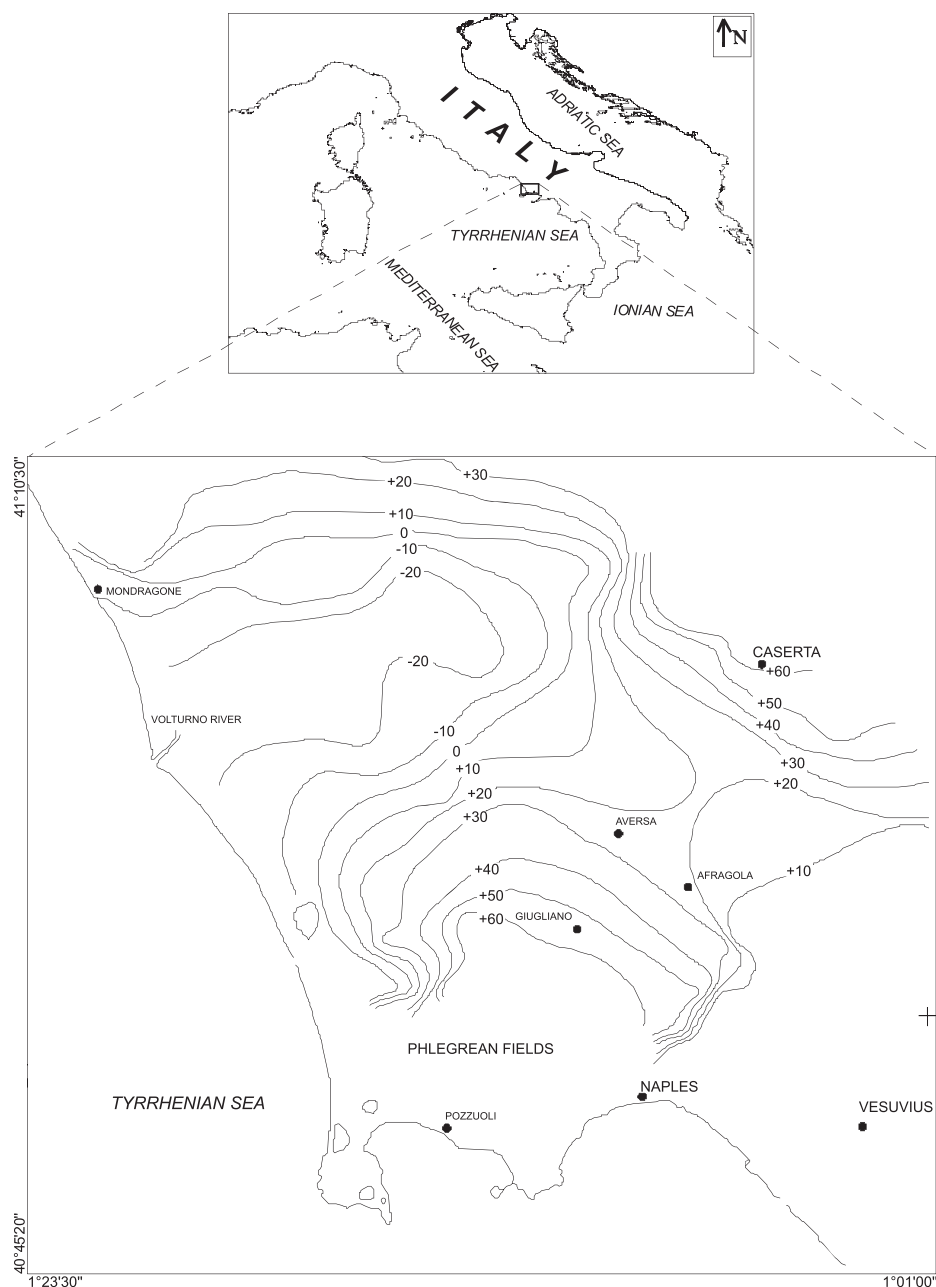
Figure 1. Distribution of the Ignimbrite Campana geological formation, a diffuse lithoid tuff, in the Campanian Plain (modified after Ortolani and Aprile, 1985). Contours are the top of the formation with respect to mean sea level.

differences method (Kelly et al., 1976; Kelly and Marfurt, 1990).

CASE STUDY IN THE NEAPOLITAN AREA

The study area belongs to Roman Volcanic Province (Ghiara et al., 1979), a K-alkaline volcanic area in which the activity started in the late Pliocene and early Pleistocene as a result of a regional strain field along northeast-southwest and, subordinately, northwest-southeast fracture systems. The main products of explosive

events that occurred in this area are the Green Ischia Ignimbrite (age 55 Ka; Vezzoli, 1988), the Ignimbrite Campana (age 39 Ka; De Vivo et al., 2001), and the Neapolitan Yellow Tuff (age 14.5 Ka; Deino et al., 2004).

The Ignimbrite Campana, or Campania Gray Tuff, is a widespread tuff formation (Fig. 1) often outcropping in the Campania Plain. It is located above the transitional marine deposits related to the isotope sub-stage 3.3, dated 55 to 50 ka B.P. (Romano et al., 1994). The Ignimbrite Campana represents the largest volcanoclastic formation of the Quaternary in southern Italy, and it extends over an area
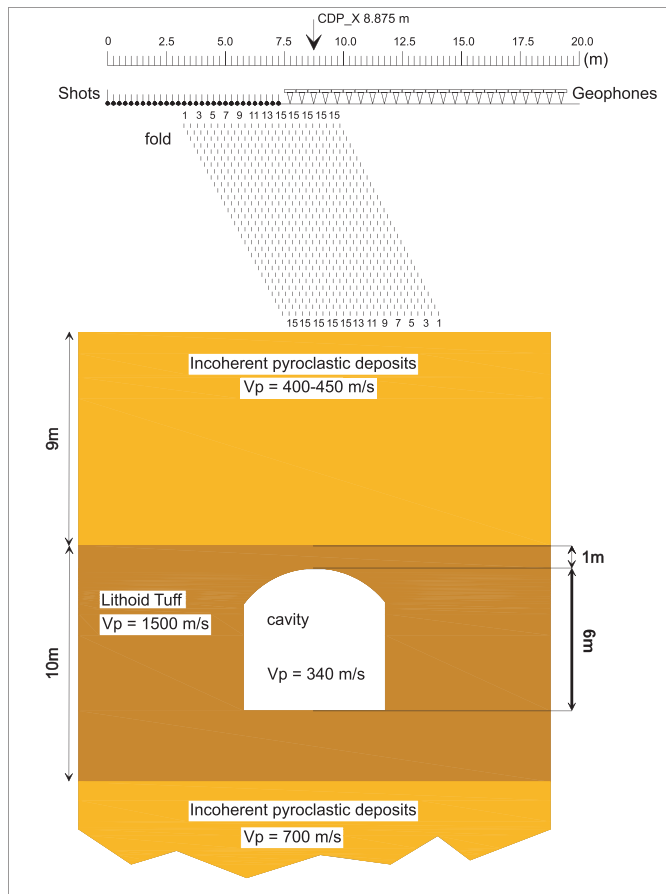
Figure 2. Field geometry and the P-wave velocity profile obtained by seismic downhole survey. The location of the CDP 8.875 m is shown.

of approximately 10,000 km^2. Figure 1 shows the trend of the top of the formation; it increases in depth in the areas surrounding the Campanian Plain towards the Volturno River.

To verify the effectiveness of the high resolution seismic-reflection method, we acquired a seismic dataset on a site with a known cavity. This site was located at Afragola, near Naples, where the local geology is typical of the Neapolitan area.

The cavity was man-made for the extraction of building material, and its presence was known before the seismic survey. Speleologists roughly mapped it. It has a vaulted roof with the top at about 10 m depth, overlain by 1m of lithoid tuff and 9 m of incoherent pyroclastic deposits (Fig. 2). Its horizontal extent is 6 by 10 m, and it is approximately 6 m high (Figs. 2 and 3). The arch of the ceiling is about 1 m deep. It lies in tuff material that has a thickness of 10 m.

The data were recorded by a 24-bit, 24-channel seismograph (Geode-Geometrics) in SEG2 format. An anti-alias filter was applied with a 40 dB/octave roll-off with a −40 dB point of 2000 Hz. A hammer-shaped seismic

source was adopted to reduce the risk related to wave propagation, since the data were recorded inside the city and fairly close to the surrounding buildings. The dataset was acquired using an end-on spread geometry (e.g., Sheriff and Geldart, 1995). The source interval was set to 0.25m, while the receiver spacing was 0.5 m (Fig. 2). The whole data acquisition consisted of thirty shot records. All horizontal distances were converted to the absolute scale of Figure 2. The acquisition parameters are summarized in Table 1. Figure 4 shows four raw shot gathers acquired at the site.

To improve the velocity-analysis control, we also carried out a downhole survey. For this, we utilized a hole of 30m deep conditioned for the borehole test. The equipment consisted of a 24-bit seismograph equipped with double 3D geophones at 10 Hz, arranged in an X-Y-Z pattern separated by 1 m. The two orthogonal, horizontal geophones were used to detect shear-wave (S-wave) arrivals, while the vertical geophone was used to detect compression-wave (P-wave) arrivals. The downhole P-wave source consisted of a hammer and an aluminium plate. To produce an identifiable S wave, the source should transmit energy to the ground with a particle motion transverse to the axis of the survey. We used an impulsive metal-beam S-wave source, a repeatable and reversible source. In the field, we applied a stack of three traces for any record.

Data Processing and Results

Weak features with low frequency and amplitude found in shot records are an indirect indication of the presence of a subsurface cavity. In addition, the presence of a subsurface cavity breaks off a reflected horizon in the seismic section when located near in depth to the reflecting horizon. Figure 5 reports shows the two-step seismic-sequence processing used. The main purposes of the applied processing are to increase the signal-to-noise ratio and the vertical and horizontal resolution. Both horizontal and vertical resolutions are controlled by the spectral content of the seismic signal. We know that the threshold for vertical resolution generally is one quarter of the dominant wavelength (Yilmaz, 1994). Horizontal resolution is how close two reflecting points can be situated horizontally and yet be recognized as two separate points rather than one.

The area that produces the reflection is known as the first Fresnel zone. Two reflecting points that fall within the Fresnel zone are indistinguishable on the seismograms. The Fresnel zone depends on wavelength and depth of the reflecting interface (Yilmaz, 1994).

Data Processing

Preliminary processing was performed to obtain a preliminary stacked section, essential to establishing the main sequence of processing. Our data were processed on a Linux machine using Seismic Unix software of the
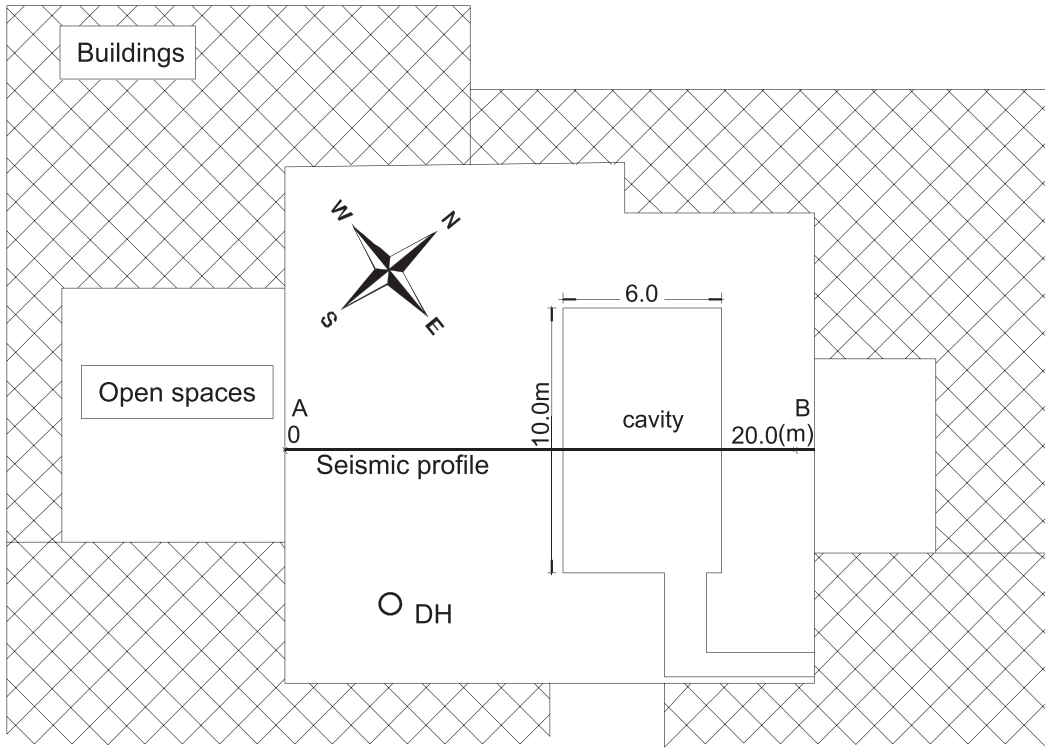
Figure 3. Site map located in Afragola, near Naples. The filled areas indicate the buildings, the white areas are open spaces. DH is the location of the down-hole survey that provided a 1D P-wave velocity field in Figure 2 and Table 2. The approximate outline of the mined cavity is shown, as is the route of the seismic line shown in Figure 2.

Colorado School of Mines (Center for Wave Phenomena, 2007). The processing was carried out using a basic CDP seismic-processing technique. A first check of the dataset was performed to estimate the data's quality. Top and surgical muting were applied to remove noise detrimental to the reflection events. Muting was concentrated in time and offset windows rich in refraction, direct wave, and airwave energy. Even though topography of the acquisition area was flat, the static corrections routine was used to minimize the effects of near-surface irregularities. In this

Table 1. Acquisition parameters P-wave.

Parameter	Specifics
Channels	24
Geophone interval	0.5 m
Geophone type	40-Hz vertical
Shot interval	0.25 m
Number of shots	57
Source	10-kg mallet on vertical steel plate
CDP bin size	0.125 m
Maximum fold	24
Recording system	Geometrics Geode
Sample rate	0.250 ms
Record length	0.50 s

paper, we replaced conventional datuming static time shift correction with wave equation datuming (Dobrin, 1976).

DATA FILTERING

A second-order Butterworth filter (-12 dB) was applied to remove the incoherent low-frequency noise. A bandpass filter was designed by a low cut-off frequency at 30 Hz and a high cut-off frequency at 150 Hz. The filtering was carried out by spectral analysis on the raw trace. An additional frequency wave number (FK) filtering was applied to the dataset to remove the ground roll noise from data, since this feature has low apparent velocity, and thus, can be easily removed in the FK domain. The fundamental parameter in FK filter design is the slope of the velocity that is to be removed or kept. Generally, in this soil type the ground roll has low apparent velocity, about 200 to 300 m/s. For this reason, taking the surface wave velocity Vs as 200 m s^{-1}, we used an equivalent slope (Vs^{-1}) of 0.005 s m^{-1} as the fan filter.

VELOCITY ANALYSIS

Velocity analysis was performed to estimate velocities for normal-move-out correction. Figure 6 represents an 8.875 m CDP_X having a maximum fold of fifteen traces (Fig. 2). The left panel of Figure 6 shows a raw CDP gather, where the ground-roll noise masks both the
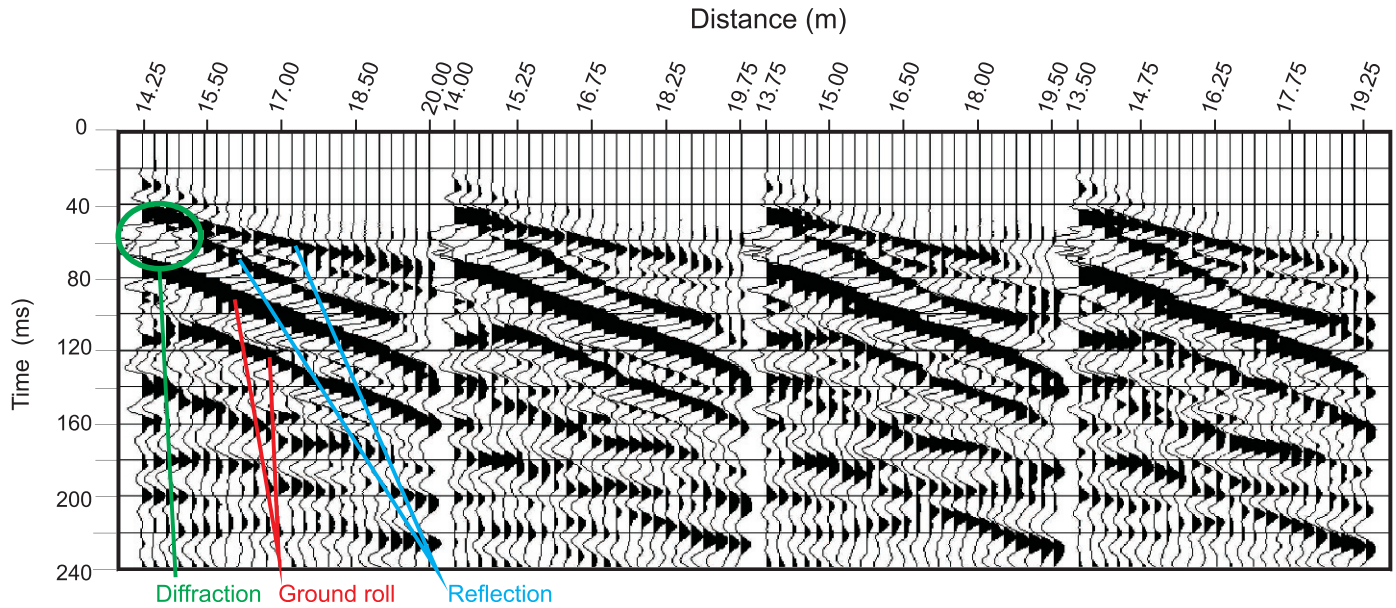
Figure 4. Four CDP gathers of raw data, with examples of direct (ground roll), refracted, and reflected phases. The presence of ground roll at low frequency and low apparent velocity is clear.
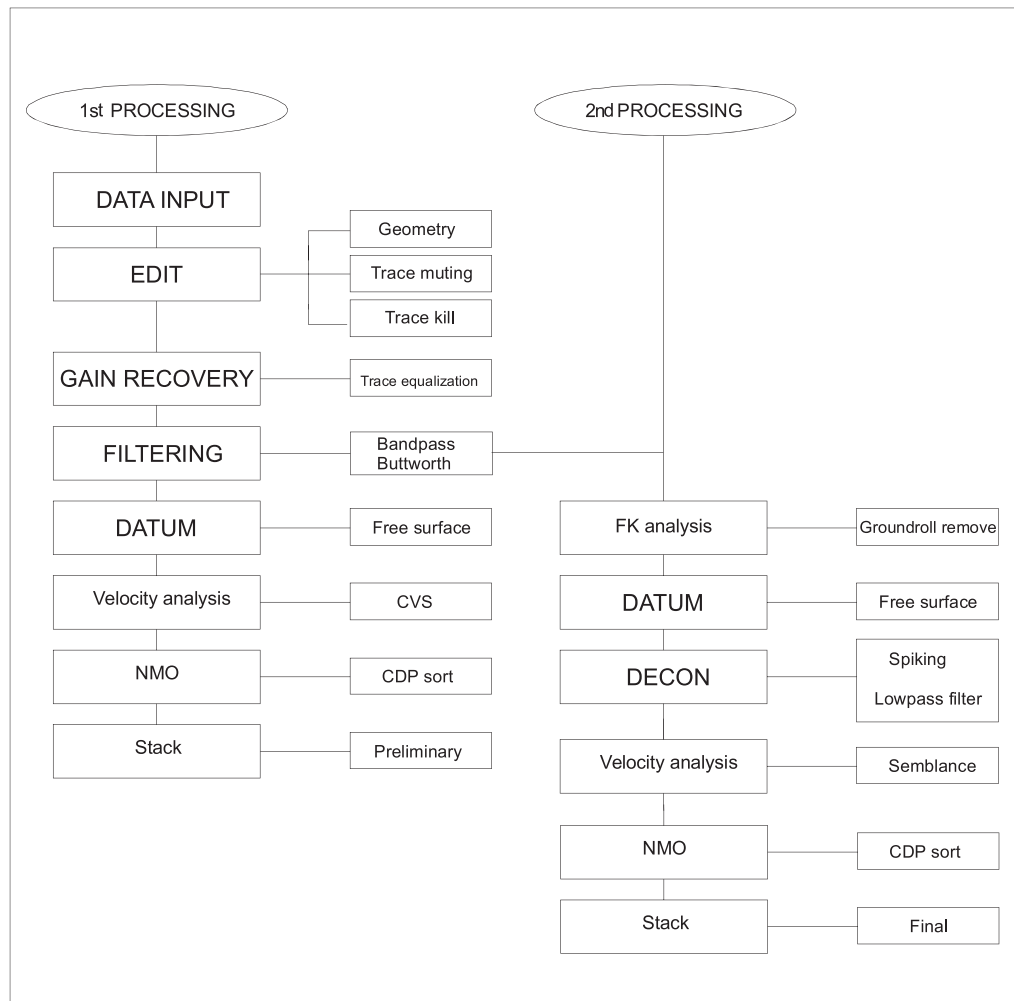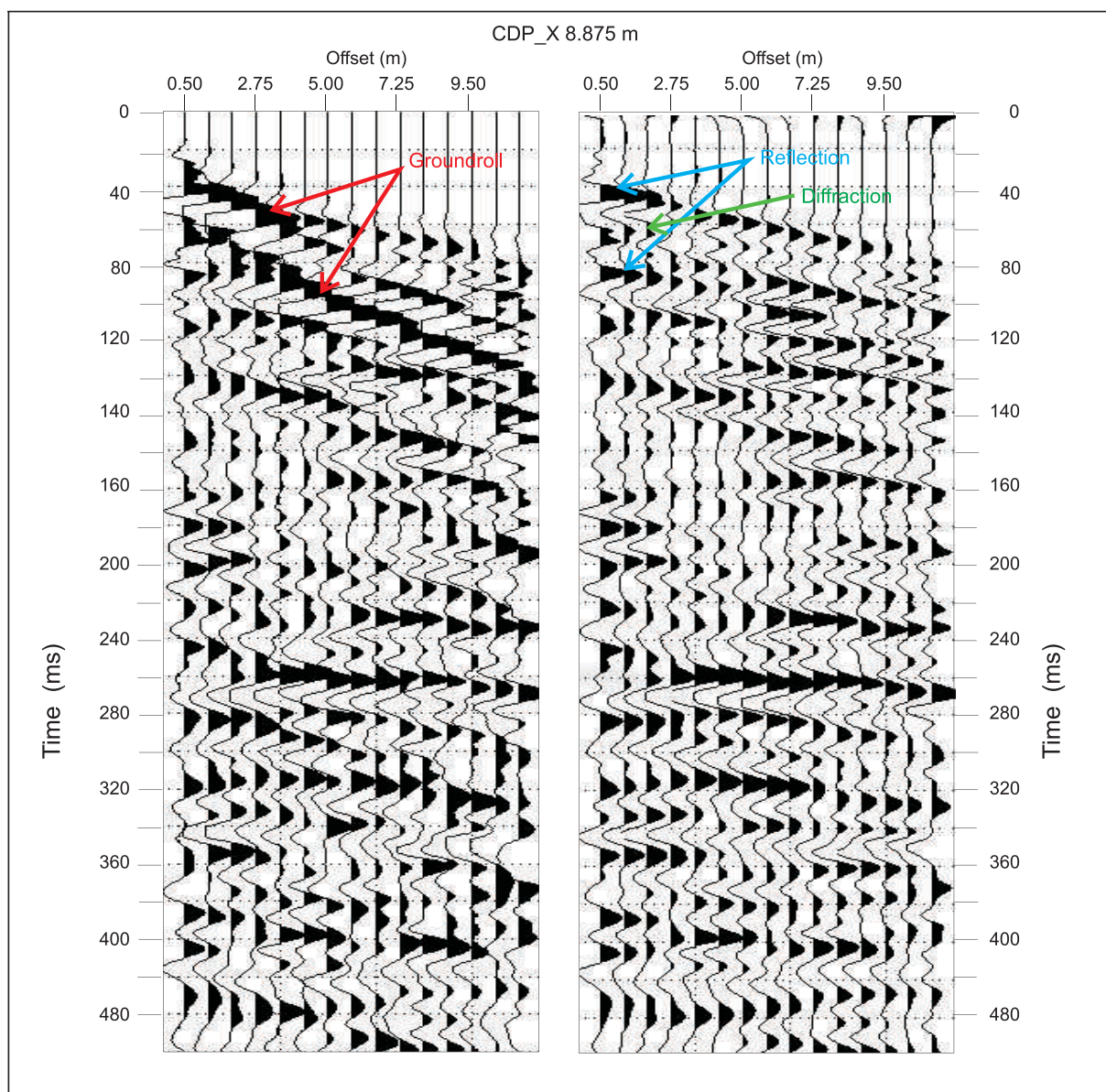

Figure 5. Processing sequences used to obtain the unmigrated final stacked section.

Figure 6. Comparison of CDP_X (8.875 m; fold=15) gather between raw data (on the left) and processed data (on the right). Note the improvement of the CDP_X data shown on the right panel, where is possible to detect the reflection and diffraction phases.

reflections and the diffractions. The right panel of Figure 6 shows the same data after the application of the processing sequence of Figure 5. Because of the higher attenuation of the ground roll, the data appear with a higher signal-to-noise ratio. The velocity was estimated by applying a semblance velocity analysis panel that provided a velocity field similar to the down-hole velocity field (Fig. 7) that was used as a guide to improve the choice of the best coherency peaks in the semblance panel. At this point, an unmigrated stack section was obtained that clearly shows the signal-to-noise ratio increasing due to the processing sequence applied (Fig. 8). In this stacked section, the diffraction is located at the CDP_X 8.875 m and at about 40 ms Two Way Time (TWT).

FORWARD MODELLING

A seismic forward modeling method was applied to the velocity model of Figure 2 to compare the field data with the theoretical data. The main advantage of using finite-difference methods in seismic modeling is that they produce the complete wave field. The different wave-types (reflections, refractions, etc.) generally will appear in the computed solution with correct amplitudes and phases.

The finite difference method is a numerical method for solving partial differential equations, and it can be applied to seismic motion to compute the displacement at any point in the given geological model (Kelly et al., 1976). It can be applied both at the ground surface, for generating synthetic seismograms to be used for comparison with
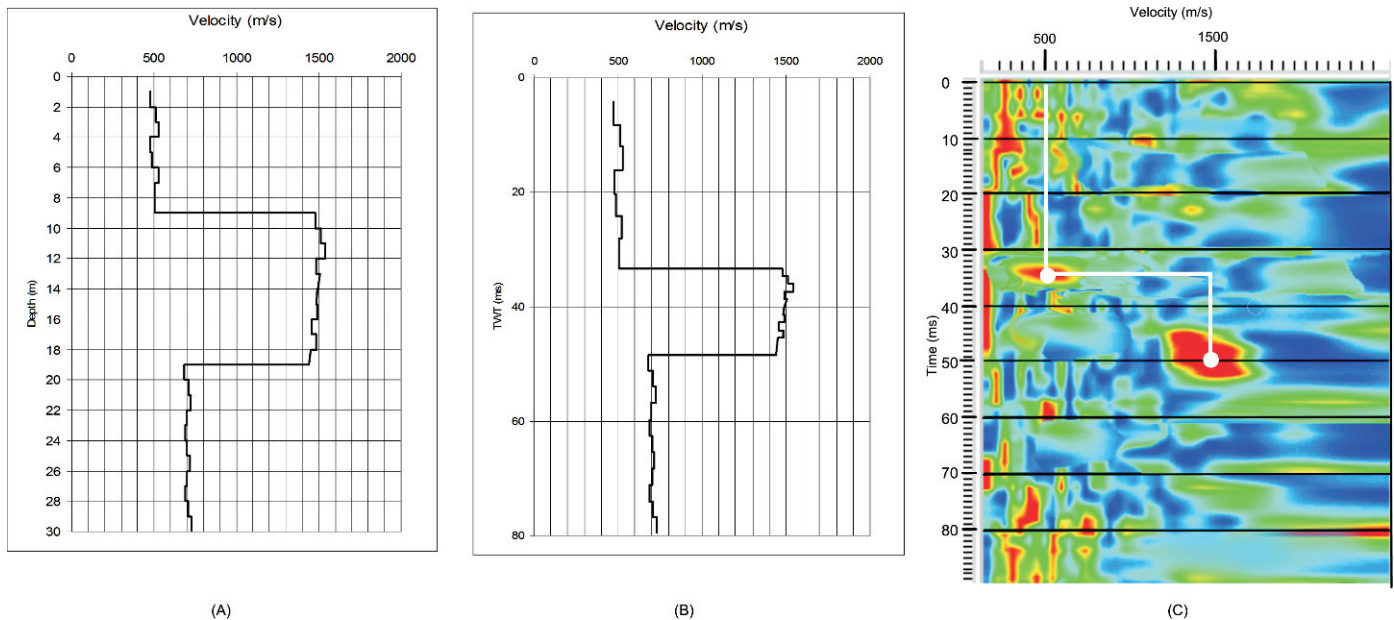
Figure 7. (A) Downhole velocity interval; (B) downhole velocity interval converted to TWT; (C) Semblance function for the CDP_ 8.875. Note the good quality of the velocity spectrum with respect to the downhole (TWT) velocity profile. CDP_8.875 location is also shown in Figure 2.

recorded data, and at depths, for doing wave-field extrapolation or downward continuation. The code used to obtain the forward modeling was slightly modified from the one proposed by Kelly and Marfurt (1990). In the analysis, we used the same geometry and sorted parameters. Table 3 reports the parameters used to carry out the synthetic seismic section of Figure 9.

Because of the small source interval (0.25 m), the diffraction move-out is very small and the ground roll is almost absent. In fact, the ground roll is present at low frequency (i.e., at low wave number). Figure 9 illustrates the unmigrated stacked section obtained by using the synthetic dataset. We can see a clear similarity with the stacked section of Figure 8, with a diffraction located in correspondence of the CDP_X 8.875 m and at 40 ms TWT.

Discussion and Conclusions

The aim of this research was to locate shallow cavities located in a lithoid tuff layer characterized by a strong contrast in terms of acoustic impedance. The application of the processing sequence was essential to locate the diffraction hyperbola caused by the cavity, because it doesn't appear clearly in the raw data (Fig. 8). A diffraction located over this horizon at about 40 ms TWT, and identifiable thanks to the presence of hyperbolic feature on the stacked section, is related to the presence of the cavity located at 10 m depth below ground level. To validate our results, the experimental data were compared with a theoretical section obtained by synthetic data (see Table 3). To obtain the synthetic seismic section, we used the model

and the field velocity obtained by a down hole survey in Figure 7, and reported in Table 2. The features related to the diffraction hyperbolas in the theoretical and experimental data have a similar character on the unmigrated stacked sections. There is only a small horizontal shift when comparing the theoretical and experimental data, probably due to slight horizontal velocity variation. The void related to the cavity was well represented on the seismic section; and therefore, the high resolution seismic-reflection method can be useful for detection of cavities located in lithoid tuff material.

To make this detection possible, however, specific techniques must be employed. These are: 1) a short geophone spacing, which helps to improve data filtering and results in a better reduction of the ground roll signal and also helps to decrease CDP distance; 2) a short distance between shots, which increases the fold; 3) high-frequency detectors, which reduce ground-role power and increase signal resolution; 4) a 24-bit resolution seismograph; 5) adequate data processing, which should include the choice of optimal frequency and FK filters, in our case the adoption of an equivalent slope 0.005 s m^{-1} cut in the FK transform that resulted in successful ground-roll noise removal; and 6) whenever possible, the application of forward modeling to compare experimental with theoretical data and strengthen the obtained results.

Although the data clearly show the cavity, the void signal appears essentially as a perturbation on a stronger reflection, and thus, it is relatively subtle if compared to the background geology. Thus, seismic reflection is shown to be a suitable method for the detection of cavities in
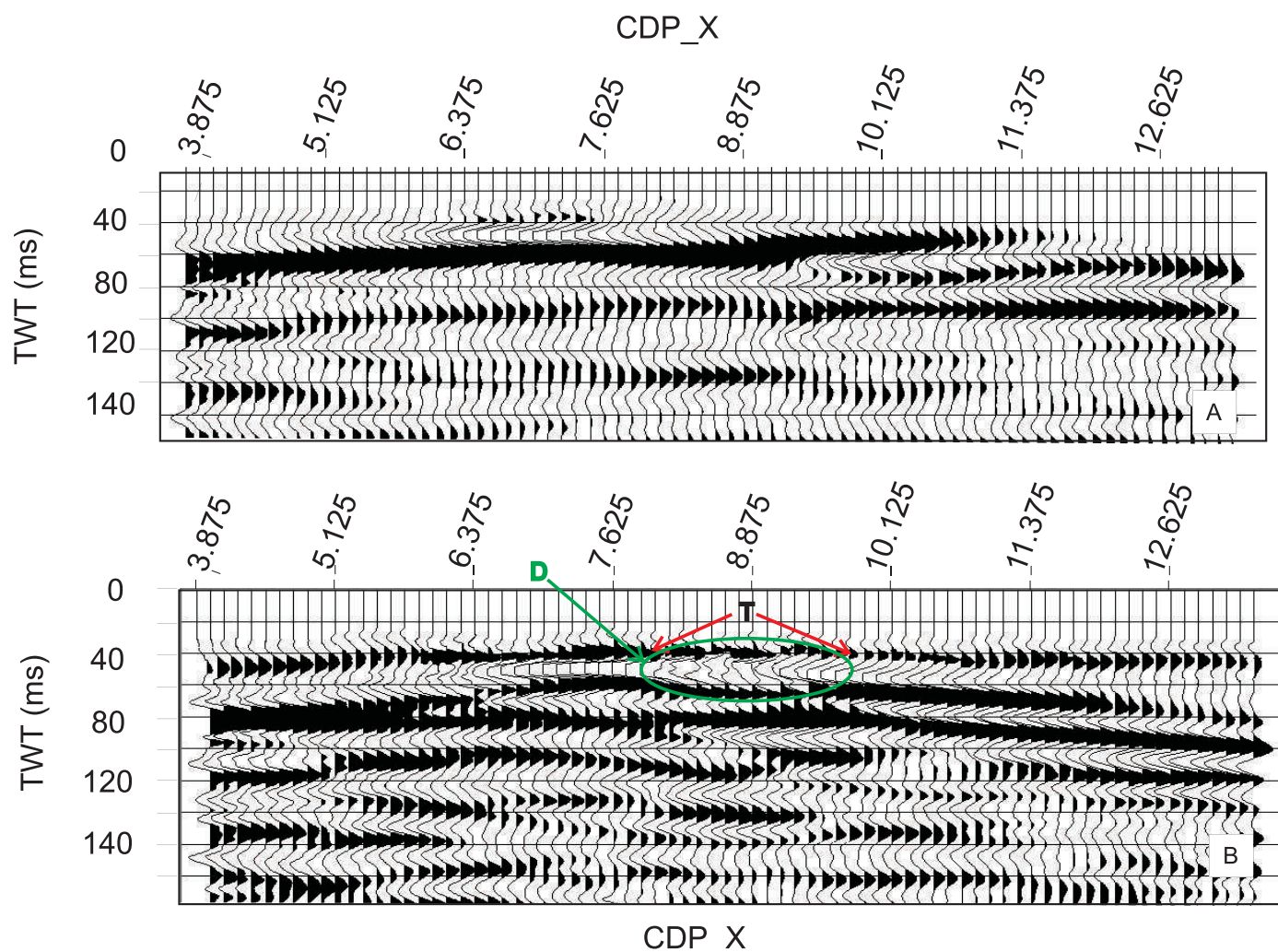
Figure 8. Unmigrated stacked section of field data before (A) and after (B) the application of the adopted processing sequences. The T horizon is related to the top of the lithoid tuff layer. Diffraction patterns D appear at about 40 ms TWT. Such hyperbole is due to the cavity presence. We can see that high amplitude diffraction occur between the CDP_X 6.375 and 10.125 m.
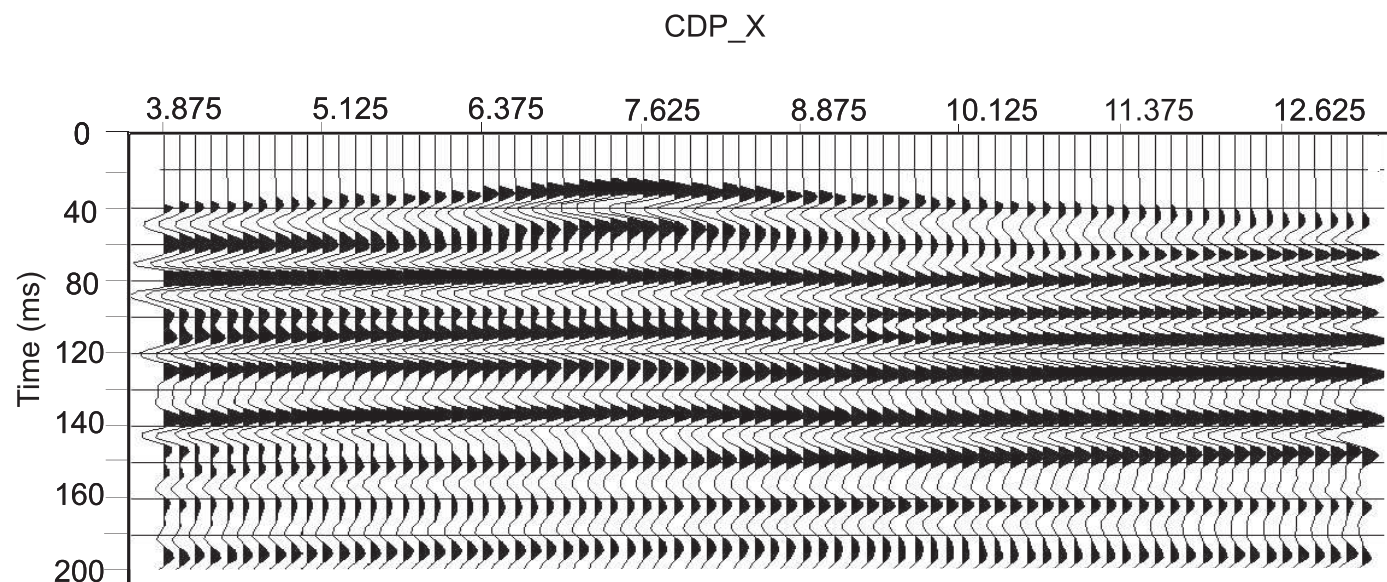

Figure 9. Unmigrated stacked section of synthetic data. It is very similar to the stacked section of field data (Fig. 8).

Table 2. Wave velocities determined from downhole data and also used in the calculation of the synthetic data in Figure 9.

Depth, m	P-wave velocity, m s^{-1}
0.00–1.50	400
1.50–9.00	450
9.00–19.00	1500
19.00– •••	700

Table 3. Parameters used to carry out the synthetic seismic section.

Boundary Condition at Interfaces	Reflecting
Depth of field for modelling	20 m
Type source	Point source model
Windows time length	500 ms
Type of source wavelet	Minimum phase Ricker
Fundamental frequency Peak Richer	50 Hz
Grid factor for step in finite difference	0.5 ms

locations where voids occur in relatively homogeneous background materials, but voids may be difficult to resolve if host rock has other heterogeneities.

REFERENCES

Branham, K.L., and Steeples, D.W., 1988, Cavity detection using high-resolution seismic-reflection methods: Mining Engineering, v. 40, p. 115–119.

Bruno, P.P., and Rapolla, A., 1997, Location of cavities buried in the Neapolitan Yellow Tuff using the seismic reflection method: Bollettino di Geofisica Teorica e Applicata, v. 38, no. 1–2, p. 25–40.

Center for Wave Phenomena, 2007, Seismic Unix (SU) Release 40, Golden, Colorado School of Mines.

De Vivo, B., Rolandi, G., Gans, P.B., Calvert, A., Bohrson, W.A., Spera, F.J., and Belkin, H.E., 2001, New constraints on the pyroclastic eruptive history of the Campanian volcanic Plain (Italy): Mineralogy and Petrology, v. 73, p. 47–65. doi:10.1007/s007100170010.

Deino, A.L., Orsi, G., de Vita, S., and Piochi, M., 2004, The age of the Neapolitan Yellow Tuff caldera-forming eruption (Campi Flegrei caldera – Italy) assessed by ^{40}Ar/^{39}Ar dating method: Journal of Volcanology and Geothermal Research, v. 133, p. 157–170. doi:10.1016/S0377-0273(03)00396-2.

Dobrin, M.B., 1976, Introduction to Geophysical Prospecting, third edition, McGraw-Hill, 630 p.

Frumkin, A., Ezersky, M., Al-Zoubi, A., Akkawi, E., and Abueladas, A.-R., 2011, The Dead Sea sinkhole hazard: Geophysical assessment of salt dissolution and collapse: Geomorphology, v. 134, no. 1–2, p. 102–117. doi:10.1016/j.geomorph.2011.04.023.

Ghiara, M.R., Lirer, L., and Munno, R., 1979, Mineralogy and geochemistry of the "low-potassium series" of the Campania volcanics (south Italy): Chemical Geology, v. 26, no. 1–2, p. 29–49. doi:10.1016/0009-2541(79)90028-7.

Grandjean, G., and Leparoux, D., 2004, The potential of seismic methods for detecting cavities and buried objects: experimentation at a test site: Journal of Applied Geophysics, v. 56, no. 2, p. 93–106. doi:10.1016/j.jappgeo.2004.04.004.

Hunter, J.A., Pullan, S.E., Burns, R.A., Gagne, R.M., and Good, R.L., 1984, Shallow seismic reflection mapping of the overburden-bedrock interface with the engineering seismograph - some simple techniques: Geophysics, v. 49, p. 138 l–1385. doi:10.1190/1.1441766.

Inazaki, T., Yamanaka, Y., Kawamura, S., and Tazawa, O., 2004, High-resolution seismic reflection survey using Land Streamers for near-surface cavity detection, Proceedings of 7th SEGJ International Symposium, Sendai, Japan, p. 475–480.

Kelly, K.R., and Marfurt, K.J., eds., 1990, Numerical Modeling of Seismic Wave Propagation, Tulsa, Oklahoma, Society of Exploration Geophysicists, 525 p.

Kelly, K.R., Ward, R.W., Treitel, S., and Alford, R.M., 1976, Synthetic seismograms: a finite-difference approach: Geophysics, v. 41, p. 2–27. doi:10.1190/1.1440605.

Miller, R.D., and Steeples, D.W., 1991, Detecting voids in a 0.6-m coal seam, 7 m deep, using seismic reflection: Geoexploration, v. 28, p. 109–119. doi:10.1016/0016-7142(91)90043-C.

Ortolani, F., and Aprile, F., 1985, Principali caratteristiche stratigrafiche e strutturali dei depositi superficiali della Piana Campana: Bollettino della Società Geologica Italiana, v. 104, no. 2, p. 195–206.

Pánek, T., Margielewski, W., Tábořík, P., Urban, J., Hradecký, J., and Szura, C., 2010, Gravitationally induced caves and other discontinuities detected by 2D electrical resistivity tomography: Case studies from the Polish Flysch Carpathians: Geomorphology, v. 123, no. 1–2, p. 165–180. doi:10.1016/j.geomorph.2010.07.008.

Pueyo-Anchuela, Ó., Casas-Sainz, A.M., Soriano, M.A., and Pocoví-Juan, A., 2010, A geophysical survey routine for the detection of doline areas in the surroundings of Zaragoza (NE Spain): Engineering Geology, v. 114, p. 382–396. doi:10.1016/j.enggeo.2010.05.015.

Romano, P., Santo, A., and Voltaggio, M., 1994, L'evoluzione geomorfologica della pianura del Fiume Volturno (Campania) durante il tardo Quaternario (Pleistocene medio-superiore–Olocene): Il Quaternario, v. 7, no. 1, p. 41–56.

Sheriff, R.E., and Geldart, L.P., 1995, Exploration Seismology, second edition, Cambridge, Cambridge University Press, 628 p.

Steeples, D.W., and Miller, R.D., 1987, Direct detection of shallow subsurface voids using high-resolution seismic-reflection techniques, in Beck, B.F., and Wilson, W.L., eds., Karst Hydrogeology: Engineering and Environmental Applications, Boston, Balkema, p. 179–183.

Steeples, D.W., and Miller, R.D., 1990, Seismic-reflection methods applied to engineering, environmental, and ground-water problems, in Ward, S., ed., Geotechnical and Environmental Geophysics, V. 1, Review and Tutorial, Society of Exploration Geophysicists, Investigations in Geophysics No. 5, p. 1–30.

Taurisano, A., Tronstad, S., Brandt, O., and Kohler, J., 2006, On the use of ground penetrating radar for detecting and reducing crevasse-hazard in Dronning Maud Land, Antarctica: Cold Regions Science and Technology, v. 45, p. 166–177. doi:10.1016/j.coldregions.2006.03.005.

van Schoor, M., 2002, Detection of sinkholes using 2D electrical resistivity imaging: Journal of Applied Geophysics, v. 50, p. 393–399. doi:10.1016/S0926-9851(02)00166-0.

Vezzoli, L., ed., 1988, Island of Ischia, Quaderni di Ricerca CNR 114, 133 p.

Yilmaz, Ö., ed., 1994, Seismic Data Processing, Tulsa, Oklahoma, Society of Exploration Geophysicists, Investigations in Geophysics no. 2, 529 p.

CHAETASPIS ATTENUATUS, A NEW SPECIES OF CAVERNICOLOUS MILLIPED FROM ARKANSAS (DIPLOPODA: POLYDESMIDA: MACROSTERNODESMIDAE)

JULIAN J. LEWIS[1] AND MICHAEL E. SLAY[2]

Abstract: This description of *Chaetaspis attenuatus,* new species, from two caves in northern Arkansas brings the total species assigned to the genus to six. *Chaetaspis attenuatus* occurs approximately 100 kilometers to the southeast of its sister species *C. aleyorum* that occurs in southwestern Missouri.

INTRODUCTION

Five species have been assigned to the genus *Chaetaspis*, a group of minute millipeds occuring in caves and edaphic habitats in the eastern United States (Lewis, 2002). The genus was erected by Bollman (1887) for *Chaetaspis albus*, which he described from an unspecified locality in Bloomington, Monroe County, Indiana, and subsequently reported from a locality in Little Rock, Arkansas (Bollman 1888). Bollman's description did not include illustrations of the gonopods, a deficiency that was rectified by Lewis (2002), who examined material from Indiana, Kentucky, Tennessee, Alabama, Mississippi, and Virginia.

Antriadesmus fragilis was described by Loomis (1943) from a female specimen collected in White's Cave, Mammoth Cave National Park, Kentucky. Causey (1959) described *A. debilis* from material collected in Walker Spring Cave, Wayne County, Tennessee, and *A. mollis* from Cumberland Caverns, Warren County, Tennessee. Hoffman (1979) synonymized *Antriadesmus* with *Chaetaspis* and placed the genus in the family Macrosternodesmidae based on gonopod similarities. These cavernicolous species remain poorly known, although *C. mollis* was found in Camps Gulf Cave, Van Buren County (Lewis, 2002), and *C. fragilis* was reported from a cave in Pulaski County, Kentucky (Lewis and Lewis, 2005).

Causey (1950) also described *Chaetaspis ohionis*, but this species remains somewhat of a mystery. The type material was apparently lost and Hoffman (1999) stated that the species was not a *Chaetaspis*, and possibly not even correctly placed in the same family.

Lewis (2002) described the first cavernicolous species of the genus from the Ozarks, *Chaetaspis aleyorum*, from Tumbling Creek Cave, Taney County, Missouri.

In this paper the term *exomere* adopted by Shear et al. (2009) from Djursvoll (2008) is followed and applied to the part of the gonopod called the ''posterior prefemoral process'' by Lewis (2002) and ''process B'' of Shear and Shelley (2007, 2008).

The species below from northern Arkansas is the second cavernicolous *Chaetaspis* species described from the Ozark Plateau physiographic province.

Order Polydesmida Pocock, 1887
Family Macrosternodesmidae Brölemann, 1916
Chaetaspis attenuatus Lewis, new species
Figs. 1–5
Antriadesmus sp.—McDaniel and Smith, 1976: 59.
Chaetaspis undescribed species 1.—Lewis, 2002: 105, 108.

Material examined—Arkansas: Independence Co., Cushman Cave, approximately 2 km west of Cushman, 5 October 1974, G.L. Harp; same locality, 19 October 1974, V.R. McDaniel; same locality, 9 July 2008, M. Slay, M. D. Kottmyer; Izard Co., Clay Cave, approximately 10 km southwest of Melbourne, 10 July 2008, M. Slay, M. D. Kottmyer. A dissected male from Cushman Cave is the holotype, the other specimens from that locality are paratypes. All specimens deposited in the Florida State Collection of Arthropods, Gainesville.

Diagnosis—Separable from all species assigned to *Chaetaspis,* except *C. aleyorum,* by the solenomere of acropodite tapering to a terminal disc covered with setules and denticles. The gonopod exomere of *C. attenuatus* tapers to a single point in lateral aspect, in contrast to the club-like shape in *C. aleyorum* that increases in size, then is slightly bifurcate apically. The proximal acroprodite is lower, non-alate in anterior or posterior aspect in comparison to the distinctly alate structure in *C. aleyorum*.

Description—Holotype approximately 5.3 mm long, 0.45mm wide, unpigmented, white in appearance, body filiform, approximately 12× as long as wide. Head wider than collum, epicranial suture distinct. Antenna densely setose, article 6 longest, clavate, with row of microsensilla along distal margin, articles 2–4 subequal, about 0.70× as long as article 6, article 7 tapering to apical disc, 4 sensory cones present.

Collum broadly rounded anteriorly (almost semi-circular), subequal in width to segment 2, with transverse rows of setae; segments 3 and 4 slightly smaller than 2 and 5; segment 7 approximately 1.7× length of preceding segment; metatergites with three rows of setae; lateral margins of pregonopodal paranota slightly undulate,

[1] Lewis & Associates LLC, Cave, Karst & Groundwater Biological Consulting, 17903 State Road 60, Borden, IN 47106-8608, lewisbioconsult@aol.com
[2] The Nature Conservancy, 601 North University Avenue, Little Rock, AR 72205
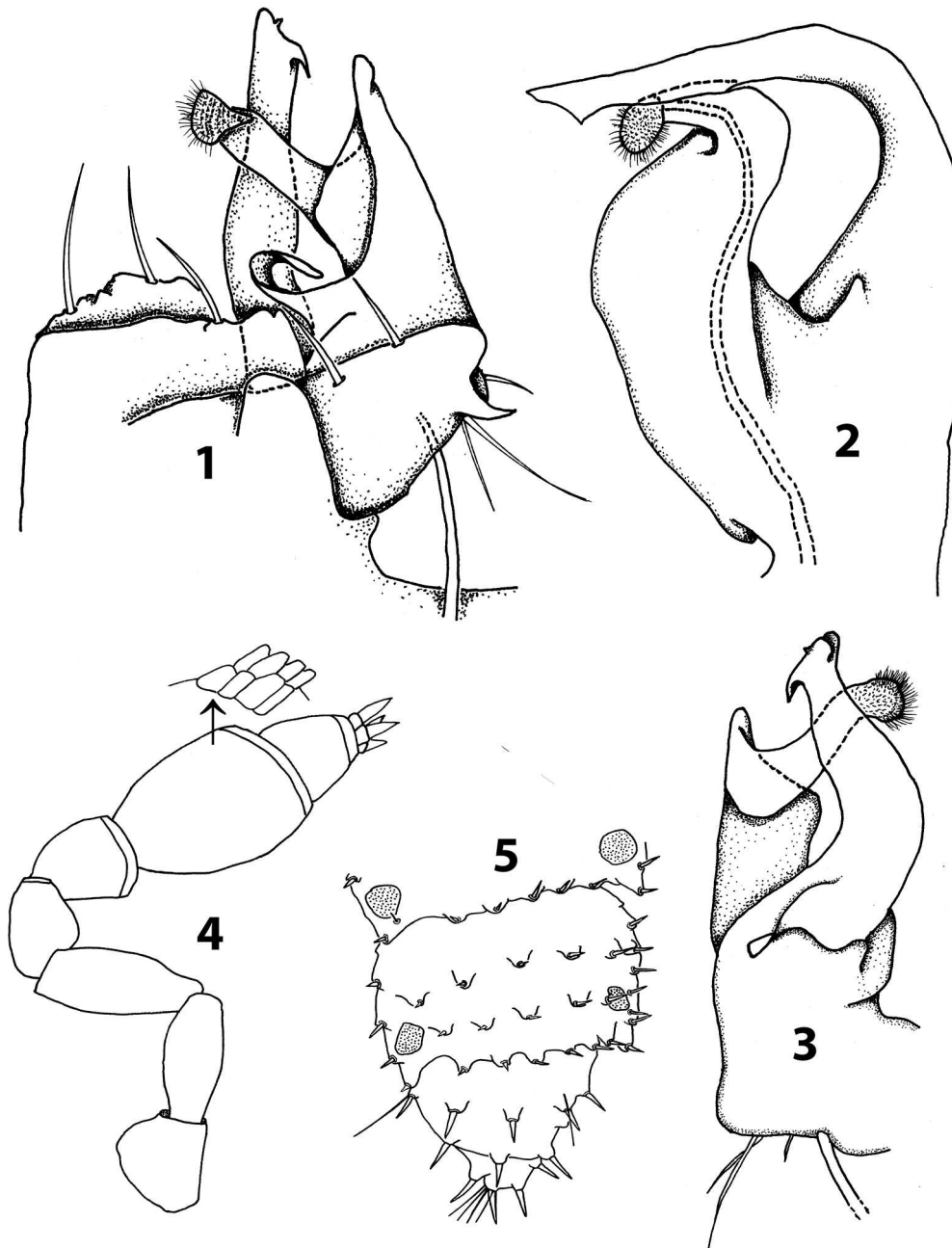
Figures 1–5. *Chaetaspis attenuatus*, holotype, Cushman Cave, Independence County, Arkansas: (1) gonopod, posterior; (2) gonopod, lateral; (3) gonopod, anterior; (4) antenna, setae omitted; (5) ornamentation of terminal segments (specimen bent to left).

post-gonopodal paranota slightly dentate; posterior lateral corners of anterior segments rounded, becoming progressively more produced on posterior segments, becoming a distinct tooth-like lobe directed posteriad in segments 17–19. Posterior margin of segments unmodified on anterior segments except for row of setae along margin, in segments 18–19 with a row of produced, rounded projections directed posteriad, each bearing a seta.

Gonopod, coxae subglobose, cannula prominent, prefemur setose. Acropodite with solenomere slender, cylindrical, apical disc with numerous minute denticles and setules,

anteriad to proximally broad process that terminates in mesial and lateral lobes; exomere tapering distally to an acute point.

Females to approximately 6.5 mm, width approximately 0.55 mm. Nonsexual characters as in male.

Distribution—*Chaetaspis attenuatus* is known from Cushman and Clay Caves in northeastern Arkansas (Fig. 6). These caves were formed in limestone of Ordovician age that occurs along the southern margin of the Salem Plateau section of the Ozark Plateau physiographic province. The caves occur along the northeastern side of the White River, separated by approximately 100 km from the
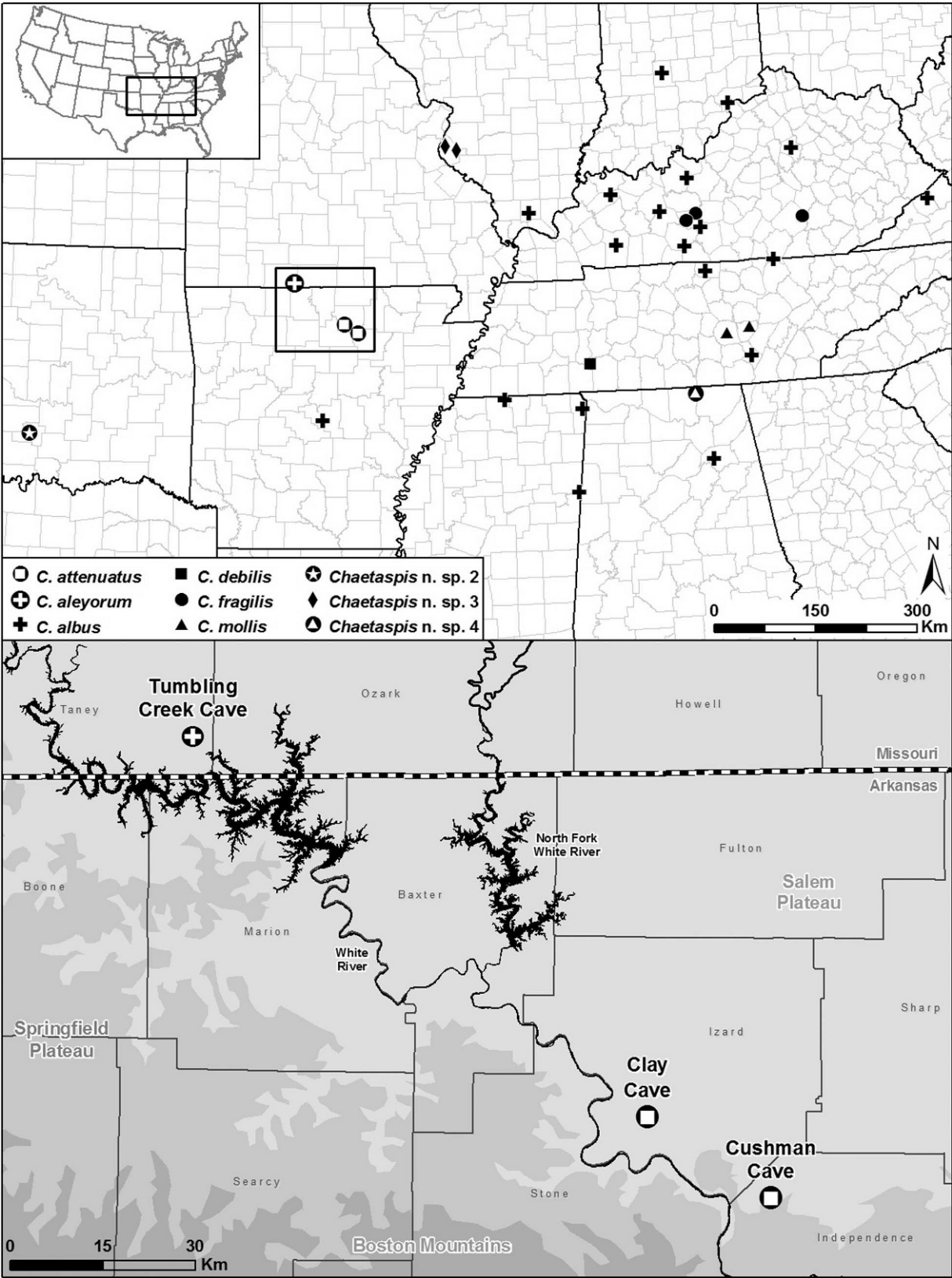
Figure 6. Distribution of *Chaetaspis* species (top) and detail for *C. attenuatus* and *C. aleyorum* (below).

only known locality of the sister species *C. aleyorum* in Tumbling Creek Cave, Taney County, Missouri.

Ecology—Cushman Cave is notable for its large entrance from which emerges a perennial stream. The cave has 2100 meters of mapped passages. In Cushman Cave the millipeds were collected in the dark zone, mostly under rocks lying in undisturbed soil or in woody organic debris. On 9 July 2008 the air temperature 2 cm above the substrate varied from 14.6 to 15.3 °C at four stations measured in the dark zone; *Chaetaspis attenuatus* occurred at three of these stations. Relative humidity at the same sites ranged from 88 to 94%. Other troglobionts observed in proximity to *C. attenuatus* included the milliped *Causyella causeyae* Shear, a pseudoscorpion *Apochthonius* sp., the isopod *Brackenridgia ashleyi* Lewis, unidentified linyphiid spiders, and rhagidiid mites.

Clay Cave receives a great deal of water during heavy precipitation, but there is not a perennial stream. Approximately 300 meters of passage are known in the cave. *Chaetaspis attenuatus* was found in the dark zone under leaf litter and associated with rotting wood. The millipeds occurred at all four stations for which temperature and humidity data were recorded on 10 July 2008. Temperature 2 cm above the floor varied from 56.0–59.5 degrees F. and relative humidity ranged from 86 to 95%. Other terrestrial taxa included the milliped *Causyella causeyae,* the isopod *Brackenridgia ashleyi*, the beetle *Ptomaphagus cavernicola* Schwarz, a harvestman *Crosbyella* sp., a collembolan *Tomocerus* sp., and rhagidiid mites.

Etymology—The name *attenuatus* is from Latin referring to the tapering gonopod exomere.

Chaetaspis sp.

Material examined—Arkansas: Marion County, Forest Trail Ridge Cave, Buffalo National River, National Park Service, 12 June 2008, Michael E. Slay, D. Fong, and M. Kottmyer; Stone County, Double Barrel Cave, Ozark-St. Francis National Forest, U.S. Forest Service, 31 March 2002, G. Graening, D. Fenolio, and C. Brickey. Oklahoma: Cherokee County, cave identified as CZ-18, 29 January 2002, G. Graening, D. Fenolio, and S. Hensley.

Notes—These records represent localities for *Chaetaspis* populations from which males, necessary for identification, have not yet been found. The Forest Trail Ridge Cave and Double Barrel Cave localities are zoogeographically interesting since they occur on the southwestern side of the White River, whereas *C. aleyorum* and *C. attenuatus* are only known from caves on the northeastern side.

Lewis (2002) reported an undescribed *Chaetaspis* collected by R. C. Harrel on 3 July 1959 from an unspecified cave in Murray County, Oklahoma. It is likely that this "unspecified cave" is actually Wild Woman Cave, where Harrel (1960, 1963) was investigating the invertebrate community. Indeed, Harrel (1963) reported on a new species of *Antriadesmus* (= *Chaetaspis*) from Wild Woman Cave that was being studied by Nell Causey. This is postulated should the need arise to collect additional material of the undescribed Oklahoma *Chaetaspis* reported in Lewis (2002). Wild Woman Cave occurs in the Arbuckle Mountains, a geographically isolated karst region of Oklahoma, and represents the only known location of *Chaetaspis* in Oklahoma, as well as the most westerly population of the group.

REFERENCES

Bollman, C.H., 1887, New genus and species of Polydesmidae: Entomologica Americana, v. 3, no. 3, p. 45–46.

Bollman, C.H., 1888, A preliminary list of the Myriapoda of Arkansas with descriptions of new species: Entomologica Americana, v. 4, no. 1, p. 1–8.

Causey, N.B., 1950, On four new polydesmoid millipeds: Entomological News, v. 61, no. 7, p. 193–198.

Causey, N.B., 1959, Some cavernicolous millipeds from the Cumberland Plateau: Journal of the Tennessee Academy of Science, v. 34, no. 4, p. 229–237.

Djursvoll, P., 2008, Revision of the Iberian millipede genus *Schizomeritus* Verhoeff, 1931 (Diplopoda, Polydesmidae), with the description of three new species: International Journal of Myriapodology, v. 1, p. 111–122. doi:10.1163/187525408X316776.

Harrel, R.C., 1960, A preliminary report of the invertebrate animals of Wild Woman Cave: Proceedings of the Oklahoma Academy of Science, v. 40, p. 29–34.

Harrel, R.C., 1963, Further notes on invertebrate animals of Wild Woman Cave, Murray County, Oklahoma: Proceedings of the Oklahoma Academy of Science, v. 43, p. 129–131.

Hoffman, R.L., 1979, Classification of the Diplopoda, Geneva, Muséum d'Histoire Naturelle, 237 p.

Hoffman, R.L., 1999, Checklist of the Millipeds of North and Middle America, Virginia Museum of Natural History Special Publication, no. 8, 584 p.

Lewis, J.J., 2002, *Chaetaspis aleyorum,* a new species of millipede from Tumbling Creek Cave, Missouri, with a synopsis of the cavernicolous species of *Chaetaspis* (Diplopoda: Polydesmida): Myriapodologica, v. 7, no. 11, p. 101–111.

Lewis, J.J., and Lewis, S.L., 2005, Cave fauna study for the Interstate 66 E.I.S. (Somerset to London, Kentucky), *in* Rea, G.T., ed., Proceedings of the 2005 National Cave and Karst Management Symposium: NCKMS Steering Committee, p. 15–20.

Loomis, H.F., 1943, New cave and epigean millipeds of the United States, with notes on some established species: Bulletin of the Museum of Comparative Zoology, v. 92, p. 371–410.

McDaniel, V.R., and Smith, K.L., 1976, Cave fauna of Arkansas: selected invertebrate taxa: Proceedings of the Arkansas Academy of Science, v. 30, p. 57–60.

Shear, W.A., and Shelley, R.M., 2007, The milliped genus *Tidesmus* Chamberlin 1943 (Polydesmida, Macrosternodesmidae): Zootaxa, 1656, p. 51–68.

Shear, W.A., and Shelley, R.M., 2008, Cave millipeds of the United States. VI. *Sequoiadesmus krejcae*, n. gen., n. sp., from Sequoia and Kings Canyon National Parks, California, USA (Diplopoda, Polydesmida, Trichopolydesmidea, Macrosternodesmidae): Zootaxa, 1693, p. 41–48.

Shear, W.A., Taylor, S.J., Wynne, J.J., and Krejca, J.K., 2009, Cave millipeds of the United States. VIII. New genera and species of polydesmidan millipeds from caves in the southwestern United States (Diplopoda, Polydesmida, Macrosternodesmidae): Zootaxa, 2151, p. 47–65.

CAECIDOTEA INSULA, A NEW SPECIES OF SUBTERRANEAN ASELLID FROM LAKE ERIE'S SOUTH BASS ISLAND, OHIO (CRUSTACEA: ISOPODA: ASELLIDAE)

JULIAN J. LEWIS

Lewis & Associates LLC., Cave, Karst & Groundwater Biological Consulting, 17903 State Road 60, Borden, IN 47106-8608, lewisbioconsult@aol.com

Abstract: Three species of obligate subterranean asellids were previously known from Ohio, all assigned to the *stygia* Group of the genus *Caecidotea*: *C. stygia, C. filicispeluncae,* and *C. rotunda. Caecidotea insula*, n. sp., is described here from two caves on South Bass Island, Ottawa County, Ohio. This island is only 7 km from the Canadian border. The new species is assigned to an assemblage proposed here as the *forbesi* Group, which includes the epigean species *C. forbesi, C. racovitzai, C. attenuata,* and *C. obtusa*. Evidence suggests that *C. insula* evolved as the result of a groundwater invasion by ancestral *C. forbesi* during the late Pleistocene.

INTRODUCTION

Three species of obligate subterranean asellid isopods were previously known from Ohio, all associated with karst habitats along the southern edge of the state (Fig. 1). Each are members of the *stygia* Group of the genus *Caecidotea* (Steeves, 1963; Lewis, 1988) containing *C. stygia, C. filicispeluncae,* and *C. rotunda. Caecidotea stygia* is one of the most widespread subterranean isopods in the eastern United States with a range extending from southern Indiana through Kentucky into northern Tennessee and west through southern Illinois to east-central Missouri. It was redescribed from specimens on the eastern edge of its range collected in southwestern Ohio (Bowman and Beckett, 1978). *Caecidotea filicispeluncae* was described from Fern Cave, Adams County (Bowman and Hobbs, 1983) and is endemic to that site. *Caecidotea rotunda* was described from collections in southern Ohio and southeastern Indiana (Bowman and Lewis, 1984).

The discovery of an obligate subterranean isopod in caves on South Bass Island, only 7 km from the Canadian border, in Lake Erie is remarkable for its occurrence there. Peck (1998) listed only four obligate subterranean species in Canada, and none were known from east of the Rocky Mountains. The potential for discovery of obligate subterranean organisms in eastern Canada should not be dismissed, especially in hyporheic and epikarstic habitats. As a case in point, the new isopod was taken from a pool collecting water dripping in from the epikarst.

FAMILY ASELLIDAE

Caecidotea Packard, 1871

forbesi Group (new species group)

Diagnosis of male—Eyes and pigmentation present or absent. Palmar margin of pereopod 1 propodus with median triangular process. Pleopod 1 subequal or shorter than pleopod 2, exopod distal margin with short, non-plumose setae. Pleopod 2, exopod, distal article ovate, large in relation to and longer than endopod, widest along mid-length, with numerous elongate plumose setae along margins; endopodite tip with broadly rounded, sclerotized caudal process, cannula relatively short, blunt, extending parallel to axis of endopod, mesial process present.

The following species are assigned to the *forbesi* Group: *Caecidotea forbesi, C. racovitzai, C. obtusa, C. attenuata,* and *C. insula*.

Caecidotea insula, new species

Figures 2–3

Material examined—OHIO: Ottawa County, drip pool in Kindt's Cave I, town of Put-in-Bay, near center of southern half of South Bass Island, collected Wittenberg University Speleological Society, 5 August 2007, holotype male; drip pool in Kindt's Cave II, Wittenberg University Speleological Society, 5 August 2007, one paratype male. The specimens have been deposited in the collection of the National Museum of Natural History, Smithsonian Institution.

Description—Eyeless, unpigmented, longest 9.3 mm, approximately 4.2× as long as wide. Margins of head, pereonites, and pleotelson densely setose. Head approximately 1.9× as wide as long, post-mandibular lobes modestly produced. Pleotelson slightly longer than wide, caudomedial lobe distinct.

Antenna 1 flagellum with 10 articles, distal 4 articles with esthetes. Antenna 2 last article of peduncle approximately 1.5× length of preceding article, flagellum with 61 articles. Mouthparts per the diagnosis of the genus (Lewis 2009).

Pereopod 1 propodus subtriangular, approximately 1.4× as long as wide, palmar margin with stout proximal seta, high triangular median process, lower rounded distal process. Dactylus slightly longer than palmar margin of propodus.

Pleopod 1 slightly shorter than pleopod 2, protopod approximately 0.7× length of exopod, 2 retinacula; exopod approximately 1.7× as long as wide, ovate, mesial and
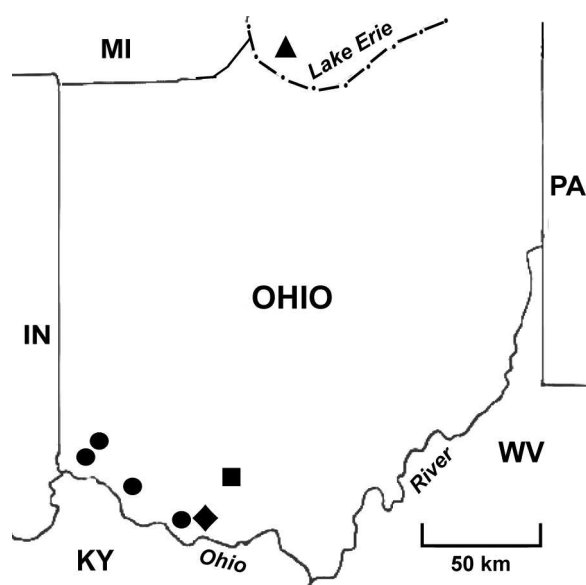
Figure 1. Approximate locations of subterranean asellid isopods in Ohio: triangle, *Caecidotea insula*; circles, *C. stygia*; diamond, *C. filicispelunca*; square, *C. rotunda*.

lateral margins broadly rounded, sparse non-plumose setae on distal margin.

Pleopod 2, protopod subquadrate, about 1.35× as long as wide; exopod about 1.6× length of endopod, proximal article with 2 small lateral setae, distal article slightly longer than endopod, ovate, with 14 plumose setae along margins increasing in size at apex; endopod with broadly rounded basal apophysis, tip with 4 processes in anterior view: (1) cannula broad, distally flat, (2) mesial process prominent, distally hooked mesiad, with endopodial groove barely visible at base; (3) lateral process low, broad, partially obscured by mesial process, extending slightly beyond margin of endopod; (4) caudal process prominent, broadly rounded, sclerotized.

Pleopod 3 exopod, proximal to transverse suture about 0.6× length of distal part; elongate plumose setae along distal and lateral margins, tapering in length to suture. Pleopod 4 exopod with 2 false sutures, proximolateral margin with 2 setae and numerous setules. Pleopod 5 exopod with 3 proximolateral setae. Uropods detached and missing from vial.

Etymology—The name is from the Latin noun *insula* = island, referring to the location of the type-locality on South Bass Island.

Vernacular name—The suggested common name is the Kindt's Cave isopod, referring to the Kindt family in honor of their stewardship of the cave.

Range—*Caecidotea insula* is known from two caves on South Bass Island, Ohio, in southwestern Lake Erie. The Kindt's Caves are clustered a little southwest of the center of the southern half of the island, within the village of Put-in-Bay. Verber and Stansberry (1953) provided a map with the locations of twenty-eight caves on the island, including

three Kindt's Caves. The potential range encompasses South Bass Island, which is approximately 6 km long by 2.4 km wide, with a narrow isthmus separating the smaller northern section from the larger southern part of the island.

Habitat—In contrast to other caves of the eastern U.S. formed by dissolution of carbonate bedrock, many caves on South Bass Island are the product of collapse of the Put-in-Bay and Tymochtee dolomites into voids created by dissolution of underlying gypsum domes (Verber and Stansberry, 1953). This produced short, crescent-shaped caves around the edge of the collapsed domes. The three Kindt's Caves are clustered around such a collapsed dome. Kindt's Cave I has been surveyed at 164 meters in length, while Kindt's Cave II is 144.4 meters long. The entrance to Kindt's Cave III has been filled for several decades and little is known about it (Athy, pers. comm., 2010). The specimens of *C. insula* were collected from shallow pools of drip water originating in the epikarst (Hobbs, pers. comm., 2010). The isopods have also been seen in the deeper, base level pool in the lowest part of the cave (Athy, pers. comm., 2010). The level of these pools is equivalent to the top of the local water table, which fluctuates with the level of Lake Erie (Verber and Stansberry, 1953).

Relationships—The morphology of *Caecidotea insula* most closely resembles *C. forbesi* (Williams, 1970), an epigean species widespread in the eastern U.S. and southeastern Canada. Although troglomorphism does not in itself imply speciation, the two species are easily separated by the absence of eyes and pigmentation in *C. insula*. *Caecidotea forbesi* has large, distinct eyes and pigmentation typical of a surface-dwelling species. The habitus of *C. insula* is not particularly vermiform as compared to other subterranean *Caecidotea*, but the male gnathopod propodus is more attenuate than that of *C. forbesi*. In *C. insula* the propodus is subtriangular and about 1.4× as long as wide. In *C. forbesi,* the propodus is subtrapezoidal and slightly wider than long (Williams, 1970). In both species the palm of the propodus has a large median process and a low distal process. The male first pleopods are essentially identical in appearance. The resemblance of the male second pleopod of the two species is strong, but differs in details of the tip structures of the endopod. In *C. forbesi,* the endopodial groove is prominent in anterior aspect, but it is barely visible in *C. insula,* where it seems to run behind the decurved mesial process. A subcaudal lateral process is present in *C. insula*, but undifferentiated in *C. forbesi*.

The morphological similarity of *C. insula* to *C. forbesi* suggests a close relationship with the group of four epigean species proposed here as the *forbesi* Group (*C. forbesi, C. racovitzai, C. obtusa, C. attenuata*) indicated by the phylogeny of Williams (1970). This is the only described subterranean asellid in North America belonging to a group of species that is otherwise entirely epigean.
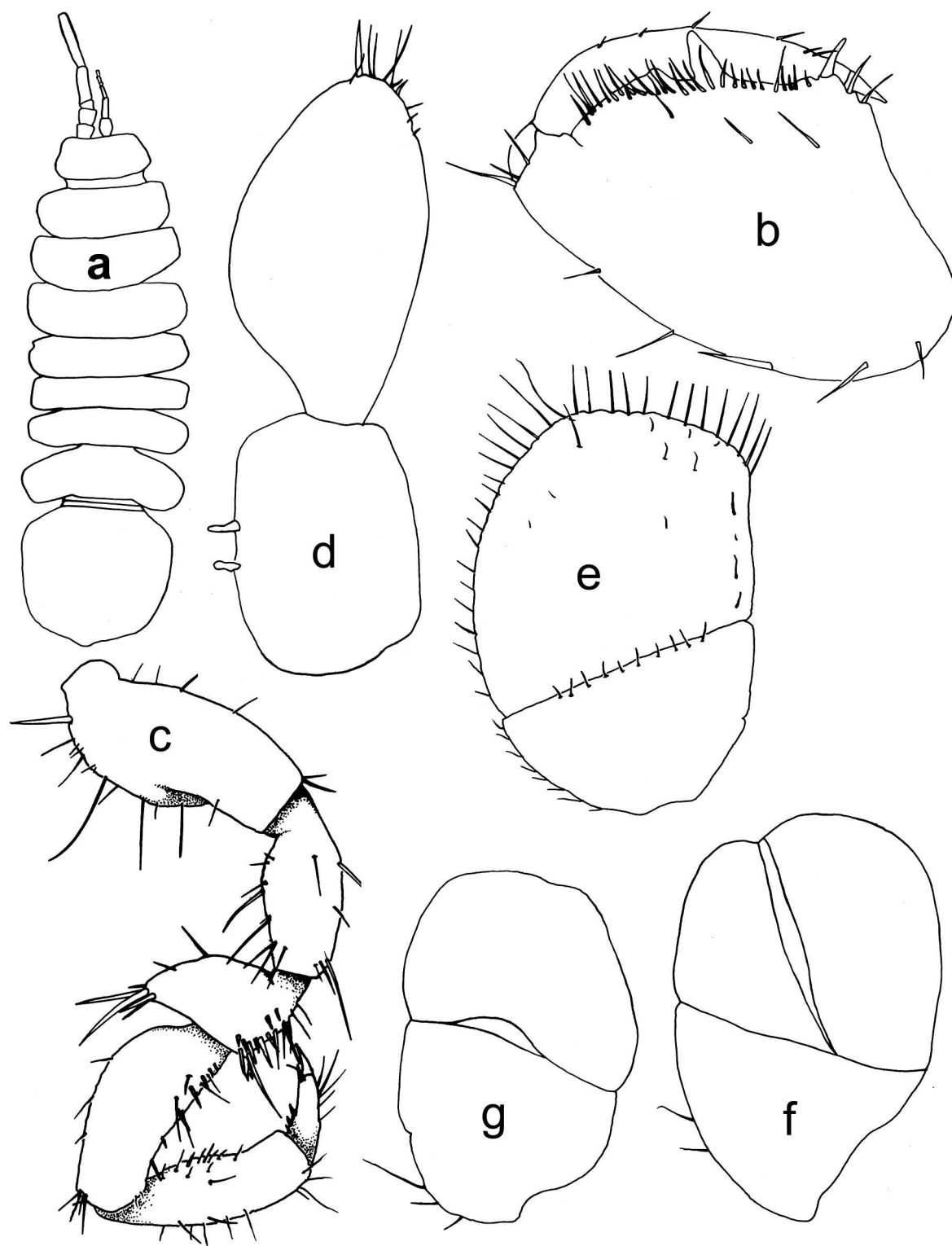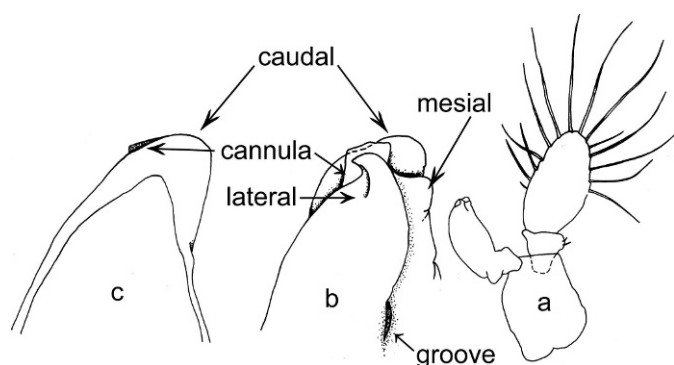
Figure 2. *Caecidotea insula*, new species: (a) habitus, (b) pereopod 1 propodus, (c) pereopod 4, (d) pleopod 1, (e) pleopod 3 exopod, (f) pleopod 4 exopod, (g) pleopod 5 exopod.

Evolution—The area where *C. insula* occurs was covered by the Wisconsinan glacier until about 14,000 years before present (Forsyth, 1988). As the glacier receded, new aquatic habitats presented opportunities for the *forbesi-insula* ancestral species. Williams (1970) reported that *C. forbesi* does not occur in Lake Erie, so as the relatively deep water lake formed in the post-glacial era, that species must have moved to other areas. Today, *C. forbesi* is one of the most

Figure 3. *Caecidotea insula*, **new species: (a) pleopod 2, (b) same, endopodite tip, anterior aspect, (c) same, posterior aspect.**

common aquatic isopods in eastern North America, including many sites peripheral to Lake Erie. A population stranded on South Bass Island was geographically, and thus genetically, isolated. It is not difficult to envision an isopod like *C. forbesi*, a frequent inhabitant of temporary pools, following water downward as its habitat dried, and thus invading and colonizing groundwater. Whatever the cause, the result was the presence of the species recognized here at *C. insula* on South Bass Island.

Steeves (1969) noted another subterranean species only slightly changed morphologically from its epigean relative. That species was designated as undescribed species D by Steeves, known only from Lawson's Cave, in an isolated valley called Burkes Garden, Tazewell County,Virginia. I have examined collections from Lawson's Cave and found the isopods to be eyeless and unpigmented, but otherwise indistinguishable from the epigean *C. racovitzai* (Lewis, 2009). Likewise, specimens from some caves in central Florida are troglomorphic, i.e., eyeless and unpigmented, but otherwise morphologically identical to *C. racovitzai*.

As the asellid fauna of eastern North America becomes better understood, trends in the evolution of the group are becoming evident. A recurrent theme that is emerging among the species of the *forbesi* Group is their penchant for recent groundwater invasions. Until the discovery of the *Caecidotea* in Kindt's Caves, none of the taxa were known from demonstrably geographically isolated sites.

The presence of *C. insula* on an island in Lake Erie is reasonable evidence of genetic isolation.

References

Bowman, T.E., and Beckett, D.C., 1978, A redescription of the troglobitic isopod, *Caecidotea stygia*, from the environs of Cincinnati, Ohio (Crustacea: Isopoda: Asellidae): Proceedings of the Biological Society of Washington, v. 91, no. 1, p. 294–302.

Bowman, T.E., and Hobbs, III, H.H., 1983, *Caecidotea filicispeluncae,* a new troglobitic asellid isopod from Ohio: Proceedings of the Biological Society of Washington, v. 96, no. 4, p. 693–697.

Bowman, T.E., and Lewis, J.J., 1984, *Caecidotea rotunda*, a new troglobitic asellid from Indiana and Ohio (Crustacea: Isopoda: Asellidae): Proceedings of the Biological Society of Washington, v. 97, no. 2, p. 425–431.

Forsyth, J.L., 1988, The geologic setting of the Erie islands, *in* Downhower, J.F., ed., The Biography of the Island Region of Western Lake Erie, Columbus, Ohio State University Press, p. 13–23.

Lewis, J.J., 1988, The systematics, zoogeography and life history of the troglobitic isopods of the Interior Plateaus of the eastern United States: Ph.D. dissertation, University of Louisville, Louisville, Kentucky, 281 p.

Lewis, J.J., 2009, Three new species of *Caecidotea*, with a synopsis of the asellids of Virginia (Crustacea: Isopoda: Asellidae), *in* Roble, S.M., and Mitchell, J.C., eds., A Lifetime of Contributions to Myriapodology and the Natural History of Virginia: A Festschrift in Honor of Richard L. Hoffman's 80th Birthday: Martinsville, Virginia Museum of Natural History Special Publication, no. 16, p. 245–259.

Peck, S.B., 1998, A summary of diversity and distribution of the obligate cave-inhabiting faunas of the United States and Canada: Journal of Cave and Karst Studies, v. 60, no. 1, p. 18–26.

Steeves, III, H.S., 1963, The troglobitic asellids of the United States: the Stygius Group: American Midland Naturalist, v. 69, no. 2, p. 470–481.

Steeves, III, H.S., 1969, The origin and affinities of the troglobitic asellids of the southern Appalachians, *in* Holt, P.C., ed., The Distributional History of the Biota of the Southern Appalachians, Part I, Invertebrates, Blacksburg, Virginia Polytechnic Institute and State University, Research Division Monograph I, p. 51–65.

Verber, J.L., and Stansberry, D.H., 1953, Caves in the Lake Erie Islands: Ohio Journal of Science, v. 53, no. 6, p. 358–362.

Williams, W.D., 1970, A revision of North American epigean species of *Asellus* (Crustacea: Isopoda), Washington, Smithsonian Contributions to Zoology 49, 80 p.

HYDROGEOLOGY OF GYPSUM FORMATIONS IN IRAN

Ezzat Raeisi*, Mohammad Zare, and Jalal A. Aghdam

Department of Earth Sciences, College of Sciences, Shiraz University, 71454, Shiraz, Iran

Abstract: The gypsum formations in Iran are mainly Upper Red (URF), Gachsaran (GF), and Sachun. The GF is divided into salt (SGF) and its non-salt equivalents (NSGF). The conductivity of the spring's water in Sachun, URF and NSGF is below 3500 μS cm^{-1}, but the conductivity of the SGF varies from 2400 to 400,000 μS cm^{-1}. Three different sites, Tangsorkh (NSGF), Ambal and Salbiz (SGF), were selected for further studies. The Tangsorkh area is composed of alternating units of marlstone and gypsum. The hydraulic connections between these units are broken by the marls and no sub-aquifer is developed in the gypsum units due to their small catchment area and lack of karst development. The Ambal area, adjacent to the large Karun River, consists of units of marl, anhydrite, and halite. Sinkholes cover all parts of the area. Contact of Karun River with the Amble ridge causes the chemistry of the river to evolve from bicarbonate type to chloride type. The presence of the Karun River inside this ridge formed a network of karstic conduits and sinkholes, which causes the marly layers to collapse such that the Ambal area cannot be considered to have several independent sub-aquifers. The Salbiz site is composed of alternating units of marl-marlstone and gypsum without any sinkholes or exposed salt layers. It consists of independent sub-aquifers with general flow directions parallel to the strike. The study indicates that the GF is mainly composed of small independent sub-aquifers due to its alternative marl or marlstone layers, resulting water flows parallel to the strike, except in the SGF under specific conditions.

Introduction

Surface outcrops of gypsiferous strata appear quite limited on the global scale. This apparent scarcity can be explained by the relatively low resistance of gypsum to denudation, rather than an actual limited occurrence of sulfate rocks, therefore, the extent of sulfate rocks is greater at depth (Klimchouk et al., 1996). Ford and Williams (1989) estimated that gypsum/anhydrite or halite deposits underlie 25% of the continental surface (approximately 60 million km^2), while Maximovich (1962), in Klimchouk et al. (1996), calculated that the area of the continents underlain by gypsum/anhydrite alone is about 7 million km^2. It is estimated that gypsum/anhydrite deposits underlie 35 to 40% of the United States' land area (Johnson, 1996), and they outcrop on 7% of Spain's land area (Gutierrez et al., 2008) and about 80,000 km^2 of Canada's land area (Ford, 1997).

As gypsum is susceptible to rapid dissolution wherever there is active circulation of groundwater that is undersaturated with respect to calcium sulfate, substantial underground voids and cave systems may develop (Johnson, 2003). Gypsum dissolution is one of the most common processes in deteriorating the water quality of aquifers. Water in gypsum karst terrains commonly contains over 1000 mg l^{-1} of sulfates, which makes them unsuitable for use as domestic water supply. Much higher concentrations of solutes are not uncommon where gypsum karstification is accompanied by dissolution of the various other salts that are associated with evaporitic sedimentary formations (Klimchouk and Andrejchuk, 1996).

Gypsum formations also outcrop in Iran, especially in the south and southwest of the country. In most of these parts, the gypsum layers are in direct contact with carbonate karstic aquifers or alluvium, deteriorating the good water quality of the adjacent aquifers. Studies on the hydrogeology of gypsum formations in Iran are limited, in spite of the great impact that it has on groundwater quality. Among the gypsum formations, the Gachsaran, with alternative layers of marls, gypsum, and halite, has the highest outcrop in southern Iran (Ashjari and Raeisi, 2006).

This study is focused on preparing a distribution map of gypsum formations in Iran, determining the lithological and hydrochemical characteristic of these formations, and presenting conceptual hydrogeological models in the three Gachsaran Formation aquifers in southern Iran.

Methods

Two distribution maps of gypsum formations in Iran were prepared based on available scientific information on the stratigraphy and geology of Iran (Stocklin and Setudehnia, 1977; Aghanabati, 2006; Darvishzadeh, 2003; Khosro Tehrani, 1987; Motiei, 1993); on 1:1,000,000, 1:250,000, and 1:100,000 geological maps from the Geological Survey and Mineral Exploration of Iran dated 1972, 1975, and 2001 or the Iranian Oil Operating Company dated 1965, 1967, 1975, 1976, and 1977; and

---

* Corresponding Author, e_raeisi@yahoo.com

on air photos. Some of the hydrochemistry data for this research were obtained from the Karst Research Center of Iran and unpublished M.Sc. thesis in the Geosciences Department of Shiraz University (Rahimi, 2006; Bagheri, 2007). The temperature, electrical conductivity, pH, and discharge of typical springs emerging from gypsum formations were measured in the field during sampling. In the laboratory, calcium and magnesium were measured by titration with EDTA, with Murexide and Erichrom Black-T as indicators. Sodium and potassium concentrations were determined by flame photometery. Sulfate and chloride were measured by the Mohr and turbidity methods, respectively. Bicarbonate was determined by titration with HCl with methyl orange as indicator. The accuracy of the analyses was estimated from the ion balance. The uncertainty was less than 5% in all the samples.

Geology and Stratigraphy of Gypsum Formations in Iran

The Zagros basin is made of 7 to 14 km thick sediments over a region along the edge of the Arabian plate. The Zagros region has evolved through different tectonic settings. The stratigraphic column of the Zagros basin contains evaporites. The Hormuz salt (Precambrian) is located at the base of the sedimentary column, and the Gachsaran Formation (GF, Miocene) is composed of widespread evaporate units (Bahroudi and Koyi, 2004). The GF was deposited under the following conditions: evaporation exceeding the supply of seawater, arid climates, and nearly isolated salt basins. The GF was a syntectonic sediment deposited in the northwest-trending synclinal troughs during active folding that divided the Zagros foreland basin into sub-basins with poor water circulation (Berbrian and King, 1981; Hessami et al., 2001). In the salt sub-basins, the two processes of dissolution of extruding Hormuz salts and evaporation were responsible for the deposition of Gachsaran salt. Chemostratigraphic analysis reveals that arid conditions and cycles of transgression–regression of the sea contributed to the formation of the evaporite sequences of the GF in the coastal Sabkha lagoon basin that was partly closed from the open sea by a shallow barrier (Bahadori et al., 2011).

Four main gypsum formations, namely Hith Anhydrite (Late Jurassic), Sachun (late Maestrichtian to early Eocene), Gachsaran (early Miocene) and Upper Red (Miocene-Pliocene) outcrop in Iran (Fig. 1). The total outcrop of the gypsum formations is about 80,000 km^2, 5% of Iran's land area. The characteristics of these formations are presented in Table 1.

The Hith Anhydrite (Late Jurassic) outcrops in south-central Iran near the Persian Gulf; its area is too small to show on Figure 1. Its thickness is about 91 m based on the type locality in Kuh-e Asaluyeh. It consists of massive anhydrite-gypsum with interbedded dolomites. The outcrop
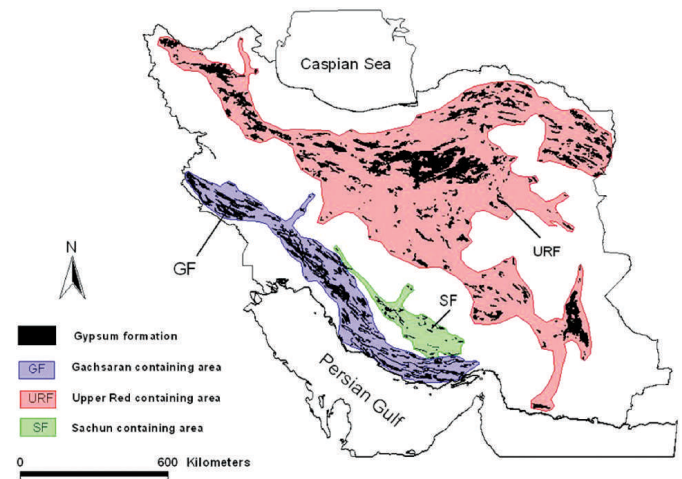
Figure 1. Areas containing outcrops (black) of the main gypsum formations in Iran. The Hith Anhydrite area is too small to show at this scale.

of this formation is only 0.2% of the total gypsum outcrop in Iran. The Hith Anhydrite is sandwiched between the limestones and dolomites of the Surmeh Formation and the limestones of the Fahliyan Formation. No hydrogeological information is available.

The Sachun Formation (late Paleocene-Eocene) is present only in south-central Iran. The outcrop of this formation is only 1.3% of the total gypsum outcrop in Iran. The type section was measured at Kuh-e Sachun, about 5 km north of the village of Sachun. The thickness at the type locality is 1414 m. The bottom 387 meters consists of marl, marlstone, and limestone. These are followed by 91.4 m of gypsum and dolomite, which are overlain by 112.8 m of marlstone and dolomite. The succession is continued with 82.3 m of gypsum with bands of dolomite. Following this are 335.2 m of chalky marlstone, dolomite, and limestone. The upper 405.4 m are composed of massive gypsum, marl, and ribs of dolomite (Stocklin and Setudehnia, 1977).

The Upper Red Formation (Miocene-Pliocene) outcrops in the north, center, and east of Iran, composing 73.2% of the total gypsum outcrop in Iran. No type sections have been specified for this formation. However, the name was first applied to the extensive exposures in the hills of the Qom plain, and it is here that the most detailed studies of the formation have been carried out in both surface and borehole sections by the geological staff of the Iran Oil Company (Mostofi and Frei, 1959). Thus, this area can be regarded as the general type area. The evaporate lower subunit consists of 300 to 500 m of salt, anhydrite, pebble layers, bituminous paper shales, and dark-red saline plastic clays. The upper subunit has a thickness of 4000 to 5000 m, consisting of gypsiferous marl and sandstone in the lower part and marl and sandstone in the upper part (Stocklin and Setudehnia, 1977).

Table 1. Area and percent of gypsum formations in Iran.

| Gypsum Formation	Geological Time	Percentage of Iran Area	Percentage of Gypsum Area	Location in Iran	Lithology
Upper Red	Tertiary	3.63	73.2	North – Center - East	marl, gypsiferous marl, sandstone
Gachsaran	Tertiary	1.25	25.3	South west – Central South	anhydrite, salt, marl, limestone, argillaceous limestone
Hith Anhydrite	Jurassic – Cretaceous	0.005	0.2	Central South	anhydrite
Sachun	Tertiary	0.07	1.3	Central South	marl, marlstone, limestone, gypsum, dolomite

A more detailed distribution map of the Gachsaran Formation is presented in Figure 2. The GF outcrops in southwest and south-central Iran with a total exposure of 20,400 km^2, making up 25.3% of the total gypsum outcrop in the country. The Zagros foreland basin is divided into sub-basins where Gachsaran salt and its non-salt equivalents were deposited (Bahroudi and Koyi, 2004). The Salt Gachsaran Formation (SGF) outcrops in a region from the Kazerun–Qatar faults to Dehloran City. The Non-Salt Gachsaran Formation (NSGF) is classified into Three Members and undifferentiated. The Three Members Gachsaran Formation (TMGF) outcrops between Bandar-e-Abbas and Firuzabad, while undifferentiated NSGF outcrops in two different regions, from Firuzabad to the Kazerun-Qatar fault and north of Dehloran City (Fig. 2). The thickness of the GF usually varies over short distances (Dunnington, 1968; O'Brien, 1957; Stöcklin, 1968), typically from several hundred up to 2000 meters (Edgell, 1996; James and Wynd, 1965; Murris, 1980; Stöcklin, 1968; Bahroudi and Koyi, 2004). Although the GF is generally considered as lower Miocene in age (James and Wynd, 1965), stratigraphic correlations between wells on Qeshm

Figure 2. Distribution map of the Gachsaran Formation and its parts in Iran. SGF is the salt Gachsaran Formation, and the non-salt Gachsaran Formation (NSGF in the text) is divided into the three member GF (TMGF; Chehel, Champeh, and Mol Members) and the undifferentiated GF (UGF).

Island in the extreme southeast of the basin reveals that its base is Oligocene or even older (Eocene). The base of the Fars group is diachoronous along the foreland basin and becomes younger with evaporite increases northwestward (Fig. 2) (Gill and Ala, 1972; Motiei, 1993; Bahroudi and Koyi, 2004).

The SGF, in the center of which lie the present oilfields, is mainly located in the southwest of Iran. Stocklin and Setudehnia (1977) divided the GF of the salt basin into seven members based on a type section from a well in the Gachsaran Oilfield. James and Wynd (1965) described the members of SGF in ascending order is as follows: Member 1 consists of 39.6 m of interbedded anhydrite and limestone associated with shale. It is important as a sealing unit over the Asmari Formation oil reservoirs. Member 2, with a thickness of 115 m, is mainly composed of salt, with some anhydrite and thin limestone intercalations. The thickness of Member 3 is 229 m. The lower half of this member consists of thick anhydrite with subordinate salt, and the upper half is composed of interbedded anhydrite, thin-bedded limestone, and marl. Member 4 is composed of 848 m of thick salt beds associated with grey marl, limestone, or anhydrite. Member 5 consists of 324 m of marl alternating with anhydrite. Member 6 is divided into three parts. The lower part (103 m) consists of alternating anhydrite, red marl, and limestone. The middle part (121 m) consists of salt and anhydrite, and the upper part (61 m) is composed of anhydrite with marl alternations. Member 7, with a thickness of 139 m, is overlain conformably by the Mishan Formation and consists of alternating anhydrite, marl, and argillaceous limestone.

Although exposures of Gachsaran rock salt are rare, it is known from wells and quarries in the south of Masjed Suleyman in the Dezful embayment (Dunnington, 1968; Gill and Ala, 1972; Kashfi, 1980; Motiei, 1993; Bahroudi and Koyi, 2004).

The NSGF is divided into undifferentiated GF and the three early Miocene Chehel, Champeh and Mol Members (James and Wynd, 1965). The lowest, Chehel Member, with a thickness of 296 m, predominantly consists of anhydrite or gypsum. Thin interbeds of limestone and
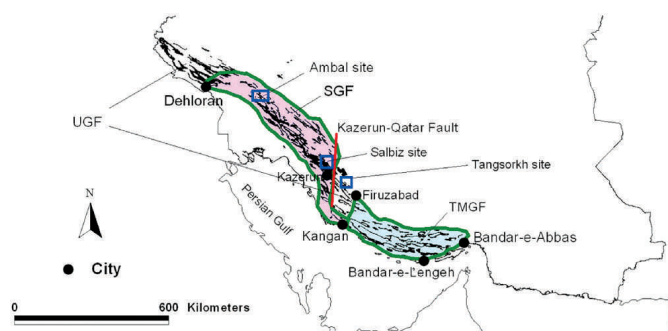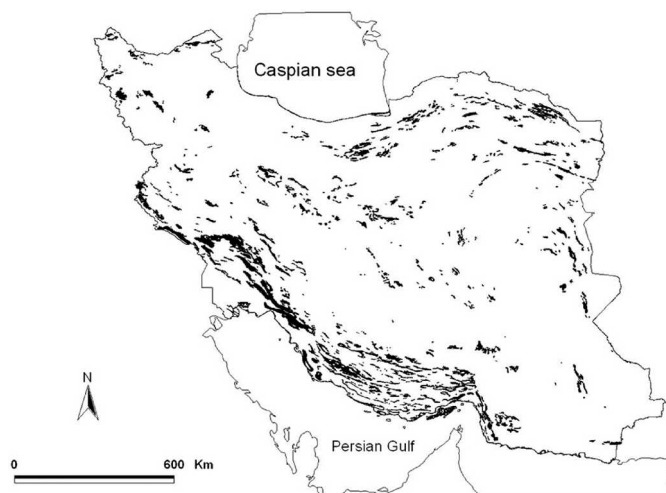
Figure 3. Distribution map of outcrops of additional gypsiferous formations, with minor beds or veins of gypsum, not shown in Figure 1.

marls are common in this unit. The Champeh Member, with a thickness of 110 m at the type locality, is the middle member of the GF. This member consists of chalky-gypsiferous limestones or dolomites, gypsiferous marl, and nodular to massive gypsum. The Mol Member, with a thickness of 52 m, consists of gypsiferous marls interbedded with thin gypsiferous limestone and gypsum. Two small parts of the GF are undifferentiated in the west and the south-central regions of Iran (Fig. 2) and were determined based on the 1965 1:250,000 geological maps of the Iranian Oil Operating Companies. No type localities were studied for the undifferentiated GF, which is mainly composed of alternating units of marl and gypsum with interbedded thin limestones and sandstones. The small 1200 km² region of undifferentiated GF in the south-central of Iran is classified into the upper and lower GF (Oveisi, 2001). The upper GF consists of gypsum rocks, gypsum-bearing limestone, marl, and marly limestone, and the lower one is composed of marly limestone, limestone, marl, interbedded sandstone, and gypsum.

The tectonically incompetent units of the Gachsaran Formation are highly subject to dissolution effects, being characterized by responsiveness to differential pressures and extreme mobility. Because of these characteristics, one seldom finds a complete sequence as described at the type locality (Stocklin and Setudehnia, 1977). It is named Gachsaran in most parts of the outcropped area (Aghanabati, 2006).

Other gypsum occurs as thin layers, veins, or inside the matrix in small parts of several formations and units in Iran, mainly marl, marlstone, sandstone, siltstone, mudstone and conglomerate. These formations and units are named gypsiferous formations, as distinct from the gypsum formations of Figure 1 and Table 1, and outcrop in 3.4% of the total area of Iran (Fig. 3). The characteristics of

these formations and units are presented in Table 2 based on the "Stratigraphic Lexicon of Iran" (Stocklin and Setudehnia, 1977).

Hydrogeology of Gypsum Formations

There are numerous small springs emerging from gypsum formations with flow rates mostly less than a few liters per second, but in exceptional cases up to 60 L s^{-1} (Table 3). There are 165 measurements available for electrical conductivity and 128 measurements for chloride concentrations of water samples, and 73 samples were analyzed for major ions. No chemical analyses are available for samples from the Sachun and Upper Red Formations. The springs in each formation were classified into four groups based only on the EC as follows: Group A less than 1000 µS cm^{-1}, Group B between 1000 and 3500 µS cm^{-1}, Group C between 3500 and 10,000 µS cm^{-1}, and Group D more than 10,000 µS cm^{-1} (Table 3).

The conductivity of Sachun Formation water varies between 300 to 1400 µS cm^{-1}, and the Upper Red Formation varies from 300 to 14,500 µS cm^{-1}. Eighty-seven percent of the Sachun Formation water samples are classified into group A and the rest into group B. Most of the water samples of the Upper Red Formations are classified into Groups A and B (94%) and only 6% into Groups C and D.

The conductivity of waters from the NSGF varies from 300 to 5000 µS/cm. The water samples of NSGF are classified as follows: 20% in Group A, 76% in Group B, and 4% in Group C. In Group A, five samples with EC's less than 750 µS cm^{-1} are bicarbonate water type, and three samples with EC's between 800 and 1000 µS cm^{-1} are sulfate type. Groups B and C are sulfate and chloride water types, respectively. Within each group, the springs show the same distributions of ion concentrations (Figs. 4a, b, c). The low EC and dominantly bicarbonate and sulfate water types are expected because the NSGF has very small amounts of halite. The bicarbonate water mainly emerged from alluvium, probably originating from the Chehel Member or sandstone layers, and the sulfate water emerged from gypsum layers.

The conductivity of water from the SGF varies from about 2000 to 400,000 µS cm^{-1}. The SGF has members of only three groups: 46% Group B, 25% Group C, and 29% Group D. Out of the forty-one water samples, thirty-two have been chemically analyzed: the water in Group B being sulfate and bicarbonate, while Groups C and D are chloride water. The springs within each group show similar distributions in ion concentration (Fig. 4 d, e, f, g). The high percentage of chloride water is expected because more than 50% of SGF thickness is composed of salt.

In spite of the limited number of springs, it can be concluded that the alternating layers of gypsum, marlstone, and halite of the Gachsaran Formation result in numerous small sub-aquifers with small discharges, with spring water

Table 2. Area and percent of gypsiferous formations (gypsum-veins bearing formations) and units in Iran.

Gypsiferous Formation, F / Unit, U	Geological Time	Percentage of Iran Area	Percentage of Total Gypsiferous Formations Area	Location in Iran	Lithology
Aghajari F.	Tertiary	2.09	61.22	South – Southwest	sandstone, gypsum-veined, marl, siltstone
E1m, E2m, E3m, E2mg U.	Tertiary	0.26	7.74	Central – East	gypsiferous marl, marl, limestone
Lower Red F.	Tertiary	0.16	4.83	Central – Northeast	silty shale, gypsiferous marl, sandstone, gypsum
M1f, Msc U.	Tertiary	0.15	4.32	Northwest – Southeast	sandstone, gypsiferous mudstone, shale, mudstone
Qom F.	Tertiary	0.13	3.85	Northwest – Central	limestone, marl, gypsiferous marl, sandy marl, sandstone
Shurijeh F.	Jurassic-	0.12	3.60	Northeast	gypsiferous marl, marl, argillaceous limestone, sandstone, conglomerate
Omrb U.	Tertiary	0.11	3.24	Northwest – Central	conglomerate, sandstone, marl, gypsiferous marl, gypsum
K1m, K2Im (U.)	Cretaceous	0.11	3.24	Northwest – Central – East	limestone, argillaceous limestone, Sandstone, gypsiferous marl, marl
Pes, Pem, Pems U.	Tertiary	0.07	2.16	East – Central	gypsiferous mudstone, gypsiferous marl, marl, sandstone, conglomeratic sandstone
Ekgy (U.)	Tertiary	0.03	0.77	Central – North	gypsum
PeEm (U.)	Tertiary	0.03	0.85	North – East	gypsiferous marl, gypsiferous mudstone, marl
Dalan F.	Permian	0.03	0.99	West	dolomitic limestone, anhydrite, limestone, dolomite
Padeha F.	Devonian	0.03	1.01	Central – Northeast	quartz arenite, dolomite, gypsum
Sabz, Makran U.	Tertiary	0.02	0.64	Southeast	gypsiferous and calcareous marl, marlstone, siltstone and sandstone
Eogy (U.)	Tertiary	0.02	0.70	North	gypsum (salt plug)
Ziarat F.	Tertiary	0.02	0.49	North	gypsiferous marl, limestone
Baidu F.	Jurassic	0.01	0.36	Central	sandstone, siltstone, limestone, marl, gypsum

Table 3. Some hydrochemistry characteristics of the gypsum formations and its classification.

Gypsum Formation	Group[a]	No. of Springs	Percent	Q, min. (L s⁻¹)	Q, max. (L s⁻¹)	Q, ave. (L s⁻¹)	EC[b], min. (µS cm⁻¹)	EC, max. (µS cm⁻¹)	Cl⁻, ave. (meq L⁻¹)	Water Type	Description
Sachun	A	7	87	0.3	4	1.3	361	993	1		1 spring with Q = 22 L s⁻¹
Sachun	B	1	13	2.5	2.5	2.5	1348	1348	1.2		
Upper Red	A	30	45	0.1	7.8	1.5	350	970	5		
Upper Red	B	33	49	0.1	8.1	1.9	1024	2840			
Upper Red	C	2	3	2	3	2.5	3620	3700			
Upper Red	D	2	3	6	9.5	7.8	14200	14200			
NSGF[c]	A	10	20	0.5	7	2.3	376	905	1	CO_3^{2-}; SO_4^{2-}	1 spring with Q = 30 L s⁻¹
NSGF	B	37	76	0.5	18	3.5	1101	3480	2.2	SO_4^{2-}	2 springs with Q = 55 and 58 L s⁻¹
NSGF	C	2	4	0.5	0.5	0.5	3540	4824	16	Cl^-	
SGF[d]	B	19	46	0.1	9	1.6	2390	3280	2.55	CO_3^{2-}; SO_4^{2-}	
SGF	C	10	25	0.4	7	2.7	3545	8840	46.46	Cl^-	
SGF	D	12	29	0.5	60	14.5	12096	404000	2048.55	Cl^-	

a Groups of water samples are defined as (A, EC < 1000; B, 1000 < EC < 3500; C, 3500 < EC < 10000; D, 10000 < EC µS cm⁻¹).
b EC is abbreviation for electrical conductivity.
c NSGF is abbreviation for non-salt Gachsaran Formation.
d SGF is abbreviation for salt Gachsaran Formation.

qualities being dependent on the lithology of the flow route. The salinity of the SGF groundwater is higher than the Upper Red and Sachun Formations due to numerous halite units in the SGF.

HYDROGEOLOGY OF THE GACHSARAN FORMATION

Three sites, namely the Tangsorkh , Ambal, and Salbiz, were selected to study the detailed hydrogeology of the SGF and the NSGF.

TANGSGORKH SITE

The Tangsorkh site is located on the northern flank of the Derak anticline. This area is located in the undifferentiated non-salt GF. A detailed geological cross section perpendicular to the strike of the formation was prepared by detailed field surveying (Aghdam, 2012). The undifferentiated non-salt GF consists of upper and lower parts with thicknesses of 908 and 359 m, respectively (Fig. 5). The GF is composed of twenty-eight, forty-eight, four, and two units of gypsum, marl and marlstone, limestone, and sandstone, respectively. The thickness of most of the gypsum units, which are sandwiched between marls and marlstones, varies from 2.5 to 17.2 m while they are sandwiched between the marl or marlstone units. No sinkholes or caves are observed in this site. The sub-aquifers are limited to four limestone, five gypsum, and one gypsum-halite units. Nineteen springs emerge from the sub-aquifers. Among them, the measured flows varied from 0.3 to 8.4 L s⁻¹, with an average of 2 L s⁻¹, respectively (Table 4). The main source of flow in most sub-aquifers is Tangsorkh River water that sinks where it crosses limestone and gypsum units. The spring waters of the Tangsorkh area emerging from GF are classified into two Groups, B and C. Group B consist of eighteen springs of sulfate water with electrical conductivities between 1000 and 3500 µS cm⁻¹. Of these eighteen springs, a sub-group of consisting of ten springs that emerge from four limestone units and three that emerge from alluvium covering the gypsum units have EC ranging from 1200 to 1800 µS cm⁻¹ (subgroup B1). The EC of the five additional springs that emerge from gypsum units varies from 2800 to 3500 µS cm⁻¹ (subgroup B2). The unexpected sulfate type of water in the limestone springs is related to recharge by the sulfate Tangsorkh River water and the adjacent marly layers. Group C has only one spring (S12 on Fig. 5) that emerges from a gypsum unit and has an average EC of 4823 µS cm⁻¹ and average discharge of 0.5 L s⁻¹. The halite in the matrix of this unit changes the type of water to sodium chloride (Table 4).

The diversity in the hydrochemistry of the springs emerging from the limestone or gypsum units indicates that the marly layers prevent hydraulic connections of the adjacent sub-aquifers, leading to flow in the direction of the bedding plane. The dominantly sulfate water in the study area confirms the lack of halite layers in the area.
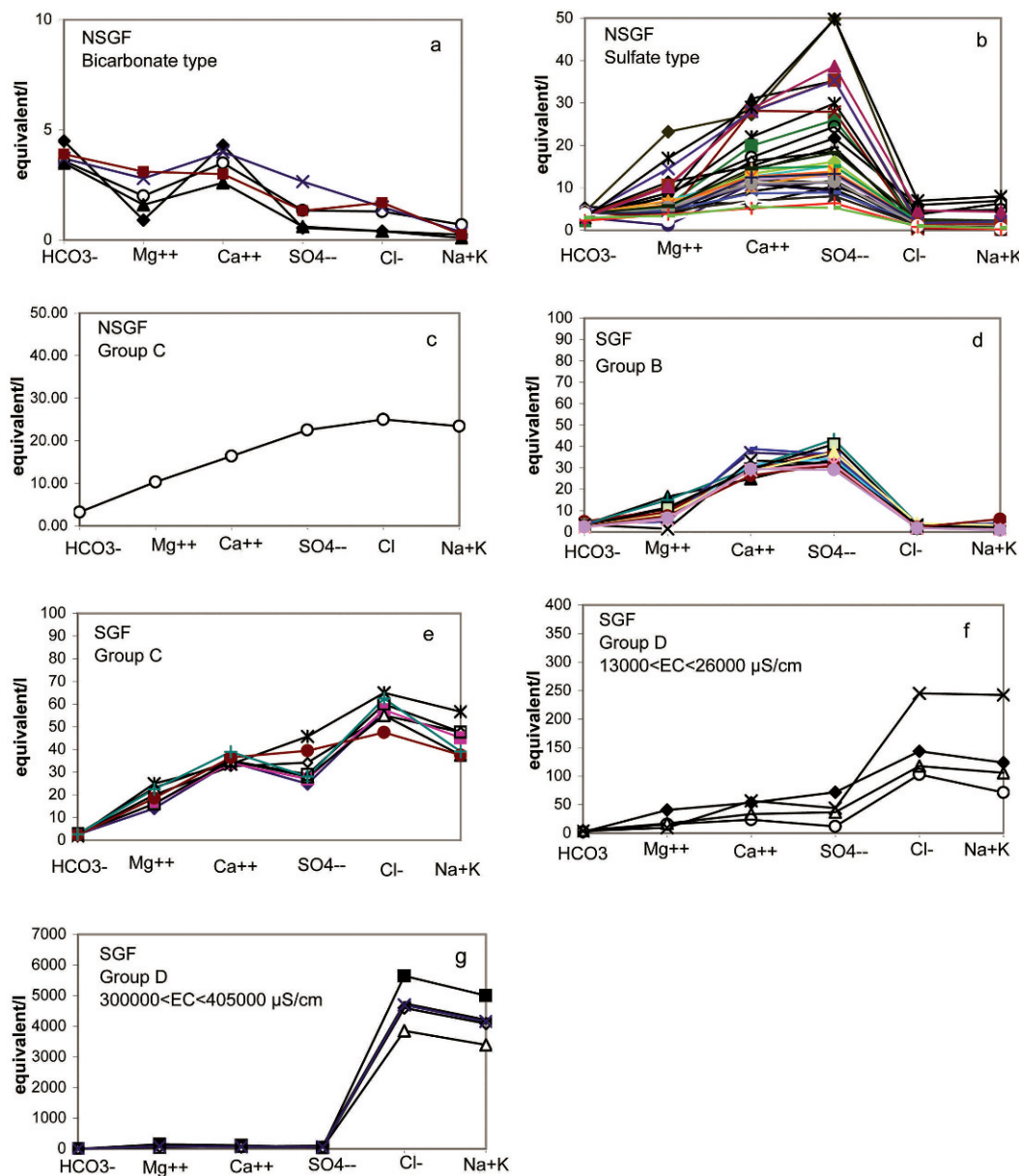
Figure 4. Ion concentrations in spring waters flowing from the non-salt Gachsaran Formation (NSGF) or the salt Gachsaran Formation (SGF), sorted by electrical conductivity groups A–D (see text or note in Table 3). Symbols and colors indentify data from a single spring. (a) NSGF group A bicarbonate water. (b) NSGF group B sulfate water. (c) NSGF group C chloride water. (d) SGF group B bicarbonate/sulfate water. (e) SGF group C chloride water. (f) SFG lower conductivity group D chloride water. (g) SGF higher conductivity group D chloride water.

No springs emerge from twenty-two of the twenty-eight gypsum layers. The main reasons for the lack of springs in those gypsum units are as follows: 1) The Tangsorkh River does not intersect these gypsum units, so precipitation is the only source of recharge. 2) The local base level of the gypsum units are dry drainages intersecting the gypsum units at maximum intervals of 2 km, therefore, the maximum catchment area of the gypsum unit is about 20,000 m^2 (maximum length and width of 2000 and 17.2 m respectively). The average annual flow rate recharging into

each gypsum unit is 0.1 L s^{-1} based on annual average precipitation of 500 mm and recharge coefficient of 0.2. The drainages are covered by coarse-grained alluvium, draining into the adjacent intersecting gypsum units. The recharge value is extremely low, such that no surface water can be observed on the drainages during the dry period. 3) The small thickness of the gypsum units and the low recharge prevent any sinkhole and conduit development. The flow is diffuse, so the recharge water stays in the top soil and a large fraction of the stored water is evaporated.
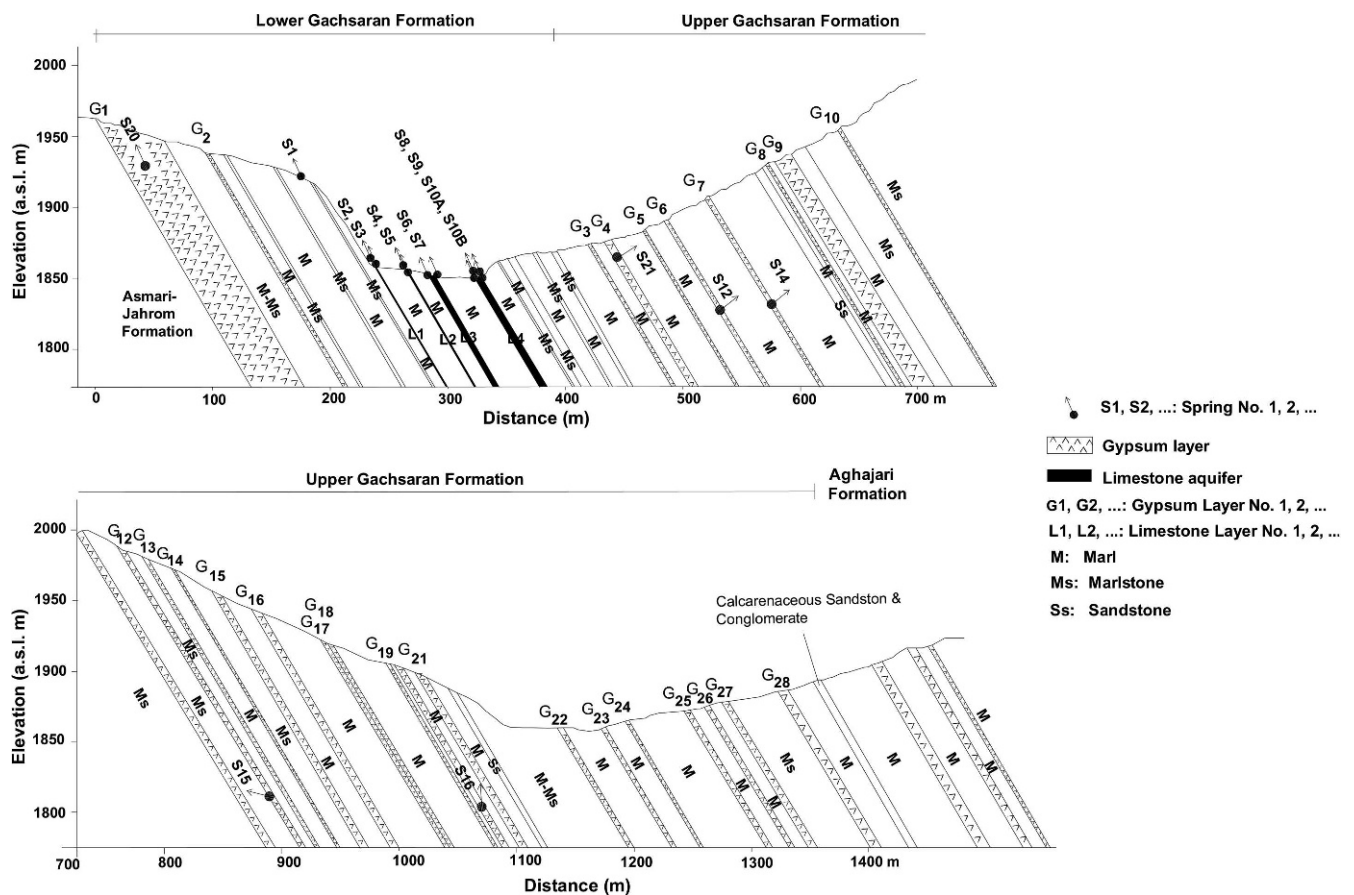
Figure 5. Detailed geological cross section along the Gachsaran Formation at the Tangsorkh site prepared by surveying the outcrop. The horizontal scale is cumulative thickness of the formation, not horizontal distance.

AMBAL SITE

This study area in the Zagros Mountains are located in the GSF. The Ambal area is a 17 km² ridge with a length of 4 km and an elevation of 100 to 340 m.a.s.l. A detailed geologic cross section, perpendicular to strike of the GF, was prepared based on borehole logs (Mahab Ghodss Consulting Engineers, 2009) (Fig. 6). The thickness of the measured cross section is about 300 meters, with additional undifferentiated GF above and below it (e.g., units of marl, anhydrite, halite, undifferentiated Gachsaran, and mixtures of thin (<5 m) beds of marl, anhydrite, halite, and occasional gypsum). The salt layers of the GF are not exposed in most parts of Iran, but they are exceptionally outcropped in some parts of this study area. The Ambal ridge area seems to be an active salt structure where tectonic pressures continuously squeeze the salt to the surface, where it is dissolved (Aghdam et al., 2012).

Sinkholes are the dominant karst features in both the gypsum and salt units of the Ambal area. Sinkhole diameters vary from 1 to 130 m. The Karun River is in direct contact with the Gachsaran Formation along 4 km of the Ambal area. Six springs emerge from the GF a few meters above the Karun River, and numerous springs rise below the water surface. The geological map and location of springs in the studied area are shown in Fig. 7. The springs are classified based on the electrical conductivity of their water into group D, with EC values ranging within 14,250 to 392,000 µS cm⁻¹, all from sodium chloride; total spring discharges are from 0.8 to 7.5 L s⁻¹.

The chemistry of Karun River during contact with the GF quickly evolves from bicarbonate type, with a TDS of ~0.4 g L⁻¹, to chloride type with a TDS of ~1.5 g L⁻¹, mainly due to halite and, to a lesser extent, gypsum. Mass balance and water budget calculations indicate that 5% of the Karun River's salinity enhancement is from direct precipitation in the Ambal area (Aghdam, 2010). The rest is due to the turbulent flow of river water sinking into the fractures and karstic conduits of the evaporite layers that dissolves the gypsum and salt layers of the GF. The borehole logs showed cavities more than 10 m in diameter below the river level (Mahab Ghodss Consulting Engineering, 2009). The flow from the Karun River inside the GF developed a network of karstic conduits and sinkholes, collapsing the marly layers between the huge conduits, and thus connecting the layers of halite and gypsum, such that the Ambal area cannot be considered to have several independent subaquifers.

Table 4. Some hydrochemistry characteristics of the Gachsaran Formation in the three sites.

Site	Group[a]	No. of Springs	Percent	Q, min. (L s^{-1})	Q, max. (L s^{-1})	Q, ave. (L s^{-1})	Q, total (L s^{-1})	EC[b], min. (µS cm^{-1})	EC, max. (µS cm^{-1})	Cl$^-$, ave. (meq L^{-1})	Water Type
Tangsorkh	B1	13	69	0.3	8.4	2.6	34.3	1234	1649	2.1	SO$_4^{2-}$
Tangsorkh	B2	5	26	0.5	0.75	0.6	3	2800	3540	3.4	SO$_4^{2-}$
Tangsorkh	C	1	5	0.5	0.5	0.5	0.5	4824	4824	25	Cl$^-$
Ambal	D	6	100	0.8	7.5	3.3	19.8	14250	392000	3043	Cl$^-$
Salbiz	B	3	23	0.5	9	3.3	10	2770	3010	2.4	SO$_4^{2-}$
Salbiz	C	8	62	1	5	2.9	23	7470	8840	57.5	Cl$^-$
Salbiz	D	2	15	0.1	1	0.6	1.1	17400	404000	2896.8	Cl$^-$

[a] Groups of water samples are defined as (A, EC < 1000; B, 1000 < EC < 3500; C, 3500 < EC < 10000; D, 10000 < EC µS cm^{-1}).
[b] EC is abbreviation for electrical conductivity.

SALBIZ SITE

This study area is located in the Salt Gachsaran Formation near the Qatar-Kazerun Fault, 20 km northwest of Kazerun (Fig. 2). The mean annual potential evaporation is 2641 mm. The study area receives an average of 650 mm of rainfall per year. No caves or sinkholes are observed in the study area. The only place in the study area with extensive exposure of the Gachsaran layers is the Salbiz Valley. The lithology of the cross-section along this valley is composed of 252 alternating units of marl-marlstone (51%), gypsum (47%), and limestone (2%) (Aghdam, 2012). No salt layers are exposed in this cross section in spite of several springs with chloride type water and elevated electrical conductivity (Table 4 and Fig. 8) and considering the study area is located on seven members of the GF with extensive salt layers in members 2, 3, 4, and 6. The salt has been leached from the top several meters of the SGF. Therefore, the exposed units are not representative of the full SGF. A full profile must be prepared based on borehole logging.

The water sources along the cross section consist of thirteen springs with the total discharge of 34.1 L s^{-1}; in addition water seeps into the Salbiz River in several locations (Fig. 8). It was not possible to measure the discharge of the seeps because most parts of the Salbiz River are inaccessible. The SGF springs are classified into Groups B, C, and D based on their electrical conductivities (Table 4). Group B consists of three springs with EC from 2770 to 3010 µS cm^{-1}, sulfate water, and a total discharge of 10 L s^{-1}. These springs emerge from gypsum units. Group C is composed of eight springs with EC ranging from 7470 to 8840 µS cm^{-1}, chloride water, and a total discharge of 23 L s^{-1}. The remaining two springs are classified into Group D, with EC ranging from 17,400 to 404,000 µS cm^{-1}, chloride water, and a total discharge of 1.1 L s^{-1}.

That ten out of the thirteen springs have chloride water confirms that the SGF here is dominantly salt layers. None of the ten chloride springs emerge directly from halite units due to the leaching of sodium chloride from the surface. The Gachsaran layers are perpendicular to the Salbiz Valley. Water originating in an area far from the river flows deep into the halite units and converges into the river bed, dissolving the deep halite units. Exposed marly layers perpendicular to the Salbiz Valley and small springs with different ranges of electrical conductivity indicate that the SGF is composed of independent sub-aquifers. The Salbiz Valley is the local base of erosion, draining the water from adjacent gypsum and halite layers, preferentially along the bedding planes. The small springs, the limited catchment areas of the sub-aquifers, and the lack of caves and sinkholes imply the absence of conduit flow in the study area.

COMPARISON OF SITES

The characteristics of the three typical Gachsaran Formation sites are summarized in Table 5. The marly
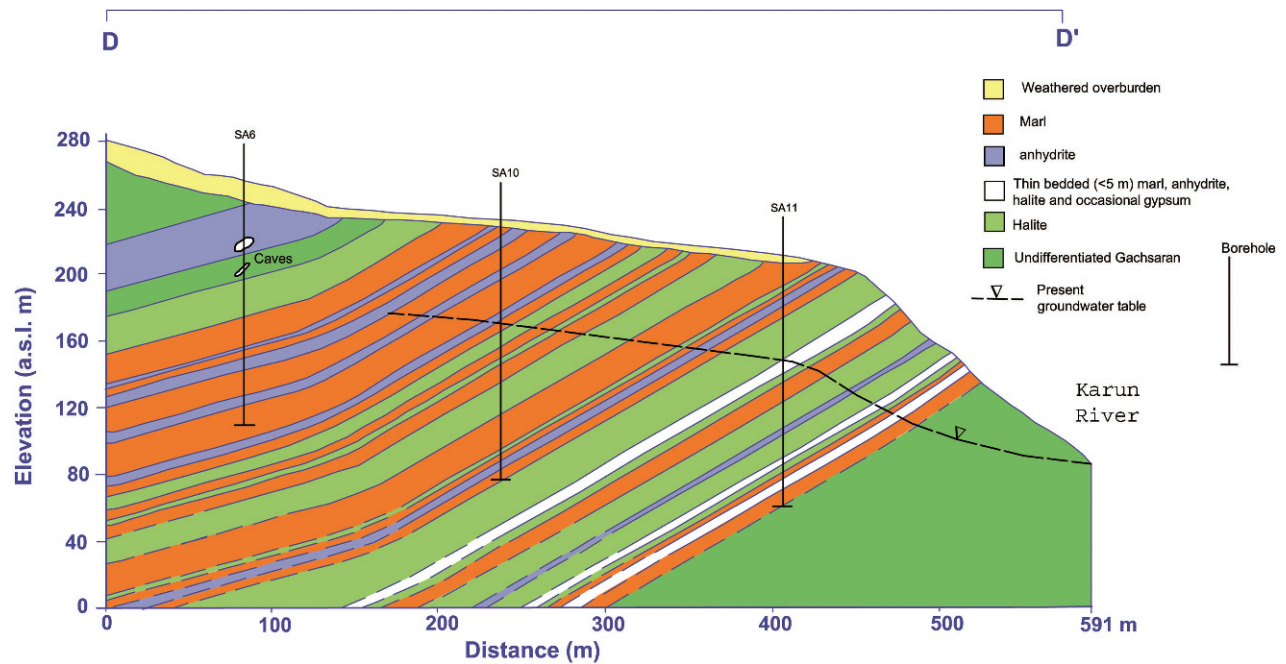
Figure 6. Detailed geological cross section through the Gachsaran Formation at the Ambal site prepared from borehole logs (Mahab Ghodss Consulting Engineers, 2009).
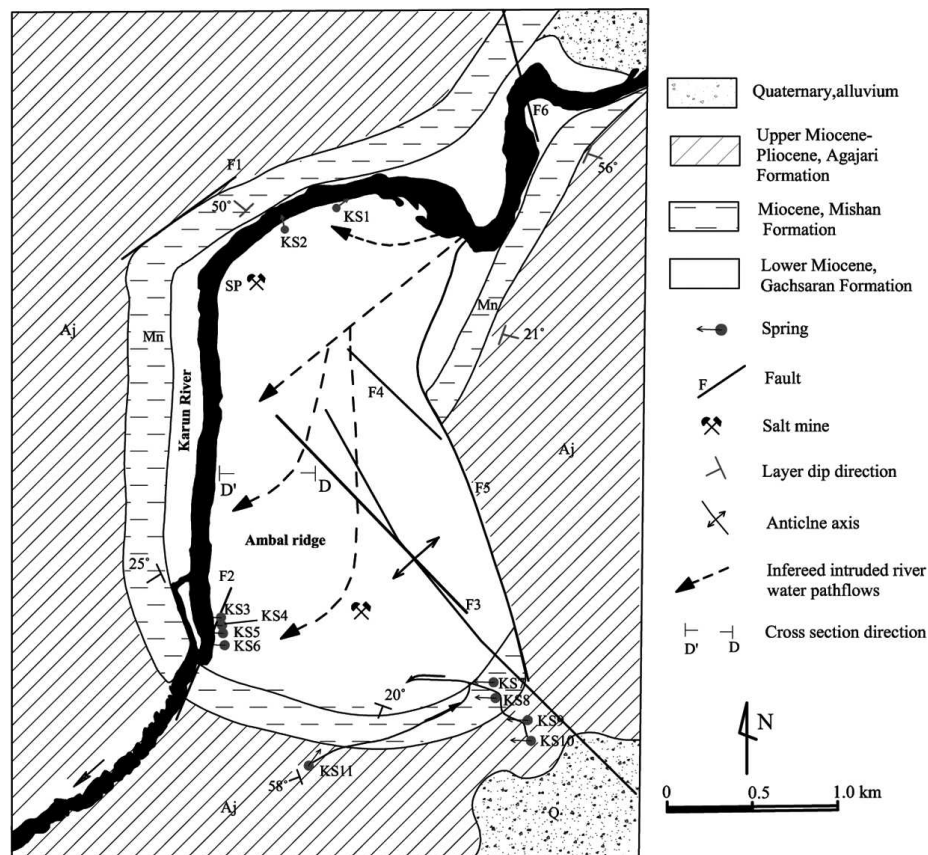

Figure 7. Geology map of the Ambal Ridge study area, including the locations of the sampling points (KS) and inferred flow paths of diverted river water.
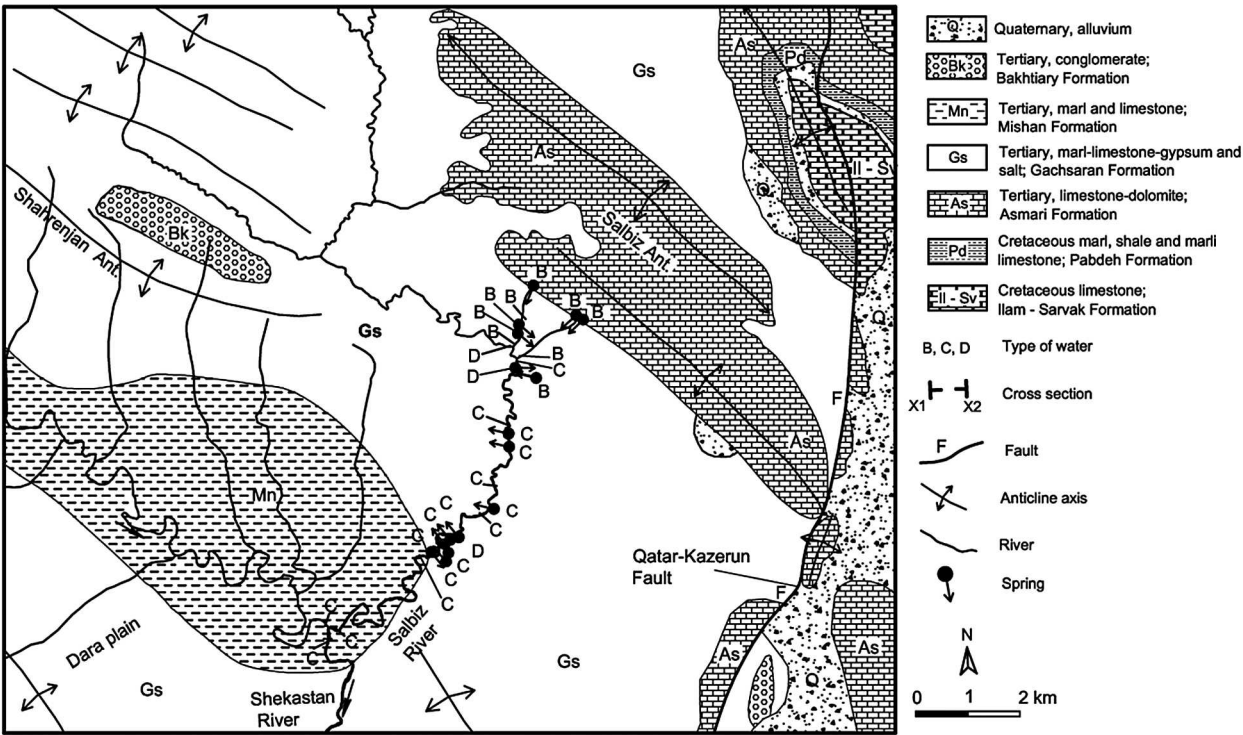
Figure 8. Geology map of the Salbiz site, including the locations of the sampling points labeled by their electrical conductivity group B–D as defined in the text or a note in Table 3. Both springs and surface water sites are shown.

units disconnect the evaporate units in the Tangsorkh and Salbiz sites, resulting in limited catchment areas, flow parallel to the bedding, low-discharge springs, absence of extensive sinkholes and caves, and flow being predominantly diffuse. Tectonic activities exposed salt rocks in the Ambal site, and inflow from the Karun River developed huge conduits beneath the Ambal Ridge, developing extensive sinkholes. As a result, the marly units collapsed, hydraulically connecting the evaporate units. These conditions resulted in a direction of flow toward base level instead of the direction of the

bedding planes. The hydrochemistry of these sites is strongly related to the lithology of the groundwater route, such that the springs are sulfate in the Tangsorkh site, with its lithology of marl and gypsum, and sulfate and chloride in the Salbiz site, with a lithology of marl, gypsum, and salt. The type of water is chloride in Ambal, in spite of the alternating gypsum and salt units and groundwater flow through both gypsum and salt units. It is the higher dissolution rate of the salt that controls the hydrochemistry of groundwater in the Ambal site.

Table 5. Comparison of the three sites.

Subject	Tangsorkh	Salbiz	Ambal
Lithology	marl, gypsum	marl, gypsum, salt	marl, gypsum, salt
Salt outcrop	no	no	extensive outcrop
Hydraulic connection between evaporites units	disconnect	disconnect	connect
Karst morphology	no cave, a few sinkholes	no cave, no sinkholes	caves and sinkholes
Springs discharge	small	small	probably large under river springs
Karst conduits	no	no	yes
Flow type	diffuse	diffuse	conduit
Hydrochemistry controlling factor	lithology	lithology	lithology
Water type	sulfate	sulfate, chloride	chloride
EC range ($\mu S\ cm^{-1}$)	mainly bellow 3,500	bellow 16,000	16,000 to 350,000

Water Use

Halite dissolution is significantly more detrimental to the quality of spring water than gypsum dissolution. Sulfate type water with electrical conductivity less than 3000 μS cm^{-1} was used for drinking in rural area a few decades ago, but currently, water from carbonate karst springs or wells is piped to rural areas. Sulfate and chloride type water with EC less than 7000 μS cm^{-1} is used for irrigation. The total discharge of the Gachsaran Formation springs is very low, so the contribution of these waters to agricultural products is not significant. Most of the saline and brine springs emerging from the GF join the permanent rivers more or less immediately, and the salinity is diluted to acceptable levels. The worst effects are on the groundwater. Saline and briney water flows from the GF into adjacent karstic Asmari or alluvium aquifers, increasing the EC up to 10,000 μS cm^{-1} (Raeisi and Moor, 1993). The Salt Gachsaran Formation outcrops in the reservoir of a few dams, for example Kowsar and Maroon, but the quality of water is not affected because no salt outcrops in the reservoir and the strike is parallel to the dam axis, so that the marly units prevent flow toward the reservoir.

Conclusions

The main gypsum formations in Iran are the Upper Red, Gachsaran, Sachun, and Hith Anhydrite, making up five percent of Iran's total land area. The Upper Red, Sachun, and Hith Anhydrite Formations are predominantly composed of gypsum and marlstone. The Gachsaran Formation is divided into the SGF and NSGF. The NSGF consists of alternating units of anhydrite or gypsum, gypsiferous limestone, or dolomites. The SGF is composed of alternating units of gypsum, marl, and salt. The quality of springs emerging from the GF strongly reflects the lithology of the groundwater route. The main characteristics of the springs emerging from NSGF and SGF gypsum units without any hydraulic connection to salt units include mostly low discharge and sulfate water type, with electrical conductivity values of less than 3500 μS cm^{-1}. Chloride type water and a wide range of ECs, up to halite saturation, are characteristics of those SGF springs with direct connection between the gypsum and salt units.

The Tangsorkh (NSGF) and Ambal and Salbiz (SGF) sites were selected to study the detailed hydrogeology of the GF. The salt units of GF are not exposed in Iran due to the high salt dissolution rate, except at the Ambal site and another small region where salt ascends continuously by tectonic pressures. In the GF, the marly layers usually hydraulically disconnect the narrow gypsum beds from unexposed halite, resulting in very low discharge from springs and dominantly diffuse flow, preventing cave and sinkhole development and causing the general flow to be parallel to the bedding plane. Recharge water in the unexposed salt units flows deep, dissolving the deep halite

units, converging towards the river bed, and ultimately emerging as saline or brine springs. Some special hydrogeological settings, for example, a tectonically active zone or where there is inflow from an adjacent river, result in the development of a conduit system, formation of collapse sinkholes in the halite and gypsum units, and consequent connection of the gypsum and halite units. In such a case, the general flow direction may not be in the direction of the bedding planes, and it will depend on other parameters of karst development, such as a highly soluble lithology or the local base level. Gachsaran Formation water with an EC of less than 7000 μS cm^{-1} is used for irrigation. The low-discharge saline and brine GF spring waters are usually diluted to acceptable levels by mixing with the good quality waters of permanent rivers, but in several cases, the salty water in the GF degrades the quality of nearby karstic and alluvium aquifers.

References

Aghanabati, A., 2006, Geology of Iran: Ministry of Industry and Mines, Geological Survey of Iran, (in Farsi) 576 p.

Aghdam, J., 2012, Hydrogeology of gypsum formations in the south of Iran [Ph.D. thesis]: Shiraz, University of Shiraz, 120 p.

Aghdam, J.A., Zare, M., Capaccioni, B., Raeisi, E., and Forti, P., 2012, The Karun River waters in the Ambal ridge region (Zagros mountain Range, southwestern Iran): mixing calculation and hydrogeological implications: Carbonates and Evaporites (in press). doi:10.1007/s13146-012-0083-8.

Ashjari, J., and Raeisi, E., 2006, Lithological control on water chemistry in karst aquifers of the Zagros Range, Iran: Cave and Karst Science, v. 33, no. 3, p. 111–118.

Bagheri, R., 2007, Leakage potential in Seymareh dam site [M.Sc. thesis]: Shiraz, University of Shiraz, (in Farsi) 225 p.

Bahadori, A., Carranza, E.J.M., and Soleimani, B., 2011, Geochemical analysis of evaporite sedimentation in the Gachsaran Formation, Zeloi oil field, southwest Iran: Journal of Geochemical Exploration, v. 111, p. 97–112. doi:10.1016/j.gexplo.2011.02.007.

Bahroudi, A., and Koyi, H.A., 2004, Tectono-sedimentary framework of the Gachsaran Formation in the Zagros foreland basin: Marine and Petroleum Geology, v. 21, p. 1295–1310. doi:10.1016/j.marpetgeo.2004.09.001.

Berberian, M., and King, G.C.P., 1981, Towards a paleogeography and tectonic evolution of Iran: Canadian Journal of Earth Sciences, v. 18, p. 210–265. doi:10.1139/e81-019.

Darvishzadeh, A., 2003, Geology of Iran, Tehran, Amir Kabir, 901 p.

Dunnington, H.V., 1968, Salt-tectonic features of Northern Iraq, in Mattox, R.B., ed., Saline Deposits: A Symposium Based on Papers from the International Conference on Saline Deposits, Geological Society of America Special Paper 88, p. 183–227.

Edgell, H.S., 1996, Salt tectonics in the Persian Gulf basin, in Alsop, G.L., Blundell, D.L., and Davison, I., eds., Salt Tectonics, Geology Society of London, Special Publication 100, p. 129–151. doi:10.1144/GSL.SP.1996.100.01.10.

Ford, D.C., 1997, Principal features of evaporite karst in Canada: Carbonates and Evaporites, v. 12, no. 1, p. 15–23. doi:10.1007/BF03175798.

Ford, D.C., and Williams, P.W., 1989, Karst Geomorphology and Hydrology, London, Unwin Hyman, 601 p.

Gill, W.D., and Ala, M.A., 1972, Sedimentology of Gachsaran Formation (lower Fars series), Southwest Iran, American Association of Petroleum Geologists Bulletin 56, p. 1965–1974.

Gutiérrez, F., Calaforra, J.M., Cardona, F., Orti, F., Durán, J.J., and Garay, P., 2008, Geological and environmental implications of the evaporate karst in Spain: Environmental Geology, v. 53, p. 951–965. doi:10.1007/s00254-007-0721-y.

Hessami, K., Koyi, H.A., Talbot, C.J., Tabasi, H., and Shabanian, E., 2001, Progressive unconformities within an evolving foreland fold–thrust belt, Zagros Mountains: Journal of the Geological Society, v. 158, p. 969–981. doi:10.1144/0016-764901-007.

James, G.A., and Wynd, J.D., 1965, Stratigraphic nomenclature of Iranian Oil Consortium Agreement Area: American Association of Petroleum Geologists Bulletin, v. 49, no. 12, p. 2182–2245.

Johnson, K.S., 1996, Gypsum karst in the United States: International Journal of Speleology, v. 25, no. 3–4, p. 183–193.

Johnson, K.S., 2003, Evaporite-karst problems in the United States, in Johnson, K.S., and Neal, J.T., eds., Evaporite Karst and Engineering/Environmental Problems in the United States, Oklahoma Geological Survey, Circular 109, p. 1–20.

Kashfi, M.S., 1980, Stratigraphy and environmental sedimentology of lower Fars Group (Miocene), South–Southwest Iran: American Association of Petroleum Geologists Bulletin, v. 64, p. 2095–2107. doi:10.1306/2F919742-16CE-11D7-8645000102C1865D.

Khosro Tehrani, K., 1987, Stratigraphy and formations type sections, Tehran, University of Tehran, (in Farsi) 260 p.

Klimchouk, A., and Andrejchuk, V., 1996, Environmental problems in gypsum karst terrains: International Journal of Speleology, v. 25, no. 3–4, p. 145–156.

Klimchouk, A., Forti, P., and Cooper, A., 1996, Gypsum karst of the World: a brief overview: International Journal of Speleology, v. 25, no. 3–4, p. 159–181.

Mahab Ghodss Consulting Engineers, 2009, Slope Stability Analysis of the Reservoir, Upper Gotvand Dam, Iran Water & Power Resources Development Company, 48 p.

Maximovitch, G.A., 1962, Karst of gypsum and anhydrite of the globe (geotectonical relations, distribution, and major peculiarities), in Obshchiye voprosi karstovedemiya: Moscow, p. 108–113 (in Russian).

Mostofi, B., and Frei, E., 1959, The main sedimentary basins of Iran and their oil possibilities, Proceedings, 5th World Petroleum Congress, New York, section 1, paper 17, 10 p.

Motiei, H., 1993, Treatise on the geology of Iran – stratigraphy of Zagros: Editor-in-Chief, A. Hushmandzadeh. Tehran, Geological Survey of Iran, (in Farsi) 536 p.

Murris, R.J., 1980, Middle East, stratigraphic evolution and oil habitat: American Association of Petroleum Geologists Bulletin, v. 64, p. 597–618.

O'Brien, C.A.E., 1957, Salt diapirism in South Persia: Geologie en Mijnbouw, v. 19, p. 357–376.

Oveisi, B., 2001, Resume of Kelestan geological map report, scale 1:100000, Geological Survey & Mineral Exploration of Iran, sheet No. 6449.

Raeisi, E., and Moore, F., 1993, The effect of evaporitic formations on the quality of karst water: Iranian Journal of Science & Technology, v. 17, no. 2, p. 91–103.

Rahimi, M., 2006, Effect of rainfall, temperature, geological factors, and level base of erosion on characteristics of Asmari-Jahrum Formations in south-central Iran [M.Sc. thesis]: Shiraz, University of Shiraz, (in Farsi) 163 p.

Stöcklin, J., 1968, Salt deposits of the Middle East, in Mattox, R.B., ed., Saline Deposits: A Symposium Based on Papers from the International Conference on Saline Deposits, Geology Society of America, Special Paper 88, p. 157–181.

Stöcklin, J., and Setudehnia, A., 1977, Stratigraphic Lexicon of Iran, Ministry of Industry and Mines, Geological Survey of Iran, Report No. 18-1971, Second Edition, 370 p.

Talbot, C.J., and Alavi, M., 1996, The past of a future syntaxis across the Zagros, in Alsop, G.I., Blundell, D.J., and Davison, I., eds., Salt Tectonics. Geological Society of London Special Publication 100, p. 89–109. doi:10.1144/ GSL.SP.1996.100.01.08.

LATE QUATERNARY CAVIOMORPH RODENTS (RODENTIA: HYSTRICOGNATHI) FROM CEARÁ STATE, NORTHEAST BRAZIL

PAULO VICTOR DE OLIVEIRA[1], ANA MARIA RIBEIRO[2], LEONARDO KERBER[2], GISELE LESSA[3]
AND MARIA SOMÁLIA SALES VIANA[4]

Abstract: In this paper we report the first remains of caviomorph rodents from the karst of the Parque Nacional de Ubajara, Ceará State, northeastern Brazil, collected with precise stratigraphic and radiometric control. The material is derived from levels with thermoluminescence dating of about 8,000 years BP, corresponding to the early Holocene. In these levels, we found remains of *Kerodon rupestris* Wied, 1820, cf. *Dasyprocta* Illiger, 1811 and *Thrichomys* Trouessart, 1880. The data here reported contribute to the knowledge of Brazilian Quaternary rodents and show the potential of the studied area for fossils.

INTRODUCTION

Caviomorphs are South American hystricognath rodents that arrived on the continent probably during the Eocene (Wyss et al., 1993; Poux et al., 2006; Antoine et al., 2011). During the Cenozoic, the group achieved great ecological and morphological diversity and occupied several niches. The oldest records of this group in Brazil are from the Oligocene Tremembé Formation (Vucetich et al., 1993; Vucetich and Ribeiro, 2003) and the Miocene of Acre State (see Negri et al., 2010). Younger records are exclusively from the late Quaternary. However, these records are poorly studied. Recent studies from several Quaternary localities in South America have shown interesting results, with descriptions of new taxa and different paleobiogeographic patterns in comparison with the modern fauna (e.g., Cartelle and Lessa, 1989; Vucetich et al., 1997; Vucetich and Verzi, 2002; Ubilla et al., 2008; Hadler et al., 2008; Kerber et al., 2011a, b; Rodrigues et al., 2011). The cited papers demonstrate the need to use multiple approaches to understand the evolution of South American Quaternary rodents.

In northeastern Brazil several records of Quaternary mammals have been reported, mainly from karsts and *tanques*. But the small mammals are poorly studied in comparison with the large- and medium-bodied taxa and are often not recovered with associated stratigraphic or radiometric data. During July 2009, an expedition to the caves of the Parque Nacional de Ubajara, Ceará State, northeast Brazil, was made to collect fossil remains with precise stratigraphic and radiometric control. In this paper, we describe the remains of caviomorph rodents collected during this expedition.

MATERIAL AND METHODS

The remains are deposited in the paleovertebrate collection of the Museu Dom José. They comprise nine specimens, including isolated teeth and fragments of dentary and maxilla.

Dental nomenclature follows Quintana (1996) for Caviidae and Patterson and Wood (1982) for Echimyidae and Dasyproctidae. However, these nomenclatures do not reflect any opinion on the homologies of these structures. The anatomical nomenclature of the dentary of Cavioidea follows Pérez (2010). The comparative specimens are listed in appendix 1. Institutional abbreviations: MCPU-M, Coleção de Mastozoologia, Pontifícia Universidade Católica do Rio Grande do Sul, Uruguaiana, Rio Grande do Sul, Brazil; MDJ M, Coleção de Mastozoologia, Museu Dom José, Sobral, Ceará, Brazil; MLP, Colección de Mastozoología, Museo de La Plata, Argentina; MN, Coleção de Mastozoologia, Museu Nacional, Rio de Janeiro, Brazil.

LOCATION AND GEOLOGICAL SETTING

The Parque Nacional de Ubajara, located in Ubajara Municipality (Fig. 1), in the Ibiapaba *Cuesta* region in northwestern Ceará (northeast Brazil), has a significant karst system. According to IBAMA (2002) the speleological province of the Ubajara region consists of nine limestone hills, in which fourteen caves are known to date. The limestone rock outcrops in the region correspond to the Neoproterozoic Frecheirinha Formation of the Ubajara Group of the Ubajara Graben (Quadros, 1996; CPRM, 2003). The Ubajara Group has an upper discordant

[1] Departamento de Geologia, Centro de Tecnologia e Geociências da Universidade Federal de Pernambuco, Av. Acadêmico Hélio Ramos, s/n°, Cidade Universitária, 50740-530, Recife, PE, Brazil, victoroliveira.paleonto@gmail.com
[2] Seção de Paleontologia, Museu de Ciências Naturais, Fundação Zoobotânica do Rio Grande do Sul, Av. Salvador França, 1427, 90690-000, Porto Alegre, RS, Brazil, ana-ribeiro@fzb.rs.gov.br; leonardokerber@gmail.com
[3] Universidade Federal de Viçosa, Departamento de Biologia Animal, Campus Universitário, s/n°, Centro, 36570-000, Viçosa, MG, Brazil, gislessa@yahoo.com.br
[4] Laboratório de Paleontologia, Museu Dom José, Universidade Estadual Vale do Acaraú (LABOPALEO-MDJ/UVA), Av. Dom José, 878, 62010-190, Sobral, CE, Brazil, somalia_viana@hotmail.com
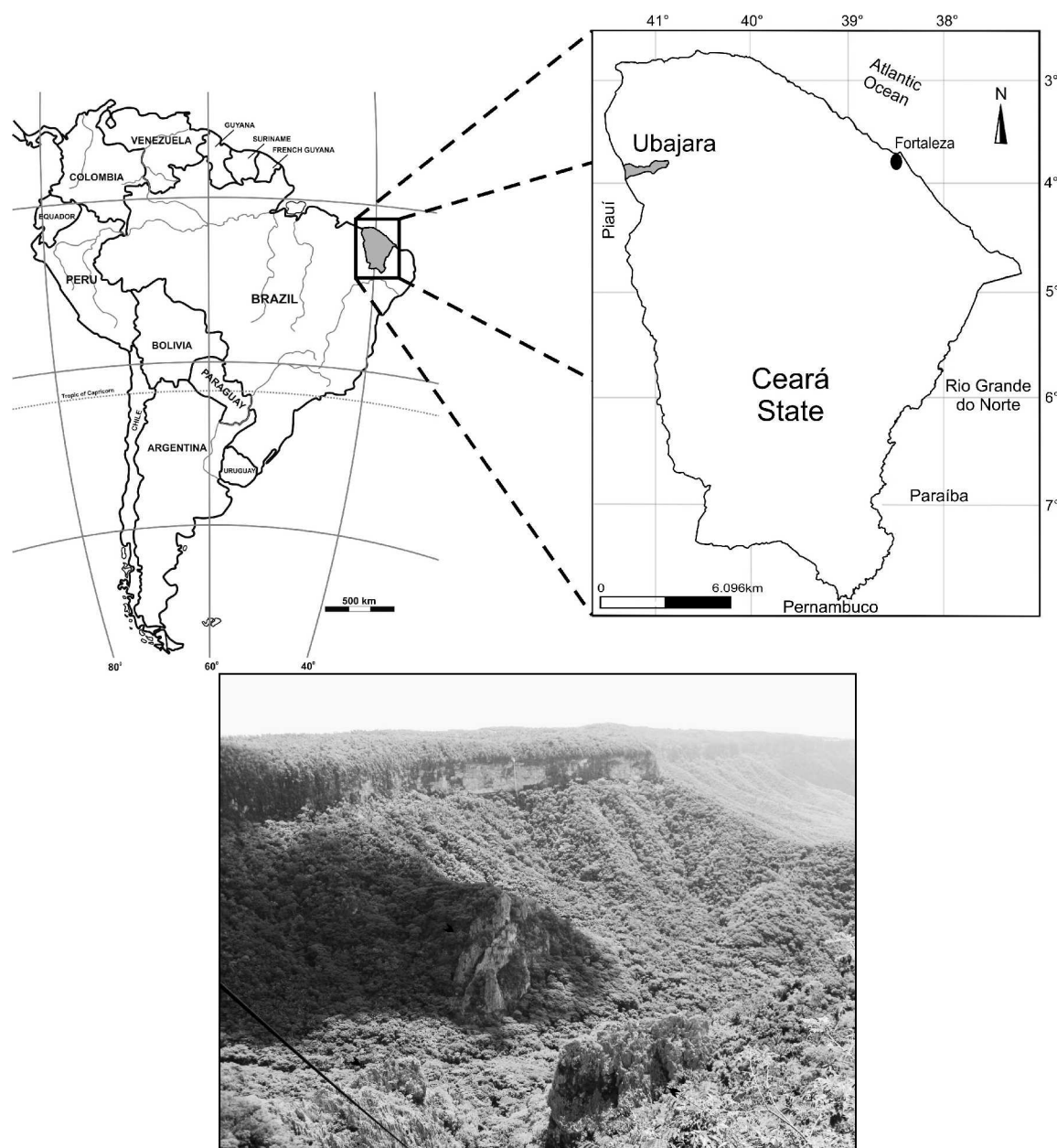
Figure 1. Location map of the Parque Nacional de Ubajara, Ceará (above) and the openings of the caves (below) indicated by arrows.

contact with the Silurian–Devonian Serra Grande Group of the Parnaíba Basin. Among the limestone hills in the studied area stands Pendurado Hill, with two caves, Urso Fóssil and Pendurado.

Previous published information about the Quaternary mammals from this area includes a bear skull and mandible assigned to *Arctotherium brasiliense* (Lund, 1840) described by Trajano and Ferrarezzi (1994). These remains were found in the Urso Fóssil cave (03°49′58″ S, 40°53′34.4″ W). The material studied here was found in one room of this cave, the Sala da Entrada. In this room we made a stratigraphically controlled excavation, exposing three levels of sedimentary deposition. A geological section provided information about

unconsolidated accumulations of sediments of both allochthonous and autochthonous origin, from top to bottom (Fig. 2):

Level 1: 0.15 m thick, is composed of clayey calcareous sediments, light yellowish in color, containing small allochthonous fragments (0.5–1 cm) of amorphous and angular limestone, as well as a great amount of recent seeds and excrement.

Level 2: 0.35 m thick, is composed of clayey sediment, light gray in color, containing allochthonous fragments of limestone (greater than 2 cm), some small geodes and
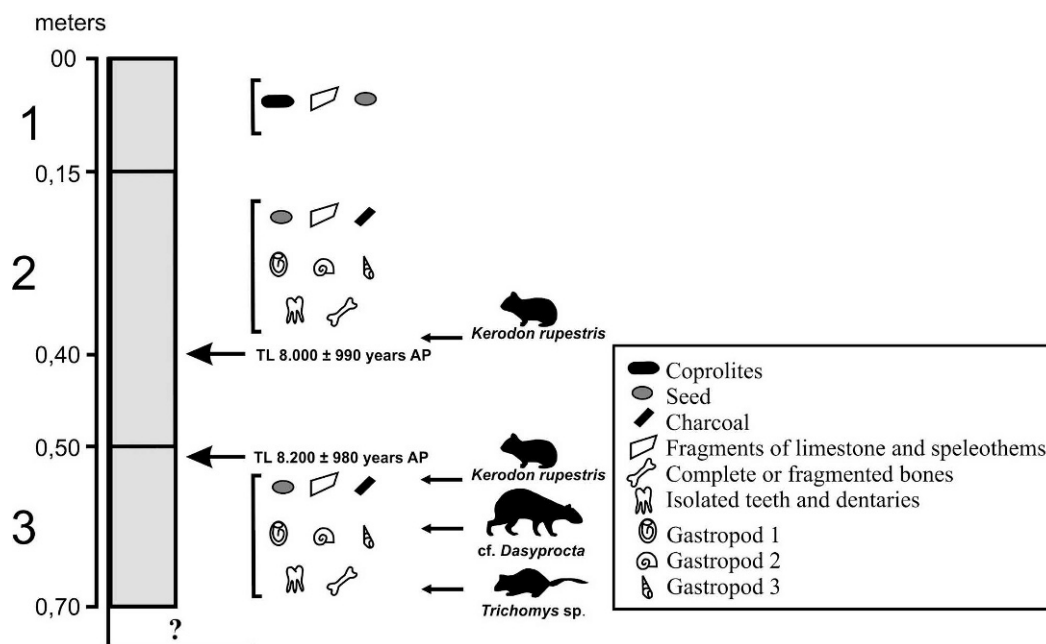
Figure 2. Stratigraphic profile of the sampled deposit in the Urso Fóssil cave, Salão dos Blocos Abatidos, Sala da Entrada, indicating where the fossils were collected.

fragments (approximately 10 cm) of stalactites and others speleothems, showing at times, concentration of iron oxide. It contains, at the top, a high concentration of two types of seeds that are still undetermined; toward the bottom of the layer, some complete shells and numerous shell fragments have accumulated. There are some small droppings covered by powdered carbonate, but still unconsolidated. At about 20 cm from the top of this layer, we collected sediment samples for thermoluminescence dating in a PVC pipe and then, below, for recovery of palynomorphs. We also collected three species of gastropods and numerous bone fragments of Didelphimorphia, Xenarthra, and Rodentia.

Level 3: 0.20 m thick, is composed of clayey sediment containing smaller autochthonous fragments of limestone and very large and angular calcareous blocks. In this level, shells and several small bone fragments occur. As in layer 2, samples for thermoluminescence dating were collected, along with the remains of squamate reptiles and mammals of the Didelphimorphia, Xenarthra, Rodentia and Artiodactyla.

These fossil assemblages could have been accumulated by predators or scavengers or overflow of owl. A taphonomic study is currently underway.

Systematic Paleontology

Rodentia Bowdich, 1821
Hystricognathi Tullberg, 1899
Caviomorpha Patterson and Wood (in Wood, 1955)
Cavioidea Fischer de Waldheim, 1817
Genus *Kerodon* Cuvier, 1825

Kerodon rupestris Wied, 1820
(Fig. 3)
Material: MDJ M-845, fragment of right dentary with incomplete p4; MDJ M-846, fragment of left dentary; MDJ M-888, fragment of right dentary with p4; MDJ M-890, toothless and incomplete right dentary.

Geographic and stratigraphic provenance: Parque Nacional de Ubajara, Pendurado Hill, Urso Fóssil cave: Sala da Entrada, levels 2 and 3.
Description: The dentary has the anteriormost area of the horizontal crest (*sensu* Pérez, 2010) at the level of the mesial area of the p4, and the anteriormost area of the notch for the insertion of the tendon of the *masseter medialis pars infraorbitalis* muscle (*sensu* Woods and Howland, 1979; and Pérez, 2010) is located below the pr. I of the m1 alveolus. The symphysis is narrow and long. The mental foramen is positioned on the lateral side of the diastema. In medial view, the alveolus of the incisor extends posteriorly up to the level of the pr. II of p4 and pr. I of the m1 contact. The p4 is euhypsodont, and the anterior additional elongation is well developed, as a true prism. The anterior additional elongation and the prisms are transversally oriented, increasing in size distally. The prisms are united by a thin and very short isthmus. On the lingual surface of the tooth there are two poorly developed furrows, one on the pr. II and another on the additional elongation. The hypoflexid extends almost the entire width of the tooth. In the lingual ends of the labial flexids there is cement.
Discussion: Traditionally, *Kerodon* was considered a member of the Caviinae. However, recent studies have
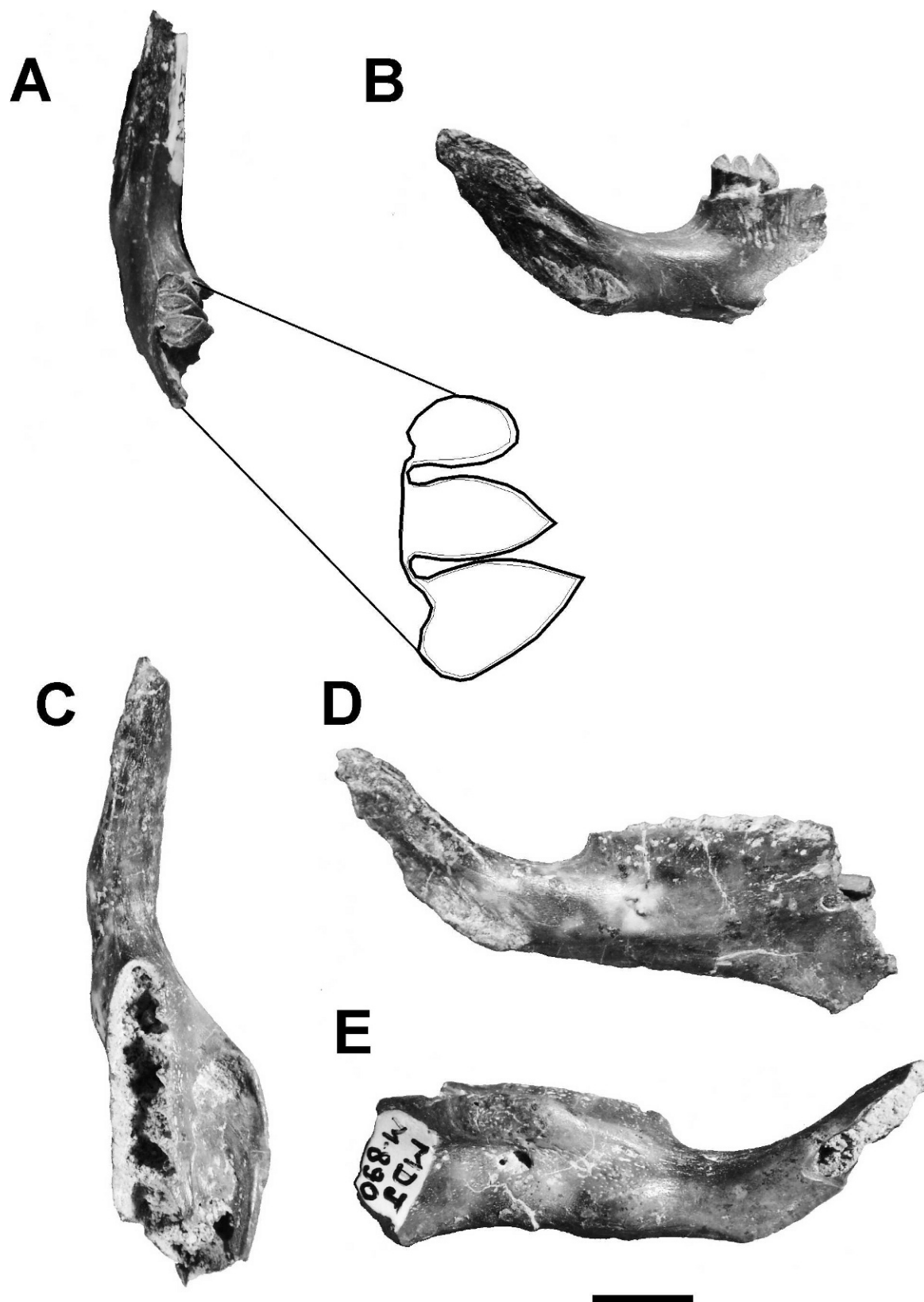
Figure 3. Right dentary of *Kerodon rupestris* from the early Holocene of Ceará. MDJ M-888 with p4 in detail, in occlusal (A) and medial (B) views. MDJ M-890 in occlusal (C), medial (D) and lateral (E) views. Scale bar: 5 mm.

Table 1. Measurements (in mm) of fossil specimens of *K. rupestris* from Ceará and comparative specimens of the living *K. rupestris* and *K. acrobata*.

Specimen	Length of the Symphysis	Height of the Dentary at Level of p4	Height of Dentary at Level of Diastema	Length of the Diastema	Mesiodistal Length (MDL) of p4 Alveolus	Linguolabial Width (LLW) of p4 Alveolus	MDL of m1 Alveolus	LLW of the m1 Alveolus	MDL of the m2 Alveolus	LLW of the m2 Alveolus
K. rupestris: Ceará State										
MDJ M-890	15.06	7.70	4.58	14.41	4.19	2.89	3.80	3.09	3.40	3.00
MDJ M-888	13.73	…	4.28	14.99	3.63	2.67	…	…	…	…
MDJ M-846	…	7.36	…	…	3.98	2.96	…	…	…	…
K. acrobata										
n	3	3	3	3	3	3	3	3	3	3
Mean	17.53	9.66	5.94	17.01	4.35	2.66	3.52	3.11	4.15	3.16
Min/Max	17.39/17.72	9.43/9.94	5.68/6.16	16.14/17.58	4.17/4.46	2.23/2.88	3.45/3.58	2.97/3.20	3.69/4.64	3.01/3.45
SD	0.16	0.25	0.34	0.76	0.16	0.35	0.06	0.12	0.47	0.24
K. rupestris										
n	25	25	25	25	25	25	25	25	25	25
Mean	12.52	7.36	4.56	12.27	3.30	2.21	3.04	2.49	3.23	2.60
Min/Max	9.8/15.21	5.82/6.69	3.36/5.3	8.56/14.36	2.64/3.77	1.74/2.86	2.45/3.69	2.09/2.97	2.28/3.84	2.02/3.22
SD	1.55	0.80	0.45	1.66	0.30	0.24	0.30	0.25	0.38	0.31

Abbreviations: n, sample size, Min, minimum, Max, maximum, SD, standard deviation.

considered it more closely related to the Hydrochoeridae (see Rowe and Honeycutt, 2002). In the cladistic analysis of Pérez (2010), *Kerodon* is the sister group of *Cardiomys* Ameghino, 1885 (Caviidae: Cardiomyinae) plus the Hydrochoeridae.

The specimens here reported differ from the other Quaternary caviids, such as *Galea* Meyen, 1832, *Microcavia* Gervais & Ameghino, 1880 and *Cavia* Pallas, 1766, in the presence of a longer and narrower symphysis and a triprismatic p4. Currently, the genus *Kerodon* has two extant species: *K. acrobata* Moojen, Locks & Langguth, 1997 and *K. rupestris*, the latter being recorded in the Parque Nacional de Ubajara (Guedes et al., 2000). The fossil specimens share with both taxa the anterior area having a horizontal crest at the level of the p4, the anterior area of the notch for the insertion of the tendon of the *masseter medialis pars infraorbitalis* muscle located below the pr. I of the m1, and a triprismatic p4 with labial furrows. However, they are different from *K. acrobata* in the presence of the anterior area of the horizontal crest being less prominent anteriorly and in having a smaller symphysis, diastema, and height of the dentary (Table 1; Fig. 4).

Kerodon are often associated with rocky and dry environments from Caatinga and Cerrado (Oliveira and Bonvicino, 2006). The fossil record of this taxon is very scarce. The only records are from the late Pleistocene/ Holocene of northeast Brazil (Guérin et al., 1993; Lessa et al., 2008; Rodrigues et al., 2011). These records are within the modern range of *K. rupestris*. Lessa and Gonçalves (1999) reported specimens of *K. rupestris* from the late Pleistocene/Holocene of Bahia, these being larger than the Recent specimens. This fact was not observed in the specimens analyzed here.

Dasyproctidae Smith, 1842
cf. *Dasyprocta* Illiger, 1811
(Fig. 5)
Material: MDJ M-882 right m1 or m2; MDJ M-880 right m1 or m2.

Geographic and stratigraphic provenance: Parque Nacional de Ubajara, Pendurado Hill, Urso Fóssil cave: Sala da Entrada, level 3.

Description: The description is based on MDJ M-882, which is better preserved (Fig. 5A). The tooth has a subrectangular outline, and the distal enamel layer is more curved than the mesial. It is protohypsodont, and the degree of hypsodonty is similar to that seen in *Dasyprocta* and *Myoprocta* and distinct from the Quaternary dasyproctid *Plesiaguti* Vucetich & Verzi, 2002, in which it is less hypsodont. It is pentalophodont, such as in the living dasyproctids (*Dasyprocta* and *Myoprocta*), and the lingual flexids are closed, forming fossetids. The lingual end of the hypoflexid is opposite the tip of the fourth flexid, but they are not confluent. The second and third flexids are connected by their labial ends, and the third lophid is interrupted.
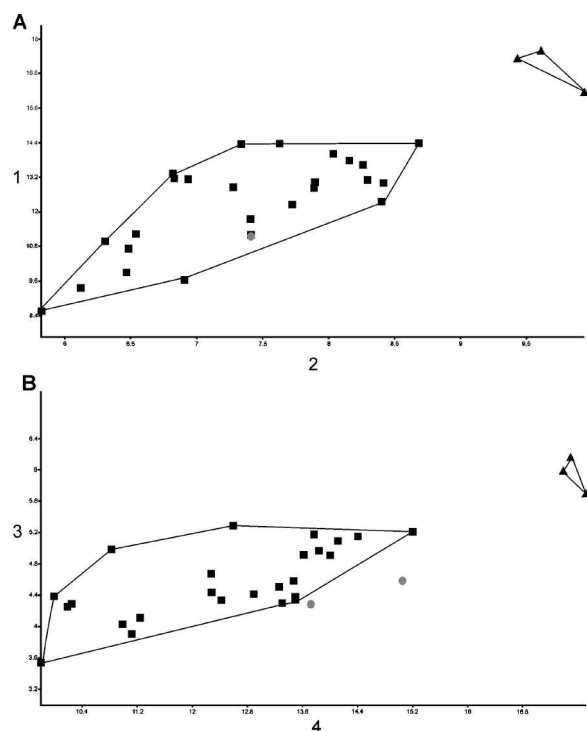
Figure 4. Bivariant diagrams of measurements of fossils of *K. rupestris* (gray circles), living *K. rupestris* (black square), and *K. acrobata* (black triangle). (A) Including the specimen MDJ M-890 and comparative specimens. (B) Including MDJ M-890, MDJ M- 888 and comparative specimens. 1. Length of the diastema; 2. Height of the dentary at the level of p4; 3. Height of the dentary at the level of diastema; 4. Length of the symphysis.
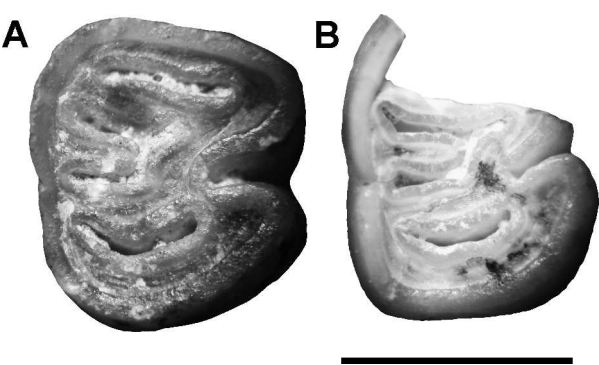
Figure 5. Right m1 or m2 in occlusal view of cf. *Dasyprocta* from the early Holocene of Ceará. (A) MDJ M-882 and (B) MDJ M-880. Scale bar: 3 mm.

Measurements of MDJ M-882: Mesiodistal length – 4.36 mm; Linguolabial width – 3.94 mm.

Discussion: The morphology of the teeth of *Dasyprocta* and *Myoprocta* are similar, but in *Dasyprocta* they are larger. The specimens described here are slightly larger than *Myoprocta* specimens used for comparison, and they are within the variation of *D. prymnolopha* (Table 2).

The living *Dasyprocta* include several species that inhabit almost all lowland tropical forest areas in the South and Central Americas. In Brazil, the review of Iack-Ximenes (1999) recognized the following species: *D. aurea* Cope, 1889, *D. azarae* Lichtenstein, 1823, *D. catrinae* (Thomas, 1917), *D. fuliginosa* Wagler, 1832, *D. croconota* Wagler, 1831, *D. leporina* (Linneus, 1758), *D. nigriclunis* Osgood, 1916, *D. prymnolopha* Wagler, 1841 and *D. aguti*

Table 2. Measurements of comparative specimens of the living dasyproctids: *Dasyprocta azarae*, *D. prymnolopha* and *Myoprocta exilis*.

Specimen	Mesiodistal Length of the m1	Linguolabial Width of the m1	Mesiodistal Length of the m2	Linguolabial Width of the m2
D. azarae				
n	11	11	11	11
Mean	4.76	4.22	4.94	4.28
Min/Max	4.03/5.05	3.19/5.04	4.57/5.61	3.58
SD	0.30	0.47	0.35	0.51
D. prymnolopha				
n	11	11	10	10
Mean	4.12	3.72	4.26	3.65
Min/Max	3.83/4.47	3.25/4.02	4.06/4.49	3.33/3.98
SD	0.20	0.25	0.16	0.23
M. exilis				
n	11	11	11	11
Mean	3.23	3.24	3.67	3.4
Min/Max	3.0/3.42	3.0/3.53	3.37/4.07	2.84/3.81
SD	0.14	0.21	0.23	0.27

Abbreviations: n, sample size, Min, minimum, Max, maximum, SD, standard deviation.
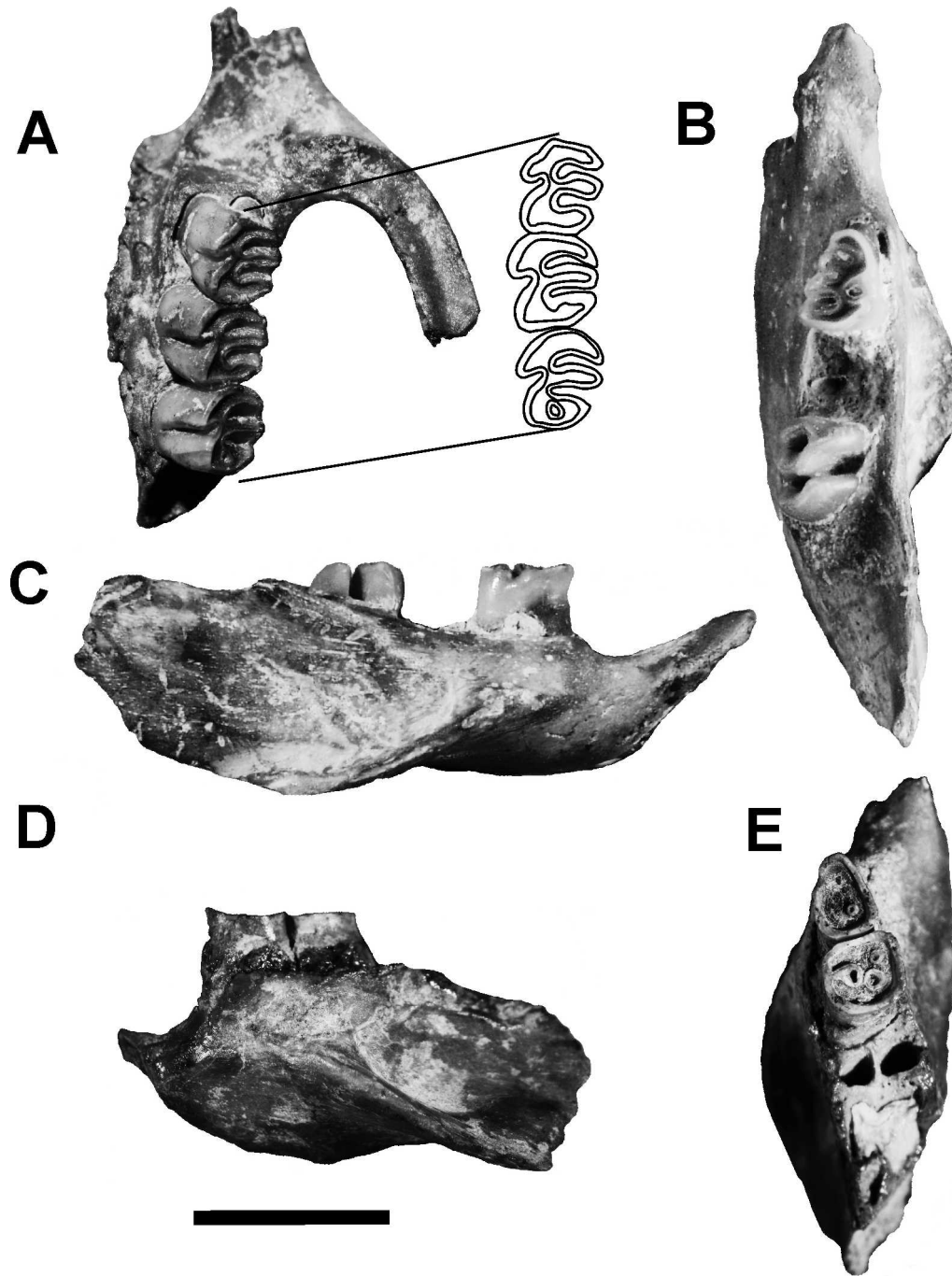
Figure 6. *Thrichomys* sp. from the early Holocene of Ceará. (A) Fragment of a left maxilla, with the DP4, M1 and M2 (MDJ M-891) in palatal view, with detail of the cheek teeth in occlusal view. (B–C) Right dentary with dp4 and m2 (MDJ M-893) in occlusal (B) and lateral (C) views. (D–E) Left dentary with dp4 and m1 (MDJ M-892), in lateral (D) and occlusal (E) views. Scale bar: 5 mm.

(Linnaeus, 1766). However, according to the list of valid species in Woods and Kilpatrick (2005), *D. aurea*, *D. catrinae* and *D. aguti* are synonyms of *D. azarae*, *D. nigriclunis* is synonym of *D. prymnolopha*, and *D. croconota* is a subspecies of *D. leporina*. *Dasyprocta* is distributed in almost all regions of Brazil, while *Myoprocta* is restricted to the Amazonian forest. According to Guedes et al.

(2000), the only living dasyproctid in the Parque Nacional de Ubajara is *D. prymnolopha*.

The living species of *Dasyprocta* are terrestrial and are often associated with water bodies, feeding mainly on fruits, seeds, roots, and leaves (Oliveira and Bonvicino, 2006). The fossil record of this genus is very scarce. According to Vucetich and Verzi (1994), the living

Table 3. Upper cheek teeth measurements of the fossil specimen of *Thrichomys* sp. from Ceará and comparative specimens of the living *T. aperoides*, *T. inermis* and *T. pachyurus*.

Specimen	Mesiodistal Length (MDL) of the DP4	Linguolabial Width (LLW) of the DP4	MDL of the M1	LLW of the M1	MDL of the M2	LLW of the M2
MDJ M-891	2.49	2.05	2.72	2.41	2.46	2.40
T. aperoides						
N	16	16	16	16	16	16
Mean	2.17	2.00	2.31	2.36	2.35	2.49
Min/Max	1.87/2.4	1.63/2.19	2.02/2.65	1.36/2.86	2.01/2.69	1.99/2.95
SD	0.13	0.14	0.16	0.37	0.19	0.30
T. inermis						
N	16	16	16	16	16	16
Mean	2.06	1.96	2.16	2.23	2.28	2.32
Min/Max	1.8/2.32	1.8/2.39	2.01/2.43	2.0/2.49	2.06/2.55	1.93/2.8
SD	0.12	0.14	0.11	0.16	0.14	0.28
T. pachyurus						
N	11	11	11	11	11	11
Mean	2.28	2.23	2.39	2.61	2.49	2.63
Min/Max	2.07/2.57	2.06/2.56	2.12/2.75	2.41/3.11	2.02/2.91	2.21/3.33
SD	0.13	0.13	0.18	0.24	0.23	0.37

Abbreviations: n, sample size, Min, minimum, Max, maximum, SD, standard deviation.

dasyproctids are not related to the taxa from the Tertiary of Argentina. These authors suggest that they have an intertropical/tropical history. Quaternary records for *Dasyprocta* are reported from the Pará, Minas Gerais, Espírito Santo, Bahia, Goiás, and Mato Grosso do Sul states of Brazil (Paula Couto, 1971; 1978; Salles et al., 1999; 2006; Toledo et al., 1999; Lessa et al., 2008). There is no definitive fossil record of *Myoprocta*.

Table 4. Measurements of lower cheek teeth and dentary of fossil specimens of *Thrichomys* sp. from Ceará and comparative specimens of the living *T. aperoides*, *T. inermis* and *T. pachyurus*.

Specimen	Mesiodistal Length (MDL) of the dp4	Linguolabial Width (LLW) of the dp4	MDL of the m1	LLW of the m1	MDL of the m2	LLW of the m2	Height of the Dentary at the Level of dp4
MDJ M -892	2.32	1.62	2.20	2.28	•••	•••	•••
MDJ M- 893	2.52	1.75	•••	•••	2.51	1.72	4.86
T. aperoides							
N	16	16	16	16	16	16	16
Mean	2.51	1.76	2.41	2.20	2.58	2.24	6.34
Min/Max	2.09/3.02	1.63/2.01	1.88/2.69	1.89/2.48	2.17/3.03	1.45/2.69	5.45/7.48
SD	0.21	0.10	0.22	0.16	0.22	0.21	0.60
T. inermis							
N	16	16	16	16	16	16	16
Mean	2.22	1.56	2.14	2.11	2.33	2.09	6.43
Min/Max	1.85/2.45	1.35/1.76	2.01/2.32	1.73/1.93	2.07/2.58	1.88/2.42	5.11/7.12
SD	0.15	0.11	0.10	0.25	0.14	0.14	0.54
T. pachyurus							
N	11	11	11	11	11	11	11
Mean	2.58	2.06	2.45	2.50	2.57	2.60	7.33
Min/Max	2.4/2.8	2.0/2.23	2.25/2.81	2.37/2.71	2.33/2.97	2.37/3.08	6.20/8.67
SD	0.10	0.07	0.16	0.09	0.18	0.22	0.79

Octodontoidea Simpson, 1945
Echimyidae Gray, 1825
Genus *Thrichomys* Trouessart, 1880
Thrichomys sp.
(Fig. 6)

Material: MDJ M-891, fragment of left maxilla with DP4, M1 and M2; MDJ M-892, fragmented dentary with dp4 and m1; MDJ M-893, fragmented dentary with dp4 and m2.

Geographic and stratigraphic provenance: Parque Nacional de Ubajara, Pendurado Hill, Urso Fóssil cave, Salão dos Blocos Abatidos; Sala da Entrada, level 3.

Description: In MDJ M-891, DP4-M2 are similar. Both are trilophodont; however, the M2 has a small fosset in the posteroloph. This fosset is present in some comparative specimens of *T. apereoides* (e.g., MN 63198), but it is reduced (e.g., MN 63200), or absent (e.g., MN 63199) in older individuals. The protocone is slightly distally oriented, and the linguodistal area of the teeth forms a slightly acute angle, more evident in the M1. The lingual area of the anteroloph, the paracone, and the metacone are transversally oriented. All the labial flexi are open, transversally oriented, and extend up to the middle of the occlusal surface, not surpassing the tip of the hypoflexus. The hypoflexus is oblique, slightly mesially oriented, and less developed than the labial flexi, and its labial end is opposite the first labial flexus.

The dp4 (MDJ M-893) is tetralophodont, with a well-developed metalophid. This character differs from other echimyids traditionally grouped in the "Eumysopinae" (see Verzi et al., 1995), such as *Euryzygomatomys* Goeldi, 1901 and *Clyomys* Thomas, 1916, in which the p4 is trilophodont, with an absent or much reduced metalophid (Verzi et al., 1995; Hadler et al., 2008). The m2 of this specimen is little worn, with the lingual flexids still open and the posterolophid isolated from the anterior elements. The m3 is not erupted. MDJ M-892 is an old individual with the dp4 deeply worn and the m1 with all flexids transformed into fossettids (hypofossettid and two lingual fossettids).

In the dentary (MDJ M-893, MDJ M-892), the masseteric crest is tilted, and its anterior area is at the level of the dp4. Considering the comparative specimens, the fossils share with *T. aperoides* the masseteric crest being less developed and the masseteric fossa being less deep than in *T. pachyurus* and *T. inermis*.

Discussion: The subfamily "Eumysopinae" comprises the echimyids with a simplified occlusal pattern, with trilophodont molars. Traditionally, the Eumysopinae encompasses the living taxa *Thrichomys*, *Carterodon* Waterhouse, 1848, *Clyomys*, *Euryzygomatomys*, *Hoplomys* Allen, 1908, *Lonchothrix* Thomas, 1920, *Mesomys* Wagner, 1845, *Proechimys* Allen, 1899, and *Trinomys* Thomas, 1921 and diverse fossil taxa, mainly from the Tertiary of Argentina. Verzi et al. (1995) considered Eumysopinae as a natural group. However, in morphological and molecular cladistic analyses, this subfamily does not form a monophyletic group (e.g., Lara et al., 1996; Carvalho and Salles, 2004; Emmons, 2005; Galewski et al., 2005).

Currently, the genus *Thrichomys* has a complex taxonomic history. Some authors have considered it a single valid species, *T. apereoides* (Lund, 1839), with several subspecies (see Reis and Pessôa, 2004), while others considered it to include, at the very least, four species: *T. apereoides, T. pachyurus* (Wagner, 1841), *T. inermis* (Pictet, 1841) and *T. laurentius* Thomas, 1904 (see Oliveira and Bonvicino, 2006). Pessôa et al. (2004), on the basis of chromosomal and morphometric analyses recognized at least two well-defined species: *T. apereoides* and *T. pachyurus*. Recently, Neves and Pessôa (2011) described some cranial traits to distinguish *T. pachyurus*, *T. inermis*, and *T. laurentius*, but unfortunately, these characters are not preserved in the fossil specimens. In size, the fossil specimens do not differ significantly from the comparative specimens (Tables 3 and 4). Thus, the remains here reported are assigned to *Thrichomys* sp. due to the fragmentary condition of the material. In recent times, *T. apereoides* has been reported in the Parque Nacional de Ubajara (Guedes et al., 2000).

Thrichomys is a scansorial rodent and has been found in several areas of Brazil, from open areas up to the forests of Cerrado, Caatinga, and Pantanal. They are herbivores and feed on leaves and fruits (Bonvicino et al., 2008). In McKenna and Bell (1997), the stratigraphic distribution of *Thrichomys* is from the late Miocene to recent. However, the Miocene fossil record of this taxon is questionable (see Verzi et al., 1995). The confident fossil record of *Thrichomys* is very scarce, represented by a few Quaternary records in the Mato Grosso do Sul, Goiás, Minas Gerais, Pernambuco, and Piauí states of Brazil (Paula Couto, 1971; Guérin et al., 1993; Salles et al., 1999; 2006; Rodrigues et al., 2011), and now in Ceará State.

FINAL REMARKS

Previous records of Quaternary rodents from northeast Brazil were exclusively from Bahia, Sergipe, Rio Grande do Norte, Pernambuco, and Piauí states (Oliveira et al., 1985; Guérin et al., 1993; Lessa et al., 2008; Dantas, 2009; Rodrigues et al., 2011), and now we are reporting a new assemblage for Ceará State. Unfortunately, some materials are very fragmented or there is a complex taxonomic situation in the living forms. Thus, it is not possible to assign a definite species name, such as in *Thrichomys* and cf. *Dasyprocta*.

The data reported here contribute to the knowledge of the Brazilian Quaternary rodents and shows the fossil potential of the studied area. Another Quaternary rodent found in Ubajara is the erethizontid *Coendou prehensilis* (Linnaeus, 1758) from the Urso Fóssil cave, but its stratigraphic provenance is not known exactly (Oliveira, 2010).

The material here reported is derived from levels with an age of about 8,000 years BP, corresponding to the early

Holocene. Like the tayassuids, marsupials, and xenarthrans from these levels (Oliveira, 2010), the caviomorphs do not indicate any faunistic turnover during the Holocene in comparison with the living fauna.

The climates of the late Pleistocene and early Holocene in the northeast region were different from the present, with more humid and colder conditions, and there was a gradual increase in drier conditions throughout the Holocene (see de Oliveira et al., 2005 and references therein). The paleoecological indications of the taxa reported here are in accordance with the mosaic composition of the current environments of the Ubajara region, with humid forest at higher altitudes and open and dryer areas on the plains.

Mammalian faunas of the Holocene, with precise stratigraphic control, have been poorly studied from a paleontological point of view in Brazil. Recent studies have revealed interesting facts in other regions, showing recent extinctions, such as the case of southern Brazil. In this region, Hadler et al. (2008) reported the presence of some rodents distinct from the recent fauna, including a new species, *Clyomys riograndensis*. Recently, Rodrigues et al. (2011) reported the presence of a new Holocene vertebrate assemblage from Pernambuco State. In that work, the authors recognized, for the first time in the Quaternary of northeast Brazil, the presence of the rodent *Phyllomys*, which indicates the presence of more humid conditions in this area during some periods of the Holocene. To analyze these aspects in the karst of Ubajara, new fieldwork should be conducted to collect more material.

ACKNOWLEDGEMENTS

REFERENCES

Antoine, P.-O., Marivaux, L., Croft, D.A., Billet, G., Ganerød, M., Jaramillo, C., Martin, T., Orliac, M.J., Tejeda, J., Altamirano, A.J., Duranthon, F., Fanjat, G., Rouse, S., and Gismondi, R.S., 2011, Middle Eocene rodents from Peruvian Amazonia reveal the pattern and timing of caviomorph origin and biogeography: Proceedings of the Royal Society B, Biological Sciences, published online. doi:10.1098/rspb.2011.1732.

Bonvicino, C.R., Oliveira, J.A. de, and D'Andrea, P.S., 2008, Guia de Roedores do Brasil, com chaves para gêneros baseadas em caracteres externos, Rio de Janeiro, Centro Pan-Americano de Febre Aftosa – OPAS/OMS, 120 p.

Cartelle, C.G., and Lessa, G., 1989, Presença de *Myocastor coypus* (Molina, 1782), Rodentia, Myocastoridae, do Pleistoceno Final-Holoceno, no centro-oeste da Bahia, in Anais, Congresso Brasileiro de Paleontologia, 11th, Curitiba, p. 583–591.

Carvalho, G.A.S., and Salles, L.O., 2004, Relationships among extant and fossil echimyids (Rodentia: Hystricognathi): Zoological Journal of the Linnean Society, v. 142, p. 445–477. doi:10.1111/j.1096-3642.2004.00150.x.

CPRM (Serviço Geológico do Brasil), 2003, Atlas Digital de Geologia e Recursos Minerais do Ceará, Brasília, Ministério das Minas e Energia, CD-ROM.

Dantas, M.A.T., 2009, Primeiro registro de fósseis de mamíferos pleistocênicos em caverna de Sergipe, Brasil: Revista Brasileira de Paleontologia, v. 12, no. 2, p. 161–164. doi:10.4072/rbp.2009.2.06.

De Oliveira, P.E., Behling, H., Ledru, M.P., Barberi, M., Bush, M., Salgado-Labouriau, M.L., Garcia, M.J., Medeanic, S., Barth, O.M., de Barros, M.A., and Scheel-Ybert, R., 2005, Paleovegetação e paleoclimas do Quaternário do Brasil, in Souza, C.R.G., Suguio, K., Oliveira, A.M.S., and de Oliveira, P.E., eds., Quaternário do Brasil, São Paulo, Holos Editora, 2005, p. 52–74.

Emmons, L.H., 2005, A revision of the genera of arboreal Echimyidae (Rodentia: Echimyidae: Echimyinae), with description of two new genera, in Lacey, E.A., and Meyes, P., eds., Mammalian Diversification, From Chromosomes to Phylogeography (A celebration of the Career of James L. Patton), University of California Press, PUblications in Zoology, v. 133, p. 247–309.

Galewski, T., Mauffrey, J.-F., Leite, Y.L.R., Patton, J.L., and Douzery, E.J.P., 2005, Ecomorphological diversification among South American spiny rats (Rodentia; Echimyidae): a phylogenetic and chronological approach: Molecular Phylogenetics and Evolution, v. 34, p. 601–615. doi:10.1016/j.ympev.2004.11.015.

Guedes, P.G., Silva, S.S.P., Camardella, A.R., Abreu, M.F.G., Borges-Nojosa, D.M., Silva, J.A.G., and Silva, A.A., 2000, Diversidade de mamíferos do Parque Nacional de Ubajara (Ceará, Brasil): Mastozoología Neotropical, v. 7, no. 2, p. 95–100.

Guérin, C., Curvello, M.A., Faure, M., Hungueney, M., and Mourer-Chauvire, C., 1993, La faune pléistocène du Piauí (Nordeste du Brésil): implications paléoécologiques et biochronologiques: Quaternaria Nova, v. 3, p. 303–341.

Hadler, P., Verzi, D.H., Vucetich, M.G., Ferigolo, J., and Ribeiro, A.M., 2008, Caviomorphs (Mammalia, Rodentia) from the Holocene of Rio Grande do Sul State, Brazil: systematics and paleonviromental context: Revista Brasileira de Paleontologia, v. 11, no. 2, p. 97–116. doi:10.4072/rbp.2008.2.03

Iack-Ximenes, G.E., 1999, Sistemática da família Dasyproctidae Bonaparte, 1838 (Rodentia, Hystricognathi) no Brasil [Master thesis]. São Paulo, Universidade de São Paulo, 429 p.

IBAMA (Instituto Brasileiro do Meio Ambiente e dos Recursos Renováveis), 2002, Parque Nacional de Ubajara: Plano de Manejo: Brasília, Ministério do Meio Ambiente, CD-ROM.

Kerber, L., Lopes, R.P., Vucetich, M.G., Ribeiro, A.M., and Pereira, J., 2011a, Chinchillidae and Dolichotinae rodents (Rodentia, Hystricognathi, Caviomorpha) from the late Pleistocene of southern Brazil: Revista Brasileira de Paleontologia, v. 14, no. 3, p. 229–238. doi:10.4072/rbp.2011.3.03.

Kerber, L., Ribeiro, A.M., and Oliveira, É.V., 2011b, The first record of *Galea* Meyen, 1832 (Rodentia, Hystricognathi, Caviidae) in the late Pleistocene of southern Brazil and its paleobiogeographic implications: Alcheringa, v. 35, no. 3, p. 445–457. doi:10.1080/03115518.2011.533985.

Lara, M.C., Patton, J.P., and Silva, M.N.F., 1996, The simultaneous diversification of South American echimyid rodents (Hystricognathi) based on complete cytochrome b sequences: Molecular Phylogenetics and Evolution, v. 5, no. 2, p. 403–413. doi:10.1006/mpev.1996.0035.

Lessa, G., Cartelle, C., and Manduca, E.G., 2008, Reevaluation of rodent assemblages from Pleistocene/Holocene of Bahia, Brazil: morphologic and environmental considerations, in Libro de Resúmenes, Congreso Latino-Americano de Paleontología de Vertebrados, 3rd, Neuquén, 137 p.

Lessa, G., and Gonçalves, P.R., 1999, Estudo comparativo de crânios de Kerodon rupestre (Mammalia, Rodentia) holo-pleistocênicos do nordeste brasileiro: Ameghiniana, v. 36, no. 1, 104 p.

McKenna, M.C., and Bell, S.K., 1997, Classification of Mammals above the Species Level, New York, Columbia University Press, 631 p.

Negri, F.R., Bocquetin-Villanueva, J., Ferigolo, J., and Antoine, P.-O., 2010, A review of Tertiary mammal faunas and birds from western Amazonia, in Hoorn, C., and Wesselingh, F.P., eds., Amazonia, Landscape and Species Evolution, A Look into the Past, Chichester, UK, Blackwell Publishing, p. 245–258. doi:10.1002/9781444306408.ch15.

Neves, A.C.S.A., and Pessôa, L.M., 2011, Morphological distinction of the species Thrichomys (Rodentia: Echimyidae) through ontogeny of cranial and dental characters: Zootaxa, no. 2804, p. 15–24.

Oliveira, J.A., and Bonvicino, C., 2006, Ordem Rodentia, in Reis, N.R., Peracchi, A.L., Pedro, W.A., and Lima, I.P., eds., Mamíferos do Brasil, Londrina, Editora da Universidade Estadual de Londrina, p. 347–400.

Oliveira, L.D.D., Souza-Cunha, F.L., and Locks, M., 1985, Um Hydrochoeridae (Mammalia, Rodentia) no Pleistoceno do nordeste o Brasil, in Campos, D.A., Ferreira, C.S., Brito, I.M., and Viana, C.F., eds., Coletânea de Trabalhos Paleontológicos, Brasília, Departamento Nacional da Produção Mineral, Série Geologia no. 27, p. 93–97.

Oliveira, P.V., 2010, Mamíferos do Neopleistoceno-Holoceno do Parque Nacional de Ubajara, Ceará [Masters thesis], Porto Alegre, Universidade Federal do Rio Grande do Sul, 167 p.

Patterson, B., and Wood, A.E., 1982, Rodents from the Deseadan Oligocene of Bolivia and the relationships of the Caviomorpha: Bulletin of the Museum of Comparative Zoology, v. 149, no. 7, p. 371–543.

Paula Couto, C., 1971, Mamíferos fósseis das cavernas de Minas Gerais: Espeleologia, v. 3–4, p. 3–14.

Paula Couto, C., 1978, Mamíferos fósseis do Pleistoceno do Espírito Santo: Anais da Academia Brasileira de Ciências, v. 50, no. 3, p. 365–379.

Pessôa, L.M., Corrêa, M.M. de O., de Oliveira, J.A., and Lopes, M.O.G., 2004, Karyological and morphometric variation in the genus Thrichomys (Rodentia: Echimyidae): Mammalian Biology, v. 69, p. 258–269. doi:10.1078/1616-5047-00141.

Pérez, M.E., 2010, A new rodent (Cavioidea, Hystricognathi) from the middle Miocene of Patagonia, mandibular homologies, and the origin of the crown group Cavioidea sensu strict: Journal of Vertebrate Paleontology, v. 30, no. 6, p. 1848–1859. doi:10.1080/02724634.2010.522432.

Poux, C., Chevret, P., Huchon, D., De Jong, W.W., and Douzery, E.J.P., 2006, Arrival and diversification of caviomorph rodents and plathyrrine primates in South America: Systematic Biology, v. 55, v. 2, p. 228–244. doi:10.1080/10635150500481390.

Quadros, M.L.E.S., 1996, Estudo tectono-sedimentar da Bacia de Jaibaras, na região entre as cidades de Pacujá e Jaibaras, noroesta do Estado do Ceará. [Masters thesis]: Belém, Universidade Federal do Pará, 134 p.

Quintana, C.A., 1996, Diversidad del roedor Microcavia (Caviomorpha, Caviidae) em América del Sur: Mastozoología Neotropical, v. 3, no. 1, p. 63–86.

Reis, S.F., and Pessôa, L.M., 2004, Thrichomys apereoides: Mammalian Species, no. 741, p. 1–5. doi:10.1644/741.

Rodrigues, P.H., Santos, J.D.F., and Silva, A.K.B., 2011, Assembleia holocênica de vertebrados de pequeno porte do Sítio Alcobaça, Estado de Pernambuco, Brasil, in Anais, Congresso Brasileiro de Paleontologia, 22th, Natal, p. 636–638.

Rowe, D.L., and Honeycutt, R.L., 2002, Phylogenetic relationships, ecological correlates, and molecular evolution within the Cavioidea (Mammalia, Rodentia): Molecular Biology and Evolution, v. 19, p. 263–277.

Salles, L.O., Cartelle, C., Guedes, P.G., Boggiani, P.C., Janoo, A., and Russo, C.A.M., 2006, Quaternary mammals from Serra da Bonoquena,

Mato Grosso do Sul, Brazil, Boletim do Museu Nacional, Nova Série Zoologia, no. 521, 12 p.

Salles, L.O., Carvalho, G.S., Weksler, M., Sicuro, F.L., Abreu, F., Camardella, A.R., Guedes, P.G., Avilla, L.S., Abrantes, E.A.P., Sahate, V., and Costa, I.S.A., 1999, Fauna de mamíferos do Quaternário de Serra da Mesa (Goiás, Brasil), Publicações Avulsas do Museu Nacional, no. 78, 15 p.

Toledo, P.M., Moraes-Santos, H.M., and Souza de Melo, C.C., 1999, Levantamento preliminar de mamíferos não-voadores da Serra dos Carajás: grupos silvestres recentes e zooarqueológicos: Boletim do Museu Paraense Emílio Goeldi, v. 15, no. 2, p. 141–157.

Trajano, E., and Ferrarezzi, H., 1994, A fossil bear from northeastern Brazil, with a phylogenetic analysis of the South American extinct Tremarctinae (Ursidae): Journal of Vertebrate Paleontology, v. 14, no. 4, p. 552–561. doi:10.1080/02724634.1995.10011577.

Ubilla, M., Oliveira, E.V., Rinderknecht, A., and Pereira, J., 2008, The hystricognath rodent Microcavia in the Late Pleistocene of Brazil (Rio Grande do Sul, South America) (Mammalia: Caviidae). Biogeographic and paleoenviromental implications: Neues Jahrbuch für Geologie und Paläontologie, Abhandlungen, v. 247, no. 1, p. 15–21. doi:10.1127/0077-7749/2008/0247-0015.

Verzi, D.H., Vucetich, M.G., and Montalvo, C.I., 1995, Un nuevo Eumysopinae (Rodentia, Echimyidae) del Mioceno tardio de la provincia de La Pampa y consideraciones sobre la historia de la subfamilia: Ameghiniana, v. 32, no. 2, p. 191–195.

Vucetich, M.G., and Ribeiro, A.M., 2003, A new and primitive rodent from the Tremembé Formation (Late Oligocene) of Brazil, with comments on the morphology of the lower premolars of caviomorph rodents: Revista Brasileira de Paleontologia, v. 5, p. 73–82.

Vucetich, M.G., Souza Cunha, F.L. de, and Alvarenga, H.M.F., 1993, Un roedor Caviomorpha de la Formación Tremembé (Cuenca de Taubaté), Estado de São Paulo, Brasil: Anais da Academia Brasileira de Ciências, v. 65, p. 247–251.

Vucetich, M.G., and Verzi, D.H., 1994, Las homologías en los diseños oclusales de los roedores Caviomorpha: un modelo alternativo: Mastozoología Neotropical, v. 1, p. 61–72.

Vucetich, M.G., and Verzi, D.H., 2002, First record of Dasyproctidae (Rodentia) in the Pleistocene of Argentina. Paleoclimatic implication: Palaeogeography, Palaeoclimatology, Palaeoecology, v. 178, p. 67–73. doi:10.1016/S0031-0182(01)00402-3.

Vucetich, M.G., Verzi, D.H., and Tonni, E.P., 1997, Paleoclimatic implications of the presence of Clyomys (Rodentia, Echimyidae) in the Pleistocene of central Argentina: Palaeogeography, Palaeoclimatology, Palaeoecology, v. 128, p. 207–214. doi:10.1016/S0031-0182(96)00050-8.

Woods, C.A., and Howland, E.B., 1979, Adaptive radiation of capromyid rodents: anatomy of the masticatory apparatus: Journal of Mammalogy, v. 60, p. 95–116.

Woods, C.A., and Kilpatrick, C.W., 2005, Infraorder Hystricognathi, in Wilson, D.E., and Reeder, D.M., eds., Mammal Species of the World: A Taxonomic and Geographic Reference, 3rd ed., Baltimore, Johns Hopkins University Press, p. 1538–1600.

Wyss, A.R., Flynn, J.J., Norell, M.A., Swisher, III., C.C., Charrier, R., Novacek, M.J., and McKenna, M.C., 1993, South America's earliest rodent and recognition of a new interval of mammalian evolution: Nature, v. 365, p. 434–437. doi:10.1038/365434a0.

APPENDIX 1—Comparative specimens: *Thrichomys apereoides:* MN-63199, MN-63198, MN-63701, MN-63217, MN-63200, MN-63202, MN-63215, MN-63202, MN-63226, MN-63205, MN-63206, MN-63210, MN-63228, MN-63216, MN-63295, MN-66059. *T. inermis:* MN-140 (79–91), MN-14098, MN-14 (100–101). *T. pachyurus:* MN-64029 – 30, MN-64112, MN-64127, MN-64060, MN-64132, MN-64062, MN- MN-64243, MN-64062, MN-64065, MN-64067. *Kerodon rupestris:* MN-263 (41–44), MN-263 (45–55), MN-26708, MN-2670 (00–04), MN-267 (10–14). *K. acrobata:* MN-22729 (holotype), MN- 22728, MN-22730. *Galea spixii:* MN-2607, MN-2031. *Microcavia australis:* MLP-683 (1–10), *Cavia aperea:* MCPU-M 007, MCPU-M 034. *Dasyprocta azarae:* MN-30477, MN-30468, MN-43172, MN-43175, MN-43169, MN-43173, MN-34387, MN-2292, MN-2296, MN-64487, MN-4857. *D. prymnolopha:* MN-43216, MN-1496, MN-43149, MN-43145, MN-43156, MN-43154, MN-43153, MN-10244, MN-7637, MN-43152, MN-7636. *Myoprocta exilis:* MN-268 (92–93), MN- 268 (96–97), MN-26899, MN-269 (00–05).

GUIDE TO AUTHORS

The *Journal of Cave and Karst Studies* is a multidisciplinary journal devoted to cave and karst research. The *Journal* is seeking original, unpublished manuscripts concerning the scientific study of caves or other karst features. Authors do not need to be members of the National Speleological Society, but preference is given to manuscripts of importance to North American speleology.

LANGUAGES: The *Journal of Cave and Karst Studies* uses American-style English as its standard language and spelling style, with the exception of allowing a second abstract in another language when room allows. In the case of proper names, the *Journal* tries to accommodate other spellings and punctuation styles. In cases where the Editor-in-Chief finds it appropriate to use non-English words outside of proper names (generally where no equivalent English word exists), the *Journal* italicizes them. However, the common abbreviations i.e., e.g., et al., and etc. should appear in roman text. Authors are encouraged to write for our combined professional and amateur readerships.

CONTENT: Each paper will contain a title with the authors' names and addresses, an abstract, and the text of the paper, including a summary or conclusions section. Acknowledgments and references follow the text.

ABSTRACTS: An abstract stating the essential points and results must accompany all articles. An abstract is a summary, not a promise of what topics are covered in the paper.

STYLE: The *Journal* consults The Chicago Manual of Style on most general style issues.

REFERENCES: In the text, references to previously published work should be followed by the relevant author's name and date (and page number, when appropriate) in parentheses. All cited references are alphabetical at the end of the manuscript with senior author's last name first, followed by date of publication, title, publisher, volume, and page numbers. Geological Society of America format should be used (see http://www.geosociety.org/pubs/geoguid5.htm). Please do not abbreviate periodical titles. Web references are acceptable when deemed appropriate. The references should follow the style of: Author (or publisher), year, Webpage title: Publisher (if a specific author is available), full URL (e.g., http://www.usgs.gov/citguide.html) and date when the web site was accessed in brackets; for example [accessed July 16, 2002]. If there are specific authors given, use their name and list the responsible organization as publisher. Because of the ephemeral nature of websites, please provide the specific date. Citations within the text should read: (Author, Year).

SUBMISSION: Effective February 2011, all manuscripts are to be submitted via Peertrack, a web-based system for online submission. The web address is http://www.edmgr.com/jcks. Instructions are provided at that address. At your first visit, you will be prompted to establish a login and password, after which you will enter information about your manuscript (e.g., authors and addresses, manuscript title, abstract, etc.). You will then enter your manuscript, tables, and figure files separately or all together as part of the manuscript. Manuscript files can be uploaded as DOC, WPD, RTF, TXT, or LaTeX. A DOC template with additional manuscript specifications may be downloaded. (Note: LaTeX files should not use any unusual style files; a LaTeX template and BiBTeX file for the *Journal* may be downloaded or obtained from the Editor-in-Chief.) Table files can be uploaded as DOC, WPD, RTF, TXT, or LaTeX files, and figure files can be uploaded as TIFF, EPS, AI, or CDR files. Alternatively, authors may submit manuscripts as PDF or HTML files, but if the manuscript is accepted for publication, the manuscript will need to be submitted as one of the accepted file types listed above. Manuscripts must be typed, double spaced, and single-sided. Manuscripts should be no longer than 6,000 words plus tables and figures, but exceptions are permitted on a case-by-case basis. Authors of accepted papers exceeding this limit may have to pay a current page charge for the extra pages unless decided otherwise by the Editor-in-Chief. Extensive supporting data will be placed on the *Journal*'s website with a paper copy placed in the NSS archives and library. The data that are used within a paper must be made available. Authors may be required to provide supporting data in a fundamental format, such as ASCII for text data or comma-delimited ASCII for tabular data.

DISCUSSIONS: Critical discussions of papers previously published in the *Journal* are welcome. Authors will be given an opportunity to reply. Discussions and replies must be limited to a maximum of 1000 words and discussions will be subject to review before publication. Discussions must be within 6 months after the original article appears.

MEASUREMENTS: All measurements will be in Systeme Internationale (metric) except when quoting historical references. Other units will be allowed where necessary if placed in parentheses and following the SI units.

FIGURES: Figures and lettering must be neat and legible. Figure captions should be on a separate sheet of paper and not within the figure. Figures should be numbered in sequence and referred to in the text by inserting (Fig. x). Most figures will be reduced, hence the lettering should be large. Photographs must be sharp and high contrast. Color will generally only be printed at author's expense.

TABLES: See http://www.caves.org/pub/journal/PDF/Tables.pdf to get guidelines for table layout.

COPYRIGHT AND AUTHOR'S RESPONSIBILITIES: It is the author's responsibility to clear any copyright or acknowledgement matters concerning text, tables, or figures used. Authors should also ensure adequate attention to sensitive or legal issues such as land owner and land manager concerns or policies.

PROCESS: All submitted manuscripts are sent out to at least two experts in the field. Reviewed manuscripts are then returned to the author for consideration of the referees' remarks and revision, where appropriate. Revised manuscripts are returned to the appropriate Associate Editor who then recommends acceptance or rejection. The Editor-in-Chief makes final decisions regarding publication. Upon acceptance, the senior author will be sent one set of PDF proofs for review. Examine the current issue for more information about the format used.

ELECTRONIC FILES: The *Journal* is printed at high resolution. Illustrations must be a minimum of 300 dpi for acceptance.

Journal of Cave and Karst Studies

Volume 75   Number 1   April 2013